SMIP91

SEMINAR ON
SEISMOLOGICAL AND ENGINEERING IMPLICATIONS OF RECENT STRONG-MOTION DATA

Sacramento, California
May 30, 1991

PREPRINTS

Sponsored by

Strong Motion Instrumentation Program
Division of Mines and Geology
California Department of Conservation

Supported in Part by

California Seismic Safety Commission

CALIFORNIA
DEPARTMENT
OF CONSERVATION

Division of Mines and Geology

The Strong Motion Instrumentation Program (SMIP) is administered by the Division of Mines and Geology, California Department of Conservation. It is advised by the Strong Motion Instrumentation Advisory Committee (SMIAC), a committee of the California Seismic Safety Commission. SMIP is funded by an assessment on construction costs for building permits issued by cities and counties in California, the Office of Statewide Health Planning and Development, and the California Department of Transportation.

DISCLAIMER

Neither the sponsoring nor supporting agencies assume responsibility for the accuracy of the information presented in this report or for the opinions expressed herein. The material presented in this publication should not be used or relied upon for any specific application without competent examination and verification of its accuracy, suitability, and applicability by qualified professionals. Users of information from this publication assume all liability arising from such use.

PREFACE

The Strong Motion Instrumentation Program (SMIP) in the Division of Mines and Geology of the California Department of Conservation promotes and facilitates the improvement of seismic codes through the Directed Research Project. The objective of this project is to increase the understanding of earthquake strong ground shaking and its effects on structures through interpretation and analysis studies of SMIP and other applicable strong-motion data. The ultimate goal is to accelerate the process by which lessons learned from earthquake data are incorporated into seismic code provisions and seismic design practices.

The Loma Prieta earthquake of October 17, 1989 produced a large set of strong-motion data from a magnitude 7.1 earthquake. This data set is very important because most previous strong-motion data are from earthquakes of lower magnitude. SMIP obtained records from a total of 94 stations, including 53 ground-response stations and 41 extensively-instrumented structures. These records have been the subject of SMIP directed research projects in the past year.

The SMIP91 Seminar is the third in a series of planned annual events designed to transfer recent research findings on strong-motion data to practicing seismic design professionals and earth scientists. In both oral presentation and poster sessions, sixteen investigators will provide state-of-the-art data and analysis results from recent research studies of SMIP data during the past year.

The papers in this volume represent interim results obtained by the investigators. Following this seminar the investigators will be preparing final reports with their final conclusions. These reports will be more detailed and will update the results presented here. SMIP will make these reports available after the completion of the studies.

TABLE OF CONTENTS

TABLE OF CONTENTS(continued)

Source, Path, and Site Ground Motion Model of The Loma Prieta Earthquake: Preliminary Results

W. J. Silva
Pacific Engineering and Analysis

C. Stark
Graduate Student, U.C. Berkeley

ABSTRACT

The objective of this study is to model the observed strong ground motion variability during the 1989 Loma Prieta earthquake. The modeling exercise is intended to assess the effects of source finiteness, crustal propagation, and site response upon the recorded motions. The ground motion model employed combines a model for the finite earthquake source as well as nonlinear soil response and crustal propagation effects with the band-limited-white-noise (BLWN) ground motion model. The combined model uses random vibration theory (RVT) to produce site specific estimates of peak acceleration and response spectral ordinates. Preliminary results indicate that the simple point-source using a 1/distance geometrical attenuation provides the optimum overall fit to observed response spectra at fault distances ranging from 1 - 80 km. In addition, knowledge of site specific kappa values reduce the uncertainty in spectral estimates for frequencies exceeding 3 - 4 Hz.

INTRODUCTION

In the near-source region of large earthquakes, dynamic and geometrical properties of the extended (or finite) earthquake source may profoundly affect the resulting ground motion. Specific properties such as rupture propagation, directivity, and source-receiver geometry may be incorporated into strong ground-motion predictions. In this study, a model for the finite-source is combined with the BLWN-RVT ground-motion model [1] to produce site-specific response spectra appropriate for engineering design. The site-response calculation includes nonlinear effects of strain-dependent soil properties on vertically propagating shear waves. In addition, to accommodate the effects of crustal structure on wave propagation at large distances ($\geq$ 50 km), the model incorporates the contributions of direct and supercritically reflected wavefields [2]. Together with the finite-source model, this combined approach yields a site-response methodology applicable to a wide range of site conditions and source distances. As a result, the model is useful in isolating and quantifying the source, propagation path, and site properties which control the variability of strong ground motions. This assessment is made by modeling a total of 25 strong motion sites (22 rock and 3 soil) which recorded the 1989 Loma Prieta earthquake. For these sites, fault distances ranged from 1 to 81 km (Table 1).

COMPUTATIONAL MODEL

To approximate the effects of an extended source at close source-receiver distances, the empirical Green function methodology [3] is followed, but in place of small-earthquake recordings the omega-square source model [4], is used to simulate a series of small earthquakes distributed across the fault plane. The model assumes constant slip in small, discretized sub-faults, and generates a small-magnitude source function over each area. The initiation of slip on the sub-fault is partially randomized to minimize artificial periodicity of sub-events. By propagating the rupture across a series of sub-faults, appropriately time-delayed, the model generates a Fourier spectrum which incorporates the effects of rupture propagation. This spectrum is then used to estimate response spectra for a finite- source within the framework of the BLWN-RVT ground-motion model. Path effects are approximated with factors for geometrical spreading (1/distance) and frequency-dependent attenuation. Amplification factors for rock sites are modeled by vertical propagation of motions through a crustal velocity model, with the near-surface exponential-decay parameter kappa [5]. At soil sites, motions are additionally propagated

through a soil profile, using an equivalent-linear approach to model the effects of strain-dependent shear modulus and damping values [6]. In order to model the effects of direct and supercritically-reflected S- waves, the point-source part of the model has been augmented to include the contributions of these wavefields [2]. This extension of the BLWN model then permits an evaluation of the appropriateness of the simple assumption of 1/distance [1] for geometrical attenuation.

INITIAL MODEL RESULTS

The M 6.9 1989 Loma Prieta earthquake produced a wealth of strong-motion recordings at source-receiver distances of less than 100 km, representing a variety of site conditions. The source model employed here is given by the slip distribution of Wald et al. [7]. The slip distribution is approximated using a grid of 3.3-by-2.5 km patches of constant slip, with each sub-event having M 5.0. Slip is initiated across the fault using a constant rupture velocity (circular rupture front) of 3 km/sec. The total rupture duration is 6.5 sec and the rise time is 1.2 sec.

In the first step of the project, rock outcrop motions at 22 rock sites at fault distances from 1 to 81 km (Table 1) were modeled. Using templates for spectral shapes as a function of kappa for an M 6.9 point-source at close distances [8], kappa values were determined for each rock site (Table 1, model 0); the average kappa is .06 sec. For crustal amplification, the velocity model of Wald et al. [7] was used. The Q model used is appropriate for WNA; $Q(f) = 150\ f^{0.6}$ (Table 1, model 0 [8]). Acceleration response spectra (5% damped) in the band .010 to 10 sec, were then simulated for the finite-fault model and for an equivalent point-source model, both using the simple 1/R geometrical term. For the point-source simulations, the magnitude and source durations were constrained to M 6.9 and 6.0 sec respectively [7]. These values result in a Brune stress drop of 238 bars for a source region shear-wave velocity of 3.6 km/sec at a depth of 12 km (depth of the largest asperity [7]). Comparisons of these simulations to the average of two horizontal components recorded at 9 of the 22 rock sites are shown in Figure 1.

In addition, response spectra were modeled at three soil sites: PAV (stiff soil), GL2 (deep stiff soil), and TRI (soft soil)(Table 1). Shear-wave velocity profiles for these sites (from surface to bedrock) are derived from downhole seismic surveys performed in close proximity to each of the strong-motion instruments (Bruce Redpath, personal communication). Shear modulus and damping for PAV and TRI sites as functions of shear strain used in the modeling are shown in Figure 2. The soil models are preliminary and currently are based upon strong-motion simulations. The soil models for GL2, also shown in Figure 2, are preliminary results from laboratory tests (Ken Stokoe, personal communication). Further refinement of the models will result from an ongoing laboratory-testing program. For input to the soil column, the same crustal velocity model was used, with a kappa of .04 sec appropriate for average western North America rock sites [8]. The soil columns were then simply placed on top of the crustal model. Comparisons of simulations to observations at soil sites are shown in Figure 1.

For rock sites, both the finite-fault and point-source models generally simulate the observed peak acceleration and spectral shape over broad spectral ranges. For periods shorter than 1.0 sec, the finite and point-source models appear to fit the data equally well. At close distances, within 20-30 km, the point-source clearly overpredicts long-period ($>$ 1.0 sec) response. At all distances, the finite-source model generally appears deficient at intermediate periods (0.5 - 3.0 sec). We attribute this deficiency to the manner in which small-magnitude earthquakes are summed to generate large earthquakes in the simulation [10].

For the soil sites (GL2, PAV, and TRI), the simulated motions agree very well for periods less than about 0.3 sec. As with the rock sites, the finite-source shows some spectral deficiency at intermediate periods and the point-source overpredicts at long periods at the close sites. For the distant soil site, TRI, the fit is very good from peak acceleration to periods of several seconds.

To illustrate the effects of soil nonlinearity at high levels of motion, Figure 3 shows 5% damped response spectra resulting from a site response analysis at GL2 using the outcrop recorded motions at GL1 as control motions. In Figure 3, the dash-dotted line represents a linear analysis using the small strain laboratory data. The resulting motions show exaggerated short period response with a peak acceleration of 0.76 g. The equivalent-linear analysis shows a good fit over the entire bandwidth with a peak acceleration of 0.37 g, in accord with the average observed of 0.37 g. The improvement at long periods using the nearby rock outcrop as control motions over the point-source model is a consequence of the exaggerated long period response of the point-source model at long periods. Also shown in Figure 3 are the low- and high- strain values of shear-wave velocity and Q (damping $\approx$ 1/2Q).

STRONG MOTION DATA INVERSION

In order to provide a more region-and site-specific ground motion model, an inversion for magnitude, corner frequency (inverse of source duration), regional Q model (Q_o and eta), and site specific kappa values was made for the 22 rock sites. Using the starting values from model 0 (Table 1), the resulting model parameters are shown in Table 1 as model 1. Interestingly, the average kappa value is changed little (0.06 sec to 0.05 sec). The moment magnitude has decreased slightly to 6.86 with an increase in duration to 6.2 sec resulting in a Brune stress drop of 184 bars. Of particular interest, the Q model has shown an increase in Q_o to 186 and a decrease in eta to 0.36. Apparently the system is more compatible with a higher Q_o and less of a frequency dependence than that assumed appropriate for WNA.

INVERSION MODEL RESULTS

Both the finite- and point- source models were rerun with the new model parameters (Table 1, model 1). For the finite-source however, the source model, based upon Wald et al. [7], was left unchanged. The simulated peak acceleration values are shown in Table 1. The results of the inversion generally show an increase in motions for the point-source resulting in a slightly better fit at distance. For the finite-source, while the motions are generally comparable, care should be taken in evaluating the difference because a point-source model was used in the inversion and neither the magnitude nor source duration was perturbed in the finite-fault run.

To provide a quantative measure of the ground motion predictions, a simple goodness of fit at each spectral period was performed by taking the difference of the logs of the observed average response spectrum and the predicted response spectrum, squaring, and summing over the 22 rock sites. Dividing the resultant by the number of sites (assuming zero bias) results in an estimate of the model variance. Figure 4 shows the natural log of the standard error plotted versus frequency for the finite- and point- source simulations using model 0 (Table 1) parameters (top frame) and model 1 parameters (lower frame). For both the point- and extended- sources, the standard errors for frequencies greater than about 2-3 Hz are comparable to those based upon empirical regression analyses. The large peak shown in the finite-fault standard error is a consequence of the intermediate-period spectral deficiency of the response spectra shown in Figure 1. Additional features of interest include the small difference between the point and extended source models and the stability of the point- source standard error to periods of several seconds. The increase in the point-source standard error with increasing period is due largely to the overprediction at close distances shown in Figure 1. For model 1, shown in Figure 4 (lower), there is a reduction in standard error for the point-source and a slight increase for the finite-source.

To examine the distance dependency of the difference in standard errors between the point- and finite- sources, Figure 5 shows an analogous set of plots for sites located within a fault distance of 55 km (sites including A2E and closer). For model 0, the finite-source shows a generally lower variance than the point-source for high frequencies ($>$ 4 Hz). Comparable levels of uncertainty are shown down

to about 1 Hz where the finite-fault spectral deficiency peaks. Also, the overprediction of the point-source at long periods is apparent in the increase in standard error at low frequencies. The value at 0.1 Hz exceeds that shown in Figure 4 by a significant amount supporting the observation that the low frequency misfit is due largely to the close stations. This may be a consequence of using an average radiation pattern coefficient in the point-source model as well as in the inversion code.

The model 1 results in Figure 5 show an improved fit for the point-source and an increase in error for the finite-source, particularly at high frequencies. Apparently, for the close-in stations, inversions for source, path, and site properties should include effects of source finiteness. However, it must be recalled that the finite-fault simulations were not rerun with a lower magnitude and slightly larger duration which resulted from the point-source inversion (Table 1, model 1).

Considering the standard errors shown in Figure 4 for all sites (1 - 81 km) and Figure 5 for the close-in sites, it appears there is not a large difference in uncertainty between the point- and extended-sources. The simple point-source, given the proper source and propagation path parameters, as well as site-specific kappa values, produces response spectral ordinates that are, on average, as reliable as those produced with a finite source.

EFFECTS OF KAPPA

In the stochastic model used here the controlling site-dependent parameter for rock sites is kappa [5,8]. In order to assess the overall improvement in fit that site-specific kappa values can provide, the point-source simulations were run with a constant average kappa. The value used (0.05 sec) is the average resulting from the inversion (Table 1, model 1). Figure 6 shows the results for all rock sites compared to the point-source with site-specific kappa values. As expected, the constant kappa variance is larger than the site-specific kappa simulations and the difference is frequency dependent. For frequencies less than about 3 - 4 Hz, site-specific kappa values provide little reduction in variance. For higher frequencies, however, the reduction in uncertainty appears to be significant and demonstrates that knowledge of an appropriate kappa value for a particular site is significant in predicting expected motions.

To examine the goodness of fit of the point-source model using a 1/R geometrical attenuation to the observed attenuation of peak acceleration, Figure 7 shows the model 1 predictions along with a curve computed using the model 1 average kappa of 0.05 sec. The model with site specific kappa values provides an acceptably good fit (standard error of about .034) to the data. The constant kappa model has a standard error for peak acceleration of about 0.47, which is still comparable to that obtained from empirical regression analyses which include interearthquake variability. The two extreme outliers in the data at about 80 km with average peak horizontal accelerations near 0.2 g are sites Presidio and Golden Gate. It is possible that these sites, which are located upon soft serpentine, experience significant local amplification (Dave Boore, personal communication). With the exception of these sites, which represent significant contributions to the model variance, the point-source model (Table 1, model 1) with site-specific kappa values provide a good estimate of the observed attenuation of peak acceleration.

EFFECTS OF WAVE PROPAGATION

In both the finite-source and point-source stochostic models presented here, geometrical attenuation was modeled as a simple 1/distance (distance to largest asperity for the point-source) dependency. In order to investigate the effects of accurately accommodating the direct and supercritically reflected rays in the point-source simulations, the method of Ou and Herrmann [2] was employed. This technique computes the appropriate geometrical attenuation and duration for the direct and supercritical rays in a manner appropriate for the stochastic ground motion model.

For a quantative comparison of the response spectral ordinates using the 1/R geometrical attenuation model and the direct plus supercritical model, the standard errors are shown in Figure 8 for both cases using model 1 parameters. The direct plus supercritical shows a larger uncertainty for frequencies greater than about 3 Hz, comparable uncertainty from about 3 Hz to about 0.3 Hz, and then lower levels of uncertainty at long periods. These results indicate that, in the stochastic model, over the period range of several seconds to over 30 Hz, the 1/R geometrical attenuation performs generally as well as the seismologically more rigorous model which includes the direct plus supercritically reflected phases.

CONCLUSIONS

An extension of the stochastic ground motion model which accommodates a finite- source as well as nonlinear soil response has been used to model the source, path, and site effects of the 1989 Loma Prieta earthquake. Based upon an analysis of variance between the observed and computed response spectra, the preliminary results indicate that the finite-fault and point-source models provide comparably low levels of uncertainty. Depending upon oscillator period, both models produce uncertainty levels comparable to the standard errors resulting from empirical regression analyses. Specifically, for sites within about 50 km of the fault, the finite-source provides slightly lower variance estimates while for all distances, the point-source results are generally lower in variance from several seconds to over 30 Hz. Using site-specific kappa values, based upon an inversion of strong motion data recorded at 22 rock sites, the variance is reduced considerably for frequencies above about 3 - 4 Hz.

Comparing the simple 1/R geometrical attenuation assumed for the stochastic model [1] with a seismologically more rigorous model which includes the direct plus supercritically reflected phases [2] resulted in nearly the same estimates of uncertainty. These results indicate that the simple stochastic point-source model with 1/R geometrical attenuation provides a good fit to the response spectra computed from observed records at fault distances varying from 1 - 80 km. For the point-source model, with site specific kappa values, the standard error of peak acceleration estimates at rock sites is about 0.34. Using an average kappa value, the standard error is increased about 40% to about 0.47.

REFERENCES

1. T.C. Hanks and R.K. McGuire, "The Character of High-Frequency Strong Ground Motion, Bulletin of the Seismological Society of America 71: 2071-2095 (1981).

2. G.B. Ou and R. B. Herrmann, "A Statistical Model for Ground Motion Produced by Earthquakes at Local and Regional Distances" Bulletin of the Seismological Society of America 80: 1397-1417 (1990).

3. S.H. Hartzell, "Earthquake Aftershocks as Green's Function", Geophys. Res. Lett.5: 1-4 (1978).

4. J.N. Brune, "Tectonic Stress and the Spectra of Seismic Shear Waves from Earthquakes", J. Geophys. Res. 75: 4997-5009 (1970).

5. J.G. Anderson and S.E. Hough, "A Model for the shape of the Fourier Amplitude Spectrum of Acceleration at High Frequencies", Bulletin of the Seismological Society of America 74:(1984).

6. G.R. Toro, R.K. McGuire and W.J. Silva, "Engineering Model of Earthquake Ground Motion for Eastern North America", EPRI NP-6074, Electric Power Research Institute, 1988.

7. D.J. Wald, D.V. Helmberger, and T.R. Heaton, "Rupture Model of the 1989 Loma Prieta Earthquake from the Inversion of Strong Motion and Broadband Teleseismic Data", submitted to Bulletin of the Seismological Society of America (1990).

8. R.B. Darragh, W.J. Silva, C. Stark, J. Schneider, and J.C. Stepp, "Engineering Characterization of Strong Ground Motion at Rock Sites in North America", Proceedings of the Fourth International Conference on Seismic Zonation, Stanford University, 1991.

9. R.W. Burger, P.G. Somerville, J.S. Barker, R.B. Herrmann, and D.V. Helmberger, "The Effect of Crustal Structure on Strong Ground Motion Attenuation Relations in Eastern North America", Bulletin of the Seismological Society of America. 77: 420-439 (1987).

10. W.B. Joyner and D.M. Boore, "On Simulating Large Earthquakes by Green's Function Addition of Smaller Earthquakes", Proceedings of the Fifth Maurice Ewing Symposium on Earthquake source Mechanics, American Geophysical Union, 1986.

TABLE 1
A) Loma Prieta Modeling Summary.

Site Name	Label	Kappa (sec) Model 0	Kappa (sec) Model 1	Fault Dist (km)	PGA(g) Avg. Obs.	PGA(g) Finite Model 0	PGA(g) Finite Model 1	PGA(g) Point* Model 0	PGA(g) Point* Model 1
Corralitos	COR	0.055	0.074	1	0.55	0.52	0.52	0.58	0.53
Gilroy 1	GL1	0.025	0.043	15	0.44	0.43	0.29	0.51	0.43
Gilroy 2	GL2	0.040	0.052	16	0.35	0.39	0.36	0.41	0.41
UC Santa Cruz	UCS	0.040	0.037	16	0.46	0.51	0.51	0.35	0.44
Gilroy 6	GL6	0.050	0.065	24	0.14	0.17	0.16	0.23	0.23
Palo Alto VA Hosp.	PAV	0.040	0.052	24	0.37	0.38	0.38	0.38	0.34
SLAC	SLA	0.060	0.062	28	0.24	0.19	0.17	0.16	0.19
Redwood City-Cañada	RDC	0.120	0.072	38	0.07	0.09	0.14	0.07	0.13
SAGO South	SAS	0.100	0.082	39	0.07	0.07	0.08	0.08	0.12
APEEL 7	A07	0.100	0.058	44	0.13	0.09	0.14	0.07	0.12
APEEL 10	A10	0.100	0.078	44	0.09	0.09	0.11	0.07	0.10
Monterey City Hall	MON	0.060	0.054	44	0.07	0.11	0.11	0.09	0.12
Belmont 2-story Bldg	BEL	0.080	0.067	46	0.11	0.12	0.13	0.08	0.11
Apeel 2E CUSH Stad.	A2E	0.040	0.059	53	0.08	0.08	0.06	0.09	0.09
Sierra Point	SSP	0.040	0.029	65	0.08	0.10	0.10	0.07	0.09
SF Diamond Heights	SFD	0.040	0.039	73	0.10	0.09	0.08	0.07	0.09
Piedmont Jr. High	PHS	0.050	0.042	74	0.08	0.06	0.07	0.06	0.08
SF Rincon	SFR	0.040	0.018	76	0.09	0.09	0.11	0.07	0.10
Yerba Buena Island	YBI	0.080	0.080	77	0.05	0.06	0.08	0.05	0.06
SF Pacific Heights	SFH	0.080	0.055	78	0.06	0.09	0.07	0.05	0.07
SF Telegraph Hill	SFT	0.040	0.048	78	0.07	0.08	0.07	0.06	0.07
SF Presidio	SFP	0.080	0.033	79	0.16	0.08	0.08	0.05	0.08
Treasure Island	TRI	0.040	0.052	79	0.13	0.14	0.14	0.14	0.14
SF Cliff House	SFC	0.080	0.048	80	0.09	0.05	0.07	0.04	0.07
SF Golden Gate	SFG	0.040	0.036	81	0.18	0.08	0.07	0.06	0.08
		AVG.** 0.06	AVG.** 0.05						

*Point source simulations use a source depth of 12 km (depth of largest asperity [7]).

**Average of rock sites

B) Source Parameters and Path Q Models

Model	M	SD (Bars)	Duration (sec)	Q_0	ETA
0	6.90	238	6.0	150	0.60
1	6.86	184	6.2	186	0.36

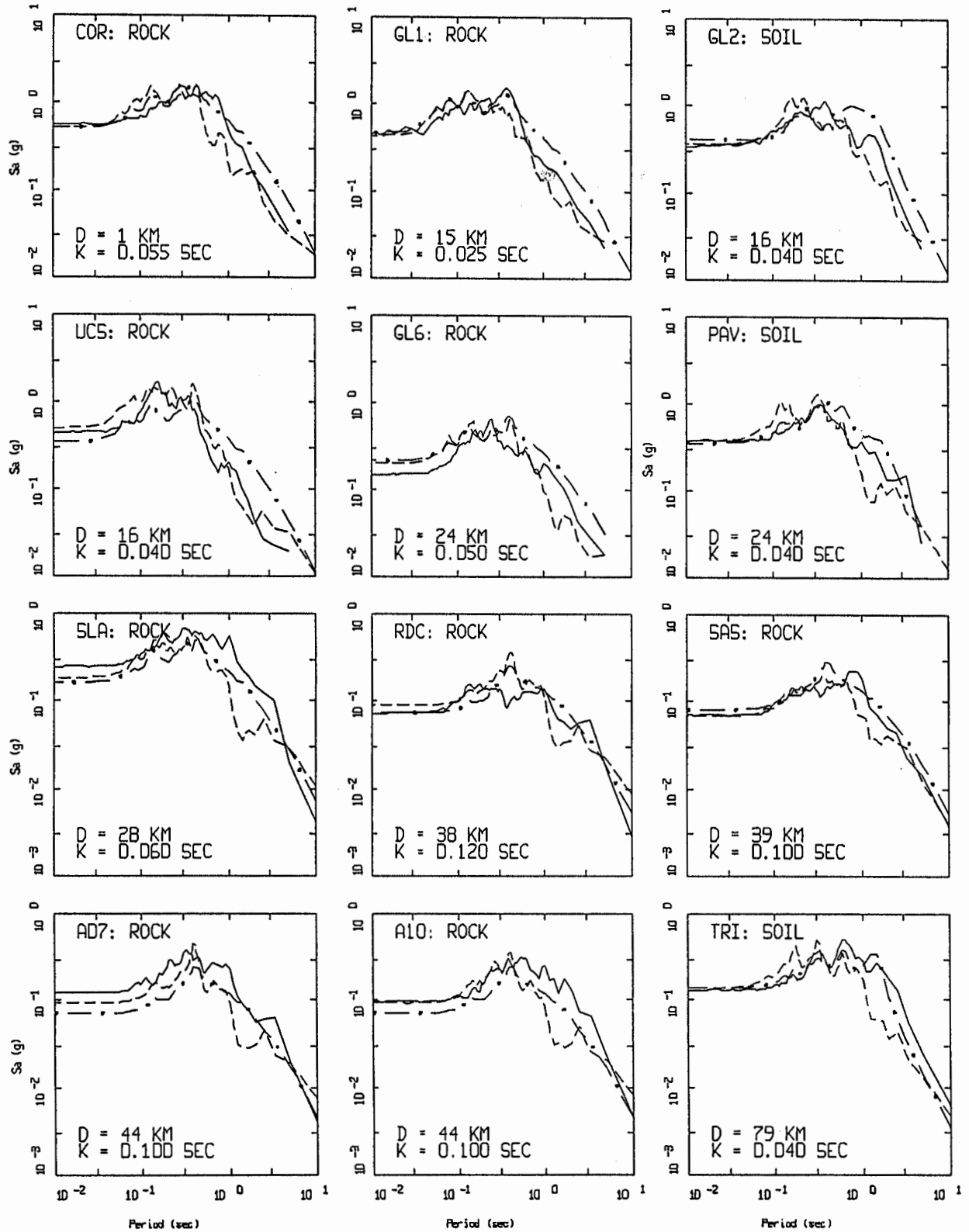

Figure 1. 5% damped response spectra for Loma Prieta earthquake at 9 rock and 3 soil sites in SF Bay Area. Shown for each site are observed data (solid), and simulations from finite fault (dashed) and point source (dash-dotted). Model parameters are shown in Table 1 (model 0).

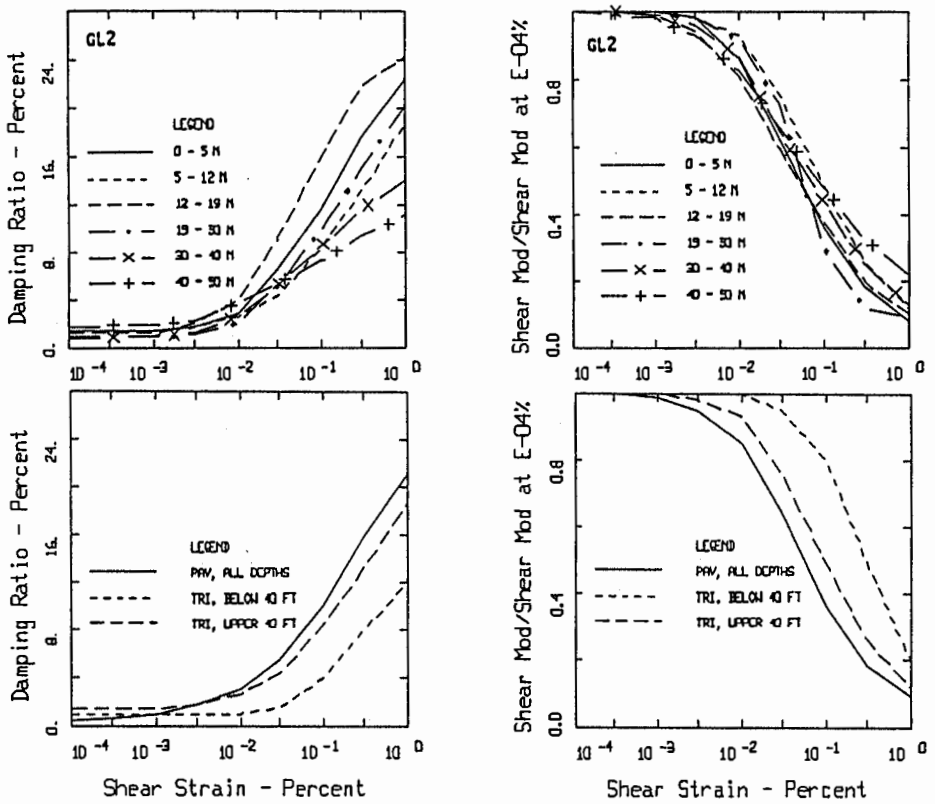

Figure 2. Modulus reduction and damping models for soil sites GL2, PAV, and TRI.

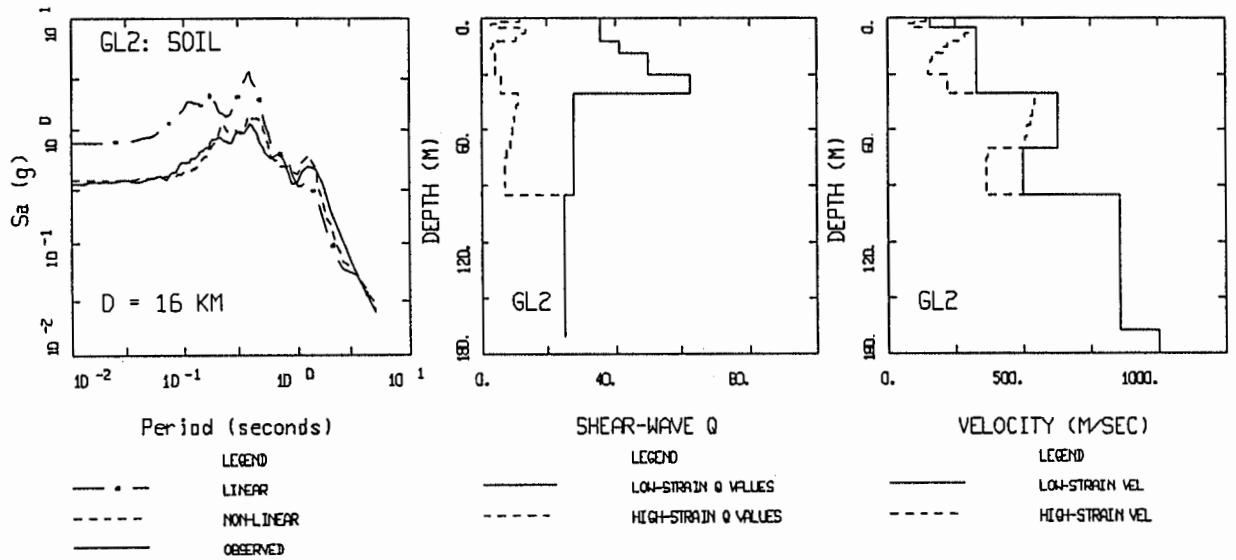

Figure 3. Results of site response analyses at GL2 using linear and equivalent-linear soil response. Rock outcrop motion at GL1 (vector sum Fourier spectra) was used as control motion. Left frame is 5% damped response spectral acceleration showing results of linear and equivalent-linear analyses. Center frame shows the initial (low-strain) and final (high-strain) soil Q profile (damping $\approx$ 1/2Q). Right frame shows the initial and final shear wave velocities. Initial (low-strain) shear wave Q is taken from the laboratory data at 10^{-4}% shear strain.

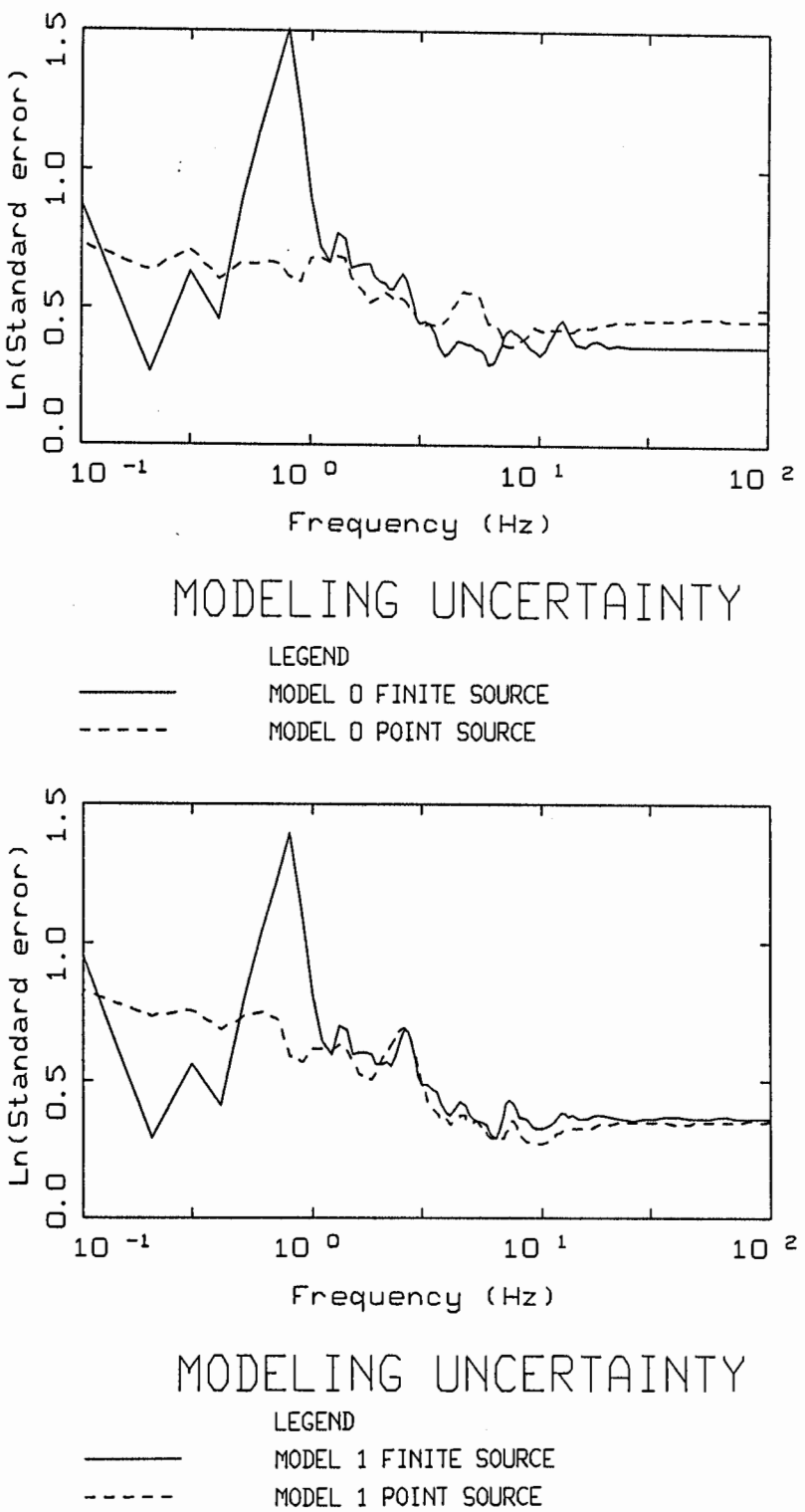

Figure 4. Plot of natural logarithm of the standard error of response spectral ordinates for finite and point source model computation at all rock sites using model 0 (upper) and model 1 (lower). Model parameters are shown in Table 1.

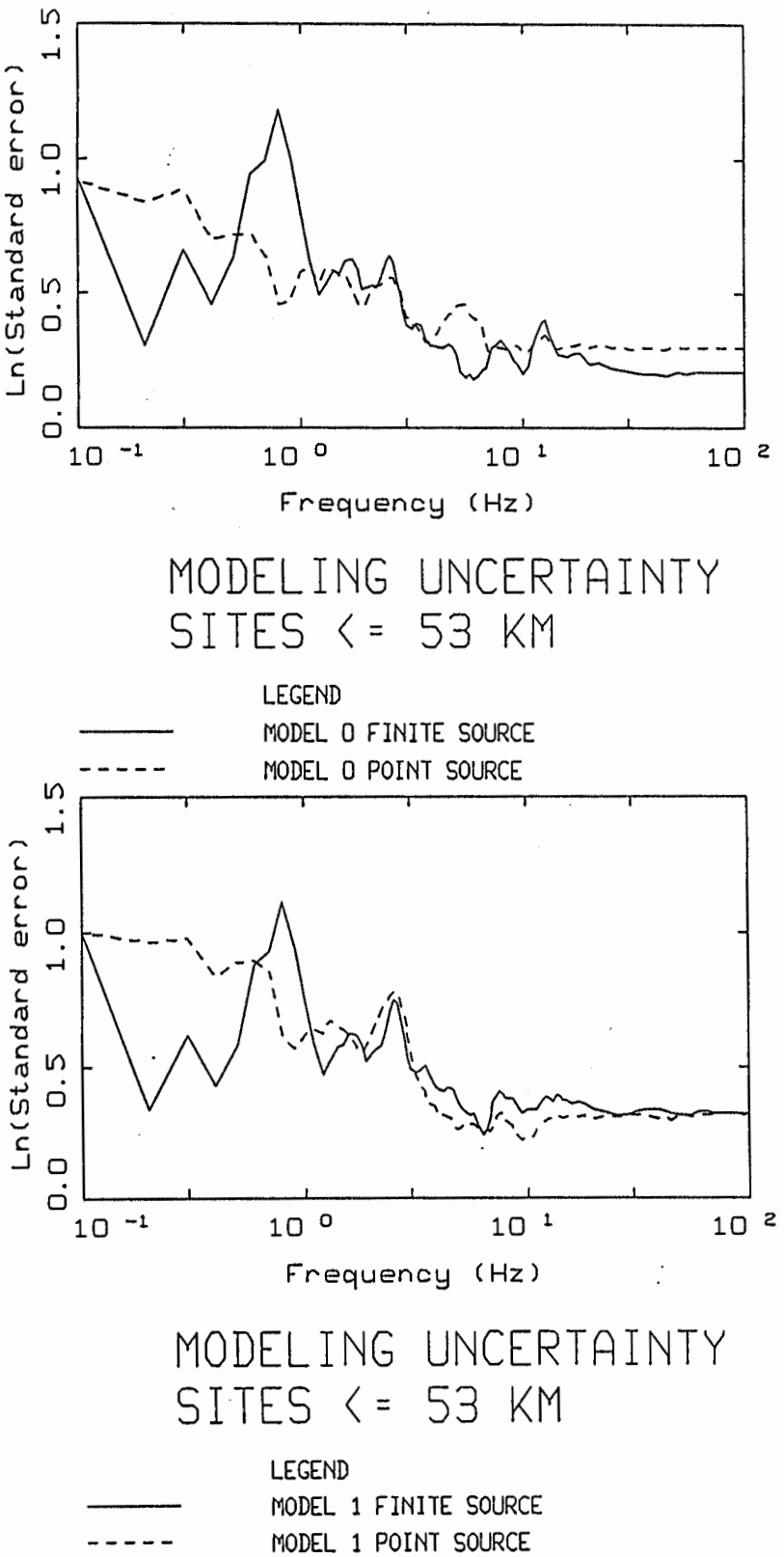

Figure 5. Plot of natural logarithm of the standard error of response spectral ordinates for finite and point source model computation at sites less than 55 km using model 0 (upper) and model 1 (lower). Model parameters are shown in Table 1.

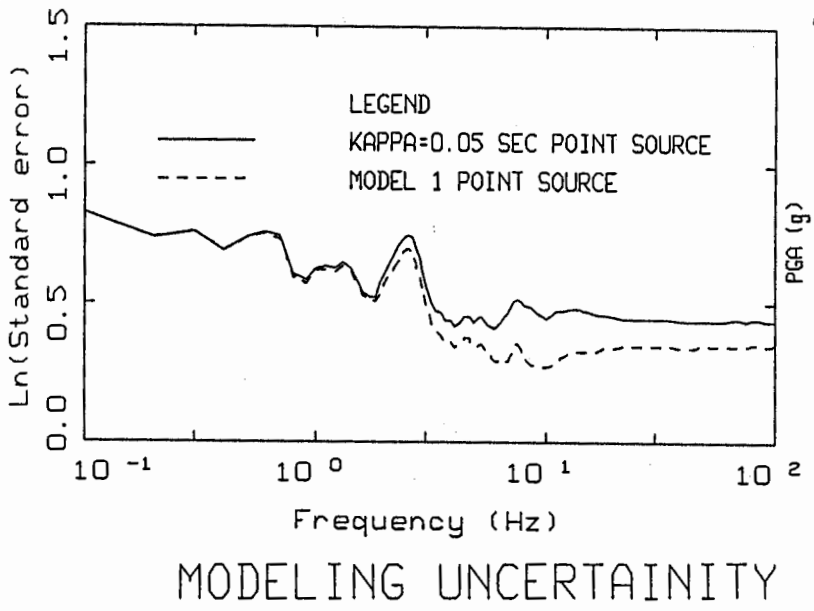

Figure 6. Left. Plot of natural logarithm of the standard error of response spectral ordinates for the point source model computation using model 1. Solid line uses a constant kappa value of 0.05 sec. Model parameters are shown in Table 1.

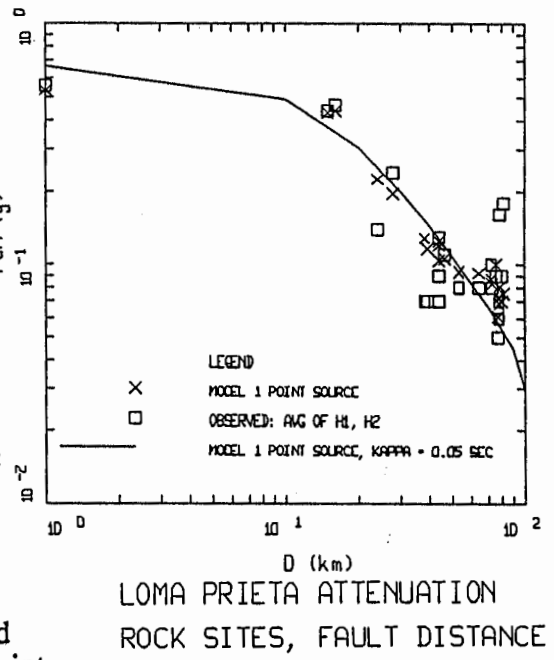

Figure 7. Right. Plot of peak acceleration attenuation: squares, average of the observed horizontal components; crosses, model 1 using site specific kappa values; solid line, model 1 with average kappa value.

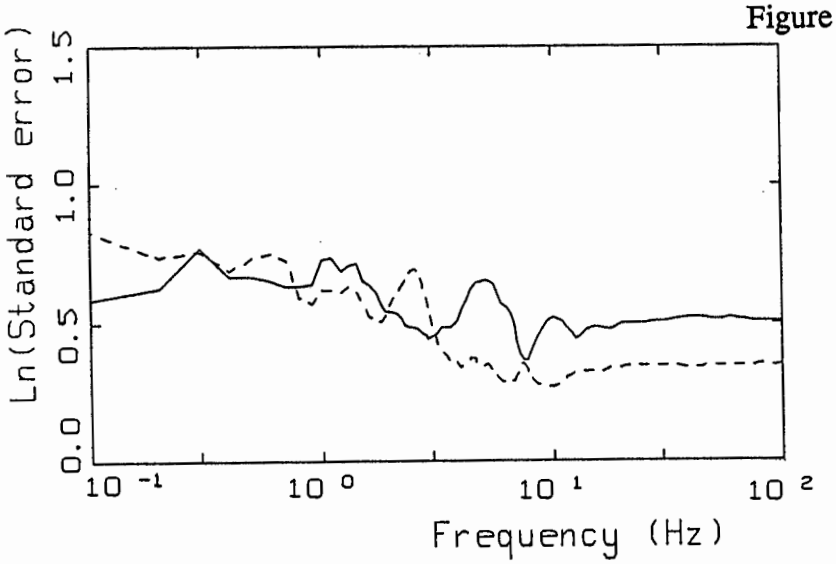

Figure 8. Plot of natural logarithm of the standard error of response spectral ordinates for the point source model computation using model 1. Solid line includes the direct plus supercritically reflected phases. Dashed line is for the simple 1/R geometrical attenuation. Model parameters are shown in Table 1.

LEGEND

——— MODEL 1 POINT SOURCE, DIRECT PLUS SUPERCRITICAL

- - - - - MODEL 1 POINT SOURCE, 1/R

THE INFLUENCE OF CRITICAL MOHO REFLECTIONS ON STRONG GROUND MOTION ATTENUATION IN CALIFORNIA

Paul Somerville, Nancy Smith, Robert Graves
Woodward-Clyde Consultants, Pasadena

Douglas Dreger
Seismological Laboratory, California Institute of Technology

ABSTRACT

Using strong motion recordings from the 1987 Whittier Narrows and 1989 Loma Prieta earthquakes, we show evidence that critical reflections from the lower crust control the attenuation of peak acceleration at distances beyond the critical distance, causing a flattening of the attenuation curve. Depending on the focal depth of the earthquake and the crustal thickness, this flattening can begin at distances from the source as close as 40 km.

INTRODUCTION

Empirical attenuation relations assume a simple monotonic decrease of peak ground motions with distance. However, models of wave propagation in a layered crust predict that the attenuation relation for a specific earthquake will have a more complex form that is controlled by the focal depth of the earthquake and the crustal structure (Burger *et al.*, 1987), as shown schematically in Figure 1. At close distances, peak horizontal ground motions are controlled by direct upgoing shear waves. However, as distance increases, the reflections of shear waves from interfaces in the lower crust (such as the Conrad and Moho discontinuities) reach the critical angle and undergo total internal reflection, producing large amplitude arrivals (S_cS and S_mS) that cause a flattening of the attenuation relation. Strong evidence of the effect of critical reflections on the attenuation of strong ground motion from the 1988 Saguenay, Quebec earthquake was described by Somerville *et al.* (1990).

The present study was motivated by the hypothesis that critical reflections from the Moho caused peak ground motion amplitudes to remain approximately uniform in the epicentral distance range of about 50 to 100 km from the 1989 Loma Prieta earthquake (Somerville and Yoshimura, 1990). Strong ground motion levels on rock and alluvium in the central San Francisco Bay area during the Loma Prieta earthquake exceeded those of empirical attenuation relations. According to the hypothesis, these large ground motions were critical Moho reflections, and contributed about equally with impedance-contrast amplification effects in generating destructive ground motions at soft soil sites in the central San Francisco Bay area.

The principal objective of this paper is to examine evidence for the influence of critical reflections on strong ground motion attenuation in other regions of California. We have done this by examining the strong motion recordings of the following large earthquakes: 1952 Kern County; 1968 Borrego Mountain; 1971 San Fernando; 1985 Coalinga; 1986 North Palm Springs; and 1987 Whittier Narrows. In this paper, we concentrate on results from the 1987 Whittier Narrows and 1989 Loma Prieta earthquakes.

1989 LOMA PRIETA AFTERSHOCKS AND MAINSHOCK

We see the influence of critical reflections most clearly in recordings of aftershocks of the Loma Prieta earthquake, because aftershocks have briefer source processes than the mainshock and therefore provide a clearer representation of wave propagation effects. On the left side of Figure 2, we show a profile of the east component of velocity recorded at stations northwest of the 1:30 am aftershock of November 5, 1989. The data are described by Mueller and Glassmoyer (1990); all of the recordings have absolute times, allowing them to be aligned in time with a travel time reduction of 3.5 km/sec. Superimposed on the profile are travel times for the direct S, Conrad

critical reflection (S_cS), and Moho critical reflection (S_mS). On the right side of Figure 2, we show a profile of synthetic seismograms for the San Francisco Peninsula (along an azimuth of 320°) generated by the reflectivity method.

Except at the closest recording station on the left side of Figure 2, the direct arrival has a small amplitude relative to later arrivals, and the first conspicuous phase has the arrival time of the critical Conrad reflection S_cS. The largest phase at all stations except the closest station occurs soon after the expected arrival time of the critical Moho reflection S_mS. These aftershock recordings indicate that at distances beyond about 50 km, the recorded peak ground motion amplitudes are controlled not by the direct S wave but by the wave that is critically reflected from the Moho. This interpretation is confirmed by the synthetic seismograms shown on the right side of Figure 2: beyond about 45 km, the largest amplitudes are associated with the Moho reflection. Analyses of other aftershocks show the same effects. The large motions that follow the Moho reflection in the recorded data suggest that there may be strong lateral variations in crustal structure along the propagation path.

Evidence of the influence of critical Moho reflections on the attenuation of strong ground motion from the mainshock was described by Somerville and Yoshimura (1990). We have updated that study using a detailed rupture model of the Loma Prieta earthquake derived by Wald *et al.* (1990). A record section of recorded accelerograms was compiled using all accelerograms to the north of the epicenter (i.e. in the San Francisco Bay region) that have known trigger time (Figure 3, left side). The recordings are from a variety of site conditions, as annotated in the figure and discussed further below, and are copies of film records published by Shakal *et al.* (1989) and Maley *et al.* (1989). On the right side of Figure 3, we show a profile of accelerograms simulated using the procedure described by Wald *et al.* (1988). The simulated accelerograms were generated using a crustal structure model having a surface shear wave velocity of 1 km/sec, appropriate for soft rock or stiff soil conditions.

At distances beyond 50 km, the onset of the largest accelerations at each station coincides with the arrival time of the critical Moho reflection S_mS in both the recorded and simulated accelerograms. The moveout of this onset with distance follows the S_mS arrival time curve and not that of direct S. The duration of strong motion following the S_mS arrival time curve is about 5 seconds, which is compatible with the 6-second duration of the source observed teleseismically (Nabelek, 1990; Kanamori and Satake, 1990). Both the recorded and synthetic accelerogram profiles suggest that, beyond about 50 km, the peak accelerations are associated not with the direct upgoing shear wave (S) but with the shear wave that has been critically reflected from the Moho (S_mS).

The average horizontal peak accelerations of the simulated accelerograms show a trend similar to that of the recorded accelerograms, as demonstrated in Figure 4(a). In this figure, the northerly profile of stations of Figure 3 has been augmented by stations that lie within 30 km of the epicenter. The peak accelerations attenuate normally to about 40 km, but then do not attenuate further until reaching an epicentral distance of 80 km. While site conditions are presumably responsible for the larger amount of scatter in recorded peak accelerations (compared with the simulated ones) at a given distance, it does not appear that site conditions explain the overall lack of attenuation between 40 and 80 km in both the recorded and simulated values. Instead, it appears that the shape of the attenuation curve is due to critical reflections, with the scatter of recorded peak values about this shape attributable in part to local site effects. The standard error of the simulations in predicting the observed response spectra is shown in Figure 5 for near-source and distant stations.

1987 WHITTIER NARROWS EARTHQUAKE

A northerly profile of strong motion recordings of the 1987 Whittier Narrows earthquake having absolute times was compiled (Figure 6, left side), and a corresponding profile of synthetic seismograms was generated using the reflectivity method (Figure 6, right side). As seen teleseismically, the Whittier Narrows earthquake had a brief but complex source function consisting of a small event followed one second later by a larger event (Bent and Helmberger, 1988). In the

distance range of zero to 20 km, the peak velocity is associated with the time of the direct S arrival from this later event in both the recorded and synthetic seismograms. However, beyond about 37 km, large arrivals also occur in the data at times corresponding to reflections from the lower crust (the mafic and Moho layers); the synthetic seismograms show that the Moho reflection becomes critical at about 70 km. For example, at Lancaster, which is at 70 km, the reflections from the lower crust produce significant ground motion amplitudes in both the recorded and synthetic seismograms. The amplitudes of the reflected arrivals increase with distance, until at Rosamond (at a distance of 86 km) the largest arrival has the time of the critical Moho reflection, and the amplitude of the direct arrival is relatively small. Thus ground motion amplitudes beyond the critical distance are controlled by critically reflected waves, causing the peak acceleration to have very gradual attenuation in the distance range of 50 to 90 km (Figure 4(b)).

An analysis of the attenuation of the entire set of strong motion recordings of the Whittier Narrows earthquake was made by Campbell (1988). His plots of residuals in peak acceleration for deep soil and hard rock are shown in the top and middle panels respectively of Figure 7. For both data sets, the residuals are predominantly negative in the distance range of 30 to 60 km, become zero on average at about 70 km, and are positive between 80 and 110 km. This indicates that the functional form that he used to model the attenuation of the Whittier Narrows data does not fit the data. The derived attenuation relation overpredicts the data by about one to two standard deviations in the distance range of 30 to 60 km, and underpredicts the data by a similar amount in the distance range of 80 to 110 km. This consistent with the expected effect of critical reflections on the attenuation of strong ground motion. A similar pattern of residuals was obtained for rock site recordings of the 1989 Loma Prieta earthquake (Boore et al., 1989), as shown in the lower panel of Figure 7. Here, the crossover from negative to positive residuals occurs at a closer distance (about 45 km compared with 70 km). This is what we would expect from the shallower depth of the Moho beneath the Loma Prieta earthquake (25 km) compared with the Whittier Narrows earthquake (32 km); the two events have comparable centroid depths of about 13 km. In both cases, the crossover distance corresponds to the critical distance for the Moho reflection.

SUMMARY OF EFFECTS ON GROUND MOTION ATTENUATION IN CALIFORNIA

We have analyzed profiles of accelerograms from five additional large California earthquakes. For the older events, the strong motion recordings did not have absolute time, and so it is more difficult to identify critical reflections in these recordings. Also, for the larger events, the source duration is sufficiently long that it obscures the individual phases that we are trying to identify. Nevertheless, we find evidence of critical reflections (in large, late wave arrivals that may be S_mS, and in the flattening of attenuation curves along specific profiles) in most of the events studied: the 1968 Borrego Mountain earthquake; the 1971 San Fernando earthquake; the 1983 Coalinga earthquake; and the 1986 North Palm Springs earthquake. This suggests that critical reflections may influence the attenuation of strong ground motion throughout California.

A contour map of crustal thickness in California is shown in Figure 8 (Mooney and Weaver, 1990). In the region of the San Andreas fault system extending from north of the Transverse Ranges to north of the San Francisco Bay area, the depth to the Moho is 25 +/- 1 km. In the region south of the Transverse Ranges, including almost all of southern California, the crustal thickness is 30 +/- 2 km. The relatively uniform crustal thickness in each of these regions, and the significant contrast in crustal thickness between them, suggests that there could be differences in ground motion attenuation between these two regions. Specifically, for a given focal depth, the effect of critical reflections should occur at closer distances and be larger in northern California than in southern California, as suggested by the residuals for the Loma Prieta and Whittier Narrows earthquakes discussed above. As a rule of thumb, we expect that the distance at which the attenuation curve for a given earthquake begins to flatten can be estimated from the critical distance of the S_mS phase, which can easily be calculated from the crustal structure and the focal depth of the earthquake.

REFERENCES

Bent, A.L. and D.V. Helmberger (1989). Source complexity of the 1 October 1987 Whittier Narrows earthquake, J. Geophys. Res. 94, 9548-9556.

Boore, D.M., L. Seekins and W. Joyner (1989). Peak accelerations from the 17 October 1989 Loma Prieta earthquake, Seismological Research Letters 60, 151-166.

Burger, R.W., P.G. Somerville, J.S. Barker, R.B. Herrmann, and D.V. Helmberger (1987). The Effect of Crustal Structure on Strong Ground Motion Attenuation Relations in Eastern North America, *Bull. Seism. Soc. Am., 77*, 420-439.

Campbell, K. (1988). The Whittier Narrows, California earthquake of October 1, 1997 - preliminary analysis of peak horizontal acceleration, Earthquake Spectra 4, 115-137.

Campbell, K. (1990). Preliminary Analysis of Strong Ground Motion from the October 18, 1989 Loma Prieta, California, Earthquake (abstract), *Seismological Research Letters, 61*, 30.

Kanamori, H. and K. Satake (1990). Broadband Study of the 1989 Loma Prieta Earthquake, *Geophysical Research Letters, 17*, 1179-1182.

Maley, R., A. Acosta, F. Ellis, E. Etheredge, L. Foote, D. Johnston, R. Porcella, M. Salsman, and J. Switzer (1989). U.S. Geological Survey Strong Motion Records from the Northern California (Loma Prieta) Earthquake of October 17, 1989, U.S.G.S. Open File Report 89-568.

Mueller, C. and G. Glassmoyer (1990). Digital recordings of aftershocks of the 17 October 1989 Loma Prieta, California earthquake, U.S.G.S. Open File Report 90-503.

Nabelek, J. (1990). Rupture Process of the October 18, 1989 Loma Prieta Earthquake from Broadband Teleseismic Body Waves, *Seismological Research Letters, 61*, 46.

Shakal, A., M. Huang, M. Reichle, C. Ventura, T. Cao, R. Sherburne, M. Savage, R. Darragh, and C. Peterson (1989). CSMIP Strong-Motion Records for the Santa Cruz Mountains (Loma Prieta), California Earthquake of 17 October 1989, Report No. OSMS 89-06, California Strong Motion Instrumentation Program.

Somerville, P. G., and J. Yoshimura (1990). The influence of critical Moho reflections on strong ground motions recorded in San Francisco and Oakland during the 1989 Loma Prieta earthquake, *Geophysical Research Letters, 17*, 1203-1206.

Somerville, P. G., J. P. McLaren, C. K. Saikia, and D. V. Helmberger (1990). The 25 November 1988 Saguenay, Quebec Earthquake: Source Parameters and the Attenuation of Strong Ground Motion, *Bull. Seism. Soc. Am., 80*, 1118-1143.

Somerville, P. G. and D. V. Helmberger (1990). The effect of crustal structure on the attenuation of strong ground motion in eastern North America, Proc. 4th U.S. National Conference on Earthquake Engineering, Earthquake Engineering Research Institute, 1, 385-394.

Wald, D. J., L. J. Burdick and P. G. Somerville (1988). Simulation of Acceleration Time Histories Close to Large Earthquakes, in Von Thun, J. L. (ed)., *Proceedings of the Earthquake Engineering and Soil Dynamics II Conference*, American Society of Civil Engineers, Geotechnical Special Publication No. 20, 430-444.

Walter, A. W. and W. D. Mooney (1982). Crustal Structure of the Diablo and Gabilan Ranges Central California: a Reinterpretation of Existing Data, *Bull. Seism. Soc. Am., 72*, 1567-1590.

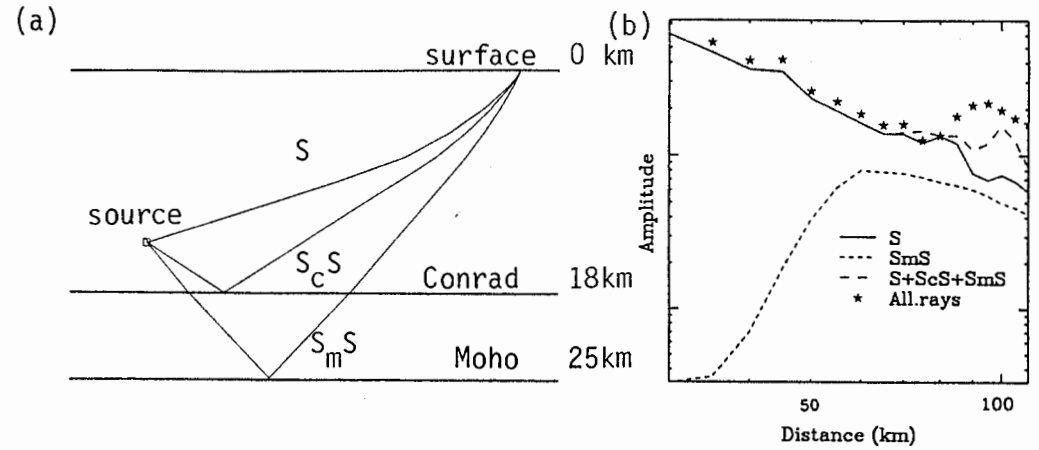

Figure 1. (a) Schematic model of wave propagation in central California showing the direct S wave and S waves reflected from the Conrad and Moho interfaces. (b) Schematic attenuation of individual rays in the wave propagation model shown in (a).

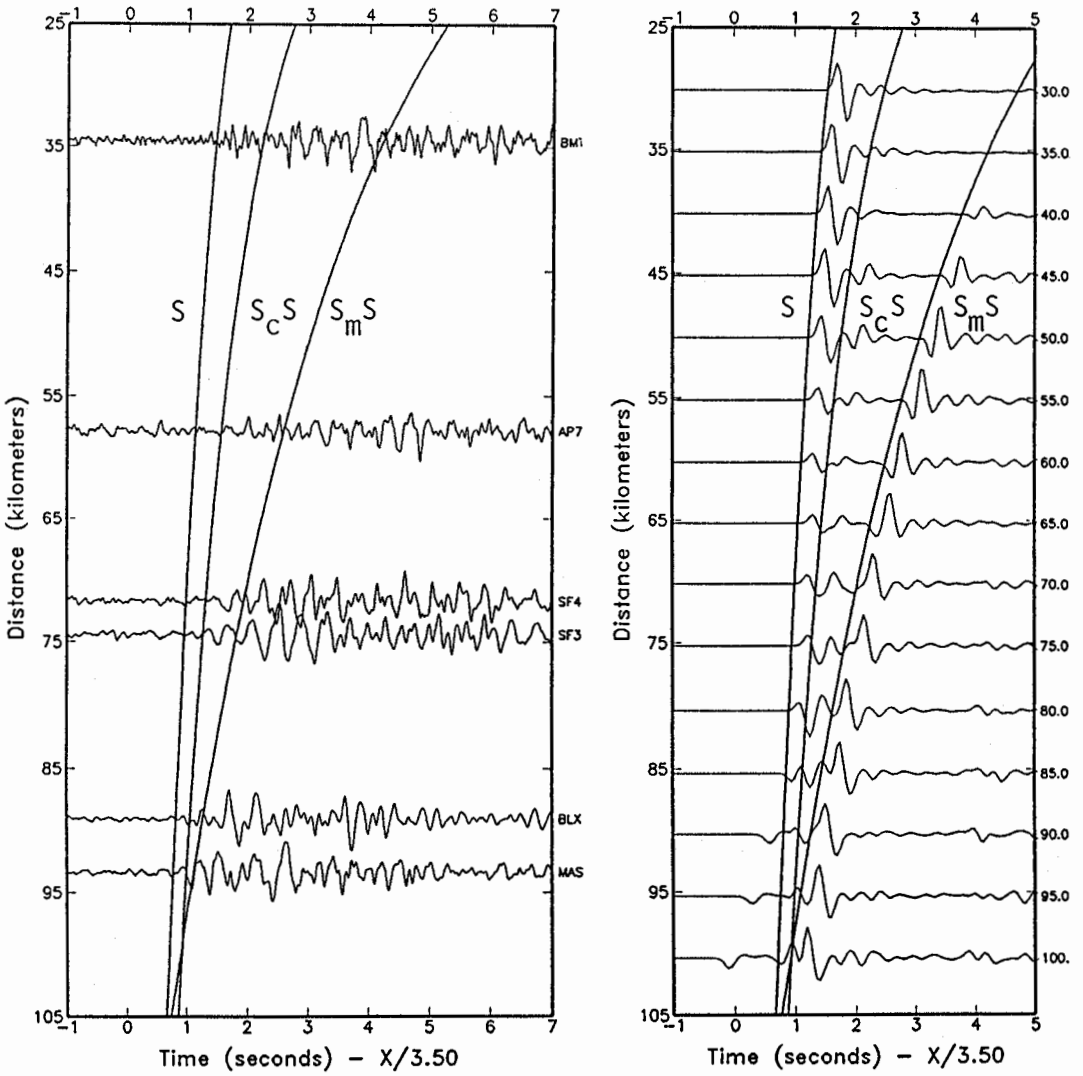

Figure 2. Profiles of recorded (left) and synthetic (right) tangential velocity of the 1:30 am, November 5 aftershock of the 1989 Loma Prieta earthquake, compiled using epicentral distance and a travel time reduction of 3.5 km/sec, and normalized to peak value. Travel time curves for the direct S, Conrad reflection (S_cS, 18 km depth) and Moho reflection (S_mS, 25 km depth) phases are shown. USGS station abbreviations are annotated on right side of traces.

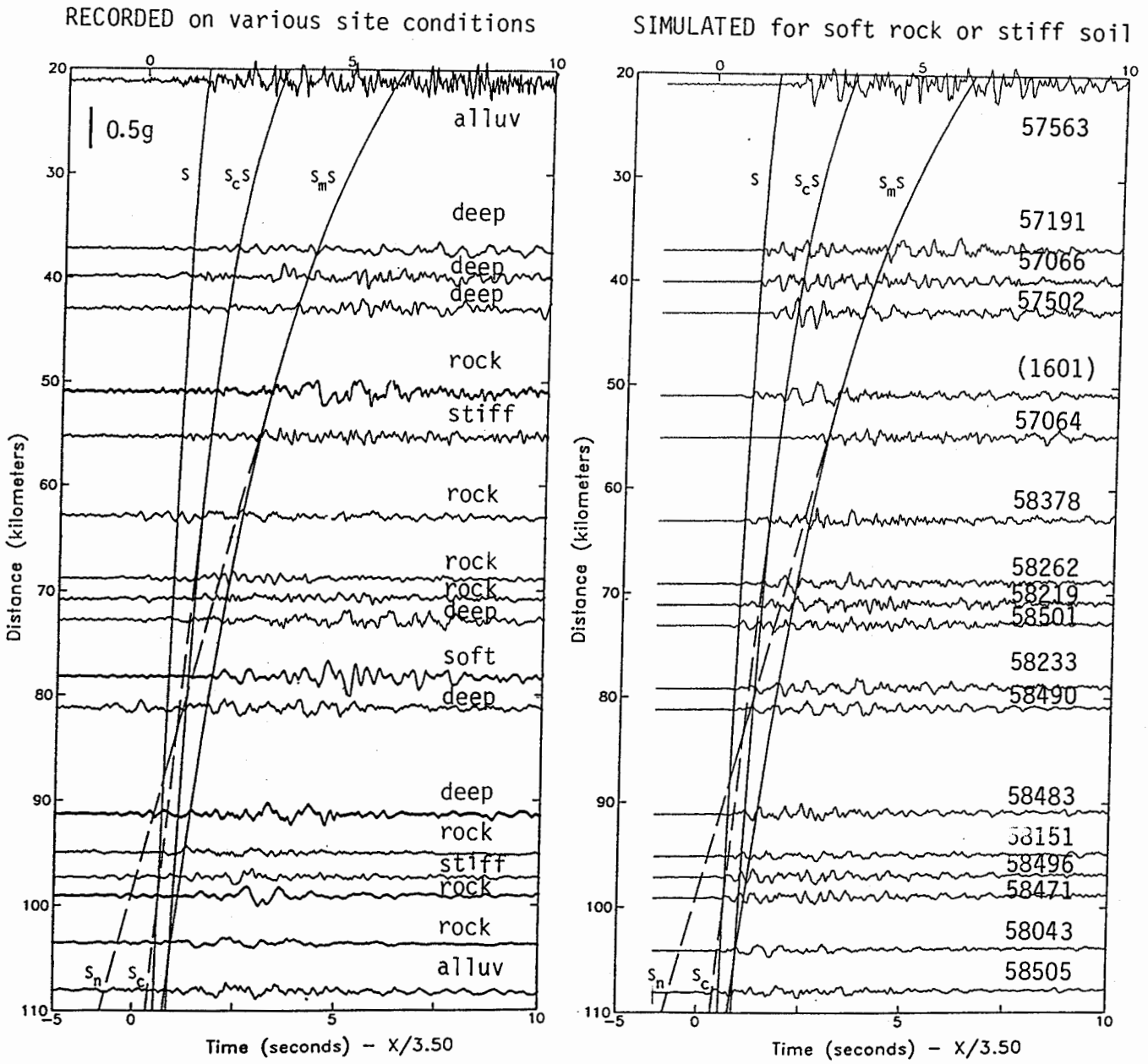

Figure 3. Profiles of recorded (left) and simulated (right) accelerograms of the 1989 Loma Prieta earthquake, compiled using epicentral distance and a travel time reduction of 3.5 km/sec, unnormalized. Travel time curves for the direct S, Conrad reflection (S_cS, 18 km depth) and Moho reflection (S_mS, 25 km depth) phases are shown. Soil conditions are annotated on recorded accelerograms, and CSMIP (and USGS in parentheses) station numbers are annotated on simulated accelerograms.

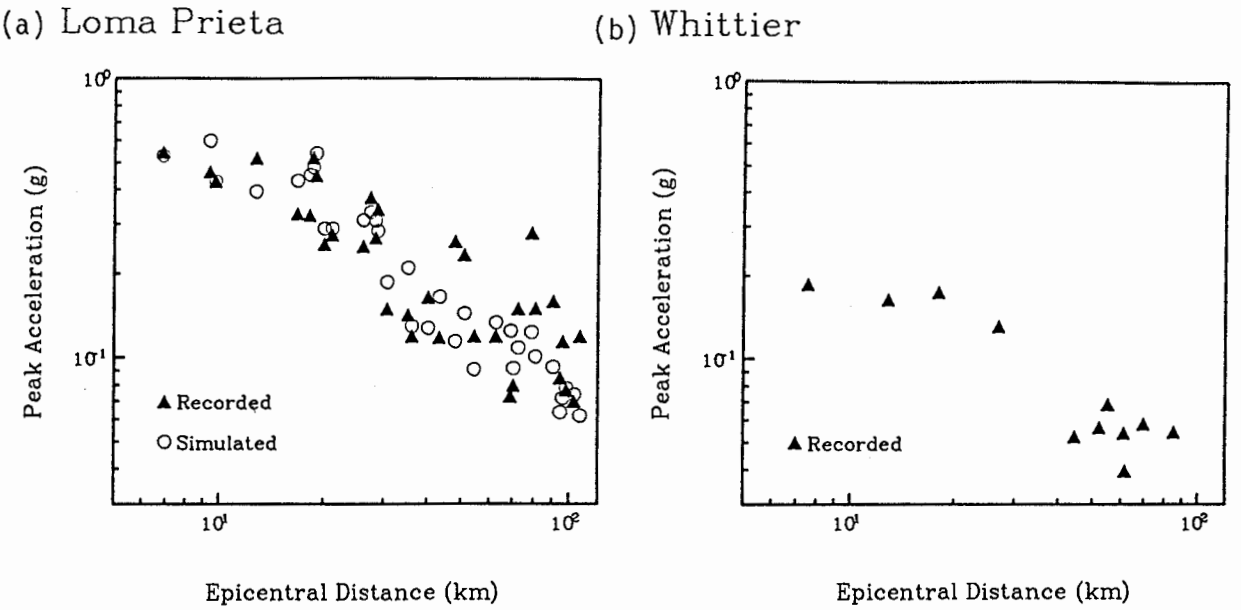

Figure 4. (a) Comparison of recorded and simulated peak accelerations as a function of distance from the Loma Prieta epicenter for recordings shown in Figure 3 and additional near-source recordings. (b) Peak tangential acceleration plotted as a function of distance from the Whittier Narrows earthquake for recording stations on the northerly profile shown in Figure 6.

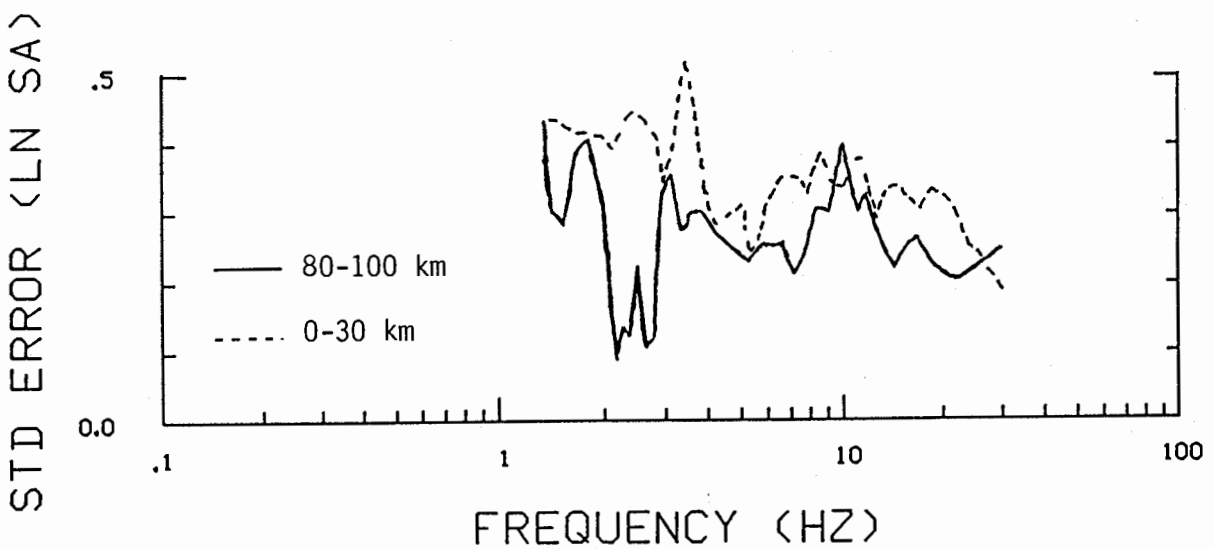

Figure 5. Natural logarithm of standard error of simulations in predicting the observed response spectrum of the Loma Prieta earthquake at near-source stations (dashed line) and at stations in San Francisco and Oakland (solid line).

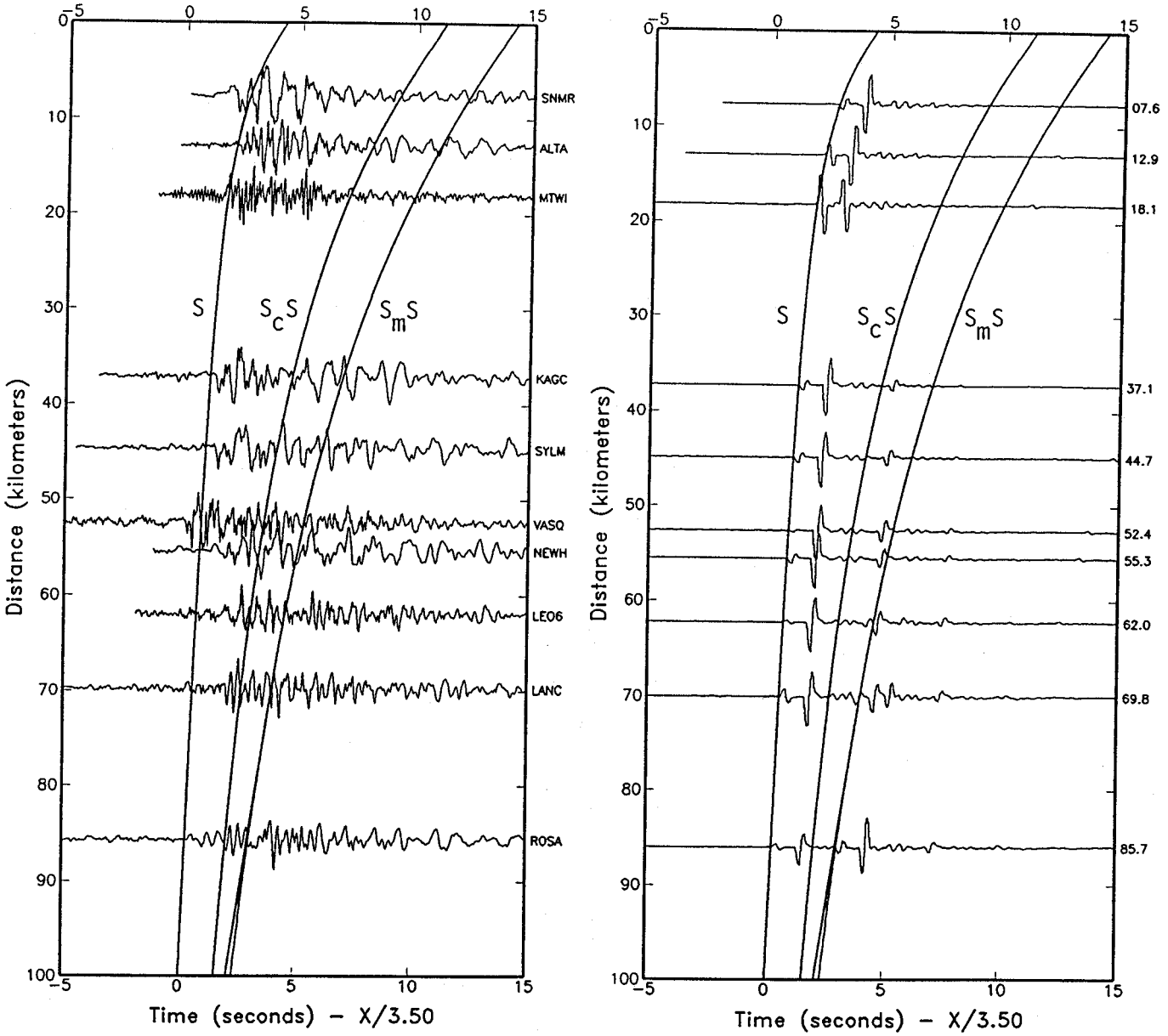

Figure 6. Profiles of recorded (left) and synthetic (right) tangential component ground velocity of the Whittier Narrows earthquake, compiled using epicentral distance and a travel time reduction of 3.5 km/sec, and normalized to the peak value. Travel time curves are shown for the direct S wave and waves reflected from the Conrad, mafic, and Moho interfaces.

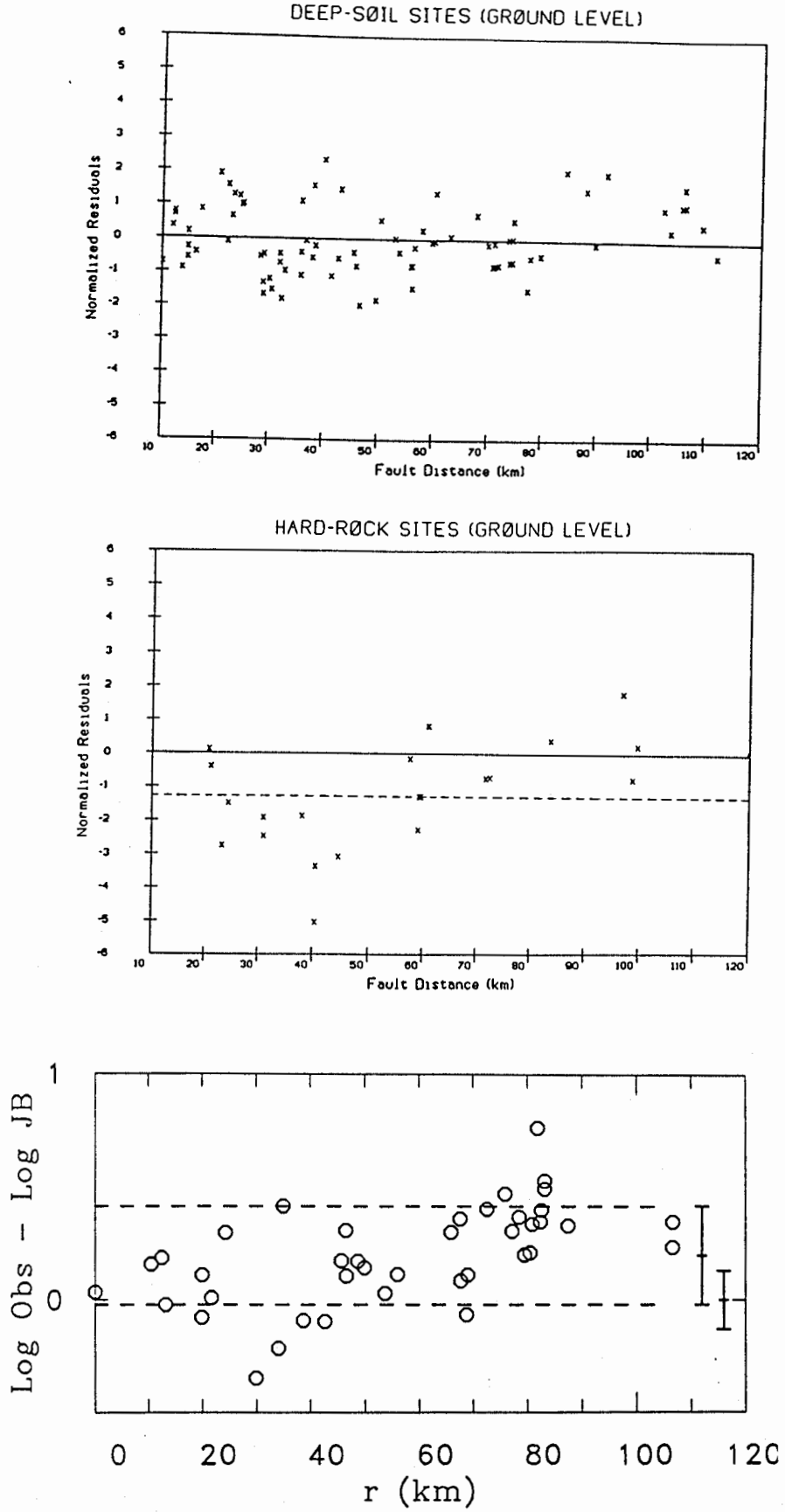

Figure 7. Top and Center: Residuals of recorded peak acceleration from the regression relations derived from deep soil and hard rock recordings of the 1987 Whittier Narrows earthquake, after Campbell (1988); Bottom: Residuals of peak acceleration from the regression relation of Joyner and Boore (1988) for rock site recordings of the 1989 Loma Prieta earthquake, after Boore et al. (1989).

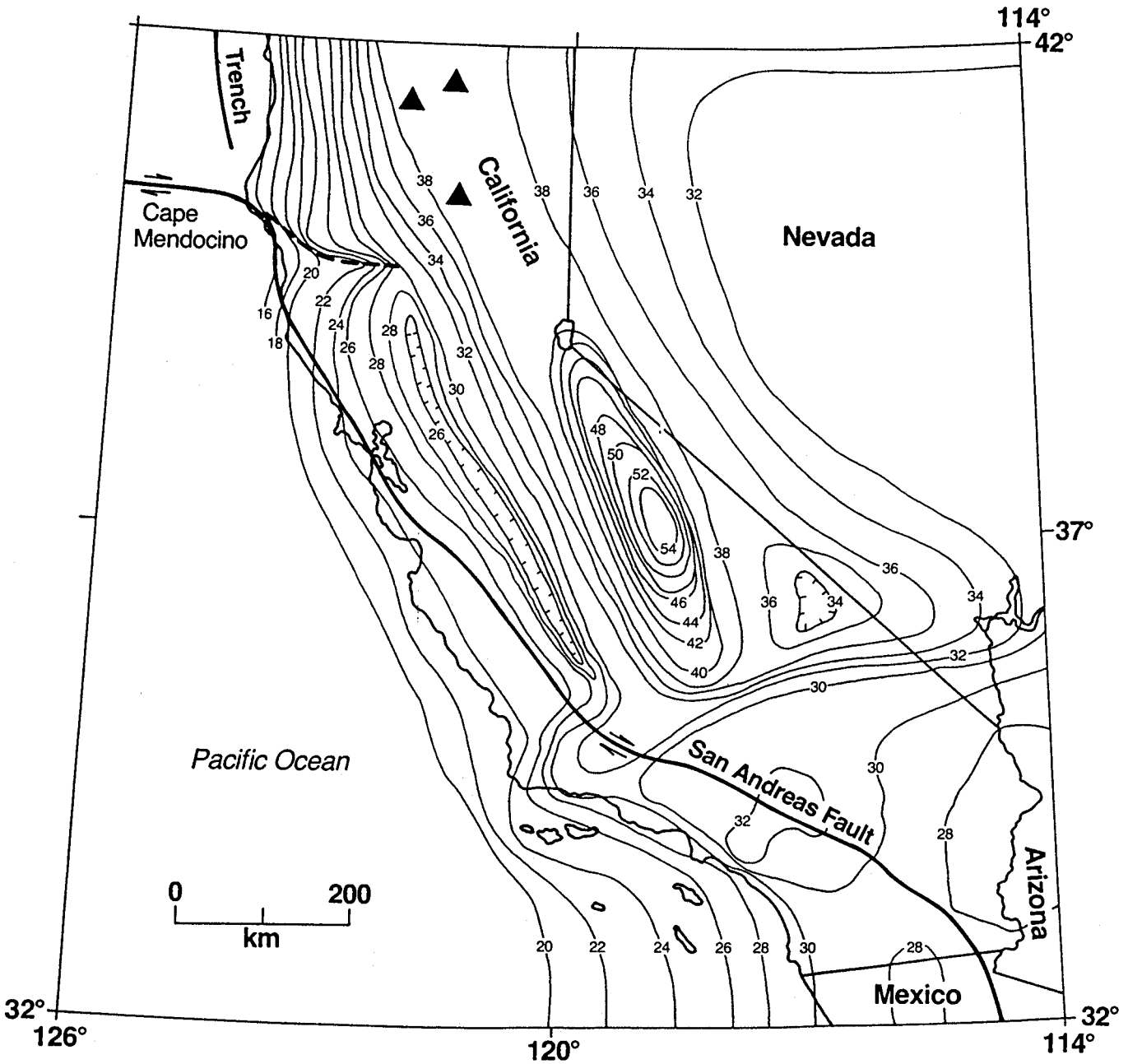

Figure 8. Contour map of crustal thickness (depth to Moho) for California. The thickness is 25 +/- 1 km in the San Francisco Bay region and 30 +/- 2 km in southern California. Source: Mooney and Weaver (1990).

Strong shaking directions from the 18 October 1989 Loma Prieta earthquake and aftershocks in San Francisco and Oakland

John E. Vidale
United States Geological Survey, Menlo Park

and

Ornella Bonamassa
University of California at Santa Cruz

Abstract

The direction of strong shaking observed at 13 California Division of Mining and Geology sites across San Francisco and Oakland at frequencies less than one Hz roughly agrees with a prediction calculated from the well-determined long-period focal mechanism. The directions of shaking at frequencies higher than one Hz, however, show little resemblance to the simple prediction, suggesting that the near-surface geology interacts with the higher frequency seismic waves in a complicated way. This interpretation is reinforced by the observation that aftershocks recorded at the CDMG sites show similar directional effects from earthquakes with a variety of mechanisms. This propagational complication suggests that the focal mechanism does not determine the direction of strongest shaking in an earthquake at this range of about 100 km at frequencies above about one Hz.

Introduction

The motion that an earthquake causes at the surface of the Earth is a combination of the details of the faulting at depth and the complications due to propagation through structures within the Earth of the seismic energy released by the faulting. Various ways of measuring the seismic source and propagational complications have been described. There exists considerable literature that documents the usefulness of the concept of a *site response*, where a particular site has a fixed set of frequencies which are amplified at that site no matter how the how the ground motion is induced (Joyner et al., 1976, Rogers et al., 1984, Borcherdt, 1970, Joyner et al., 1981). Seismic wave interaction with large-scale structures such as major sedimentary basins can be described deterministically; these structures can be shown to distort seismic waves in a semi-predictable way (Vidale and Helmberger, 1988, Kawase and Aki, 1989, Kagami et al., 1986). Bridging the gap between well-understood large-scale structures and fine structure where only the amplitude versus frequency behavior has been studied is the goal of considerable recent research.

This paper will concentrate on empirically quantifying the distortion to the direction of strongest shaking caused by earth structures, since it has been suggested that the direction of shaking is sometimes a feature of the recording site (a *directional site resonance*) rather than the earthquake (Vidale et al., 1991, Bonamassa et al., 1991, Bonamassa and Vidale, 1991). These and other observations of horizontal ground motion above one Hz frequency (Chouet, 1989, Abrahamson et al., 1989) show very small lateral correlation distances, less than 10's of meters for frequencies above a few Hz. Also, comparisons of seismograms written by surface and borehole instruments have shown that propagation through the shallowest 10's of meters of the Earth can severely distort seismic pulses (Haukkson et al., 1987, Malin et al., 1988, Aster and Shearer, 1991).

While the near-surface layers of the earth appear to scramble high-frequency waves, at long periods the Earth often affects seismic waves in a predictable way that may be stripped off to study the earthquake source. This paper focuses on finding the transition frequency where earth structure, and mainly near-surface geology, begin to obscure the signature of the seismic source at the range of 100 km. We will find a transition frequency near one Hz.

Data

The Loma Prieta earthquake of 18 October 1989, often and perhaps more appropriately called the Santa Cruz Mountains earthquake, was the largest to strike the San Francisco Bay area since 1906. It caused considerable damage and loss of life.

On the positive side, this earthquake was captured by more than a hundred strong motion seismometers, producing an unprecedented opportunity to investigate details of the earthquake and earthquake hazards in general. Numerous investigators are reconstructing the spatial and temporal patterns of fault movements during the 5 to 10 seconds it took for the earthquake to occur (Loma Prieta source references, 1990).

This paper will concentrate on observations of the effect of earth structure on the seismic waves radiated by the earthquake. To achieve this end, we examine the Loma Prieta mainshock records of 13 accelerometers located near San Francisco. The regional setting is shown in Figure 1. The seismometers are spread across San Francisco and Oakland, as shown in Figure 2. The station numbers, names, locations, and geologic settings are given in Table 1. These are all free-field, basement, or first floor installations, and all except station 480 are in two- or fewer story structures. The recordings, which were originally captured on film, have been digitized and disseminated by the California Strong Motion Instrumentation Project, managed by the California Division of Mines and Geology.

This data is well-suited for analysis of seismic wave propagation because of the large size of the Loma Prieta mainshock and the close spacing of the instrument sites relative to the distance to the earthquake. The large size of the earthquake

generated sufficient long-period seismic energy that ground motion at least down to 0.2 Hz (5 seconds period) were reliably measured by the strong motion instruments. Similar periods were recovered from the 1971 San Fernando earthquake, but fewer instruments were deployed at that time. The Whittier Narrows earthquake was recorded at a comparable number of stations, but strong motion recordings of the M_L 5.9 quake did not have recoverable energy at less that 0.5 Hz. This group of 13 stations lies within 20 km by 10 km area, but is 60 to 100 km from the fault plane that broke as estimated from aftershocks (Oppenheimer, 1990). Consequently, the stations only span about 10 to 15° in azimuth from the earthquake, and the signal that would be recorded across these stations would be similar in the absence of structural complications, particularly in their direction of shaking.

The similarity of the motions at long period shown below agrees with reflectivity simulation (Muller, 1985) with a simple source. The oblique thrust mechanism of the Loma Prieta earthquake produces a large pulse of shear wave energy on the transverse component, and little motion on the radial and vertical components of motion at this azimuth and range, which is close to directly along the San Andreas fault. A simple two-layer crust over Moho model was assumed in our calculation. A more complicated earthquake, extending ten's of kilometers, as the Loma Prieta event probably did (Loma Prieta source references) would produce more complicated radiation, but it still would maintain a similar, simple particle motion. The primary variation in particle motion across the array seen in Figure 3a is the rotation of the transverse direction of motion clockwise as one considers the stations progressively towards the east. The large transverse pulse, which can also be thought of as an incipient Love wave, dominates all stations, and would appear for all frequencies considered in this paper.

The observed ground motions show some resemblance to the prediction of the reflectivity simulation. Figure 3 shows the particle motion directions seen in the acceleration records in four different passbands. Comparison of the synthetic particle motion directions with the observed directions shows a simple and unambiguous pattern: The directions of strongest motions at frequencies less than one Hz shown in Figure 3a (as well as the passbands 0.1 to 0.2 and 0.2 to 0.4 Hz, which are not shown) generally agree with the direction expected from the simulation and the directions at frequencies above one Hz shown in Figures 3b, c and d show directions of shaking that bear little relation to the direction expected.

Aftershock recordings at the CDMG sites allow us to check whether the deviations from the particle motion predicted from the mechanism are repeatable and perhaps predictable, as the examples appeared to be in Vidale and Bonamassa (1991) and Bonamassa et al. (1991). The USGS deployed GEOS aftershock recorders at 18 CDMG sites, allowing us to compare strong and weak particle motions. We present only a comparison of the mainshock with one aftershock at station 131 in Figure 4. This aftershock is located underneath the peninsula, and thus has quite a different path and angle of incidence to the station than the mainshock. The primary direction of motion in each passband is similar, and the directions of the largest motions are in

various directions. The results suggest that the polarization features seen in Figure 3 are persistent. We also draw a similar conclusion from examination of 5 more aftershocks and one additional station, but space limitations preclude presentation of that data here.

Some caveats must be noted. Time domain information has been suppressed in this presentation, so it remains possible that the initial S wave arrivals exhibit the polarization direction expected from the focal mechanism even at high frequencies as has been observed by Bonamassa and Vidale (1991) and has also been observed for P waves by Menke (199?). Individual stations may record bizarre phenomenon; for example, Treasure Island (Station 117) underwent liquefaction near the CDMG site, Cliff House (Station 132) is situated on steep topography (Borcherdt, 1990), Oakland (Station 472) is located on a wharf that may be subject to water waves in the bay, and Oakland (Station 480) is placed in the basement of an 18-story building that may sway. Despite these potential outliers, the pattern is quite consistent across the array of strong motion stations.

Conclusions and Unanswered Questions

This relatively dense array of strong motion stations has provided one of the best fairly broadband (0.1 to 5.0 Hz) glimpses to date of the seismic wavefield generated by a large earthquake less than 100 km distant. The transition from particle motion that indicates source character to particle motion that is strongly affected by propagation through the Earth clearly takes place around 1 Hz. This highly variable high-frequency polarization is consistent with most previous studies; Vidale et al. (1991) and Bonamassa and Vidale (1991) see similar gross distortion of the 2 to 20 Hz seismic waves, probably caused by near-surface geology. As mentioned above, comparisons of seismic waves recorded on the surface and in boreholes have documented the scrambling effects of the near-surface (Aster and Shearer, 1991, Haukkson et al., 1987).

The coherence below 1 Hz is also consistent with previous work. Trifunac (1988) showed that the 0.5 to 1.0 Hz seismic waves generated by the Whittier Narrows earthquake were fairly coherent. Helmberger and Liu (1985) have done a similar exercise at a closer range of 5 to 20 km, with a comparable transition from source to structural domination of two Hz. Innumerable local, regional, and teleseismic earthquake source inversions have invariably proceeded on the assumption that seismic waves interact with Earth structure that is a stack of layers in the most complicated case, and source studies often interpret seismic energy up to frequencies near 1 Hz as indicating details of rupture propagation.

In contrast, Ebel (1988) finds that the 10 Hz particle motions of small earthquakes sometimes do reflect the focal mechanism. His study is in the stable craton in Germany, however, so perhaps the confounding effect of the near surface is strongest in active tectonic regions like California, where all the other cited works were sited.

The question that remains is: What geologic structures scramble the high-frequency polarization characteristics? The low spatial coherence suggests shallow structure, the borehole studies suggest shallow structure, and to the extent that common sense applies, the observation that the near surface is the least consolidated and most highly variable volume along the seismic ray path suggests that the structure lie near the surface. Candidates for these near surface structures include surface topography (Bard and Gariel, 1986, Kawase and Aki, 1989) and topography on the soil rock interface (Bard and Tucker, 1985). Candidate for wave interactions include focusing through seismic velocity gradients acting as lens (Rial, 1989, Langston and Lee, 1983), body-wave to surface-wave conversions at sharp, laterally heterogeneous velocity contrasts (Bard and Gariel, 1986, Vidale and Helmberger, 1988, Kawase and Aki, 1989), energy that becomes trapped and reverberates between high contrast interfaces (Novaro et al., 1990).

The task remaining is the construction of simulations with methods like three-dimensional finite differences (Frankel *et al.*, 1990) that reproduce to complexity we observe in the seismic wavefield using realistic velocity models. This task also relies on the equally difficult chore of accurately estimating realistic three-dimensional velocity models of the near surface.

It is important to learn the processes affecting high-frequency seismic waves for earthquake hazard mitigation, earthquake source determination, and seismic array design goals. So far, our 3-D site characterization is empirical, not based on an understanding of the physics involved. Clearly, optimal high frequency seismic arrays that aim to study seismic sources will minimize the interference from earth structures. Earthquake source inversions must allow sufficient variance in the solutions to withstand the randomization of the high-frequency waves by structure. Finally, site characterization for seismic hazard mitigation might become a more precise science when phase as well as amplitude information is incorporated into predictions of shaking in future earthquakes.

Table 1 - Location of thirteen CSMIP stations used

Name	Location	Near-surface geology
043	Point Bonita	2 m of broken rock, sandstone
117	Treasure Island	Fill
130	SF - Diamond Heights	Franciscan chert
131	SF - Pacific Heights	Franciscan sandstone, shale
132	SF - Cliff House	Franciscan sandstone, shale
151	SF - Rincon Hill	Franciscan sandstone, shale
163	Yerba Buena Island	Franciscan sandstone
222	SF - Presidio	Serpentine
224	Oakland - 2-story building	Alluvium
338	Piedmont - Jr. High	Weathered serpentine
471	Berkeley - LBL	Thin alluv. on shale, siltstone

472	Oakland - outer harbor wharf	Bay mud
480	Oakland - 18 story bldg.	Fill over bay mud

Table 2 - The aftershock presented

Origin time	Lat.	Long.	Depth	Mag.
301 8:35	37° 42'	-122° 33'	9.6 km	2.5

References

Abrahamson, N.A., J.F. Schneider, and J.C. Stepp, 1989. Spatial Coherency of strong ground motion for application to soil structure interaction, *Seism. Res. Lett.*, **60**, 3.

Aster, R., and P. Shearer, 1991. High-frequency seismic polarizations and site effects observed in boreholes in the San Jacinto fault zone, southern California, submitted to *Bull. Seism. Soc. Am.*.

Bard, P.-Y., and J.C. Gariel, 1986. The seismic response of two-dimensional sedimentary deposits with large vertical velocity gradients, *Bull. Seism. Soc. Am.*, **76**, 343-360.

Bard, P.-Y., and B.E. Tucker, 1985. Underground and ridge site effects: A comparison of observation and theory, *Bull. Seism. Soc. Am.*, **75**, 905-923.

Bonamassa, O., J.E. Vidale, H. Houston, and S.Y. Schwartz. Directional site resonances and the strong influence of near-surface geology on ground motion, submitted to *Geophys. Res. Lett.*.

Bonamassa, O., J.E. Vidale, 1991. Observations of directional site resonances from the Loma Prieta earthquake sequence, submitted to *Bull. Seism. Soc. Am...*

Borcherdt, R.D., 1970. Effects of local geology on ground motion near San Francisco Bay, *Bull. Seism. Soc. Am.*, **60**, 29-61.

Borcherdt, R.D., 1990. Influence of local geology in the San Francisco bay region, California on ground motions generated by the Loma Prieta earthquake of October 17, 1989, Proceedings of the International Symposium on Safety of Urban Life and Facilities, November, Tokyo, Japan.

Dietel, C., B. Chouet, K. Aki, V. Ferrazzi, P. Roberts, and R.Y. Koyanagi, 1989. Data summary for dense GEOS array observations of seismic activity associated with magma transport at Kilauea Volcano, Hawaii, Open File Report, US Geological Society, 171 p.

Ebel, J.E., 1988. Moment tensor inversion of small earthquakes in southwestern Germany for the fault plane solution, *Geophys. J. Int.*, **101**, 133-146.

Andrews, D.J., 1986. Objective determination of source parameters and similarity of earthquakes of different size, *Earthquake Source Mechanics*, AGU monograph **37**, Das, Boatwright, and Scholtz, ed., 259-267.

Frankel, A., S. Hough, P. Friberg, R. Busby, 1990. Analysis and modeling of waveforms of Loma Prieta aftershocks recorded on a dense array in Sunnyvale, California, *Eos*, **71**, 1456.

Haukkson, E., T.-L. Teng, T.L. Henyey, 1987. Results from a 1500 m deep, three-level downhole seismometer array, *Bull. Seism. Soc. Am.*, **77**, 1883-1904.

Joyner, W.B., R.E. Warrick, T.E. Fumal, 1981. The effect of Quaternary alluvium on strong ground motion in the Coyote Lake, California, earthquake of 1979, *Bull. Seism. Soc. Am.*, **71**, 1333-1351.

Joyner, W.B., R.E. Warrick, and A.A. Oliver, III, 1976. Analysis of seismograms from a downhole array in sediments near San Francisco Bay, *Bull. Seism. Soc. Am.*, **66**, 937-958.

Kagami, H., S. Okada, K. Shiono, M. Oner, M. Dravinski, and A.K. Mal, 1986. Observation of 1-5 second microtremors and their application to earthquake engineering. Part III. A two-dimensional study of site effects in the San Fernando Valley, *Bull. Seism. Soc. Am.*, **76**, 1801-1812.

Kawase, H. and K. Aki, 1989. A study on the response of a soft basin for incident S, P, and Rayleigh waves with special reference to the long duration observed in Mexico City, *Bull. Seism. Soc. Am.*, **79**, 1361-1382.

Langston, C.A., and J. Lee, 1983. Effect of structure geometry on strong ground motions; the Duwamish river valley, Seattle, Washington, *Bull. Seism. Soc. Am.*, **73**, 1851-1863.

Liu, H.L., and D.V. Helmberger, 1985. The 23:19 aftershock of the 15 October 1979 Imperial Valley earthquake: More evidence for an asperity, *Bull. Seism. Soc. Am.*, **75**, 689-709.

Loma Prieta source references, 1990. More than 50 papers and abstracts in Special Sections of *Geophys. Res. Lett.*, **17**, *Seism. Res. Lett.*, **61**, and *Eos*, **71**.

Malin, P.E., J.A. Waller, R.D. Borcherdt, E. Cranswick, E.G. Jensen, and N. Van Schaak, 1988. Vertical seismic profiling of Oroville microearthquakes: velocity spectra and particle motion as a function of depth, *Bull. Seism. Soc. Am.*, **78**, 401-420.

Menke, W., and A.Lerner-Lam, 1991. The transition from linear to complex polarization in regional compressive waves, in press in *Bull. Seism. Soc. Am.*.

Muller, G., 1985. The reflectivity method: A tutorial, *J. Geophys.*, **58**, 153-174.

Novaro, O., T.H. Seligman, J.M. Alvarez-Tostado, J.L. Mateos, and J. Flores, 1990. Two-dimensional model for site effect studies of microtremors in the San Fernando Valley, *Bull. Seism. Soc. Am.*, **80**, 239-252.

Oppenheimer, D.H., 1990. Aftershock slip behavior of the 1989 Loma Prieta, California earthquake, *Geophys. Res. Lett.*, **17**, 1199-1202.

Rial, J.A., 1989. Seismic wave resonance in 3-D sedimentary basins, *Geophys. J. Roy astr. Soc.*, **99**, 81-90.

Rogers, A.M., R.D. Borcherdt, P.A. Covington and D.M. Perkins (1984). A comparative ground response study near Los Angeles using recordings of Nevada nuclear tests and the 1971 San Fernando earthquake, *Bull. Seism. Soc. Am.*, **74**, 1925-1949.

Trifunac, M.D., 1988. The Whittier Narrows, California earthquake of October 1, 1987 - Note on peak accelerations during the 1 and 4 October earthquakes, *Spectra*, **4**, 101-113.

Vidale, J.E., 1989. Influence of focal mechanism on peak accelerations for the Whittier Narrows, Ca. earthquake and an aftershock, *J. Geophys. Res.*, **94**, 9607-9615.

Vidale, J.E., O. Bonamassa, and H. Houston. Directional Site Resonances Observed from the 1 October 1987 Whittier Narrows Earthquake and the 4 October Aftershock, to appear in February, 1991 issue of *Earthquake Spectra*.

Vidale, J.E., and D.V. Helmberger, 1988. Elastic finite-difference modeling of the 1971 San Fernando, Ca. earthquake, *Bull. Seism. Soc. Am.*, **78**, 122-142.

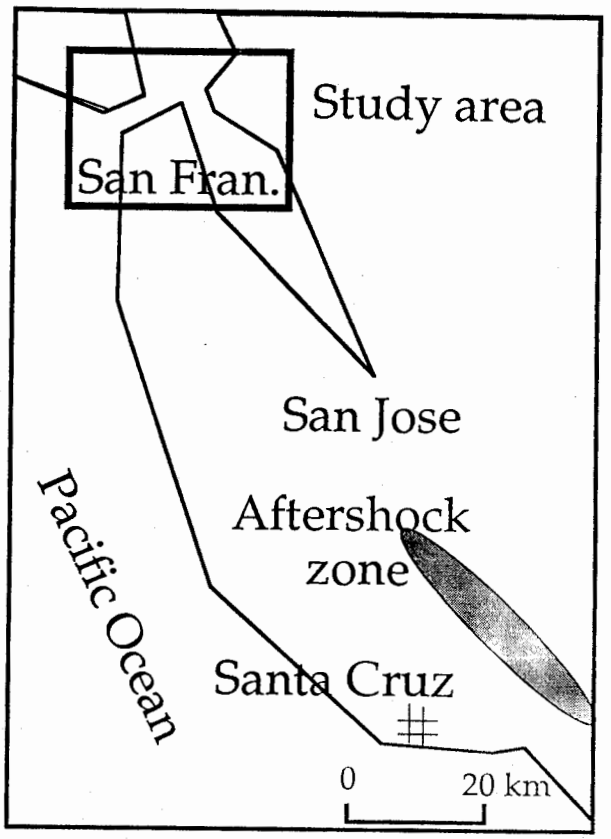

Figure 1. Location of the area of this study in relation to the aftershock zone of the 18 October 1989 earthquake. This study area is shown in more detail in Figure 2.

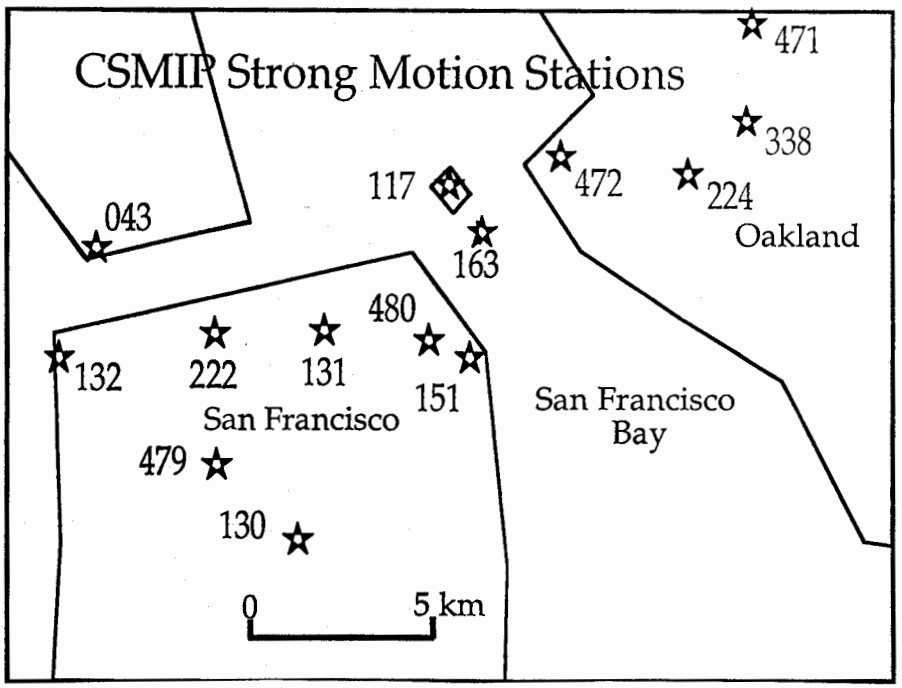

Figure 2. Location of the 13 California Strong Motion Instrumentation Program stations whose recordings are used in this paper. The name and surficial geology of each station are given in Table 1.

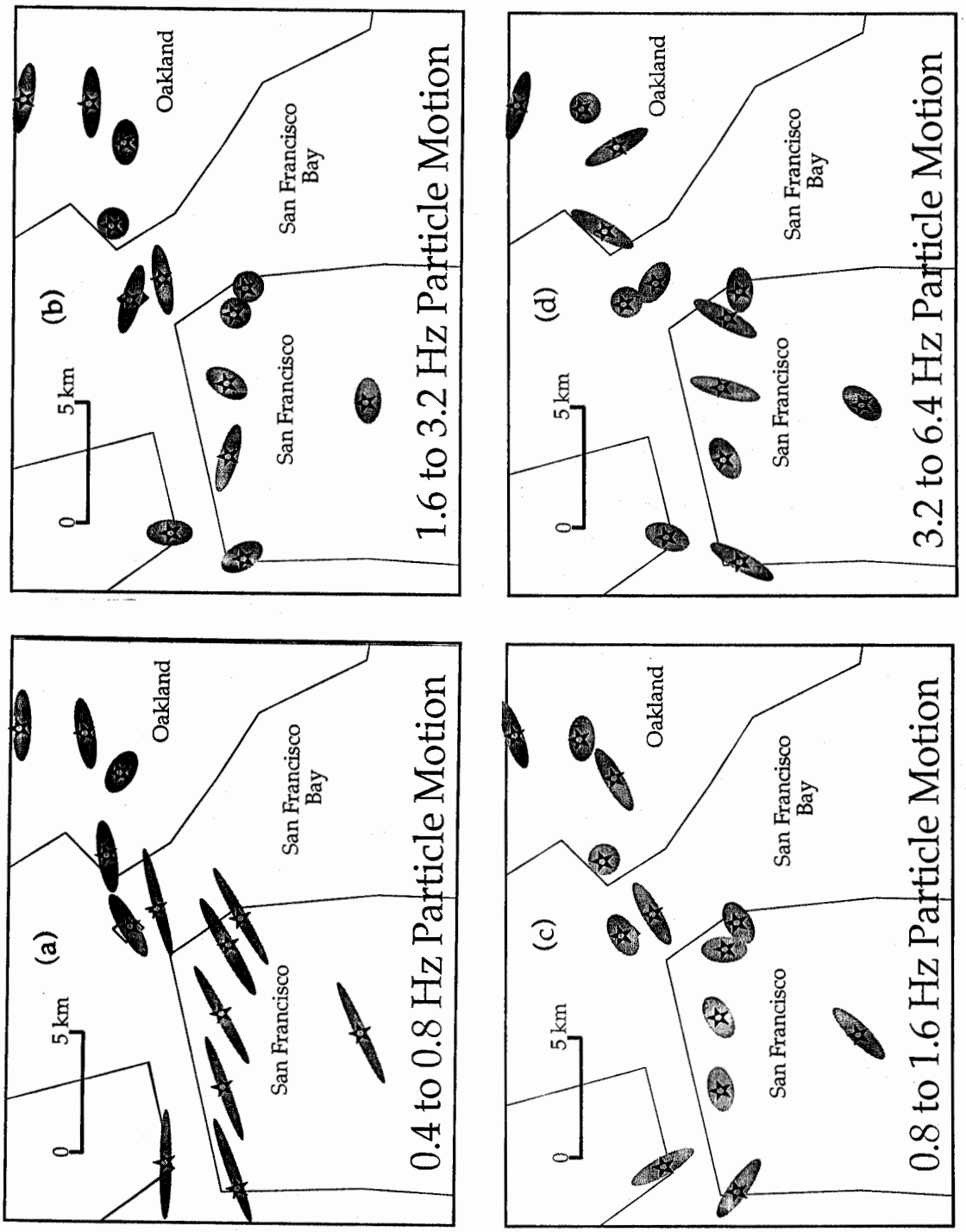

Figure 3. Particle motion diagrams for observations of the 13 stations listed in Table 1 of the 18 October 1989 Loma Prieta earthquake: (a) In the passband from 0.4 to 0.8 Hz (1.25 to 2.5 second period). (b) In the passband from 0.8 to 1.6 Hz. (c) In the passband from 1.6 to 3.2 Hz. (d) In the passband from 3.2 to 6.4 Hz. Two passes of a three pole Butterworth filter were applied.

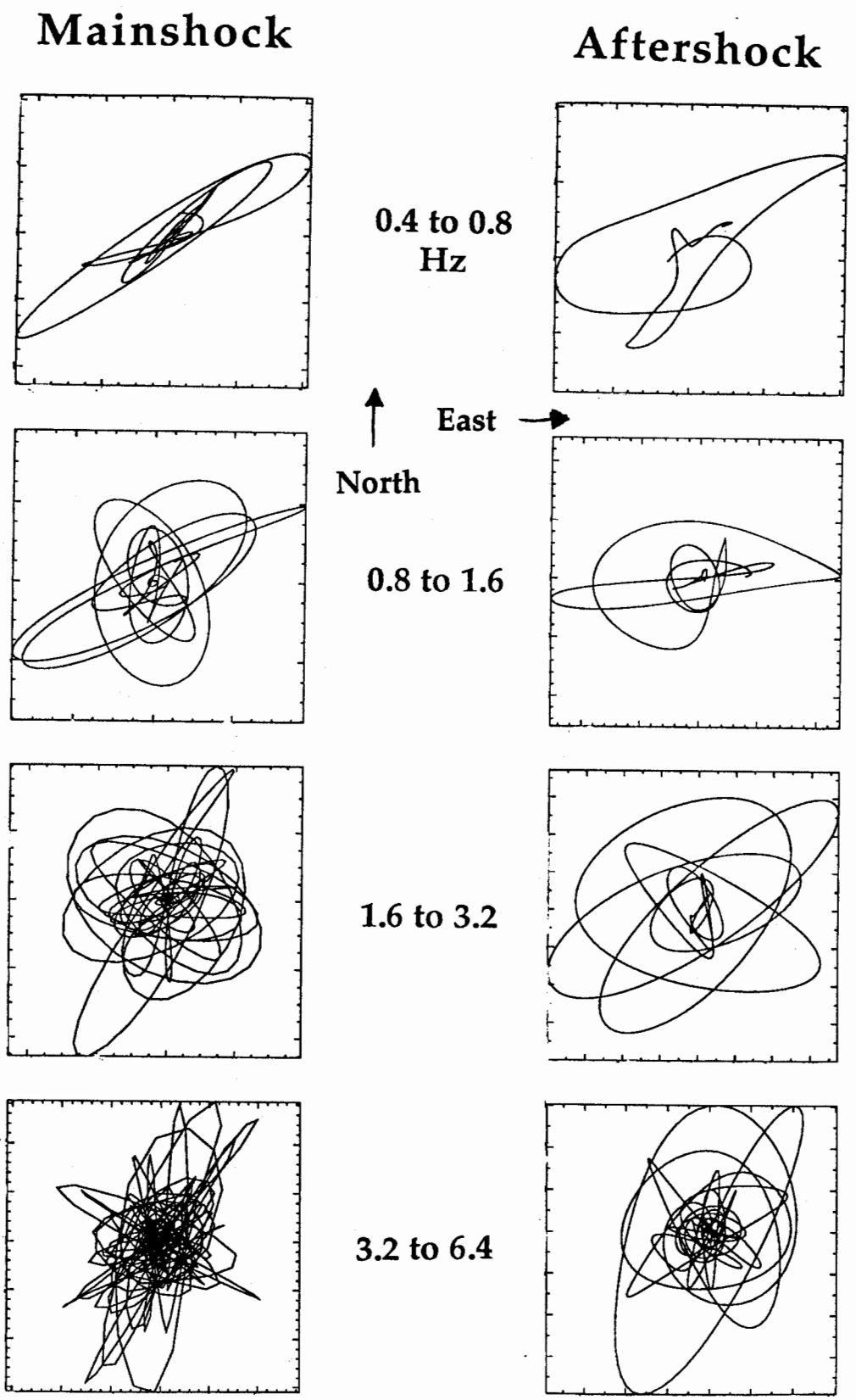

Figure 4. Comparison of weak and strong motions for mainshock and aftershock (Table 2) for all passbands at station 131.

EVALUATION OF STRUCTURAL RESPONSE FACTORS USING GROUND MOTIONS RECORDED DURING THE LOMA PRIETA EARTHQUAKE

Eduardo Miranda
Research Engineer, Earthquake Engineering Research Center
University of California at Berkeley

Vitelmo V. Bertero
Professor, Earthquake Engineering Research Center
University of California at Berkeley

ABSTRACT

Present procedures of defining seismic design forces are based on the use of elastic spectra reduced by a response modification factor which only depends on the type of structural system. This paper summarizes the results of an analytical study concerning strength reduction factors. Strength demand and strength reduction spectra were computed using simplified elastic and inelastic bilinear SDOF structural models and 36 ground motions recorded during the 1989 Loma Prieta earthquake. Special emphasis was given to the influence of local site conditions. Results show that strength reduction factors are significantly affected by the level of inelastic deformation, the period of vibration and by local site conditions.

INTRODUCTION

While current building codes accept structural damage in the event of a major earthquake, the estimated loss of 10 billion dollars produced by the 1989 Loma Prieta earthquake was not expected and was beyond what could be considered as an acceptable damage during moderate earthquake ground motions.

The procedure now commonly used is to design for lateral forces that are obtained from reducing a Smoothed Linear Elastic Design Response Spectra, SLEDRS by a force reduction factor referred as either a response modification factor, R, in the National Earthquake Hazard Reduction Program (NEHRP) [1] and the Applied Technology Council (ATC) [2] design recommendations, or as a system performance factor, R_w, in the 1988 Uniform Building Code [3]. There is no rational procedure from which the recommended factors have been derived and, as presently specified, they are empirical and only dependent on the type of structural system, thus, assuming that force reductions are the same regardless of the period of vibration or the local site conditions. By using this procedure combined with present methods of allowable stress design used in steel structures and of the method referred as strength method used in reinforced concrete structures codes may lead to conservative or unconservative design for the maximum credible event, depending on the type of structure (i.e. the response modification factor that is used).

While the rational way to design should be based on the use of Smoothed Inelastic Design Response Spectra, SIDRS, derived from statistical studies of inelastic response spectra of all possible critical earthquake ground motions that might occur at the structure site, at present, most of the practicing structural engineers are not familiar with the derivation and use of such SIDRS. Most designers prefer to obtain the seismic design forces through the use of SLEDRS and the use of response modification factors. Therefore based on the information that has been gathered from recent

earthquakes, it is of primary importance to be able to specify more reliable SLEDRS and to derive more reliable values for the response modification factors.

Previous studies have investigated strength reductions due nonlinear behavior, however, the effect of local soil conditions has not been taken into account or the study has been limited to only one type of soil conditions [4,5,6]. The main objective of this investigation is to improve the understanding of strength reduction factors through the use of ground motions recorded during the 1989 Loma Prieta earthquake and simplified elastic and inelastic bilinear single-degree-of-freedom, SDOF, structural models.

STATISTICAL STUDY ON THE RESPONSE OF SDOF SYSTEMS

Selected Ground Motions: A total of 36 ground motions recorded during the October 17, 1989 Loma Prieta earthquake. The selected ground motions are listed in Table 1. They were obtained at recording stations with epicentral distances between 7 and 100 km and site conditions and geologic conditions that range from rock to soft clayey soils (bay mud). Additionally, strong ground motions recorded in previous earthquakes were used to compare the results to those obtained using Loma Prieta data. The following records were used for this purpose: El Centro (1940 Imperial Valley), Taft (1952 Kern County), Sendai (1978 Miyagi-Ken-Oki), James Road (1979 Imperial Valley), Llolleo (1985 Chile), SCT (1985 Mexico), San Salvador (1986 El Salvador), and Colonia Roma (1989 Acapulco, Mexico). The ground motions were classified into three groups according to the geologic conditions at the recording station. These groups were rock, alluvium and very soft soil.

Results from the Statistical Study: Constant ductility nonlinear spectra were computed for all records in each soil group. Strength demands for each record were then normalized using peak ground acceleration (PGA). Details on the procedure used to compute the constant ductility nonlinear spectra can be found in Ref.7. For ground motions recorded on rock or alluvium sites, nonlinear spectra were computed for a fixed set of 50 periods between 0.05 and 3.0 seconds. In the case of ground motions recorded on very soft soil, spectra were computed for a fixed set of 50 ratios of T/T_g, where T_g is the predominant period of the ground. The reason for using T/T_g instead of T is that T_g can have large variations depending on the shear wave velocity of the soil and the depth of the soft deposits. For statistical analyses of spectra it makes no sense to average spectral ordinates at a certain period for ground motions with significantly different predominant periods. For structural design purposes, it is important to characterize the seismic demands on structures with periods shorter, longer or near the predominant period.

In this study the predominant period was computed as the period corresponding to the maximum spectral velocity ordinate. It can be shown that essentially the same predominant period would be obtained if the Fourier amplitude spectrum or the input energy spectrum are used instead of the velocity spectrum because of the relationship between these three spectra.

Computation of constant ductility response spectra involves iteration on the yielding strength of the system. The iteration is successful when the computed ductility reaches the specified (target) ductility within a certain tolerance that can be specified by the user. In this study, ductilities were considered satisfactory if they were within 1% of the target ductility. The displacement ductility ratio is defined as the ratio of the maximum absolute value of the displacement response divided by the yield displacement of the system,

$$\mu = \frac{u_{max.}}{u_y} \tag{1}$$

The following values of ductility were selected for this study: 1 (elastic), 2, 3, 4, 5 and 6. Details on the procedure used to compute the constant ductility nonlinear spectra can be found in Ref.7. Due to the large computational effort involved in calculating constant ductility nonlinear spectra, the study was limited to bilinear systems with a post-elastic stiffness of 3% of the elastic stiffness and with a damping ratio of 5% of critical.

Inelastic strength demand spectra normalized with respect to the maximum ground acceleration ($\eta = C_y/\ddot{x}_{g_{max}} / g$) for the six ground motions representative of all three site conditions are presented in Figure 1. As shown in this figure, spectral shapes for inelastic strength demands differ significantly from elastic (μ=1) spectral shapes. For soft soil records (SCT and Emeryville) and periods smaller than the predominant period of the site there is a small difference between the strength demands for ductilities between 2 and 6. This implies that small changes in the strength of yielding structures in this period range may produce large changes in ductility demands.

The strength reduction factor in a SDOF system undergoing a certain displacement ductility μ_i, is defined as

$$R_\mu = \frac{C_y(\mu=1)}{C_y(\mu=\mu_i)} \tag{2}$$

where $C_y(\mu=1)$ is the strength demand on a linear elastic system (i.e. the strength required to maintain the system elastic) and $C_y(\mu=\mu_i)$ is the strength demand on a nonlinear system undergoing a displacement ductility μ_i.

Computed strength reduction factors of six ground motions are shown in Figure 2. For each ground motion, reduction factors are plotted for displacements ductilities of 6, 5, 4, 3, and 2 (from top to bottom). Examples of predominant period of 4 soft soil sites in the San Francisco Bay Area and 2 sites in Mexico City are shown in Figure 3. It can be seen that, even within soft soil sites, large variations occur in the predominant site period depending on the shear wave velocity of the different soil layers and total depth of the soft soil deposits.

Mean inelastic strength demands of 14 ground motions recorded at rock sites during the Loma Prieta earthquake are shown in Figure 4. It can be seen that the shape of the elastic strength demands (μ=1) differs significantly from the shape of inelastic strength demands, suggesting that the currently used procedure which accounts for inelastic behavior by specifying a reduced spectra with the the same shape as the elastic is inadequate. Mean inelastic strength demands of 14 ground motions recorded at soft soil (bay mud) sites in the San Francisco Bay Area during the Loma Prieta earthquake are shown in Figure 5. For structures responding elastically and with fundamental periods that are close to the predominant period of the site experience large amplification of seismic forces. These large amplifications, however, are significantly reduced when inelastic behavior occurs. For ductilities larger than 3, inelastic strength demands decrease monotonically with increasing periods.

By comparing the average spectra of ground motions recorded on rock and soft soil it can be seen that the largest dynamic amplification for elastic response (μ=1) is produced for soft soil sites. These results are different to those reported previously by Seed et al. [8] who computed larger amplifications for rock and alluvium sites than for soft soil sites. Moreover, the maximum amplification (with respect to PGA) for soft soil sites computed in that study is nearly 30% smaller than the maximum amplification computed here. For rock and alluvium sites the maximum amplifications computed in this study are practically the same as those found by Seed et al. with a smaller set of ground motions.

Mean strength reduction factors of 14 ground motions recorded at rock sites during the Loma Prieta earthquake are shown in Figure 6. It can be seen that strength reductions are by no means constant as implied by current seismic recommendations. Reduction factors which are based on assuming that the maximum displacement is the same in elastic and inelastic systems (i.e. $R_\mu=\mu$) is unconservative in the short period range. Reduction factors which are based from assuming equal energy in elastic and inelastic systems ($R_\mu=[2\mu-1]^{1/2}$) are also unconservative in this period range.

Mean strength reduction factors of 14 ground motions recorded at bay mud sites during the Loma Prieta earthquake are shown in Figure 7. Strength reduction factors in this case are characterized by small values for periods smaller than the predominant site period ($T/T_g < 1$) and by very large reductions for periods close to the predominant site period. Strength reduction factors are approximately equal to μ for T/T_g ratios greater than 2.5.

CONCLUSIONS

Elastic and inelastic response spectra were computed for 36 ground motions recorded during the Loma Prieta earthquake and 8 ground motions recorded in previous earthquakes. The results indicate that the shape of the inelastic strength demands differs from the shape of elastic strength demands. It is concluded that strength reductions produced in nonlinear systems are strongly affected by the natural period of vibration, the level of inelastic deformation, and the local site conditions. For soft soil sites, the estimation of the predominant period of the site is particularly important on the estimation of inelastic strength demands. The use of period-independent strength reduction factors, as currently specified in many seismic design recommendations, may lead to unconservative designs.

ACKNOWLEDGEMENTS

The research presented in this paper was supported by the California Department of Conservation, Division of Mines and Geology, Strong Motion Instrumentation Program under contract No. 1089-502.

REFERENCES

[1] National Earthquake Hazard Reduction Program, "*Recommended Provisions for the Development of Seismic Regulations for New Buildings*," Building Seismic Safety Council, Washington, D.C., 1988.

[2] Applied Technology Council, "*Tentative Provisions for the Development of Seismic Regulations for Buildings*," Publication No. ATC 3-06, Palo Alto, California, June 1978.

[3] International Conference of Building Officials, "*Uniform Building Code*," 1988 Edition, Whittier, California, 1988.

[4] Riddell, R., and Newmark, N.M., "Statistical Analysis of the Response of Nonlinear Systems Subjected to Earthquakes," *Structural Research Report No. 468*, Department of Civil Engineering, University of Illinois, Urbana-Champaign, August 1979.

[5] Riddell, R., Hidalgo, P., and Cruz, E., "Response Modification Factors for Earthquake Resistant Design of Short Period Buildings," *Earthquake Spectra*, 5(3): 571-590, 1989.

[6] Krawinkler, H., and Nassar, A., "Damage Potential of the Whittier Narrows Earthquake Ground Motions," *SMIP89, Proceeding of the Seminar on Seismological and Engineering Implications of Recent Strong-Motion Data*, California Department of Conservation, Sacramento, California, May 1989.

[7] Miranda, E., "Seismic Evaluation and Upgrading of Existing Buildings," *Ph.D. Thesis*, University of California at Berkeley, Berkeley, California, May 1991.

[8] Seed, H.B., Ugas, C., Lysmer, J., "Site-Dependent Spectra for Earthquake-Resistant Design," *Report No. EERC 74-12*, Earthquake Engineering Research Center, University of California, Berkeley, November, 1974.

STATION NAME	GEOLOGY	EARTHQUAKE DATE	MAGN.	EPICTR. DIST.[km]	DIRECTION	PGA [g's]
CORRALITOS Eureka Canyon Road	Landslide deposits	Loma Prieta October 17, 1989	7.1(M_S)	7	90 360	0.47 0.62
SANTA CRUZ UCSC	Limestone	Loma Prieta October 17, 1989	7.1(M_S)	16	90 360	0.41 0.43
SAN FRANCISCO Cliff House	Franciscan sandstone	Loma Prieta October 17, 1989	7.1(M_S)	99	90 0	0.11 0.07
SAN FRANCISCO Pacific Heights	Franciscan sandstone	Loma Prieta October 17, 1989	7.1(M_S)	97	360 270	0.05 0.06
SAN FRANCISCO Presidio	Serpentine	Loma Prieta October 17, 1989	7.1(M_S)	98	90 0	0.20 0.10
SAN FRANCISCO Rincon Hill	Franciscan sandstone	Loma Prieta October 17, 1989	7.1(M_S)	95	90 360	0.09 0.08
YERBA BUENA ISLAND	Franciscan sandstone	Loma Prieta October 17, 1989	7.1(M_S)	95	90 360	0.06 0.03
CAPITOLA Fire Station	Alluvium	Loma Prieta October 17, 1989	7.1(M_S)	9	90 360	0.39 0.46
HOLLISTER South & Pine	Alluvium	Loma Prieta October 17, 1989	7.1(M_S)	48	90 360	0.17 0.36
OAKLAND 2-Story Office Bldg.	Alluvium	Loma Prieta October 17, 1989	7.1(M_S)	92	290 200	0.24 0.19
STANFORD Parking Garage	Alluvium	Loma Prieta October 17, 1989	7.1(M_S)	51	360 90	0.26 0.22
EMERYVILLE Free Field South	Bay mud	Loma Prieta October 17, 1989	7.1(M_S)	97	350 260	0.21 0.26
EMERYVILLE Free Field North	Bay mud	Loma Prieta October 17, 1989	7.1(M_S)	97	350 260	0.20 0.22
OAKLAND Outer Harbor Wharf	Bay mud	Loma Prieta October 17, 1989	7.1(M_S)	95	305 125	0.27 0.29
TREASURE ISLAND Naval Base	Fill	Loma Prieta October 17, 1989	7.1(M_S)	98	90 360	0.16 0.10
SAN FRANCISCO International Airport	Bay mud	Loma Prieta October 17, 1989	7.1(M_S)	79	90 360	0.33 0.23
SAN FRANCISCO 18-Story Comercial Bldg.	Fill over bay mud	Loma Prieta October 17, 1989	7.1(M_S)	95	980 350	0.13 0.16
FOSTER CITY Redwood Shores	Bay mud	Loma Prieta October 17, 1989	7.1(M_S)	63	90 0	0.28 0.26

Table 1. Loma Prieta earthquake ground motions selected for this study

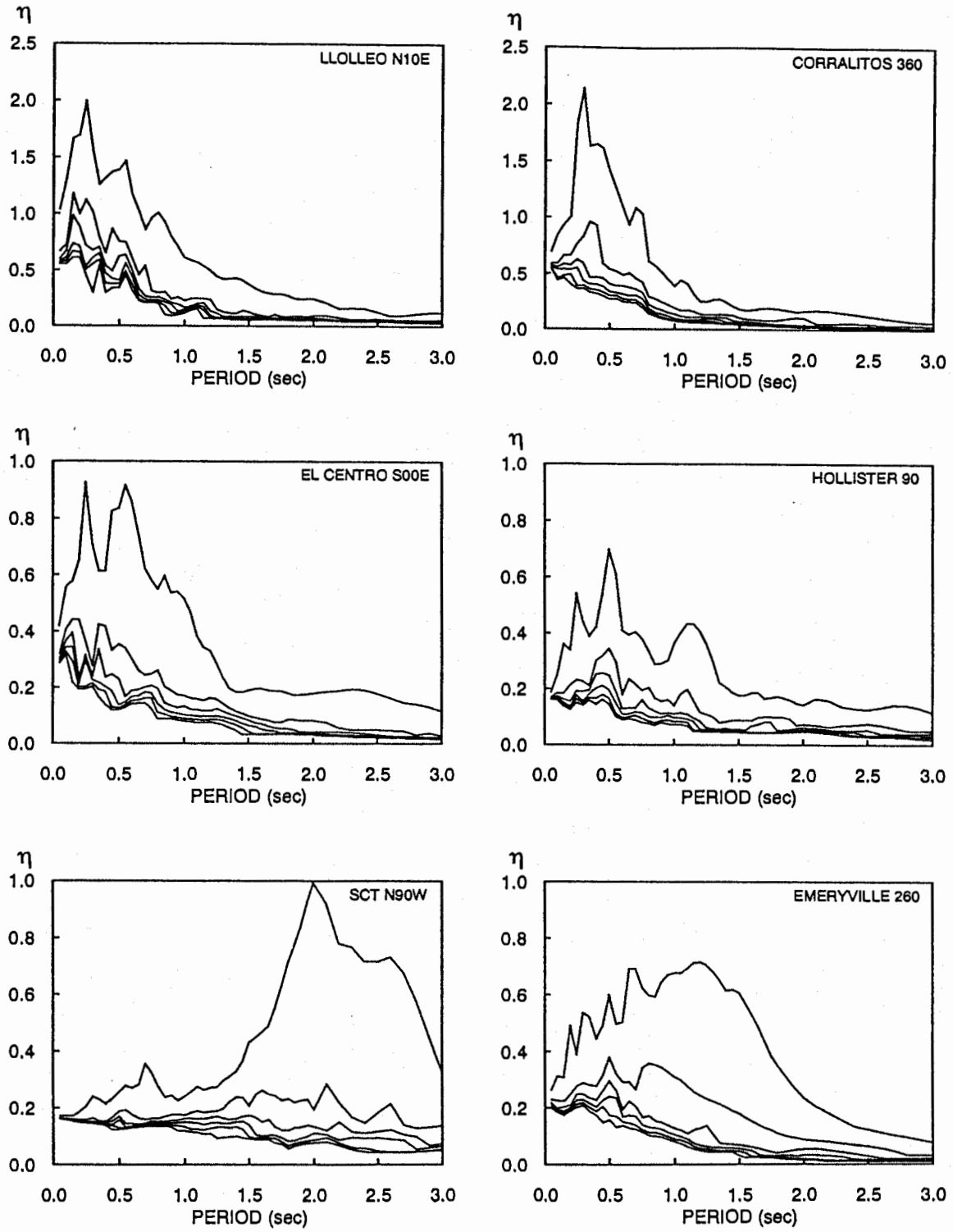

FIGURE 1. Normalized inelastic strength demands (μ=1,2,3,4,5,6).

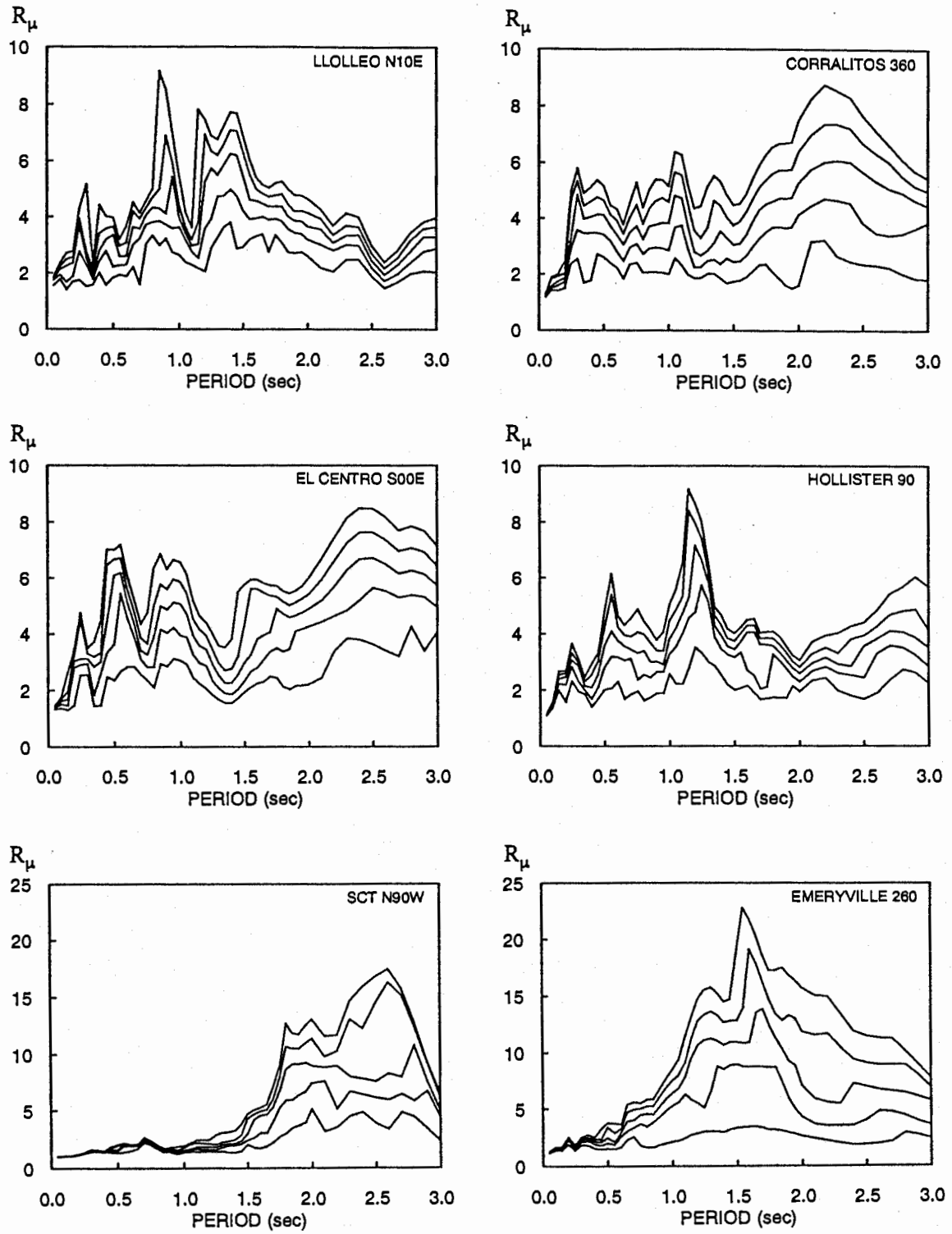

FIGURE 2. Strength reduction factors (μ=6,5,4,3,2).

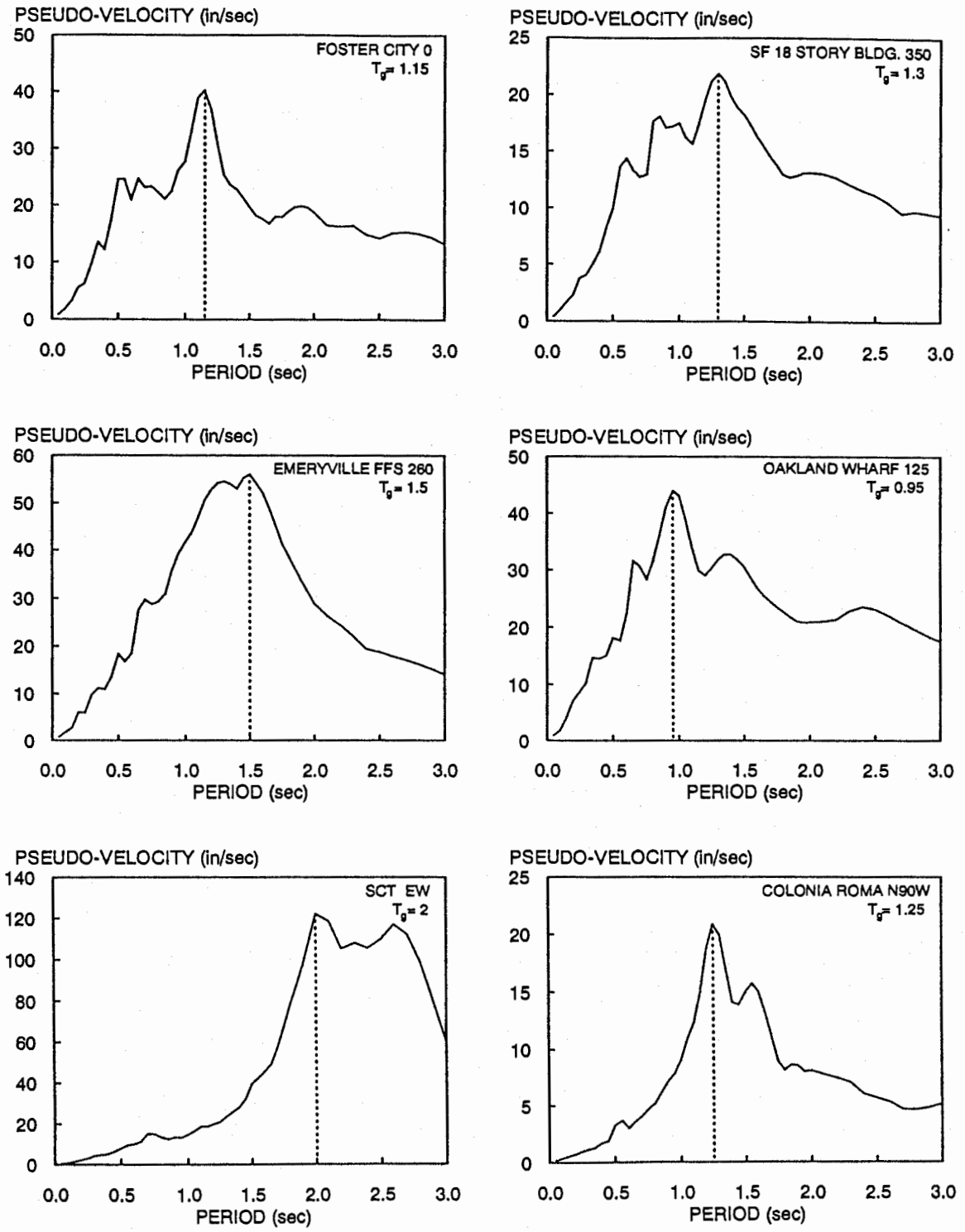

FIGURE 3. Predominant periods for various soft soil sites in the San Francisco Bay Area and Mexico City.

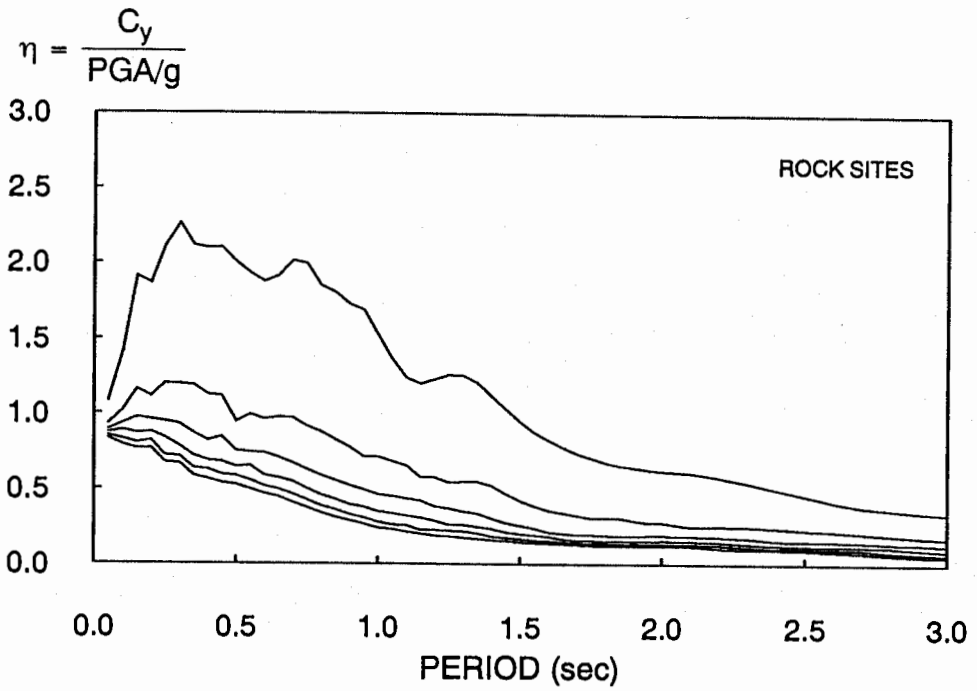

Figure 4. Mean strength demands of ground motions recorded on rock when normalized using PGA (μ=1,2,3,4,5,6).

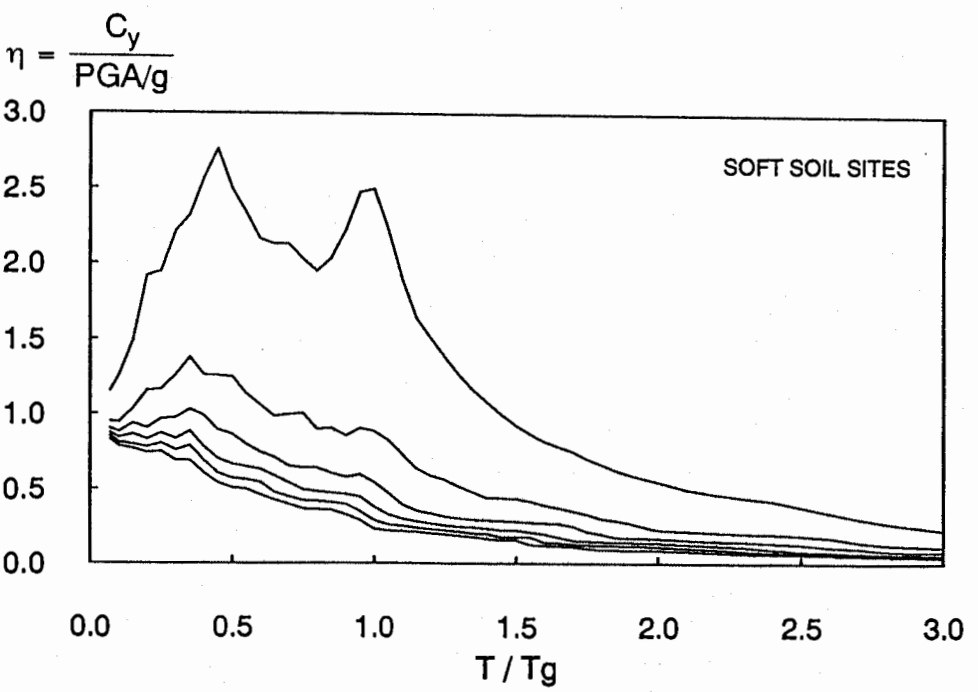

Figure 5. Mean strength demands of ground motions recorded on soft soil when normalized using PGA (μ=1,2,3,4,5,6).

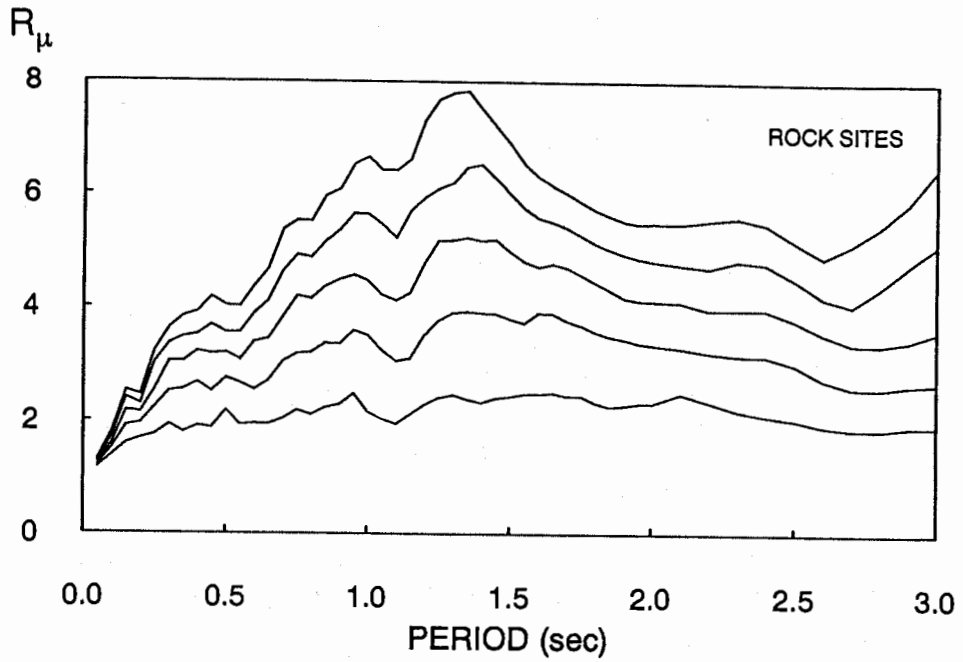

Figure 6. Mean strength reduction factors of ground motions recorded on rock (μ=6,5,4,3,2).

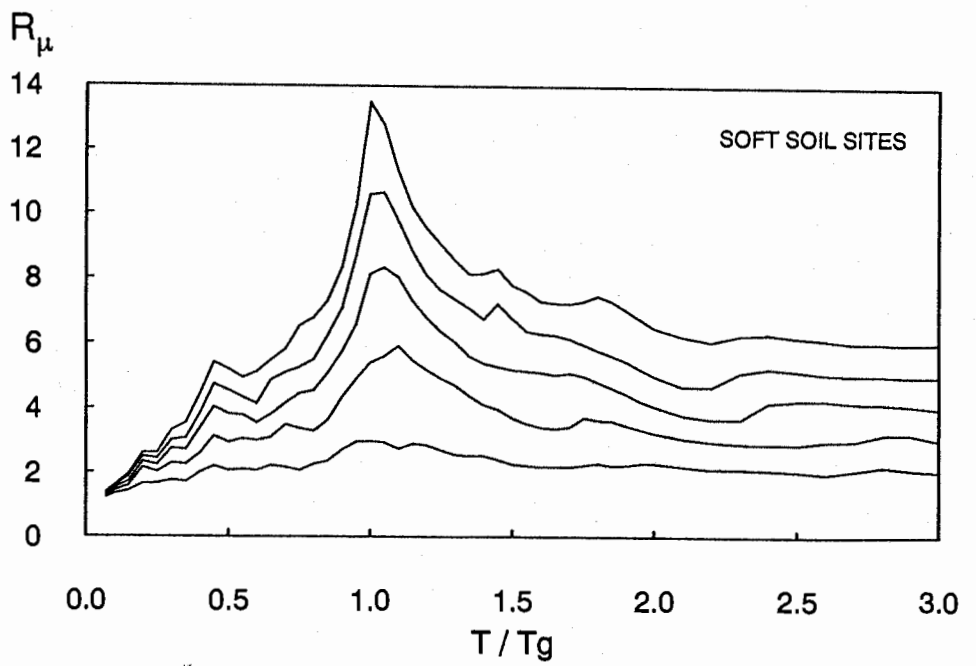

Figure 7. Mean strength reduction factors of ground motions recorded on soft soil (μ=6,5,4,3,2).

EVALUATING DESIGN PROVISIONS AND ACTUAL PERFORMANCE OF A MODERN HIGH-RISE STEEL STRUCTURE

Abolhassan Astaneh, Associate Professor
David Bonowitz, Graduate Student
Cheng Chen, Graduate Student

Department of Civil Engineering and
Earthquake Engineering Research Center
University of California at Berkeley

ABSTRACT

The objectives of this project were to study CSMIP records obtained during the October 17, 1989 Loma Prieta earthquake at a 49-story steel structure and to conduct an investigation of current structural engineering design procedures related to the response. The recorded data indicated that the top 6 stories of the building have experienced much greater drift than lower floors due to discontinuity of mass and stiffness. The results of elastic and inelastic dynamic analyses compared to CSMIP records confirmed validity of many design assumption currently used while resulting in better understanding of actual behavior of these modern structures and possible refinement of design procedures.

INTRODUCTION

The California Strong Motion Instrumentation Program (SMIP) of Division of Mines and Geology of California has many strong motion recording stations throughout the greater San Francisco Bay Area. When Loma Prieta earthquake of 1989 occurred, a 49 story instrumented steel high rise in San Francisco was shaken among many other structures. The building had 18 accelographs and all instruments recorded more than 120 seconds of valuable acceleration response of the building. This paper summarizes important aspects of a study of the response of this building during the Loma Prieta earthquake and lessons learned.

The building is located in downtown San Francisco and was designed in 1977-78 and its construction was completed in 1979. A view of the building is shown in Figure 1. The seismic design was according to UBC-76 and included modal analysis and response spectra analyses (3). The floor system consists of 2.5 inch concrete over a 3 inch metal deck connected to steel framing by shear studs and puddle welds. The structural framing system consists of special moment resisting space frames in both East-West and North-South directions. However, for extra lateral stiffness, moment frames in narrow direction (N-S) have two bays braced using eccentric braces. The length of shear links in eccentric braces is about 4.5 feet. The building is supported by

a 5 feet thick mat foundation which in turn is supported by 150-200 feet deep composite steel/concrete piles. Figure 2 shows details of a typical floor and the East-West and North-South frames.

The building is instrumented by the Strong Motion Instrumentation Program of California Department of Mines and Geology of Department of Conservation and has 18 accelerographs installed at various levels and directions as shown in Figure 3. During the Loma Prieta earthquake, all strong motion instruments were activated and all have collected reliable data for more than 120 seconds.

RESEARCH METHODOLOGY

Major phases of the study were:

1. Collect data on geometry, material, non-structural elements, equipment, dead and live load and any damage.

2. Obtain, process and analyze data recorded by CSMIP.

3. Construct realistic elastic and inelastic computer models of the structure above the top of foundations.

4. Subject the elastic computer model of the structure to base excitations recorded during the Loma Prieta earthquake using ETABS computer program and study the response and predictions of the dynamic analysis. The ETABS software represents typical dynamic analysis software used in design offices today.

5. Subject the inelastic 2-dimensional computer model of the structure to base excitations recorded during the Loma Prieta earthquake as well as to scaled-up base excitations. The objective here was to obtain insight to the inelastic behavior of the structure during future strong earthquakes.

6. Study the code provisions and seismic design practice used in design of the building and investigate the adequacy and accuracy of the current seismic design practice.

7. Formulate recommendations with regard to refining the existing instrumentation installed in the building.

8. Formulate recommendations that can be used to improve seismic design practice and code provisions.

RECORDED RESPONSE OF THE BUILDING TO LOMA PRIETA EARTHQUAKE

A. Accelerations

Figure 4 shows time histories of the E-W and N-S components of acceleration recorded at the 44th floor and at the Basement "B" level (4). The ratios of maximum peak acceleration of 44th

floor to basement B were 2.53 in E-W direction and 4.73 in the N-S direction.

SIGNIFICANT RESULTS

A report on the study (1) is in preparation which provides detailed information on the study. Due to space limitations, some significant results available at the time of this writing are provided here.

A. Period

Table 1 shows selected periods of vibration of the structure obtained from the recorded data as well as from various analyses.

Table 1. Selected Modal Periods of Vibration

Mode Number	CSMIP Records	TABS-4 (Ref.3)	ETABS 3-Dim.	ETABS 2-Dim.	N/10 Rules	UBC 1976	UBC 1991
1	6.5X	6.41X	6.54X	6.62X	4.90X	4.70X	4.05X
2	--	5.13Z	5.09Z	--	--	--	--
3	5.0Y	5.00Y	4.70Y	5.14Y	4.90Y	4.00Y	4.05Y
4	2.0X	2.34X	2.35X	2.36X	1.63X	--	--
5	--	1.80Z	1.72Z	--	--	--	--
6	1.8Y	1.70Y	1.69Y	1.72Y	1.63Y	--	--
7	1.3X	1.41X	1.39X	1.39X	.98X	--	--
8	--	1.05Z	1.01Z	--	--	--	--
9	1.0X	1.03X	1.00X	1.00X	.98Y	--	--
10	--	.98Y	.98Y	.99Y	--	--	--

NOTES: X and Y indicate modes in E-W and N-S directions respectively.
T indicates torsional mode.

B. Damping Ratio

A preliminary analysis of the CSMIP data indicated that the damping during the earthquake was about 1.7 for the N-S braced frame direction and about 2.0-2.6 percent for the E-W moment frame direction. However, the results of elastic analyses matched the recorded data better when a constant critical damping ratio of 3% was used. In the inelastic analyses, a critical damping ratio of 2.75 was used.

C. Deflected Shape of the Structure

Figure 5 shows the animated plots of the CSMIP recorded displacements in the N-S and E-W direction. The motion of the structure in the N-S direction was dominated by the higher modes during the first 30 seconds of the motion while ground motion was being applied. After the first 30 seconds, the vibration of the structure was dominated by the first mode. In the E-W direction the motion was dominated by the first mode throughout the recorded motion. Figure 6 shows drift ratios for N-S and E-W

directions. As figure indicates, drift ratios for top six stories in the N-S direction were relatively high compared to the rest of the structure.

Maximum displacement in the N-S direction occurred after 47 seconds of motion and was equal to 6.45 inches at 44th floor. The maximum displacement in the E-W dirction occurred during first 30 seconds and was equal to 10.67 inches at 44th level.

Figure 7 shows a comparison of the displacement histories of 44th floors in the E-W direction obtained from elastic analysis and CSMIP records. The elastic analysis was done using ETABS and the structure was modeled as a modern structure would be modeled in a design office without very refined research oriented modeling. The comparison shows that predictions of the current dynamic analyses in design offices for this case were very good compared to the recorded response.

In order to obtain an understanding of inelastic response of the structure, two inelastic 2-dimensional time history analyses were conducted. In one analyses, acceleration time history recorded at the basement of the building was considered to be a representative of magnitude 7 earthquake and was used as base excitation. In the second inelastic analysis, to cause severe yielding, the amplitude of the Loma Prieta acceleration time history was multiplied by 2.75 to obtain a base excitation history that will represent a magnitude 8.3 severe earthquake.

In seismic design of the structure (3) two response spectra with maximum peak accelerations of .84g and 1.16g were developed to represent magnitudes 7 and 8.3 earthquakes respectively. These spectra are shown in Figure 8 along with response spectra of Loma Prieta record at the building basement level as well as a spectra corresponding to 2.75 times Loma Prieta record. The design spectra which were based on the assumption of the rupture of nearby faults and on the assumption of rock support shows peaks over the short periods of abouts 0.4 seconds whereas the Loma Prieta spectra show larger amplifications for longer periods of about 1.5 seconds.

Figure 9 shows a comparison of the displacement time histories for 16th and 44th floors due to the Loma Prieta record, 2.75 time the Loma Prieta and the CSMIP recorded response. The analyses indicated that the E-W frames remained elastic during the Loma Prieta earthquake and experienced inelasticity and plastic hinge formations when subjected to 2.75 times Loma Prieta acceleration records. Figure 10 shows plastic hinges that formed during the initial 60 seconds of the motion when the frame on line "E" was subjected to 2.75 times the Loma Prieta record of the Basement B.

CONCLUSIONS AND RECOMMENDATIONS

The comparative study of the response data recorded by the CSMIP and the results of elastic and inelastic dynamic analyses indicated that:

1. The currently available design office computer programs used for 3-D dynamic analyses, adequately predicted the response of the building to Loma Prieta.
2. The stiffness and mass discontinuities of the top 6 stories affected the behavior of the whole structure significantly.

3. It appears that the structure will experience hinge formations and inelasticity during a magnitude 8.3 earthquake, however, maximum displacement of 44th floor in the E-W direction will be in the order of 27 inches.

4. To capture a obtain a cimplete set of strong motion data, it is recommended that at least 10 more instruments be added to this structure to capture E-W response and vertical response of cantilevers more accurately.

ACKNOWLEDGMENTS

The project was sponsored by the Strong Motion Instrumentation Program of the Division of Mines and Geology of the California Department of Conservation under grant No. CAL-DOC 1089-501, 1990. The efforts of A. Shakal and M. Huang of CSMIP in providing the strong motion data are sincerely appreciated. Rubin Boroschek, graduate research assistant assisted the investigators in processing and analysis of the recorded data particularly by using his versatile ANIM-2d program. D. Bergman and J. Nicolleti of URS/John A. Blume and Associates assisted the authors in defining the structure and Skidmore, Owings and Merrill of San Francisco provided computer support for the elastic analyses. The ETABS program used in this study was donated to the project by Computers & Structures Inc. of Berkeley.

REFERENCES

1. Astaneh, A., Bonowitz, D. and Chen, C. "Studies of a 49-Story Instrumented Steel Structure Shaken During the 1989 Loma Prieta Earthquake", EERC Research Report, in preparation, Earthquake Engineering Research Center, University of California at Berkeley, to be released in 1991.

2. "CSMIP Strong Motion Records from the Santa Cruz Mountains (Loma Prieta) California Earthquake of October 17, 1989), 1989

3. Merovich, A.T., Nicoletti, J.P., and Hartle, E., "Eccentric Bracing in Tall Buildings", Journal of Structures Division,, ASCE, Vol 108, NO. ST9, September 1982, pp. 2066-2081.

4. "Plots of the Processed Data for San Francisco 47-Story Office Building from the Santa Cruz Mountains (Loma Prieta) Earthquake of October 17, 1989", CSMIP, 1990.

5. "Uniform Building Code", 1976 & 1991 Editions, International Conference of Building Officials, Whittier, CA. 1976, 1991.

Figure 1. A View of the Structure

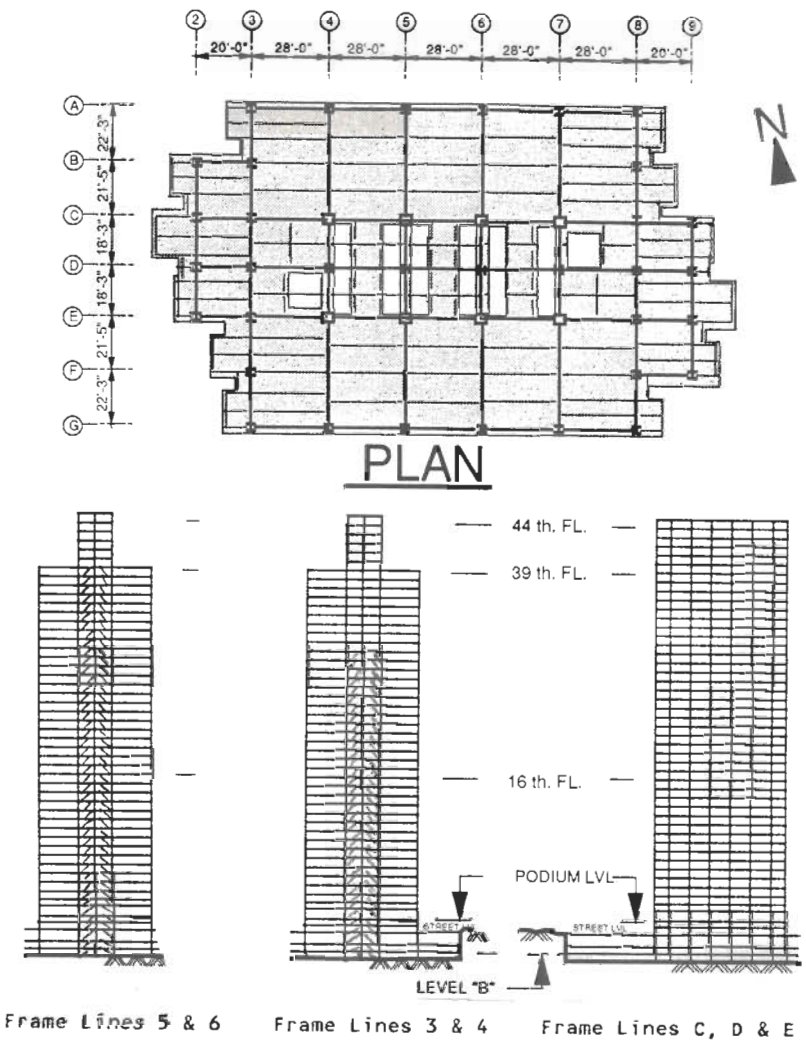

Figure 2. Typical Framing Plan, East-West and North-South Frames

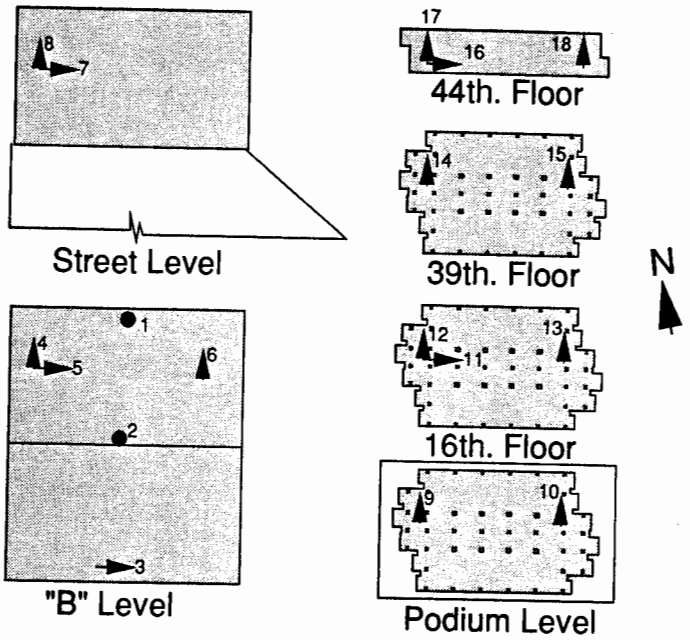

Figure 3. Plan of SMIP Instrumentation

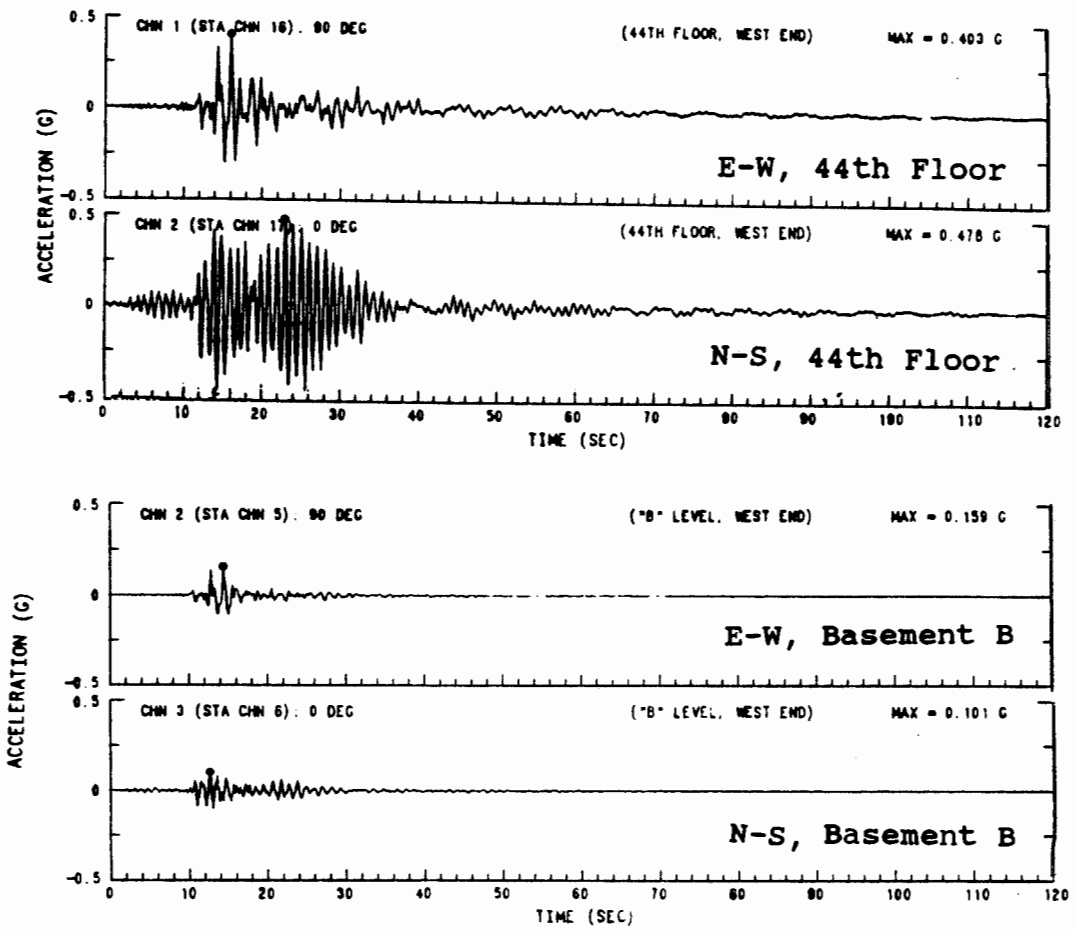

FIgure 4. Acceleration Time Histories for 44th Fl. and Basement

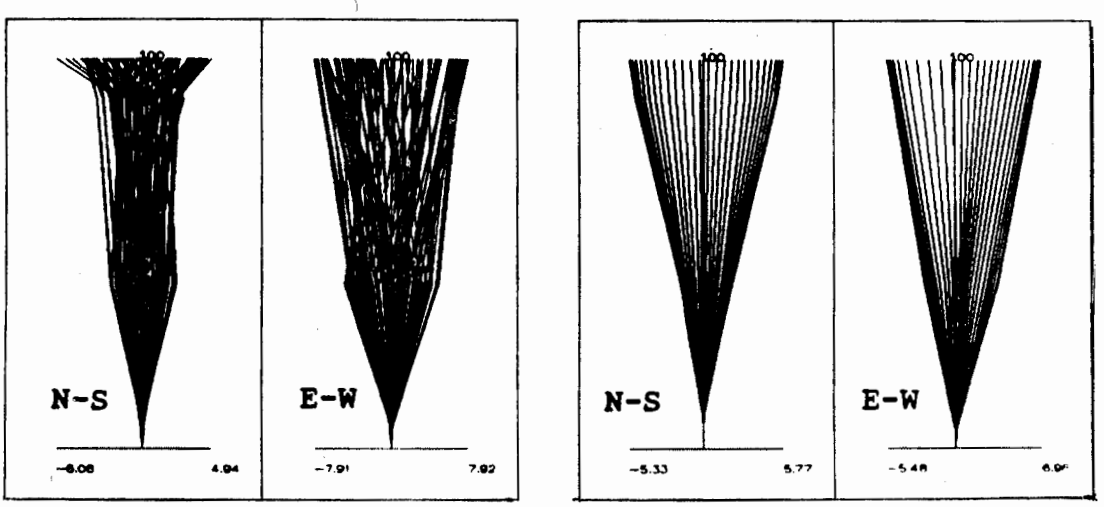

Figure 5. Animated Deflected Shape of the Structure
(a) During Ground Shaking
(b) After Ground Shaking Subsided

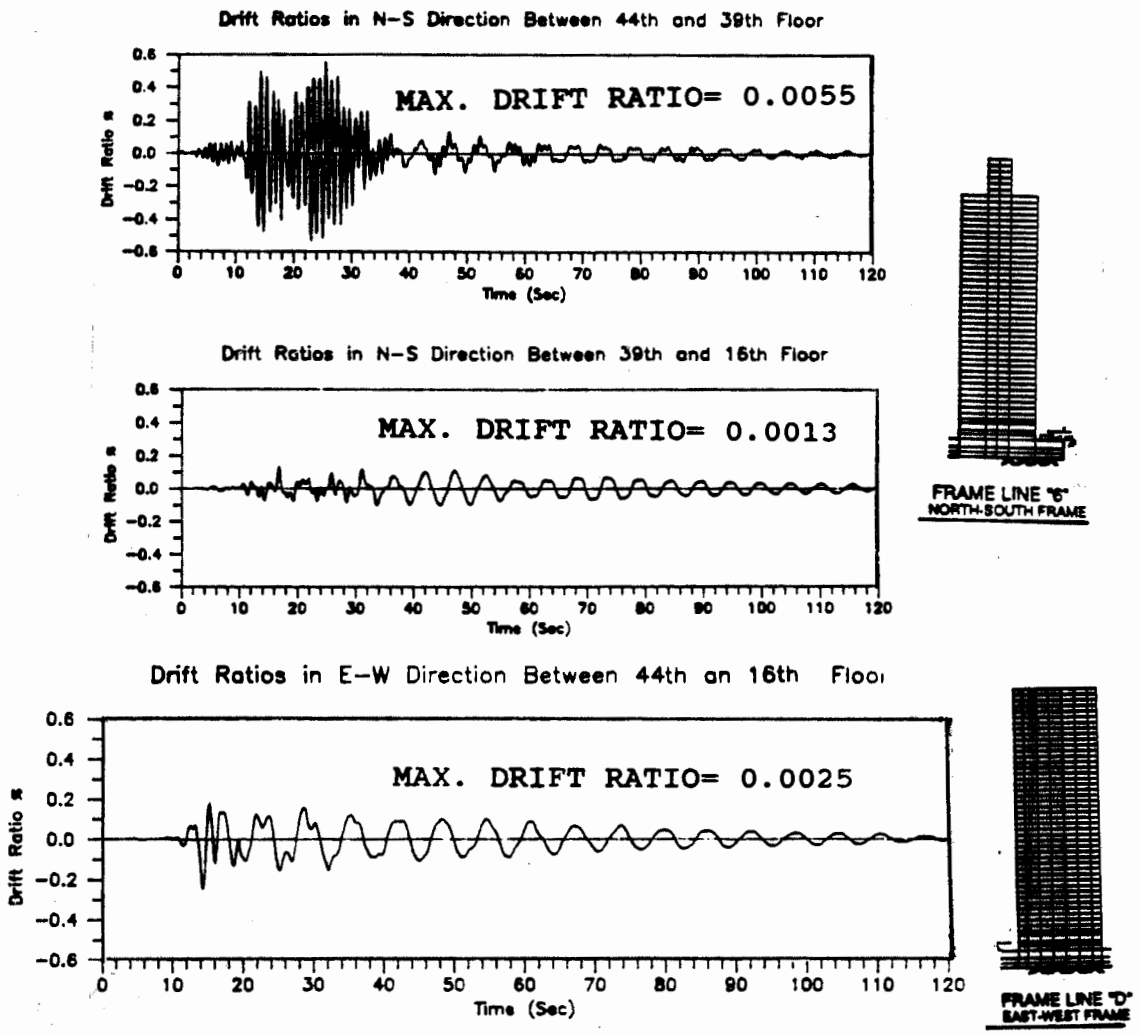

Figure 6. Drift Time Histories

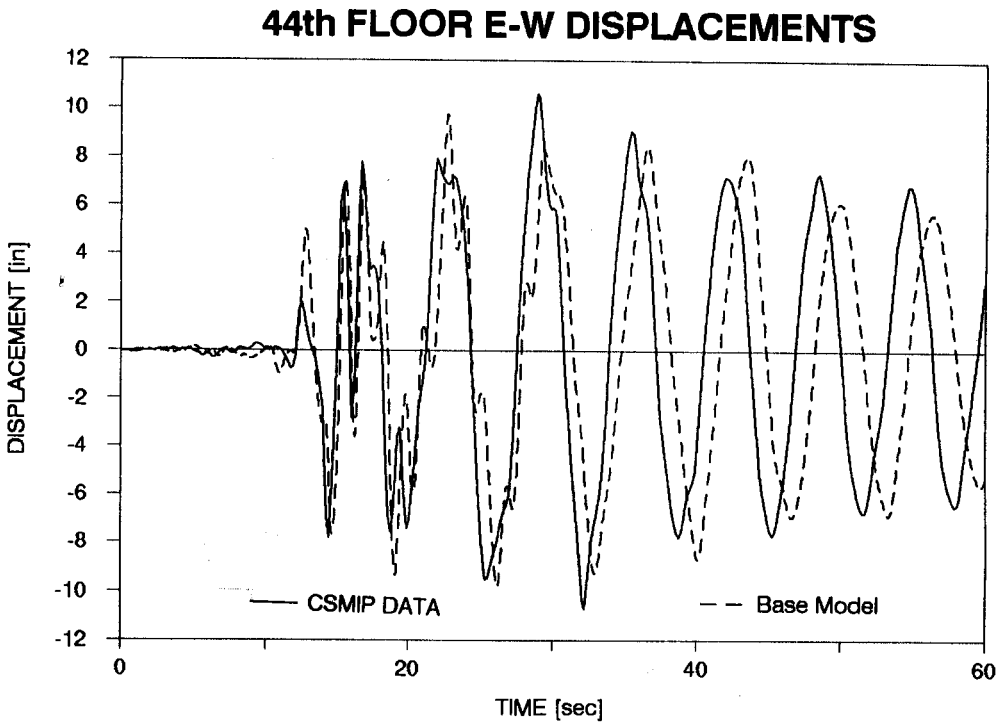

Figure 7. Comparison of the Displacement Time Histories

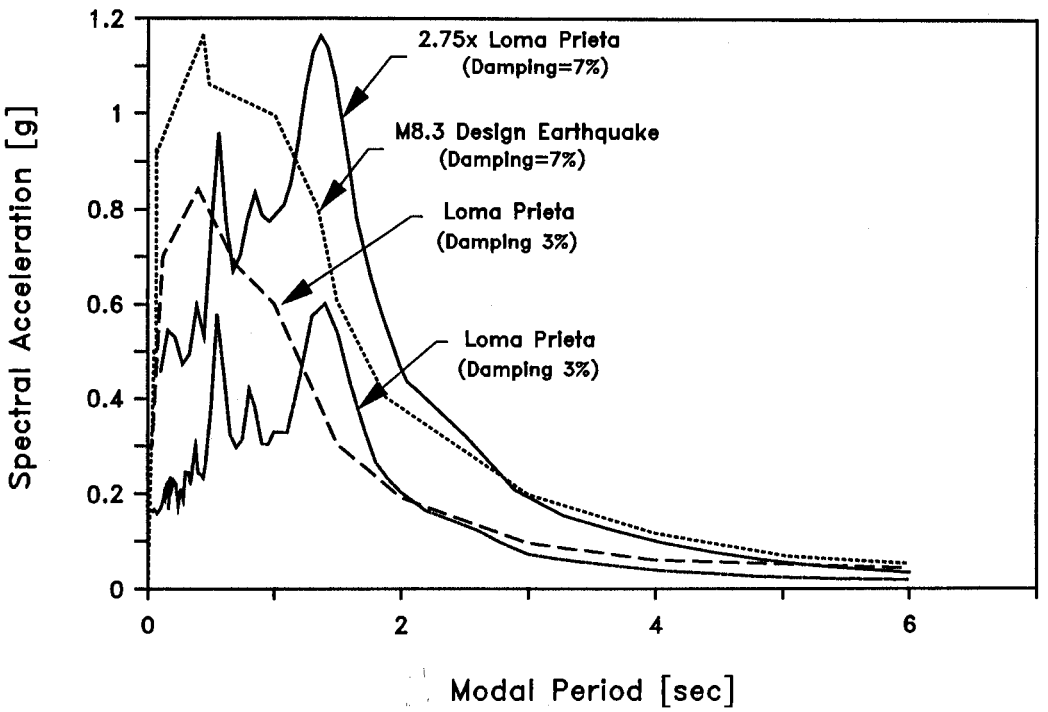

Figure 8. Response Spectra Used in Design and Obtained from Loma Prieta

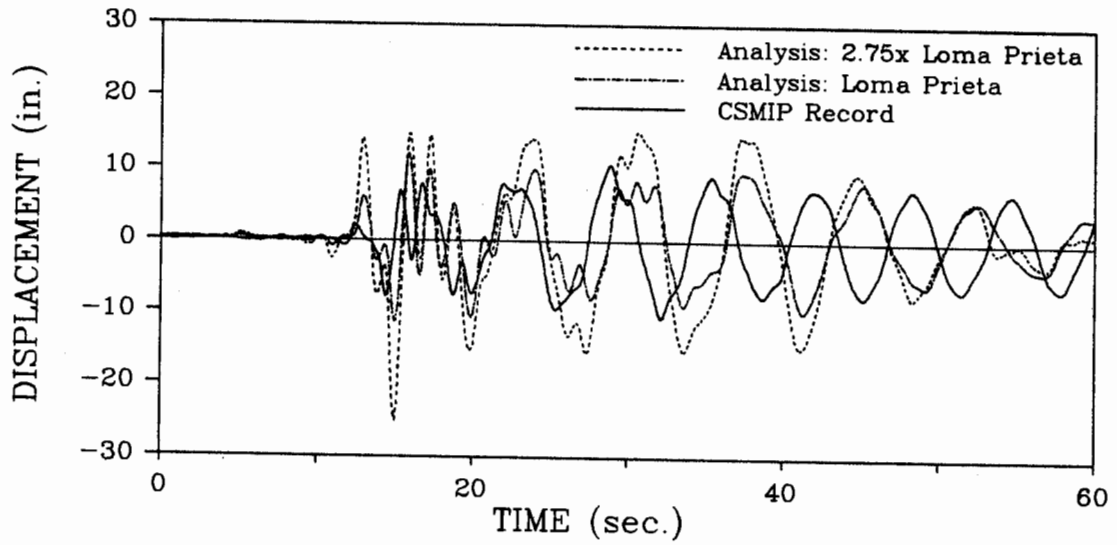

Figure 9. Displacement Time Histories for the E-W Direction Obtained from Inelastic Analyses

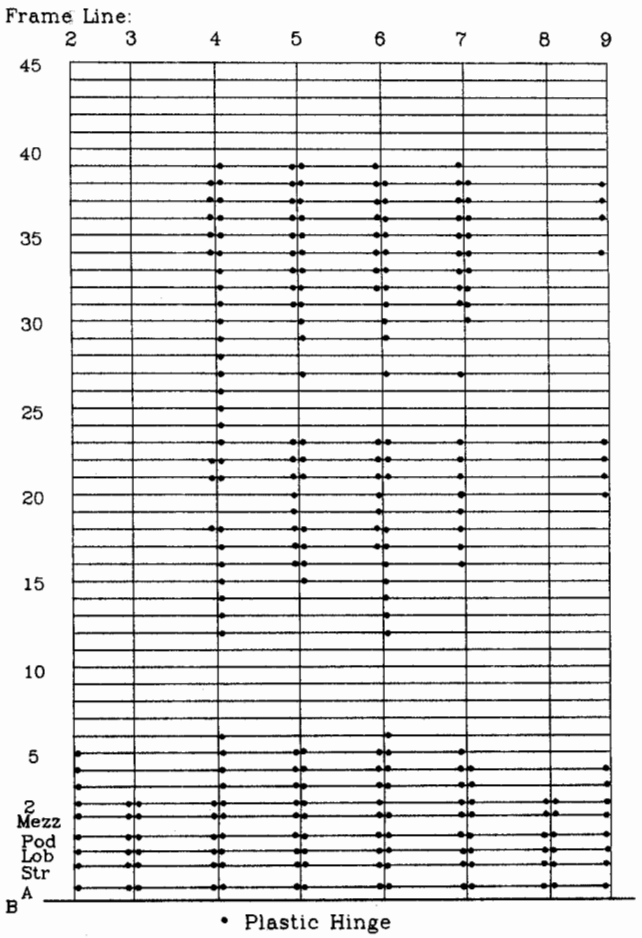

Figure 10. Plastic Hinges Formed in the E-W Frame

Degradation of Plywood Roof Diaphragms under Multiple Earthquake Loading

J. B. Bouwkamp
Professor of Civil Engineering, Technical University
Darmstadt, W. Germany

R. O. Hamburger, S.E.
Associate, EQE International

J. D. Gillengerten, S.E.
Project Manager, EQE International

ABSTRACT

This paper summarizes the interim findings of research examining the recorded response of three buildings with concrete walls and plywood roof diaphragms to repeated strong motion events. Observed stiffness characteristics of the diaphragms are compared for each successive event and with that predicted by design formula and available data from static tests. Recorded response of the diaphragms indicates an initial dynamic stiffness substantially in excess of that predicted by static tests and design formulae. Damping for these diaphragms is determined to be low, on the order of 5% or less. Degradation of dynamic stiffness, of highly stressed diaphragms with large aspect ratios is apparent. However, the observed degraded stiffness of these diaphragms is still in excess of that predicted by conventional design formulae. Research was performed under a grant from the California Division of Mines and Geology.

INTRODUCTION

The use of long span plywood roof diaphragms, with large aspect ratios, has been common practice in low rise commercial and industrial construction throughout California and other western states. Commonly used in combination with tiltup concrete and reinforced masonry walls, these diaphragms are often heavily loaded and are expected to experience large deformations under seismic loads. The performance of early structures of this type in strong ground motion has been poor. Failures occurred in the 1964 Alaska earthquake[1], the 1971 San Fernando Earthquake[2] and the 1987 Whittier earthquake[3]. These failures could be attributed to two principal failure modes: 1- cross grain tension or flexural failure of the wood framing at plywood margins; or 2- pull-out failure of the nails through the edges of the plywood.

Subsequently, the Structural Engineers Association of California recommended[4] and the Uniform Building Code[5] adopted detailing provisions intended to prevent such failures. These provisions included prohibition of the use of wood framing in cross-grain tension or flexure and requirements for providing continuous ties across the width of the diaphragms to prevent

tensile failure. The performance of buildings designed to these more recent provisions has been substantially improved, however, evidence of secondary modes of diaphragm degradation have been reported[3]. Observed damage has included substantially weakened nailing of the plywood to framing members, including nail withdrawals as well as edge failures resulting from nails pulling through the edges of plywood sheets.

Concern has been expressed that typical post-earthquake damage inspections of these structures may not indicate the presence of such damage unless it is extreme, and degraded plywood diaphragms may never be restored to their original condition. This presents a significant potential problem in zones of high seismicity, where structures may experience several strong ground motion events in the course of their useful lives, with continual degradation of their capacity to resist such motions. Buildings in the San Jose, California region for example have been subjected to strong ground motion several times over the last 10 years. Events have included the 1979 Halls Valley (M6.0), 1984 Morgan Hill (M6.2), 1988 Alum Rock (M5.5) and 1989 Loma Prieta (M7.1) earthquakes. Although only the latter event could be considered a major earthquake, it should be remembered that buildings of this type have seen significant damage in low magnitude events such as Whittier Narrows (M5.9).

A primary objective of this research is to determine if recordings of ground motion and structural response for three concrete tiltup buildings with plywood roof diaphragms, in successive earthquake excitations, indicate any significant degradation in structural rigidity, as evidenced by their response. Secondary objectives for this research are to determine if conventional design assumptions on the stiffness and loadings assigned to these structures are realistic in light of observed response.

SUBJECT BUILDINGS

The three buildings investigated in this research are a single story warehouse in Hollister (CSMIP Station No. 47391), a single story gymnasium structure at the West Valley College in Saratoga (CSMIP Station No. 58235) and a two story office structure in Milpitas (CSMIP Station No. 57502). Table 1 summarizes the ground motion records reviewed for each building under this project. The performance of the West Valley College Gymnasium building, during the 1984 Morgan Hill Earthquake has previously been evaluated by other researchers[6]. Due to a delay in obtaining data on the buildings and recorded ground motions, analysis of all three buildings is not complete as of this writing. The findings on the studies of the West Valley College Gymnasium, a single story structure in Saratoga, and the two story Milpitas Office building will be presented in an additional paper.

The single story Hollister warehouse has overall dimensions of 100 feet east to west by 300 feet north to south. It is constructed of 6" thick precast concrete wall panels, with heights of 30 feet and widths varying from 18 to 22 feet. Panel joints consist of cast-in-place pilasters, in which horizontal panel steel is embedded. The roof is a panelized plywood system consisting of glulam beams at 18 feet, spanning north to south between the pilasters and a single row of columns; 4 x 14 sawn timber purlins spanning east to west at 8 feet; 2 x 4 sub purlins; and plywood sheathing. Plywood at

the ends of the structure is 3/4 inch thick with 10d nails at 1-3/4" for boundaries, 3" for discontinuous edges and 12" in the field. The balance of the plywood sheathing is 1/2 inch thick with nail spacing varied as required for shear. No interior partitions are present. Figure 1 is a photograph of the building while Figure 2 indicates the basic construction and instrument locations.

Anchorage of the precast concrete walls to the roof diaphragm is accomplished with a double row of nails from the edge plywood into a 3x nailer along the top of the wall. Nails straddle the line of bolts anchoring the nailer to the wall and avoid placing the nailer into cross grain tension. Diaphragm cross ties are provided by Simpson MST hardware across purlin lines and by bolted splice plates across glulam connections.

ANALYSIS

A code analysis of the Hollister structure was performed to determine the diaphragm capacity.[7] Based upon the design provisions of the 1988 *Uniform Building Code* (UBC)[7], the roof diaphragm has a sufficient capacity to resist a ZPA earthquake of 0.406g. This equates to an equivalent static lateral design force of 0.186g. The design lateral capacity of the diaphragm is limited by the shear in the plywood.

In the Morgan Hill and Hollister earthquakes, the Hollister warehouse was subject to moderate ground shaking, with PGA's of 0.08g and 0.11g, respectively in the direction of interest, which is east to west. The east-west PGA at the site in the Loma Prieta Earthquake was 0.25g. Peak roof accelerations at the center of the diaphragm, the base of the north wall, the top of the north wall, and demand-capacity ratios of the roof diaphragm are presented in Table 2. The Loma Prieta earthquake, with a PGA of 0.25 g, produced peak horizontal accelerations at the center of the roof (D/C_a in Table 2) over 4 times the code level static design load. Very little amplification of motion between the ground and the top of the tilt-up walls (channels 3 and 8) was observed, indicating that the walls are behaving as rigid bodies. The response of the structure is dominated by the dynamic properties of the roof diaphragm.

The above behavior is contrary to the typical model assumed by designers of these structures. UBC design procedures assume that the entire diaphragm responds at the modified spectral acceleration, taken as ZC/R_W, or $0.458Z$, where Z is the peak ground acceleration, C is the spectral amplification taken as 2.75 and R_W is a response modification coefficient taken as 6. The observed behavior indicates a variation in accelerations along the diaphragm length, starting at nearly Z adjacent to the end walls and peaking at approximately 3Z at the diaphragm center. This would result in an average effective spectral acceleration, over the length of the diaphragm, of approximately 2Z. The column of D/C_V values in Table 2 expresses the relationship between the average spectral acceleration calculated for the diaphragm in each event to that implied by code, and is a measure of overstrength shear demand on the diaphragm.

Data published by the APA indicates that working stress values for plywood diaphragms incorporate a factor of safety slightly in excess of 4

against the ultimate strength condition. The code level diaphragm shear demand of 0.458Z with an APA factor of safety of about 4.2, yields an ultimate diaphragm capacity of about 1.9Z, which compares favorably with the observed average response of about 2Z. This indicates that current code design strength levels for these structures are appropriate.

Plywood diaphragms exhibit highly non-linear behavior[8], and therefore they do not possess a single fundamental frequency, except under low levels of excitation. However, for a given input motion, a predominant frequency range can be obtained. A Fast Fourier Transform (FFT) was applied to selected pairs of acceleration, velocity, and displacement records, from which the predominant structural frequencies of the roof diaphragm were extracted. Figures 3, 4, and 5 show representative plots of the frequency versus acceleration transfer function magnitude for roof and ground records in the Morgan Hill, Hollister, and Loma Prieta earthquakes, respectively.

Comparing the plots of the acceleration FFT's for the Morgan Hill and Hollister earthquakes with the plot for the Loma Prieta earthquake, a shift in the predominant frequency of the roof diaphragm is noted. This indicates a softening of the diaphragm stiffness. The magnitude of change in predominant frequency and the associated changes in the relative diaphragm stiffness between the three earthquakes is presented in Table 3. This degradation or softening of plywood diaphragms under high loads has been previously noted in static tests[8]. Non-cyclical tests of plywood diaphragms have shown them to be highly non-linear. A substantial portion of this non-linearity can be attributed to nail slip, a progressive and degenerative process. A representative load-deflection curve of test on a full size 1/2 inch plywood diaphragm, showing degradation of diaphragm stiffness with increasing load is shown in Figure 6.

Plots of acceleration versus displacement at the center of the roof (channel 4) for the Hollister and Loma Prieta earthquakes are shown in Figures 7 and 8. The acceleration versus displacement plot for the Hollister earthquake (Figure 7) is generally linear, indicating that the diaphragm remained essentially elastic and suffered no apparent degradation in stiffness due to the earthquake. This correlates well with the computed D/C_V of 0.93. The plot for the Loma Prieta earthquake (Figure 8) shows considerable softening of the diaphragm, as evidenced by the trend towards decreasing slope in the acceleration versus displacement plot. The magnitude of the change in diaphragm stiffness is in good agreement with the change in stiffness predicted by the period shifts observed using the FFT.

In order to compare the computed diaphragm stiffness to the stiffness actually observed, and to evaluate the accuracy of current methods for predicting wood diaphragm displacements, a simple linear-elastic finite element model of the roof diaphragm was constructed. The model properties were tuned to produce deflections under static lateral load equal to those obtained using the deflection formula in the 1988 UBC Standard 25-9[9]. For the purposes of this model, flexural properties were calculated as those produced by chords consisting of a one-half height strip of the side walls. The fundamental frequency of this "code" model was evaluated, and found to be 0.83 hertz, less than one half the predominant frequencies observed in both the Morgan Hill and Hollister events. By increasing the model diaphragm shear stiffness to 4.5 times the shear stiffness computed per UBC Standard 25-9, a

fundamental frequency comparable to the predominant frequency observed in the Hollister and Morgan Hill events was obtained. To match the model fundamental frequency to the predominant frequency observed in the Loma Prieta earthquake, it was necessary to increase the diaphragm shear stiffness to 2.3 times the UBC stiffness.

There are several possible sources for the wide difference between the observed diaphragm stiffness and that computed by conventional methods. Principal components of the UBC stiffness calculation are the flexural contribution of the chords, slip in chord connections (neglected in this case), elastic properties of the wood membrane, and slip of the nails. In the current model, flexural effects account for approximately half of the diaphragm flexibility. In a building with relatively solid and rigid side walls, such as the Hollister warehouse, conventional simple span assumptions may be highly inaccurate. Further, elastic properties of the wood membrane and nail slip values are based upon moderate duration, statically applied loads. Under short duration dynamic loading, it would be reasonable to expect stiffer response.

Using the roof diaphragm frequencies obtained from the FFT's and the recorded peak roof accelerations, the damping of the roof system was estimated using the ground response spectra prepared by CDMG for each event. In all cases, damping was found to be substantially less than 5% of critical. This is confirmed by the relatively closed loops observed on the time history plots of acceleration versus displacement, indicating little hysteretic behavior.

CONCLUSIONS

A study of the earthquake records of the Hollister warehouse for three successive events has been completed, and is underway for two other structures. The last event, the Loma Prieta earthquake, produced peak accelerations in the center of the diaphragm over 4 times the psuedo-static design acceleration. Based upon the available data, the following observations were made:

- In the Loma Prieta earthquake, the roof diaphragm of the Hollister warehouse showed a marked decrease in stiffness, when compared to its performance in the more moderate Morgan Hill and Hollister events. However, the degraded stiffness of the diaphragm was still several times greater than that predicted by conventional design models.

- Peak ground accelerations experienced by the Hollister warehouse in the Loma Prieta earthquake were approximately 65% of the nominal design basis of 0.4g. Diaphragm performance at this level was acceptable.

- Conventional design models for structures of this type assume dynamic amplification in the shear walls and a uniform acceleration of the diaphragm. Observed response indicates negligible amplification in the walls and significant diaphragm response and amplification. Regardless, conventional design

ppprocedures and force levels appear to provide adequate strength for the criteria earthquake.

- The method presented in UBC Standard 25-9 for computing displacement of plywood diaphragms is a poor predictor of the dynamic stiffness of these structures at working stress levels. It also appears that actual dynamic displacements during strong ground motion are substantially over-estimated. Additional data would be required to evaluate the dynamic displacements of the diaphragms at ultimate load.

LIST OF REFERENCES

1- National Research Council. Division of Earth Sciences. 1973. "The Great Alaska Earthquake of 1964." Washington, D.C.: National Academy of Sciences

2- U.S. Department of Commerce. National Oceanic and Atmospheric Administration. 1973. "San Fernando, California, Earthquake of February 9, 1971, Effects on Building Structures." Vol. 1

3- Hamburger, R.O.; McCormick, D.L.; and Hom, S.: "Performance of Tilt-Up Buildings in the October 1, 1987 Whittier Narrows Earthquake", Earthquake Spectra, Volume 4, No. 1, February 1988, Earthquake Engineering Research Institute, El Cerrito, California

4- Structural Engineers Association of California. 1973. "Recommended Lateral Force Requirements and Commentary." San Francisco, California.

5- International Conference of Building Officials. 1973. "Uniform Building Code." Whittier, California

6- Celebi M.,Bongiovanni, G. Safak, E. Brady A.G., "Seismic Response of A Large-Span Roof Diaphragm". Earthquake Spectra, Volume 5 No. 2, May, 1989. Earthquake Engineering Research Institute, El Cerrito, California

7- International Conference of Building Officials. 1988. "Uniform Building Code." Whittier, California

8- Elliot, James R. 1980. "Wood Diaphragm Testing - Past, Present, Planned". In *Proceedings of a Workshop on Design of Horizontal Wood Diaphragms*, Berkeley, Applied Technology Council.

9- International Conference of Building Officials. 1988. "Uniform Building Code Standards." Whittier, California

TABLE 1

SUMMARY OF DATA INVESTIGATED

Building	Station	Constructed	Earthquake	PGA
Hollister Warehouse	47391	1979	1984 Morgan Hill	0.06g
			1986 Hollister	0.13g
			1989 Loma Prieta	0.35g
West Valley College	58235	1971	1984 Morgan Hill	0.1g
			1989 Loma Prieta	0.53g
Milpitas 2 story	57502	1984	1988 Alum Rock	
			1989 Loma Prieta	0.14g

TABLE 2

BUILDING RESPONSE - TRANSVERSE (EAST-WEST) DIRECTION

Event	Recorded Peak Accelerations (g) Channel 8	Channel 3	Channel 4	D/C_a Ratio	D/C_v Ratio
1984 Morgan Hill	0.08	0.09	0.25	1.37	0.93
1986 Hollister	0.11	0.13	0.29	1.58	1.15
1989 Loma Prieta	0.25	0.25	0.79	4.32	2.84

Channel 8 - at grade, North wall
Channel 3 - at roof, North wall
Channel 4 - at center of roof

Code Static Design Force C = 0.183 g
Demand D = peak acceleration, Channel 4
D/C_a = the ratio of peak diaphragm acceleration to code design acceleration
D/C_v = the ratio of average peak diaphragm acceleration to code design acceleration

TABLE 3

OBSERVED CHANGE IN DIAPHRAGM STIFFNESS

Event	Predominant Frequency (hz)	Relative Stiffness
1984 Morgan Hill	1.77	1.00
1986 Hollister	1.72	0.94
1989 Loma Prieta	1.23	0.48

Relative Stiffness normalized to that observed in the 1984 Morgan Hill earthquake.

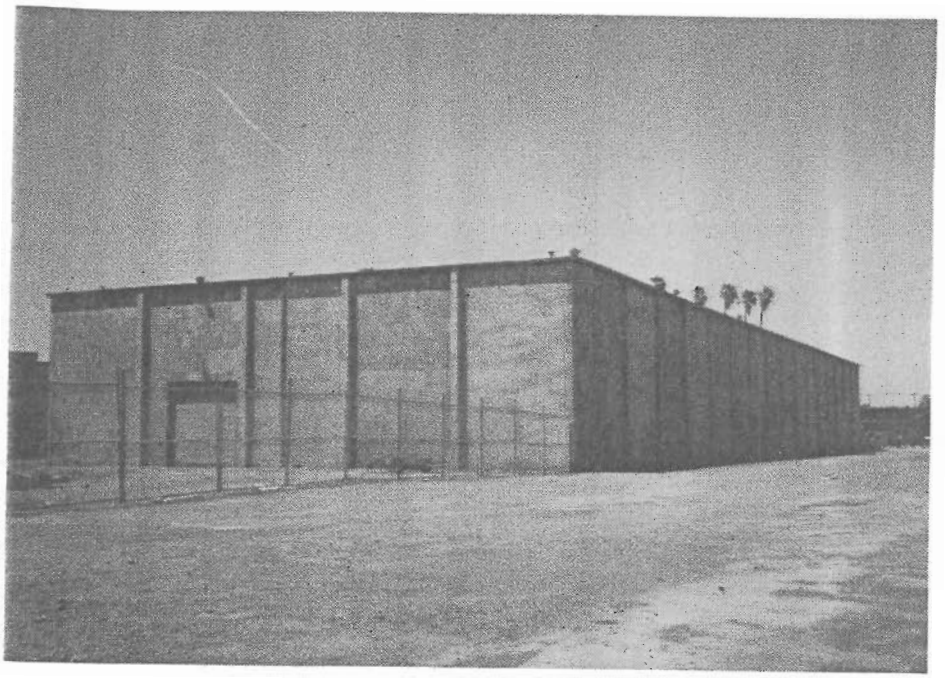

Figure 1. Hollister Warehouse

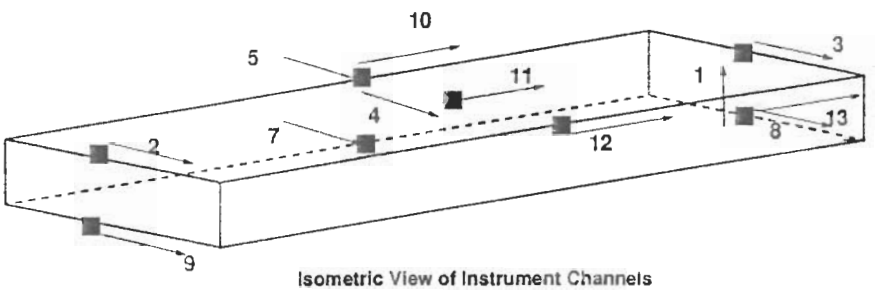

Isometric View of Instrument Channels

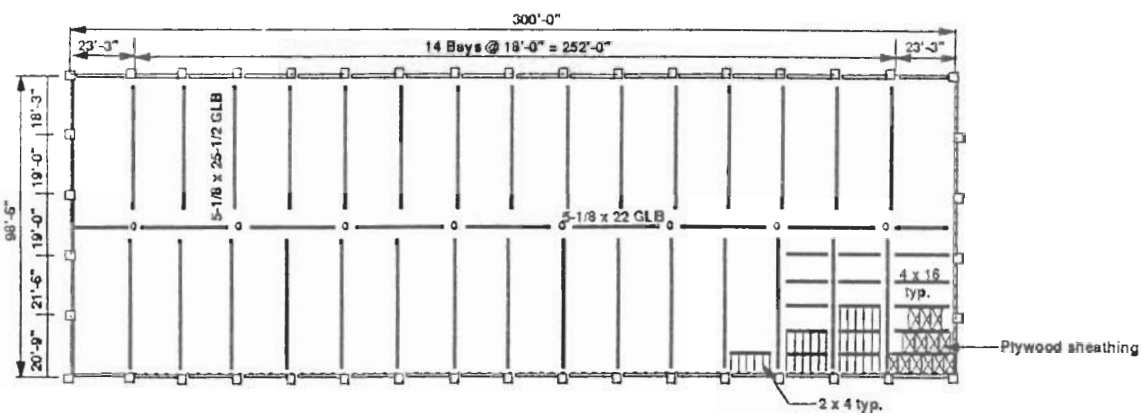

Figure 2. Hollister Warehouse, Roof Plan and Instrument Layout

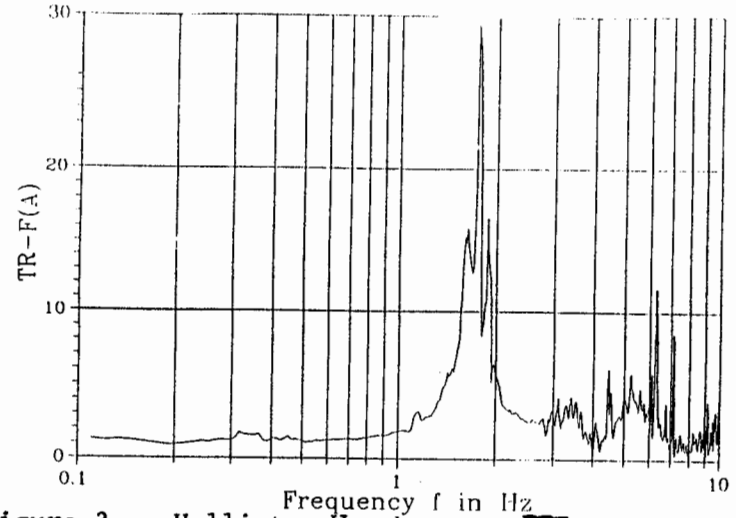

Figure 3. Hollister Warehouse - FFT(A) vs. Frequency
Morgan Hill earthquake, April 24, 1984.

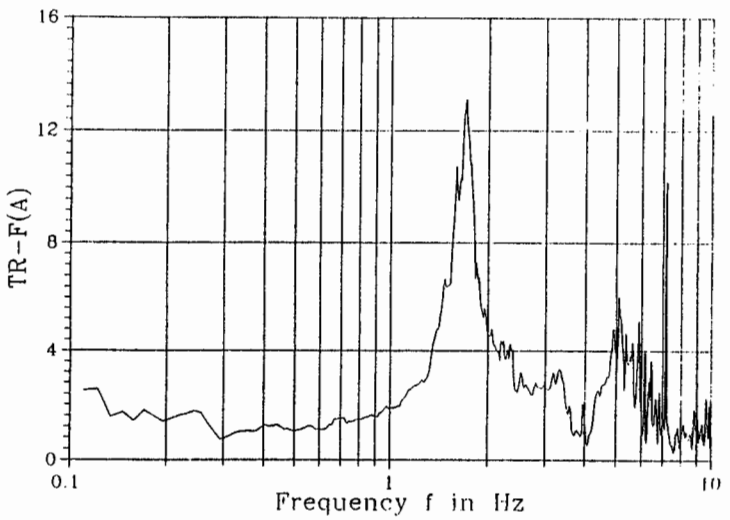

Figure 4. Hollister Warehouse - FFT(A) vs. Frequency
Hollister earthquake, January 26, 1986.

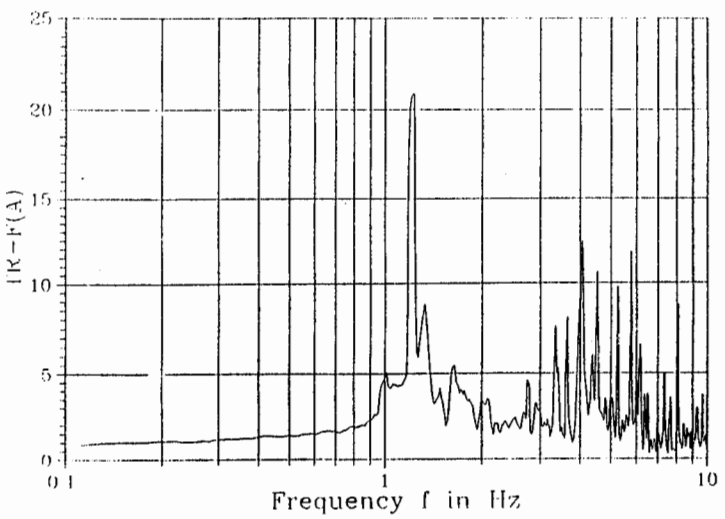

Figure 5. Hollister Warehouse - FFT(A) vs. Frequency
Loma Prieta earthquake, October 17, 1989.

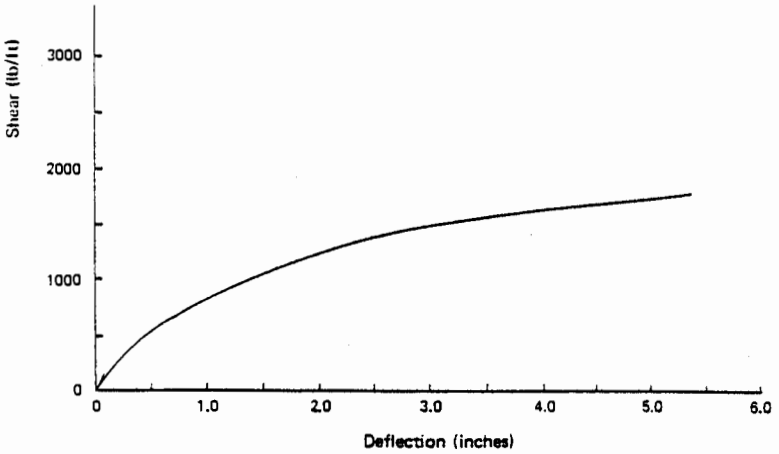

Figure 6. Shear-Deflection Plot for 1/2 inch Plywood Diaphragm. (APA)

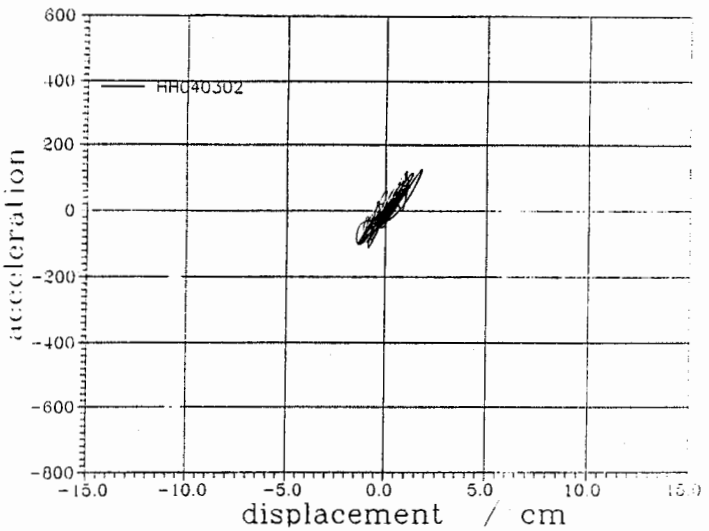

Figure 7. Acceleration vs. Displacement Hollister earthquake, January 26, 1986.

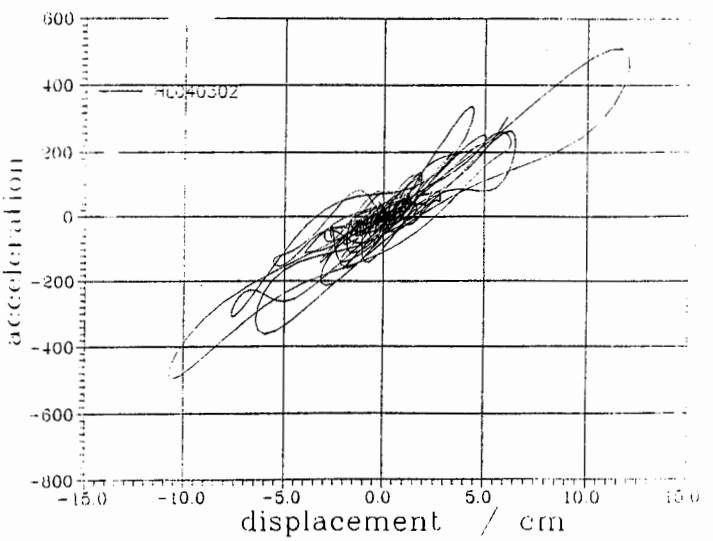

Figure 8. Acceleration vs. Displacement Loma Prieta earthquake, October 17, 1989

Evaluation of Code Accidental Torsional Provisions Using Strong Motion Records from Regular Buildings

Juan C. De la LLera
Research Assistant, U.C. Berkeley

Anil K. Chopra
Professor of Civil Engineering, U.C. Berkeley

ABSTRACT

A procedure was developed for evaluating building code provisions for accidental torsion from analysis of recorded motions of nominally symmetric-plan buildings during earthquakes. This procedure was applied to the motions of a three story office building in Richmond (CSMIP station no 58506), California recorded during the Loma Prieta earthquake. The results for this particular earthquake show that the prescribed code accidental eccentricity value of $0.05b$ predicts reasonably well the torsional effects experienced by the structure.

INTRODUCTION

Building codes require that the effects of torsion be considered by applying the equivalent lateral forces at a distance e_d from the center of rigidity (CR), resulting in story torques in addition to shears and overturning moments. The design eccentricity, e_d, specified in U.S. codes and design recommendations [1, 2] is of the form $e_d = e_s \pm 0.05b$, where e_s is the static stiffness eccentricity—i.e. the distance between the center of mass (CM) and CR— and b is the plan dimension of the building perperdicular to the direction of ground motion. The first term, e_s, is intended to account for the coupled lateral torsional response of the building arising from lack of symmetry in plan. The additional $\pm 0.05b$, known as *accidental eccentricity*, is introduced to account for eccentricities due to discrepancies between the mass, stiffness, and strength distributions used in analysis and true distributions at the time of an earthquake; torsional vibrations induced by a rotational component of ground motion; and other sources of torsion not considered explicitly in analysis.

Most of the research investigations of coupled lateral-torsional response of buildings, including the work aimed towards evaluating the adequacy of torsional provisions in building codes, have been concerned with structures with asymmetric plan. Perhaps there are two major reasons. Firstly, buildings with asymmetric floor plan tend to suffer greater damage. Secondly, the dynamics of asymmetric plan buildings are amenable to analytical study; elastic as well as inelastic systems have been investigated [3, 4, e.g].

On the other hand, the subject of accidental eccentricity is not amenable to investigation by traditional analytical approaches. Standard dynamic analyses cannot predict torsion in symmetric-plan buildings. However, it has been possible to investigate analitically the torsional response of such buildings due to rotational ground motion [5]. These studies are based on ground motion assumptions which so far have not been verified for lack of suitable ground motion records. Therefore, analysis of recorded motions of nominally-symmetric-plan buildings during earthquakes would be the most direct means of developing an understanding of the torsional responses of such buildings and for evaluation of building code provisions for accidental torsion.

BUILDING CONSIDERED

Ideal for the purposes of the investigation would be buildings with nominally symmetric floor plans, rigid floor diaphragms, and negligible soil structure interaction effects, for wich three independent components of acceleration have been recorded at the ground level and at each floor. A three-story office building in Richmond, California (CSMIP station no 58506) satisfies these requirements. Records of motions of the this building during the Loma Prieta earthquake are available.

A typical framming plan of this steel structure is shown in Figure 1. It consists of moment-resisting frames 1 and 7 in the Y-direction. Between frame lines 3 and 6, frames A and C are also designed for lateral load resistance. All other frames with semi-rigid connections are designed to carry only gravity loads.

The floor decking system is formed by a steel corrugated metal sheet filled with lightweight concrete. The roof deck is lighter but has additional insulating concrete. The foundation system consists of rectangular column footings interconnected by grade beams. In the Y-direction only footings for columns of frames 1 and 7 are inter-connected.

RECORDED MOTIONS

The locations of the accelerographs in the building are shown in Figure 2. The strong motion records obtained from the Loma Prieta earthquake are shown in Figure 3. The peak accelerations at the ground level are $0.083g$ in the X-direction and $0.11g$ in the Y-direction. These motions were amplified to $0.31g$ and $0.27g$, respectively at the roof level. The building experienced no damage during the earthquake.

The vibration frequencies and shapes of the first mode in the X-direction, the first mode in the Y-direction, and the first torsional mode were determined from the recorded motions. The results are summarized in Table 1.

STRUCTURAL IDEALIZATION

The building was idealized for analysis by the ETABS computer program, wherein floor diaphragms are assumed to be rigid and the building mass is lumped at the floor levels. The building was treated as fixed at the level defined by the slab on grade. Each frame was modeled with appropiate beam-column joints: moment resistant (or rigid) connections and semi-rigid connections. The latter were divided into two groups: connections of column flanges with beams were modeled as rigid and connections of column webs with beams as pinned.

The vibration frequencies and mode shapes of the idealized system computed by ETABS program are also presented in Table 1. The agreement between these results and the values obtained from the recorded responses is satisfactory.

DYNAMIC ECCENTRICITY

First, consider the simplest possible problem: a one-story, nominally-symmetric-plan building with a rigid roof-diaphragm with accelerations $a_1(t)$, $a_2(t)$, and $a_3(t)$ of the roof recorded during an earthquake (Figure 4). From these records, $a_x(t)$ and $a_y(t)$, the x and y acceleration components at the CM, and $a_\theta(t)$, the torsional acceleration of the diaphragm (Figure 4) can be determined. The associated lateral forces are ma_x and ma_y in the x and y directions, respectively, and the associated torque is $I_p a_\theta$, where m is the mass of the roof, and I_p is the polar moment of inertia of the distributed mass about the CM. These forces are statically equivalent to each of the following force sets: (1) ma_x at the CM and ma_y at eccentricity e_x (Figure 5) where

$$e_x(t) = I_p a_\theta(t)/ma_y(t) \tag{1}$$

and (2) ma_y at the CM and ma_x at eccentricity e_y where

$$e_y(t) = I_p a_\theta(t)/ma_x(t) \tag{2}$$

The time-dependent quantities $e_x(t)$ and $e_y(t)$ may be interpreted as the instantaneous accidental eccentricities. They can be computed from the accelerations $a_x(t)$, $a_y(t)$, and $a_\theta(t)$, determined from the recorded

motions. This approach to evaluate the accidental eccentricities is very appealing as it is based exclusively on recorded motions and does not require modeling of the structure or estimates of its stiffness properties. The only structural properties needed are the mass and polar moment of inertia of the roof.

This procedure for one-story systems can be extended to determine the accidental eccentricities for each floor of a multistory building with rigid floor diaphragms. The shears and torques in the j^{th} story can be determined by using simple statics from the floor inertia forces which are known from the floor masses and recorded accelerations.

$$V_{xj}(t) = \sum_{i=j}^{N} m_i a_{xi}(t) \tag{3}$$

$$V_{yj}(t) = \sum_{i=j}^{N} m_i a_{yi}(t) \tag{4}$$

$$T_j(t) = \sum_{i=j}^{N} I_{pi} a_{\theta i}(t) \tag{5}$$

Thus the accidental eccentricities at the j^{th} floor are defined by equations (6) and (7).

$$e_{xj}(t) = \frac{T_j(t)}{V_{yj}(t)} \tag{6}$$

$$e_{yj}(t) = \frac{T_j(t)}{V_{xj}(t)} \tag{7}$$

Required in evaluating the accidental eccentricities of a multistory building are the accelerations $a_{xi}(t)$, $a_{yi}(t)$ and $a_{\theta i}(t)$ at each floor.

From the recorded motions shown in Figure 3 these accidental eccentricities were computed for the selected building. The results for the first floor are presented in Figure 6 wherein the base shear and base torque are presented together with accidental eccentricities $e_{x1}(t)$ and $e_{y1}(t)$. These computed eccentricity values grossly exceed the code value of $0.05b$ intermittently during the earthquake. However, this result does not imply that the code provisions are deficient because the largest peaks in the eccentricity-time plot are usually associated with small values of base shear. Therefore, a large value for the accidental eccentricity by itself is not meaningful and should be considered in conjunction with the instantaneous base shear value; i.e. the combined effects of shear and torque should be considered in evaluating the code provisions.

STORY SHEARS AND TORQUE

The base shears and torque at each instant of time are given by equations (3) to (5) with $j = 1$. These forces were computed for the selected building from its floor floor masses and the recorded accelerations (Figure 3). Each point in Figure 7a represents the values of V_{x1} and T_1 at a particular instant of time, similarly V_{y1} and T_1 values are presented in Figure 7b.

According to the Uniform Building Code [6] the base shear is given by equation (8) :

$$V = \frac{ZIC}{R_w} W \tag{8}$$

For the selected building, estimates of the fundamental periods were obtained earlier from the recorded motions: $Tx = 0.59sec$ and $Ty = 0.76sec$. For analysis in the X-direction the code formula leads to a base shear of $V_{x1} = 161.2kips$, which combined with an eccentricity of $0.05b$ where $b = 77ft$, leads to a base torque $T_1 = 621kip - ft$. The code values of V_{x1} and T_1 are identified in Figure 7a; V_{y1} and T_1 are shown in Figure 7b. Only the dead weights were included in W in calculating code values of base shear.

In order to evaluate the code accidental torsional provisions, these code forces are amplified by a factor chosen to increase the base shear value to the peak value of $V_{x1}(t)$ determined from equation (3). The

amplified code values are identified in Figure 7a. Each point on the straight line AB represents a combination of base shear and torque that produces the same member force as the amplified code combination, denoted by point C (Figure 7a). In particular, point A denotes the value of base shear alone (without any torque) that produces the same member force. For the selected building the straight lines AB and $A'D'$ denote combinations of base shear and torque which produce the same bending moment (and shear force) in column 4 (Figure 1) in the first story. This is the element with the largest bending moment (and shear force) under the forces corresponding to point C. Straight lines $A'B'$ and AD denote combinations of base shear and torque which produce the same bending moment (and shear force) in column 22 (Figure 1) at the first story. The straight lines AB, AD, $A'B'$ and $A'D'$ represent "equivalent" code limits. The corresponding results for analysis in the Y-direction are presented in Figure 7b.

At a particular time instant the base shear and torque computed from the recorded motions (equations (3) to (5), represents a point on the base shear-torque diagram. A point outside the "equivalent" code region represents a combination of base shear and torque which, together with the code specified heightwise distribution of lateral forces, produces member forces in the first story column 4 wich exceed the amplified code forces associated with point C. Such a condition would suggest that the accidental eccentricities should be increased beyond the code specified value of $0.05b$. For the selected building and recorded motions all combinations of V_{y1}-T_1 and V_{x1} - T_1, except the one denoted by **a**, fall within the "equivalent" code limits (Figures 7a and 7b). This one point falls only slightly outside the "equivalent" code limit indicating that the accidental eccentricity of $0.05b$ seems satisfactory.

For the particular recorded response of this building during the Loma Prieta earthquake, the torsional effects are so small that it may not be necessary to consider accidental eccentricity at all. Figure 7 indicates that only a couple of points fall outside the "equivalent" code limit with zero accidental eccentricity.

MEMBER FORCES

Additionally, the member forces associated with the recorded motions can be compared with those resulting from the amplified code forces defined earlier. At each time instant during the earthquake, the member forces are determined by static analysis of the building , using the ETABS computer program, subjected to the floor inertia forces $m_j a_{xj}(t), m_j a_{yj}(t)$ and $I_{pj} a_{\theta j}(t)$. The results of such static analyses are plotted in Figures 8 and 9, where the shear force and bending moment in the first story columns 22 and 18 are presented. Also shown is the member force associated with the amplified code forces defined by the base shear-torque combination of point C in Figure 7. It is seen that the column 18 forces during the earthquake remain below the amplified code values. The same is true for column 22 forces, except for one peak (This peak corresponds to point **a** in Figure 7). Even at this peak the actual member force exceeds the amplified code value only slightly. Thus the accidental eccentricity of $0.05b$ seems to be satisfactory in representing the torsional response of the building during the Loma Prieta earthquake.

Also shown in Figures 8 and 9 , are the member forces associated with the amplified code forces modified for zero accidental eccentricity. These lower values are slightly exceeded for both columns only by a single peak, suggesting that the torsional response of this building during the Loma Prieta earthquake is so small that it may not be necessary to consider accidental eccentricity at all.

CONCLUSIONS

A procedure has been developed for evaluating building code provisions for accidental torsion from analysis of recorded motions of nominally symmetric-plan buildings during earthquakes. This procedure has been applied to the motions of a three story office building in Richmond, California recorded during the Loma Prieta earthquake. It is demonstrated that the code accidental eccentricity of $0.05b$ seems to be satisfactory in representing the torsional motion of this building during this particular earthquake. Furthermore it appears that the accidental eccentricity need not even be considered in this case. Because the building analyzed is almost perfectly symmetric, these conclusions may not apply to all nominally-symmetric buildings for which the code accidental eccentricity is intended.

REFERENCES

[1] Recommended Lateral Force Requirements and Tentative Commentary. Structural Engineers Association of California, 1990.

[2] Tentative Provisions for the Development of Seismic Regulations for Buildings , ATC3-06. Applied Technology Council ,Palo Alto, California, 1978.

[3] R. Hejal and A.K. Chopra. "Lateral-Torsional Coupling in Earthquake Response of Frame Buildings". *Journal of Structural Engineering, ASCE*, 15(4):852–867, April 1989.

[4] R. K. Goel. "Inelastic Seismic Response of One-Story Asymmetric-Plan Systems". Report no UCB/EERC-90/14, Earthquake Engineering Research Center, University of California, Berkeley, October 1990.

[5] N. M. Newmark and E. Rosenblueth. *Fundamentals of Earthquake Engineering.* Prentice-Hall, Inc., Englewood Cliffs, N.J., 1971.

[6] Uniform Building Code. International Conference of Building Officials (ICBO), 1988.

	X-lateral mode		Y-lateral mode		Torsional mode	
	Recorded	Computed	Recorded	Computed	Recorded	Computed
Frequency (Hz)	1.317	1.321	1.672	1.657	2.242	2.212
Mode Shape						
Floor 3	1	1	1	1	1	1
Floor 2	.75	.73	.69	.77	.73	.76
Floor 1	.46	.38	.35	.44	.42	.42

Table 1: Vibration frequencies and shapes of first three modes from recorded motions and computed using structural model

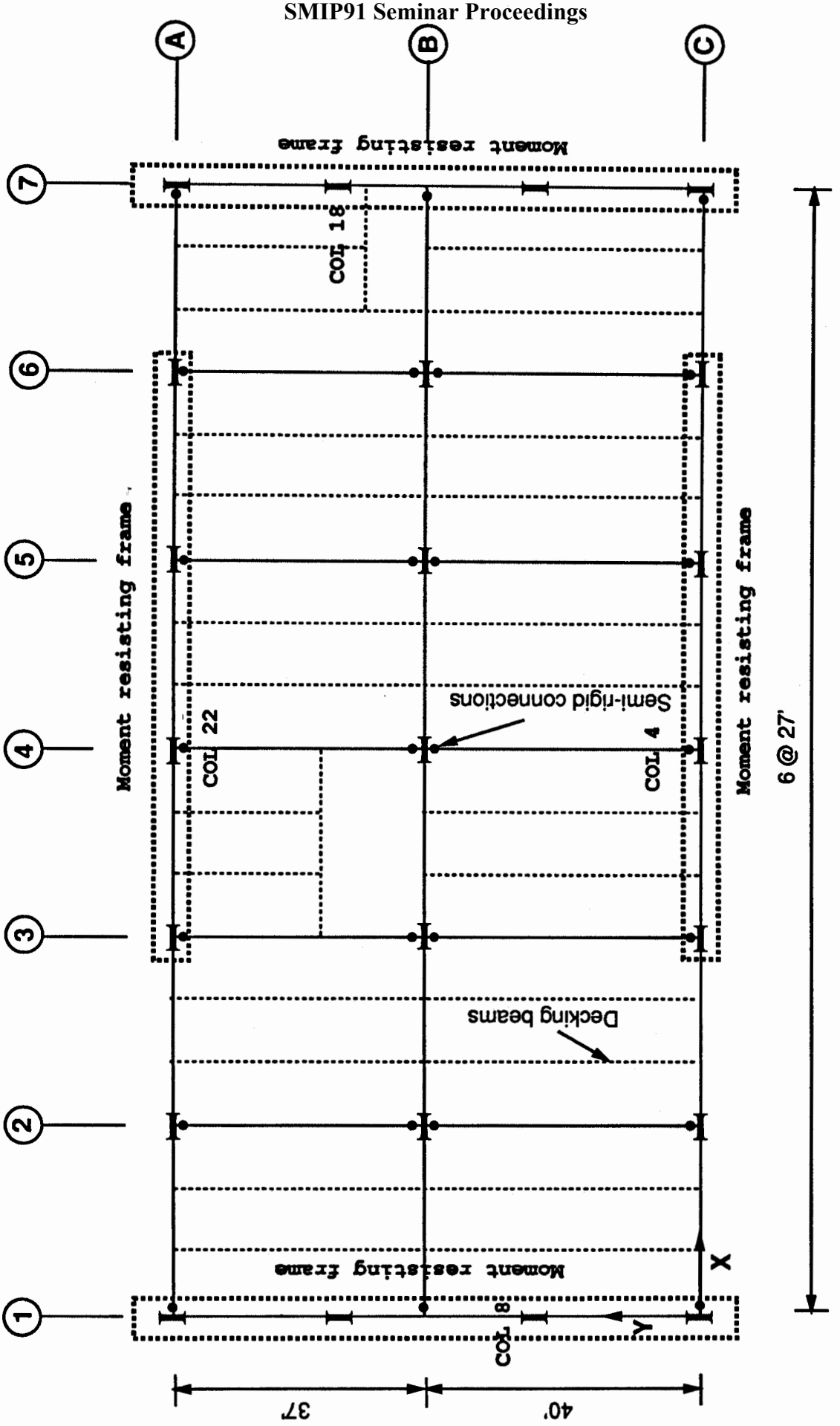

Figure 1: Framing plan

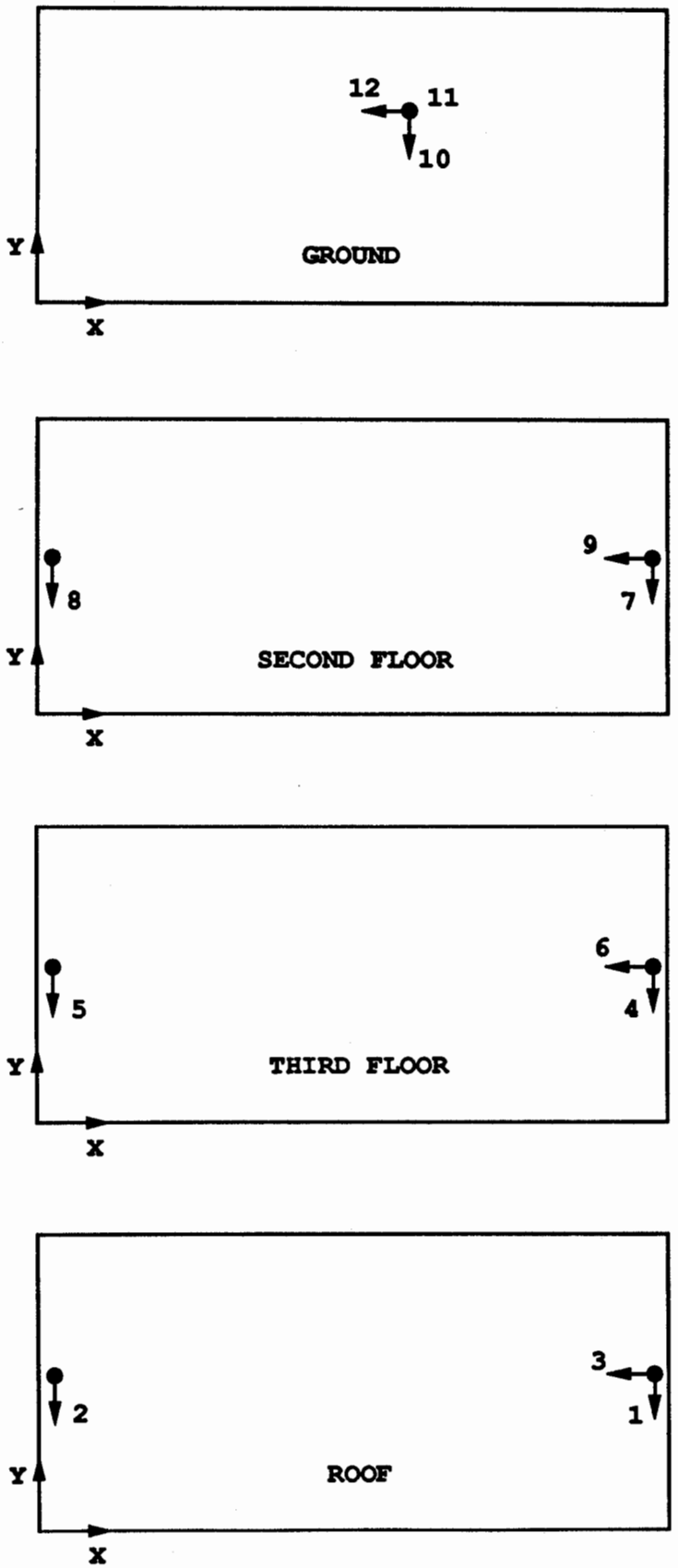

Figure 2: Instrument locations

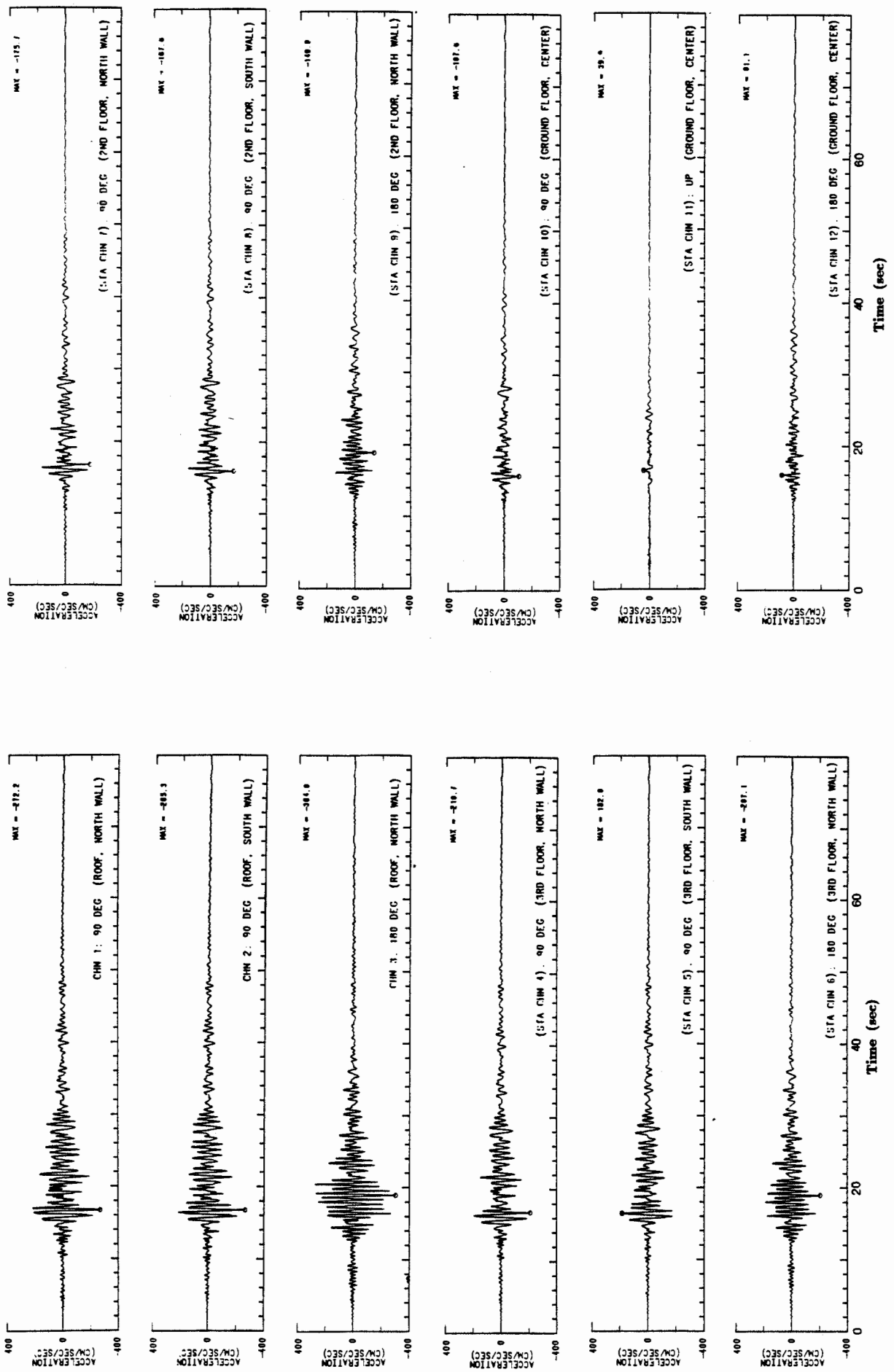

Figure 3: Recorded motions during Loma Prieta earthquake

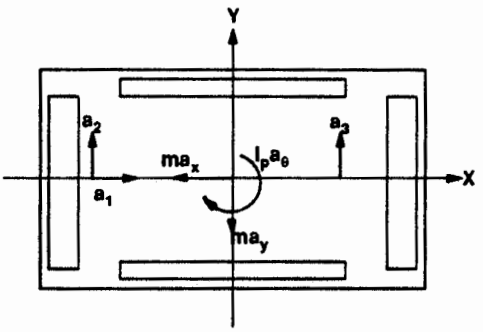

Figure 4: Recorded accelerations and floor forces

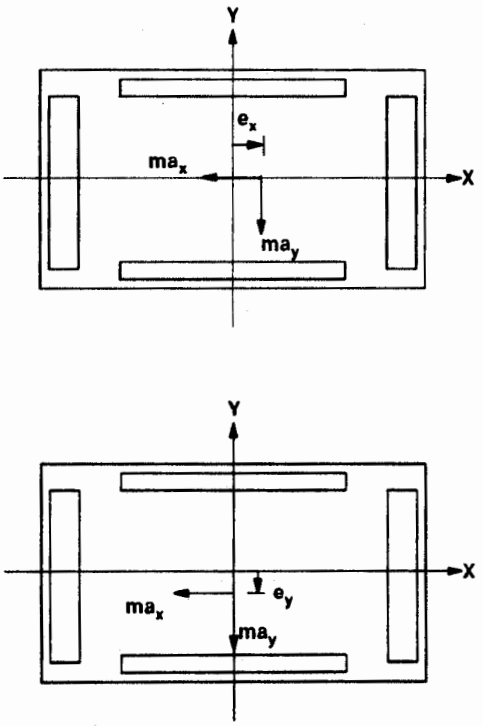

Figure 5: Accidental eccentricities, e_x and e_y

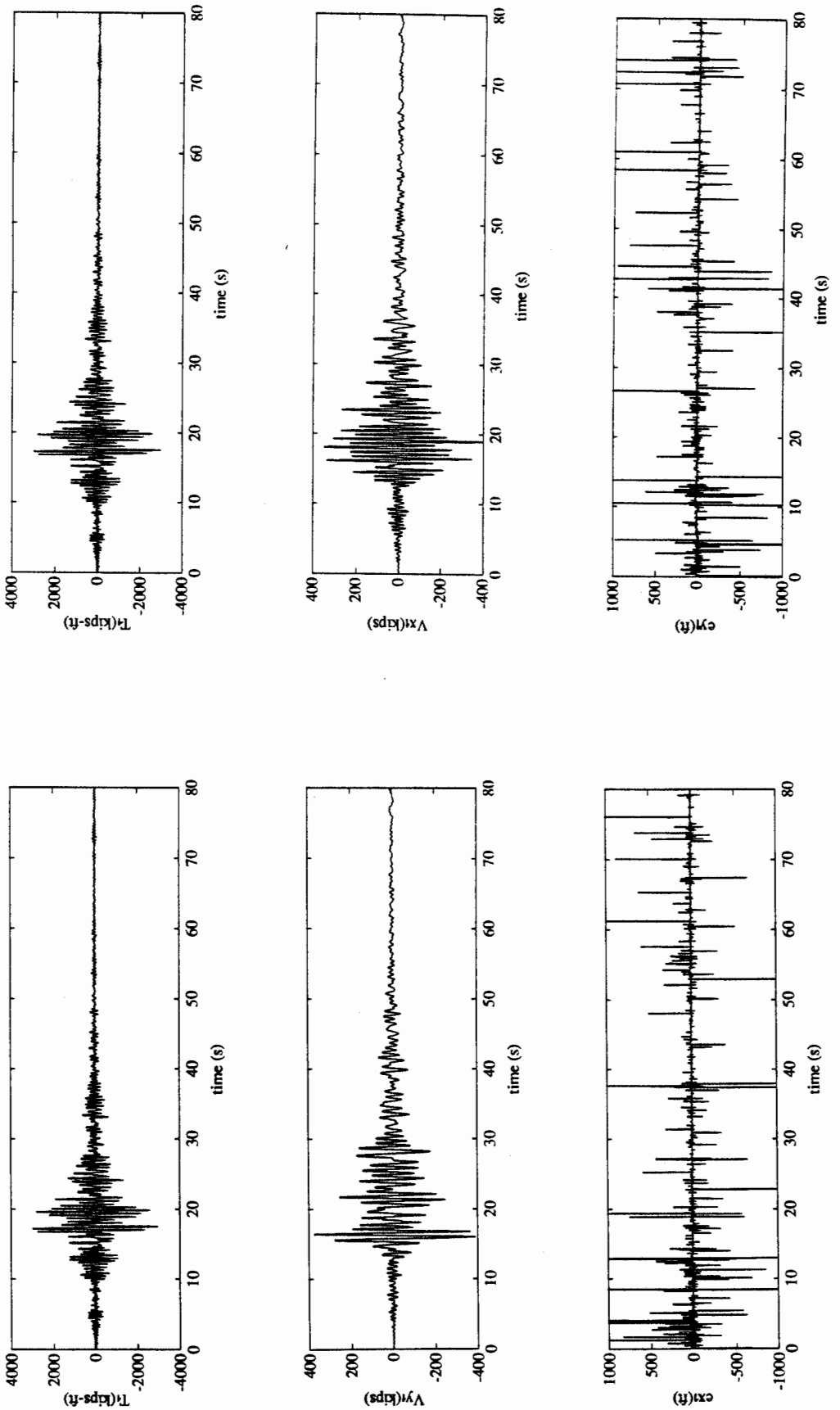

Figure 6: Base shears, base torque and first floor accidental eccentricities computed from recorded accelerations

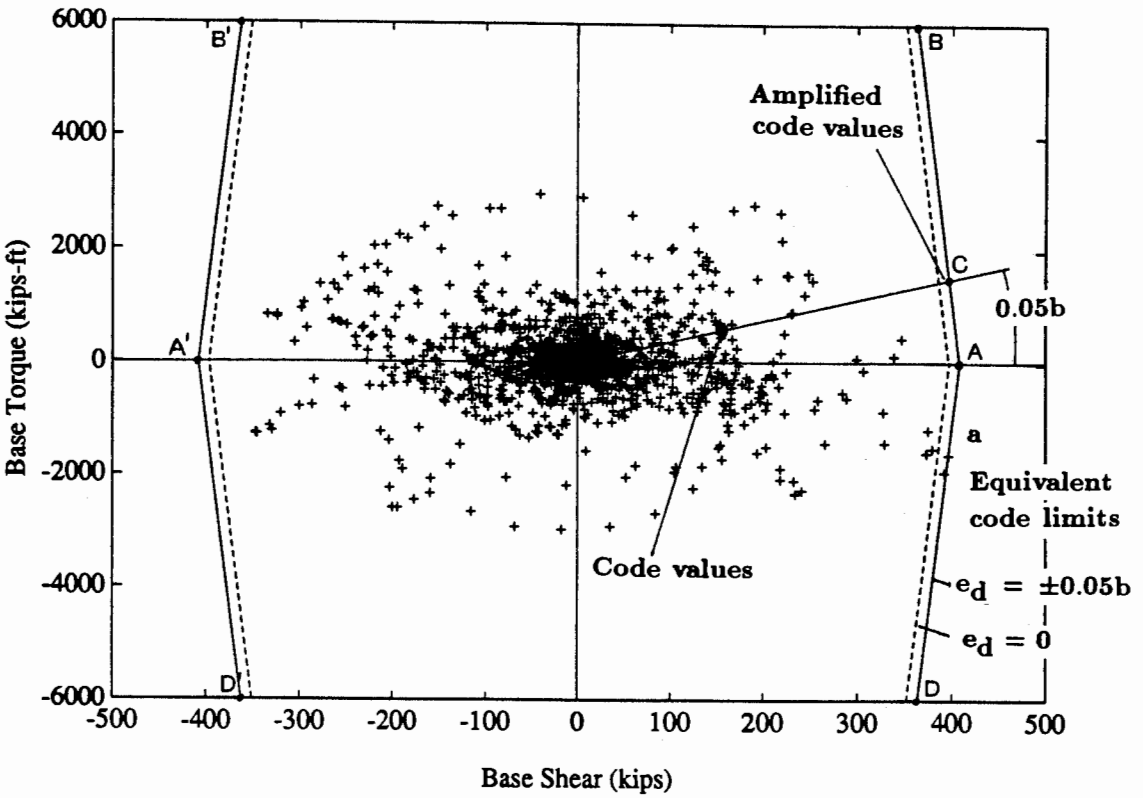

a)

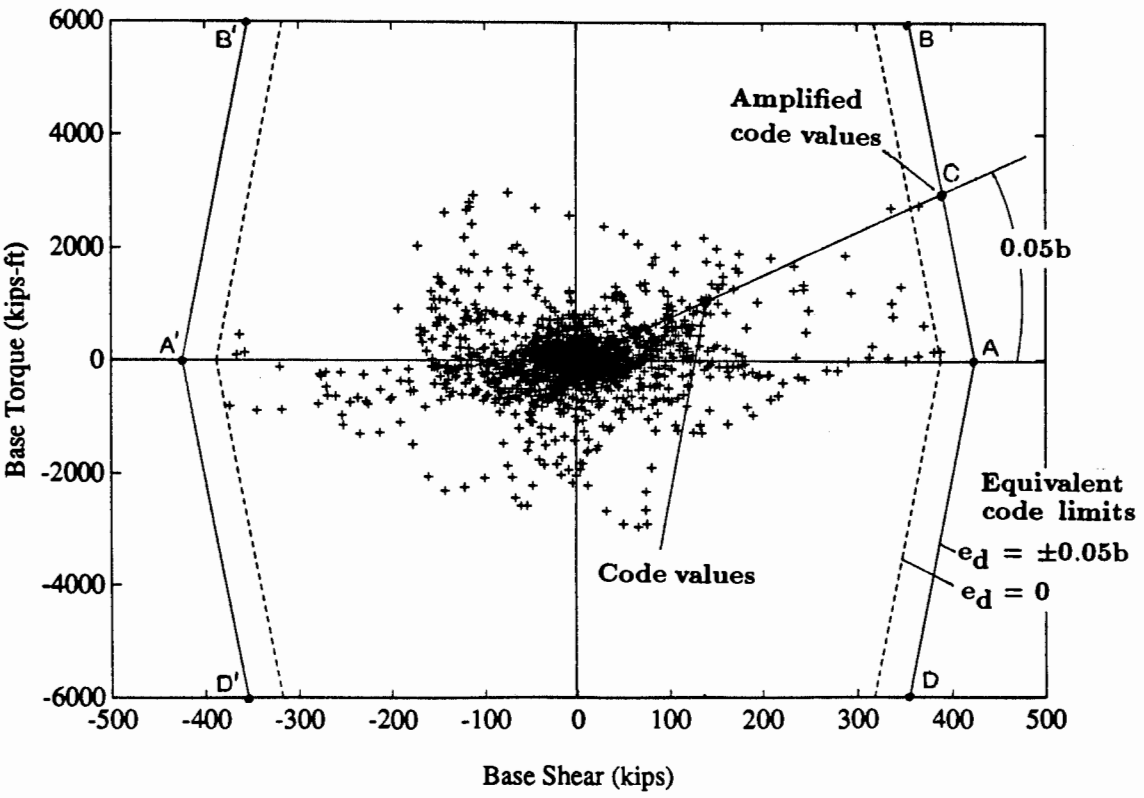

b)

Figure 7: Comparison of dynamic base shear and base torque with code values, and "equivalent" code limits

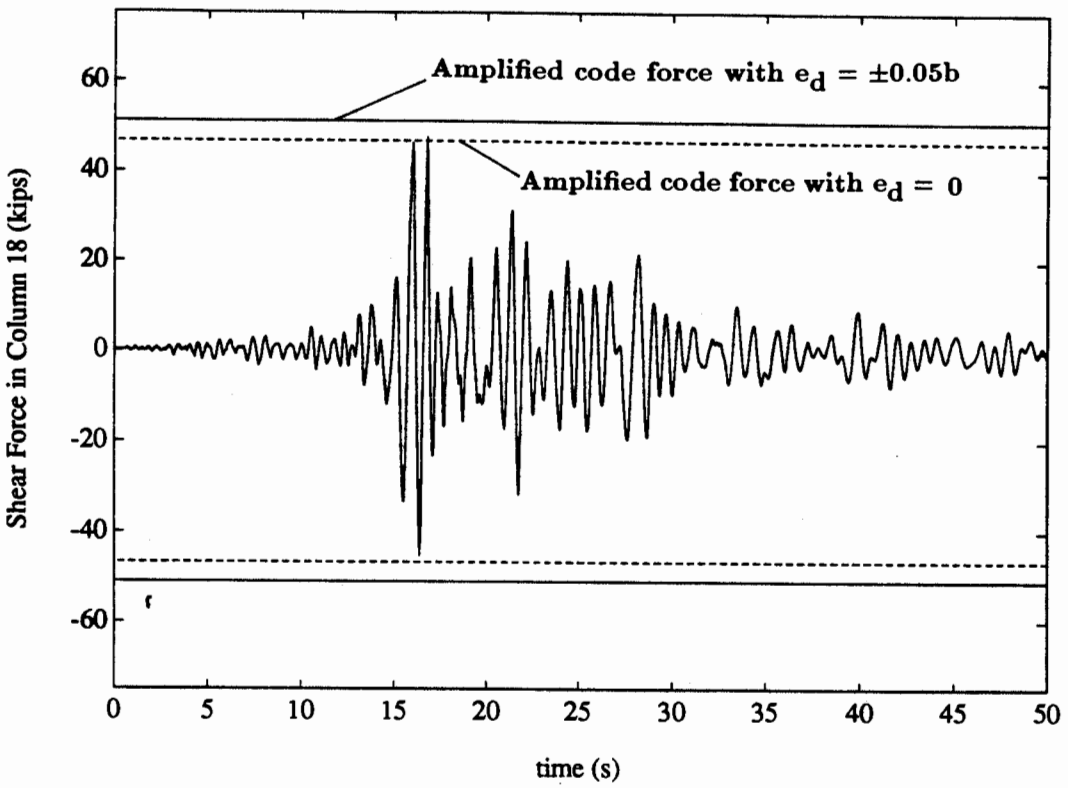

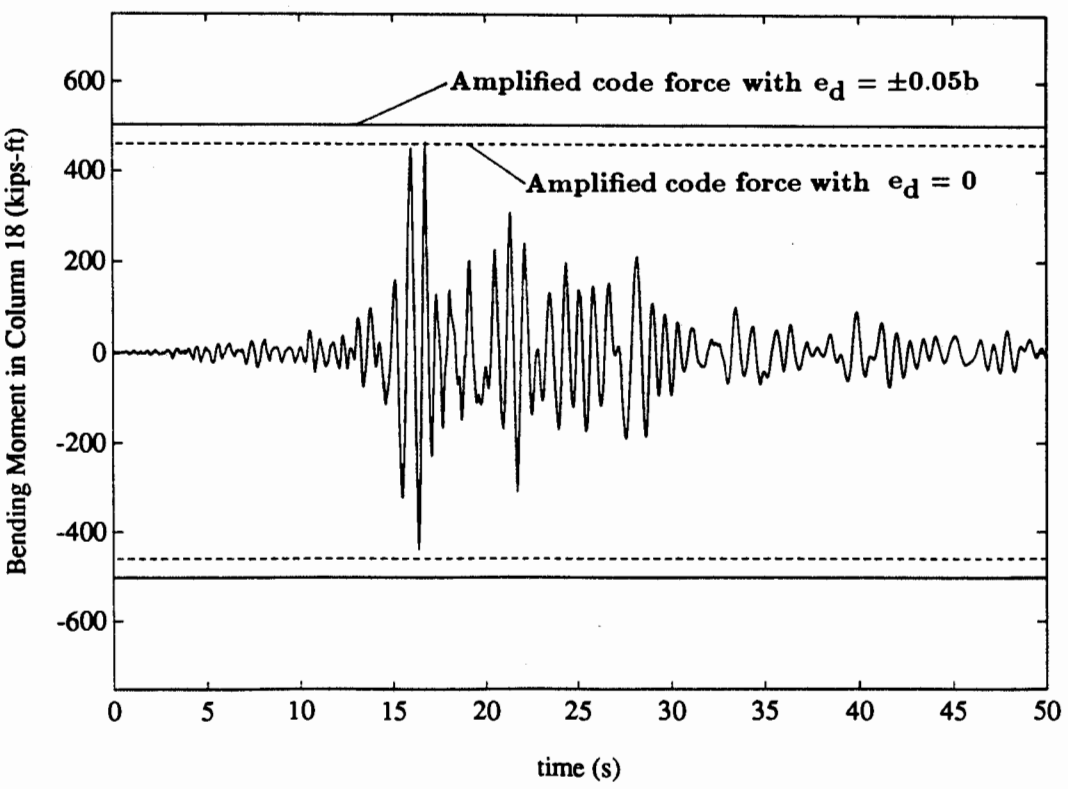

Figure 8: Comparison of earthquake-induced forces in column 18 with amplified code values

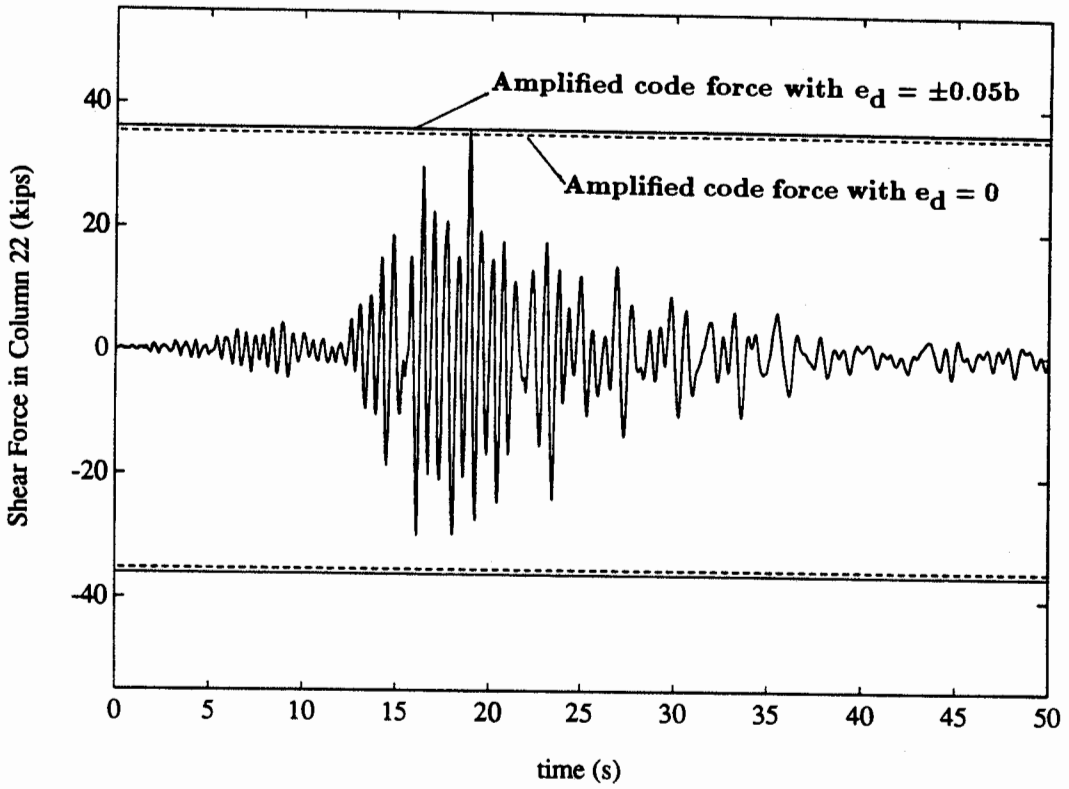

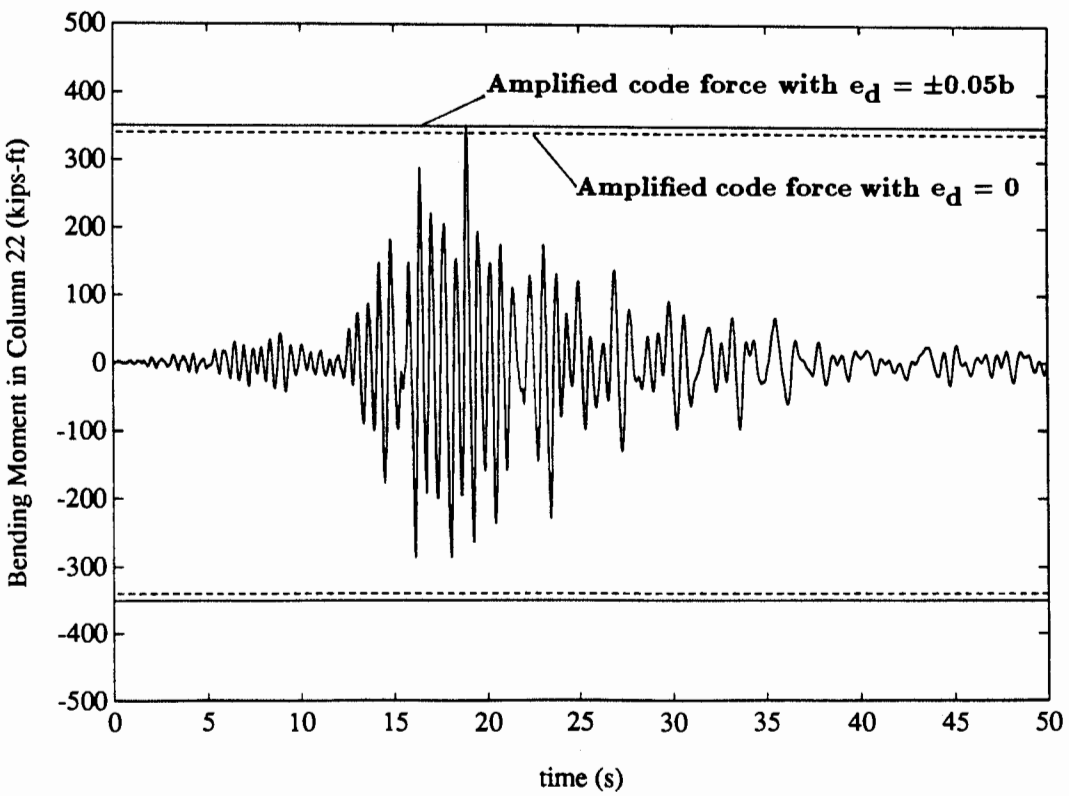

Figure 9: Comparison of earthquake-induced forces in column 22 with amplified code values

TORSIONAL RESPONSE CHARACTERISTICS OF REGULAR BUILDINGS UNDER DIFFERENT SEISMIC EXCITATION LEVELS

Hassan Sedarat[1], Sunil Gupta[2], Stuart D. Werner[2]

ABSTRACT

Torsional response characteristics of three regular buildings in San Jose and one in Watsonville, California, were studied by analyzing the strong motion records from three recent earthquakes: 1989 Loma Prieta, 1986 Mt. Lewis, and 1984 Morgan Hill. The story shear forces, torsional moments and dynamic eccentricities for these buildings during the three earthquakes were obtained from an analysis of the recorded motions. The fundamental period of vibrations and damping ratios for these buildings were also estimated for the three earthquakes. These results were then compared with the provisions of the 1988 Uniform Building Code. This comparison indicates that the provisions of the UBC may not realistically account for the torsional response of buildings during earthquakes.

INTRODUCTION

The real response of buildings to ground motion excitations can, in general, be affected by the coupling of translational vibrations with rotational vibrations. This coupling may occur because of several reasons, such as the presence of static eccentricity due to unsymmetrical distribution of mass and/or stiffness in the plan, and/or accidental eccentricity due to factors such as non-uniform ground motions across the foundation of the structure, torsional components in the ground motions, and detailing of non-structural components, etc. Recent research [1,2,3] on the analytical response of one-story idealized structures indicates that the lateral-torsional response of a structure during earthquakes can be much larger than what can be estimated by linear elastic static analysis. This is mainly due to the dynamic amplification of eccentricity during strong ground shaking. This dynamic amplification can be more pronounced for structures with small static eccentricities, i.e., for regular structures. The current provisions 1988 UBC to account for torsional effects in regular buildings can, therefore, sometimes be unconservative.

The objective of this investigation is to analyze strong motions recorded in regular buildings during past earthquakes to study their torsional response characteristics. In this investigation, the distribution of shear forces, torsional moments and dynamic eccentricities over the height of the selected buildings has been estimated for three different levels of excitation during the 1989 Loma Prieta, 1986 Mt. Lewis, and the 1984 Morgan Hill earthquakes. The fundamental period of vibration and damping ratios are also estimated from the recorded motions. These response quantities are then compared with the provisions of the 1988 Uniform Building Code (UBC).

---

[1]Staff Engineer, Dames & Moore, San Francisco, CA
[2]Associate, Dames & Moore, San Francisco, CA

DESCRIPTION OF BUILDINGS AND STRONG MOTIONS STUDIED

Four regular buildings in the San Jose and Watsonville area were selected for this study. These buildings are: 10-story residential, 10-story commercial, and 13-story government buildings, all in San Jose; and a 4-story telephone building in Watsonville. The basic structural features, and the motions recorded in these buildings during the Loma Prieta, Mt. Lewis, and Morgan Hill earthquakes are summarized in Table 1.

TABLE 1 - SUMMARY OF RECORDED MOTIONS IN SELECTED BUILDINGS

Bldg. Location (and type)	CSMIP Station Number	Stories	Lateral Force System	Peak Acceleration, g					
				Loma Prieta Earthquake (1989)		Mt. Lewis Earthquake (1986)		Morgan Hill Earthquake (1984)	
				Base	Roof	Base	Roof	Base	Roof
San Jose (Residential)	57356	10	SW	0.13	0.37	0.04	0.12	0.06	0.22
San Jose (Commercial)	57355	10	SW/MRCF	0.11	0.39	0.04	0.08	0.06	0.22
Watsonville (Telephone)	47459	4	SW	0.66	1.24	N.A.	N.A.	0.11	0.33
San Jose (Government)	57357	13	MRSF	0.11	0.36	0.04	0.32	0.04	0.17

Notes: SW = Reinforced Concrete Shear Wall; MRSF = Moment Resisting Steel Frame; MRCF = Moment Resisting Concrete Frame; N.A. = Not Available

The selected buildings represent different types of structural systems. The configurations of these buildings and the location of their lateral loads resisting elements is fairly regular, except for the 4-story building which has significant static eccentricity due to non-symmetric location of shear walls. The selected buildings have relatively rigid in-plane floor diaphragms and all are relatively well instrumented to allow estimation of the torsional accelerations and their distribution over the height of the structure.

METHODOLOGY

The following methodology was used for each building:

Step 1: From the information shown on the structural drawings for the buildings provided by the CDMG, the mass, location of the center of mass (CM), the radius of gyration, and the mass moment of inertia for each floor of each building were computed. Relative floor stiffness and the location of the center of stiffness (CS) for each floor were obtained by simplified hand calculations.

Step 2: The acceleration time-histories at those floors that were not instrumented were obtained by interpolation using 2nd order polynomial functions. From the translational accelerations at the two ends of the floor diaphragm, the rotational and translational acceleration time-histories in the transverse direction of the building were then calculated at the center of mass of each floor by assuming rigid floor diaphragm behavior. These were used to calculate

the coupled shear force time-histories at the CM and the torsional moment time-histories about the CS for each floor.

Step 3: In this step, the fundamental period of vibrations, mode shapes and the damping ratios for the buildings were estimated. For this purpose, a transfer function was computed as the ratio of the Fourier amplitude spectrum (FAS) of the roof motions to the FAS of the corresponding ground motions. The FAS transfer functions exhibited well defined peaks. The fundamental frequency of vibration in the transverse direction of the building was taken as the frequency at the location of the first peak and the damping ratio was estimated by applying the half-power method to that peak. The fundamental mode shape was taken as the deflected shape of the building at the instant of peak roof acceleration.

Step 4: The estimated fundamental periods, damping ratios, and mode shapes were used to compute the spectral accelerations and uncoupled lateral forces by assuming a fundamental mode response. In this, the spectral accelerations and story shear forces at each floor are a function of the modal damping ratios estimated under Step 3 using the half power method which, as discussed later in this paper, are probably not fully reliable. For this reason, the spectral accelerations and lateral forces were estimated for a range of different damping ratios (2%, 5%, and 10%). The total dynamic eccentricity at each floor was then obtained by dividing the torsional moment about the CS calculated in Step 3 by the story shear obtained from the uncoupled lateral forces.

Step 5: The design shear forces and the torsional moments were calculated using the provisions of the 1988 UBC. Since the buildings selected are fairly regular and under 240 feet in height, the static force procedure of the UBC was used for these computations. These values were then compared with those obtained for the three earthquakes from Step 1 to 4 above. The ratios of the total dynamic eccentricity as obtained in Step 4, to the total design eccentricity as prescribed by the UBC were also obtained.

The processed data from the Loma Prieta earthquake for the 13-story government building was not available until very recently. Therefore, the analysis of this building for the Loma Prieta earthquake could not be completed at the writing of this paper.

DISCUSSION OF RESULTS

Fundamental Period of Vibration: The fundamental periods of vibration for the four buildings as obtained from the FAS transfer functions are summarized in Table 2 for the three earthquakes. This table also shows the building periods as obtained from Method A in the 1988 UBC. These results indicate that, except for the 13-story government building, the building periods predicted by UBC are 25% to 100% higher than the periods estimated from the recorded motions. This discrepancy was higher for the stiffer 4-story building. This suggests that the UBC equation for period calculation may sometimes be unconservative when used to calculate earthquake design forces using the static force procedure. For the 13-story building, the periods estimated from recorded motions were actually 100% higher than those given by UBC. These results also show lengthening of periods for the Loma Prieta earthquake, indicating that the buildings probably experienced some inelastic deformations during the Loma Prieta earthquake. The periods obtained here also compared well with those from previous studies [4], including those utilizing more sophisticated system identification methods [5].

TABLE 2 - FUNDAMENTAL PERIOD OF BUILDINGS

EARTHQUAKE	PERIOD (Seconds)			
	10-story Residential Building (E.W.)	10-story Commercial Building (E.W.)	4-story Telephone Building (N.S.)	13-story Government Building (E.W.)
Loma Prieta	0.45	0.7	0.22	--
Mt. Lewis	0.42	0.6	N.A.	2.2
Morgan Hill	0.42	0.6	0.21	2.2
UBC 88	0.61	0.74	0.46	1.01

Damping Ratios: Table 3 summarizes the damping ratios obtained by applying the half-power bandwidth method to the FAS transfer functions. For each building, two damping ratios, corresponding to FAS transfer functions for the motions recorded at the two ends of the diaphragm, were obtained. A large variation in the damping ratio so obtained was observed. The damping ratios for the 10-story residential and commercial buildings also did not agree well with those obtained for these buildings from system identification methods [5]. This suggests some inherent limitations in the half-power method. The unreliability of half-power method for estimating damping may stem from several factors, such as: the presence of noise in the measured response; representation of complex energy dissipation phenomena with a simplified viscous damping ratio; the representation of actual nonlinear behavior with linear behavior; and, for some structures, closely spaced modes. Some of these difficulties in the use of half-power method have been pointed out by Beck and Beck [6].

TABLE 3 - DAMPING RATIO FOR BUILDINGS

EARTHQUAKE	DAMPING (%)			
	10-story Residential Building (E.W.)	10-story Commercial Building (E.W.)	4-story Telephone Building (N.S.)	13-story Government Building (E.W.)
Loma Prieta	3.7 to 9.8	4.1 to 4.6	7 to 11	--
Mt. Lewis	5.5 to 8.0	2.6 to 3.3	N.A.	3.4 to 4.7
Morgan Hill	2.1 to 2.8	2.4 to 2.6	5.1 to 13.9	4.3

Shear Forces: From the time-histories of the story shear forces the maximum shear forces over the height of all four buildings were obtained. These are shown in Figure 1. It can be observed that the maximum base shear experienced by the 10-story Residential building during the Loma Prieta earthquake was about 15% larger than the UBC base shear, whereas, for the Mt. Lewis and Morgan Hill earthquakes, it was about 62% and 32% smaller than the 1988 UBC base shear. For the 10-story Commercial building, the total base shear experienced during the Loma Prieta earthquake was about 59% larger than the UBC base shear. For the Mt. Lewis earthquake the total base shear was about 64% smaller than the UBC base shear, while for the Morgan Hill earthquake it was approximately on the same order as the UBC base shear. For the 4-story Telephone building, the total base shear during the Loma Prieta earthquake was observed to be about 144% larger than

the UBC base shear, while during the Morgan Hill earthquake the total base shear was about 29% smaller than the UBC base shear. For the 13-story government building the total base shear forces during the Mt. Lewis and Morgan Hill earthquakes were 38% and 18%, respectively, smaller than the UBC base shear.

Torsional Moments: The variation of maximum torsional moments over the height of the three buildings as obtained from the time-histories for the torsional moments is shown in Figure 2. This figure shows that for the 10-story residential and commercial buildings and the 4-story telephone building, the torsional moments during Mt. Lewis and Morgan Hill earthquakes are smaller than those obtained by using 1988 UBC and are larger for the Loma Prieta earthquake. For the 13-story government building, however, the maximum story torsional moments during the Mt. Lewis and Morgan Hill earthquakes were larger than the UBC torsional moments, even though the maximum story shears during these earthquakes were smaller than the UBC story shears. This interesting observation indicates that there is a large amplification in the eccentricity in this building and may be indicative of strong torsional coupling which probably led to the unusually long duration of response recorded in this building during the past three earthquakes. The ratio of the base torsional moments experienced by the buildings during the earthquakes to those obtained from UBC are summarized in the Table 4.

TABLE 4 - RATIO OF COMPUTED EARTHQUAKE TO UBC BASE TORSIONAL MOMENTS

Building / Earthquake	10-Story Residential	10-Story Commercial	4-Story Telephone	13-Story Government
Loma Prieta	1.15	1.64	1.98	---
Mt. Lewis	0.52	0.49	---	1.30
Morgan Hill	0.74	1.00	0.61	1.65

Dynamic Eccentricities: As explained earlier, it was difficult to obtain the real damping ratios for the buildings. Therefore, the total dynamic eccentricities were calculated for a range of damping ratios: 2%, 5%, and 10%. The total dynamic eccentricities, as obtained from the analysis of the recorded motions, include both the dynamic eccentricity and the accidental eccentricity. The total dynamic eccentricities obtained here were compared with the total UBC design eccentricities, which in turn consist of static eccentricity and the 5% accidental eccentricity. The ratios of the total dynamic eccentricity for different damping ratios to the UBC design eccentricity were also calculated over the height of each building during the three ground motions and are shown in Figure 3.

From Figure 3 it can be observed that the maximum amplification of eccentricity occurs in the first story. The ratios of total dynamic eccentricity to the total UBC design eccentricity in the first story of each building during the three earthquakes are summarized in Table 5.

TABLE 5 - RATIO OF FIRST STORY TOTAL DYNAMIC ECCENTRICITY TO THE UBC DESIGN ECCENTRICITY

Building	10-story Residential			10-story Commercial			4-story Telephone			13-story Government		
Earthquake	2%	5%	10%	2%	5%	10%	2%	5%	10%	2%	5%	10%
Loma Prieta	0.98	1.07	1.18	0.92	1.06	1.14	0.53	0.71	0.95	--	--	--
Mt. Lewis	1.21	1.50	1.77	1.57	1.62	1.84	N.A.	N.A.	N.A.	2.14	2.57	3.39
Morgan Hill	1.13	1.25	1.41	0.99	1.07	1.16	0.53	0.66	0.79	1.50	2.28	3.54

The information presented in Figure 3 and Table 5 shows that the total dynamic eccentricity for the buildings during the earthquakes is generally larger than the total design eccentricity from 1988 UBC. This is especially true for regular buildings with small static eccentricities. Only for the 4-story building, which has a high static eccentricity, was the UBC prescribed total eccentricity observed to be larger than the total dynamic eccentricity. This observation is consistent with the results obtained from analytical studies of idealized one-story structures [2,3]. The amplification in the eccentricity was observed to be especially pronounced for the 13-story government building which may indicate that this building experienced severe torsion during the past earthquakes which would not be realistically estimated by the UBC requirements.

CONCLUSIONS AND RECOMMENDATIONS

The CSMIP directed research program for the analysis of strong motions recorded in structures has provided a unique opportunity to investigate the actual behavior of buildings during earthquakes, and to assess the adequacy of current analytical methods and Code design provisions. The present investigation was undertaken to study the torsional response of four regular buildings by analyzing the strong motions recorded during the 1989 Loma Prieta, 1986 Mt. Lewis, and 1984 Morgan Hill earthquakes and to compare them with the provisions of 1988 UBC. The primary observations from this investigation are summarized below:

1. The transfer functions of the Fourier amplitude spectra of the recorded building motions can be used to obtain realistic estimates of fundamental building period. It is observed that the building periods obtained using Method A of the UBC may sometimes be unconservative, especially for stiffer buildings, when used to calculate earthquake design forces using static force procedure. CDMG's Strong Motion Instrumentation Program has resulted in a significant data base of recorded motions in different types of building structures which may be used to make a more comprehensive assessment of the adequacy of the current provisions in the UBC for the estimation of fundamental building periods.
2. The real damping in structures cannot be accurately and reliably predicted using the half power method. This may be due to the representations of complex energy dissipation phenomenon with a simplified viscous damping ratio, noise in the recorded motions, and, for some structures, closely spaced modes.
3. The maximum shear forces estimated in the buildings for the Loma Prieta Earthquake were generally higher than the UBC prescribed shear forces. The

maximum shear forces in the buildings during the Mt. Lewis and Morgan Hill earthquakes were generally smaller than the UBC shear forces.

4. The torsional moments during the Loma Prieta earthquake were higher than the UBC prescribed torsional moments for all buildings. For the Mt. Lewis and Morgan Hill earthquakes, the actual torsional moments in the 10-story residential, 10-story commercial, and 4-story telephone buildings were smaller than the UBC. For the 13-story government building, the moments during these two earthquakes were larger than those obtained from UBC even though the earthquake shear forces were smaller than the UBC shear forces.
5. The total dynamic eccentricities as obtained from the analysis of recorded motions were larger than the total design eccentricities given by the UBC for all buildings except for the 4-story telephone building. For 5% damping ratio, this increase in eccentricity ranged from 5% to 60% for the 10-story residential and commercial buildings. The increase was especially pronounced for the 13-story government building and was on the order of 150%. This amplification of eccentricities is most likely due to lateral-torsional coupling and is consistent with the observations from previous analytical studies. Many building codes, such as Mexican and Canadian, have recognized this amplification of eccentricity by requiring that the computed static eccentricity be multiplied by a factor of 1.5. An amplification of static eccentricity by using the response spectrum amplification factors has also been suggested by Newmark and Hall [7]. In the light of these observations, the provisions of the current UBC, which do not require an amplification in the static eccentricities, may require further evaluation by performing a more comprehensive study of the recorded building motions.

REFERENCES

1. H. Sedarat, V.V. Bertero, "Effects of Torsion on the Linear and Nonlinear Seismic Response of Structures," Report No. UCB/EERC-90/12, Earthquake Engineering Research Center, University of California, Berkeley, September 1990.
2. R. Hejal, A.K. Chopra, "Earthquake Response of Torsionally-Coupled Buildings," Report No. UCB/EERC-87/20, Earthquake Engineering Research Center, University of California, Berkeley, 1987.
3. W.K. Tso, Dempsey, "Seismic Torsional Provisions for Dynamic Eccentricity," Earthquake Engineering and Structural Dynamics, Vol. 8, pp. 275-289 (1980).
4. R.L. Boroschek, S.A. Mahin, C.A. Zeris, "Seismic Response and Analytical Modeling of Three Instrumented Buildings," Proceedings of Fourth U.S. National Conference on Earthquake Engineering, pp. 219-228, Volume 2, May 20-24, 1990, Palm Springs, California.
5. S.D. Werner, A. Nisar, and J.L. Beck, "Assessment of Seismic Design Code provisions for Buildings Using Recorded Earthquake Motions" (to be published).
6. R.T. Beck, J.L. Beck, "Comparison Between Transfer Function and Modal Minimization Methods for System Identification," Report No. EERL 85-06, Earthquake Engineering Research Laboratory, California Institute of Technology, Pasadena, California, November 1985.
7. N.M. Newmark and N.J. Hall, "Earthquake Spectra and Design," Earthquake Engineering Research Institute Monograph.

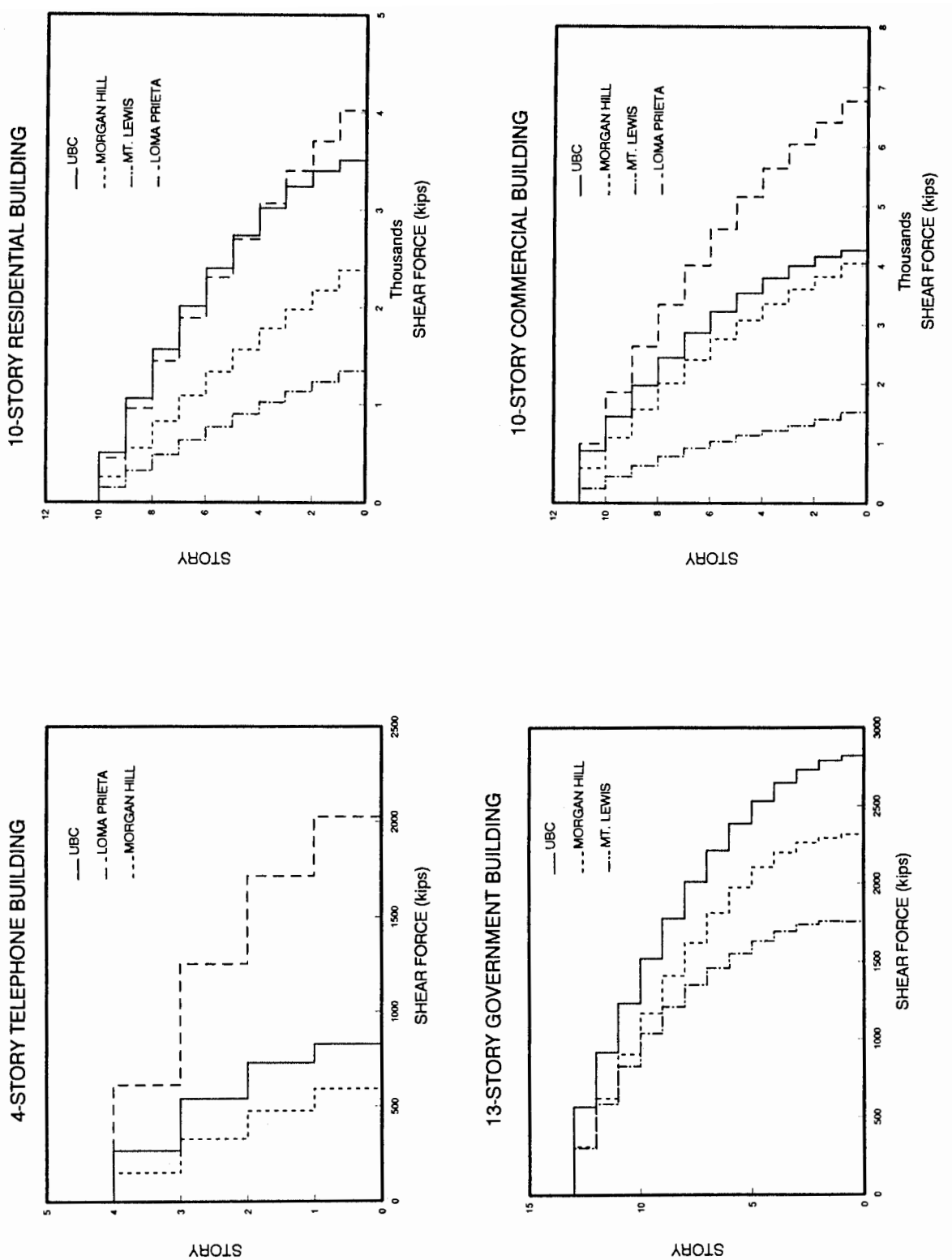

Figure 1: Variation of the Maximum Shear Forces Over the Height of the Buildings

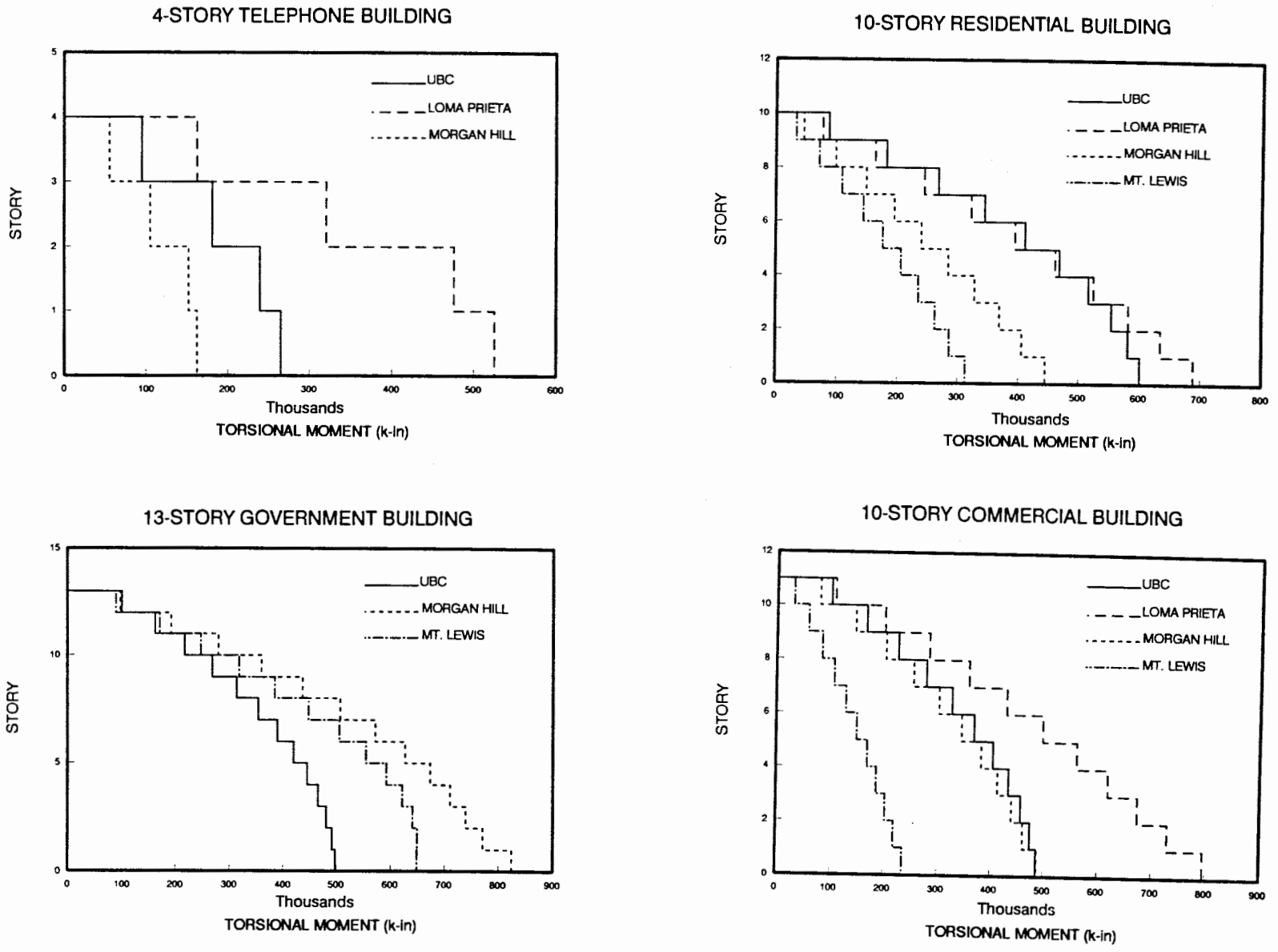

Figure 2: Variation of the Maximum Torsional Moments Over the Height of the Buildings

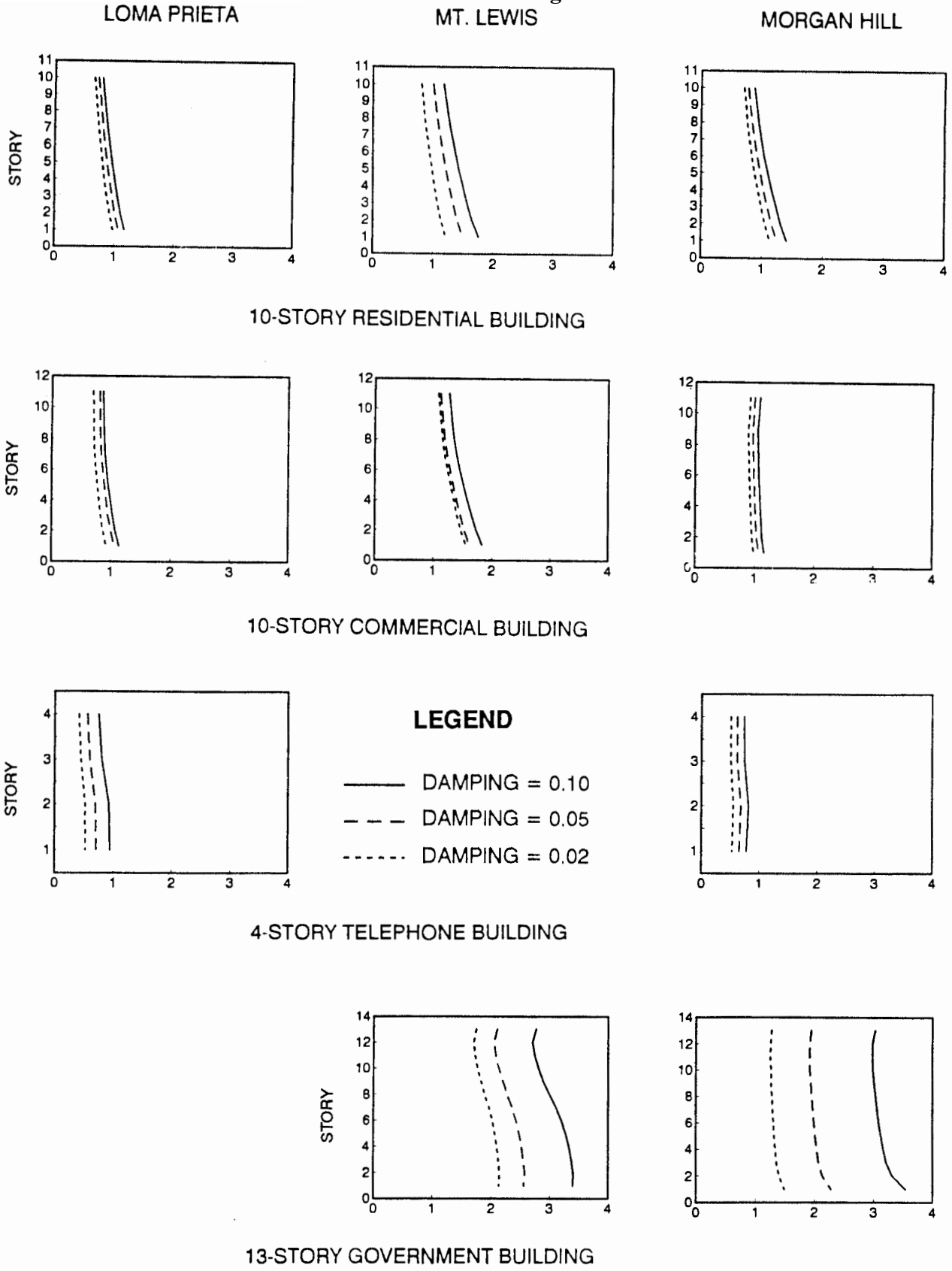

Figure 3: Variation of Total dynamic to Total Design Eccentricity Over the Height of the Buildings

SEISMIC PERFORMANCE INVESTIGATION OF THE HAYWARD-BART ELEVATED SECTION INSTRUMENTED UNDER CSMIP

Joseph Penzien, Wen S. Tseng, and Ming S. Yang
International Civil Engineering Consultants, Inc., Berkeley, CA

ABSTRACT

This paper presents the results of a seismic performance investigation of the Hayward-BART elevated section, instrumented by the California Division of Mines and Geology under its Strong Motion Instrumentation Program (CSMIP), using the acceleration time-histories recorded during the October 17, 1989 Loma Prieta earthquake. The recorded structural responses are correlated with corresponding theoretically predicted responses. Adjustments of structural parameters and modelling concepts required to achieve satisfactory correlations are discussed, along with their implications to procedures of standard engineering practice. Recommendations are made toward improving the arrangement of CSMIP strong-motion instruments at the Hayward-BART site.

INTRODUCTION

The design of the present Bay Area Rapid Transit (BART) system started in 1963 and continued over a number of years. The state-of-the-art in the analysis and design of earthquake-resistant transportation structures has improved significantly since that time. Observing the performances of such structures during past earthquakes has been a major factor in bringing about this improvement. Most notably is the San Fernando earthquake of February 9, 1971, during which many elevated freeway structures collapsed. Following this event, major changes were made to the earthquake code provisions leading to improved structures form a seismic performance point of view (Ref. 1). As evidence of this fact, no freeway structures of post-San Fernando design suffered damages during the Loma Prieta earthquake while many of such structures of pre-San Fernando design were heavily damaged and/or collapsed.

While the BART aerial structures were undamaged during the Loma Prieta earthquake, that fact alone does not insure satisfactory performance under future moderate to maximum credible earthquake conditions. Considering that the CSMIP-instrumented section of the Hayward-BART aerial structure experienced deck-level peak horizontal accelerations as high as 0.60g during the Loma Prieta earthquake, even though the peak free-field horizontal ground acceleration at the site was only about 0.16g, its performance under free-field ground motions of two to four times this intensity of shaking is of considerable concern. Fortunately, the CSMIP recordings of structural response at this site have made it possible to develop realistic modelling of this structure, allowing not only an assessment of its performance during the Loma Prieta earthquake but an assessment of its expected performance during an earthquake of much higher intensity, say 0.70g peak ground acceleration (PGA).

DESCRIPTION OF STRUCTURE INVESTIGATED

The structure investigated under this research program is a three-span, nearly-straight section of the BART elevated system located immediately to the north of the BART Hayward Station. The structure consists of 3 simply-supported twin box-girders constructed of prestressed concrete, which are supported on four single-column piers designated as P132, P133, P134, and P135; see Figure 1.

The reinforced concrete single-column piers have a hexagon cross-section with a 5-foot dimension between opposite faces and they are reinforced with two rings of #18 Grade 60 reinforcing bars. Each column of piers P132, P133, and P135 has 28-#18 bars in its outer-ring which run the full height and

16-#18 bars in its inner ring which are cut at various heights; thus, for each column, a total of 44-#18 bars are present at its base. The column of pier P134 has 24 full-length #18 bars in its outer-ring and 12-#18 bars cut at various heights in its inner ring; thus, it has a total of 36-#18 bars present at its base. All columns are provided with #5 spiral bars running at 3-inch pitch covering almost the full height of column.

Each pier-column of P132, P133, and P135 is supported on an 18' x 18' square footing 5.5' deep, which is, in turn, supported by 18 one-foot diameter reinforced concrete piles, each having a capacity rating of 60 tons. Pier P134 is supported on a 16' x 16' square footing, 5.5' deep, and on 16 piles of the same capacity rating. Except for the vertical piles located along the horizontal axes of symmetry of the footing, all others are battered with a slope of 8:1 for the inner piles and 4:1 for the outer piles. All piles were driven into the soils to depths of 40 to 50 feet below the bottoms of the pier footings. The soil condition at the site, as indicated by the soil boring-logs for bore holes located near the site, consists of layers of sandy clay and silty sand. The water table at the site is located about 60 feet below ground surface.

Each prestressed-concrete box-girder is hinged at its north end to its corresponding pier-beam support through two vertical concrete-filled 5-in. diameter steel pipes and it rests on a bearing support at its south end allowing freedom of movement longitudinally relative to the support. Freedom of relative movement transversely is prevented however since the south end of each girder is hinged to the north end of the adjacent girder. All hinges of the girders have a 1-inch gap, tight fitted with a non-laminated elastomeric material and the girders themselves are supported on the tops of pier beams through two 15" x 12" x 1" elastomeric pads at each end of each girder. Thus, even for small relative displacements ($<< 1$ inch), the stiffnesses of the elastomeric pipe-hinge fillers and bearing pads play a role in controlling the girder vibration frequencies.

The BART train rails are fastened rigidly to the prestressed-concrete girders at 3-ft intervals longitudinally. Thus, even though the girders are simply supported between adjacent piers, stiffness coupling across the girder joints between spans exists due to the stiffnesses of the continuous rails which are rigidly fastened to the girders. Such coupling is very significant in the longitudinal direction due to the high axial stiffness of the rails but is not too significant in the transverse direction. As will be discussed later, the high stiffness coupling in the longitudinal direction did indeed play a major role in the seismic response behavior as recorded by the CSMIP instruments during the Loma Prieta earthquake.

DESCRIPTION OF INSTRUMENTATION AND DATA COLLECTED DURING LOMA PRIETA EARTHQUAKE

The CSMIP instrumentation of the structure under investigation consists of 18 strong-motion acceleration sensors installed both on the structure and in the free-field. These sensors will be designated herein as Channel Nos. 1 through 8 and 10 through 19 (Channel No. 9 was not installed). The locations and directions of sensors are shown in Fig. 1.

During the October 17, 1989 Loma Prieta Earthquake, accelerograms were recorded by all 18 sensors. These accelerograms are shown as time-history plots in Fig. 2. The free-field recordings show that during the earthquake, the site region experienced ground-surface peak-accelerations of 0.16g horizontally and 0.08g vertically. The peak accelerations experienced at the girder deck level ranged from 0.39g to 0.60g in the transverse direction and from 0.21g to 0.26g in the longitudinal direction.

ANALYSIS OF RECORDED DATA AND OBSERVATIONS

The acceleration time-history data collected from the Loma Prieta earthquake shown in Fig. 1 have been analyzed extensively in this research program in an attempt to understand the seismic response

behavior of this structure during the earthquake. In general, the data analyses performed consisted of: (1) computing and plotting acceleration response spectra (ARS) for a 2% damping ratio for the recorded acceleration time-history data; (2) computing and plotting Fourier spectra of acceleration time histories and the transfer functions (complex Fourier spectrum ratios) between the structural response motions and the free-field motions; (3) doubly integrating the acceleration time-histories to give displacement time histories from which selected relative displacement time-histories of interest were obtained; and (4) generating cross-correlation functions between pairs of selected recorded motions from which the apparent phase lags between these pairs of motions were determined. From the results of the data analyses described above, significant features of the seismic response of the structure during the earthquake were observed and deduced. These are summarized below.

Free-Field Motions - The 2%-damped ARS computed from the free-field recorded motions indicate that even though the recorded PGA values are the same for the NS and EW directions, the EW motion, which is in the transverse direction of the structure, contains significant components of motion in a narrow frequency range near 1 Hz; whereas these same components of motion are nearly absent in the NS motion. The significant content of motion near 1 Hz for the EW motion has a significant effect on the transverse response of the structure.

Longitudinal Structural Response at the Deck Level - The longitudinal structural response motions at the deck level recorded at sensor locations, 3, 4, 5, 6, 7, and 8 shown in Fig. 1 indicate that the longitudinal responses at all these sensor locations along the 3-span length are almost identical, indicating that, even though joints are present, the girders are strongly coupled longitudinally by the rails; thus, they behave essentially as a unit in this direction with almost no relative motions taking place across the joints. The relative displacement time-history obtained from recorded data of Sensors 4 and 5 indicate that the maximum relative displacement experienced at this joint was about 2 mm (0.08 inch) which is less than 10% of the joint gap of 1 inch.

Transverse Structural Response at the Deck Level - The transverse structural response motions at the deck level recorded at sensor locations 10, 11, and 12 shown in Fig. 1 indicate that, transversely, the girder and the pier-beam basically responded as a unit with very little relative motion across the elastomeric bearing pads. The maximum relative displacement between the girder and the pier beam obtained from the recorded data is 5.5 mm (0.216 inch). Using this amount of relative displacement and the transverse inertia force of the girder tributary to Pier 132, the apparent shear modulus of the elastomeric bearing pads, calculated taking into account the sitffnesses of elastomeric fillers around the hinges, is in the range of 500 to 600 psi which is about 4 to 5 times higher than the 120 to 155 psi given in the AASHTO code.

Structural Response Behavior at P132 - Pier 132 has been instrumented with the largest number of sensors as indicated in Fig. 1, namely, Sensors 2, 3, 4, and 6 measuring the longitudinal response motions and Sensors 11, 12, and 13 measuring the transverse response motions. Examining the 2%-damped ARS and the transfer function amplitudes obtained from analyses of recorded data shown in Fig. 3, one can observe that, longitudinally, the structural system at P132 has a major structural response peak at the frequency of 3.5 Hz and a minor peak at about 2.1 Hz; transversely, it has a major structural response peak at the frequency of 1.8 Hz and a minor peak at 3.6 Hz. Using the half-power bandwidth method, the modal damping values of the system associated with the major response modes at 3.5 Hz for the longitudinal response and 1.8 Hz for the transverse response are estimated to be 4% and 3.6%, respectively.

Structural Responses at the Bases of P132 and P135 - Two sets of triaxial sensors were installed at the bases of piers P132 and P135 which are separated by a distance of 231 feet (70.4 m). The recorded motions and their integrated displacement time-histories at these two locations indicate that these response motions are nearly identical with the response at P132 lagging behind P135 by a small amount, indicating that the seismic waves propagated in the general direction from South to North which is consistent with the relative location of the epicenter to the site. The time lags determined from the cross-

correlation functions computed form the recorded motions are estimated to be 0.03 second for the longitudinal motions and 0.07 second for the transverse motions, giving the apparent wave propagation velocities of these motions at about 2.4 km/sec and 1.0 km/sec, respectively.

DEVELOPMENT OF ANALYTICAL MODELS

Based on the dynamic response behaviors of the structure observed from the results of data analyses described previously, analytical models intended for capturing the gross dynamic response behaviors observed were developed. Since as described previously, the longitudinal and the transverse structural responses observed show essentially decoupled behaviors, separate longitudinal and transverse models could be used for the structure in capturing its overall behavior. Furthermore, since the structures of all three spans are essentially the same and their observed responses are quite similar, it is only necessary in developing analytical models to consider the structure and foundation system of a typical span. Since Pier 132 has been most extensively instrumented, a representative one-span structure tributary to it was used for developing the analytical models. Because the recorded data have indicated significant soil-structure interaction effects, the dynamic impedance characteristics of the pier foundation system were included in developing the analytical models.

Transverse Model - For response prediction in the transverse (EW) direction of the structure, a lumped-mass generalized-beam-stick model was used to represent the one-span structure tributary to pier P132 as indicated in Fig. 4. As shown in this figure, the model consists of: 2 lumped masses representing the twin box girders, which respond essentially as rigid bodies due to their very high fundamental horizontal frequency (10 Hz) relative to the critical system frequency (1.8 Hz); 3 lumped masses representing the pier-beam and column; and one lumped mass representing the pier footing (pile cap). For each lumped mass, its tributary rotary inertia is also included. The girder lumped masses are connected to the lumped mass representing the rigid pier beam through two shear springs (K_p) representing the apparent shear stiffnesses of the elastometric bearing pads. The lumped masses of the column are interconnected by elastic beam elements which have stiffness properties based on the gross uncracked concrete section of the column. The modal damping ratios for the fixed-base structure are assumed to be 2.5% for all modes.

The dynamic characteristics of the soil-pile foundation system are represented by a set of frequency-independent foundation impedances (i.e., soil springs and dampers). A set of translational soil spring and damper (K_{xx} and C_{xx}) and a set of rocking soil spring and damper ($K_{\theta\theta}$ and $C_{\theta\theta}$) are attached to the pier footing a distance H above its center of mass as shown in Fig. 4. This distance H is intended to simulate the effect of foundation embedment which results in increases in the foundation impedance values and creates a coupling impedance ($K_{x\theta}$ and $C_{x\theta}$) between the foundation translation and rocking rotation. The numerical values of the translation and rocking spring stiffnesses (K_{xx} and $K_{\theta\theta}$) were estimated using the results of a pile group test conducted recently by Caltrans (Ref. 3) and the axial stiffnesses of the battered piles. The stiffnesses as obtained were further adjusted considering the soil shear modulus degradation effect due to the free-field soil shear strains induced during the earthquake. The values of the translation and rocking damper coefficients (C_{xx} and $C_{\theta\theta}$) were derived by assuming a critical damping ratio of 20% for both the rigid body translation and rocking modes of the rigid structure on the flexible foundation. Distance H was left as a parameter to be adjusted in optimizing the correlation between the predicted and measured responses.

Longitudinal Model - For predicting the longitudinal (NS) response of the structure, the analytical model selected to represent a typical span of structure tributary to pier P132 is essentially the same as that of the transverse model described above; however, recognizing that the structure in the longitudinal direction is highly coupled to the stiffer and much more massive structure of the Hayward BART Station through the high axial stiffnesses of the girders and the rigidly-fastened rails across the girder joints, the longitudinal model for a representative span is coupled longitudinally through two axial links to a stiffer and more massive model representing the gross dynamic characteristics of the structures of the Hayward BART

Station immediately to the south. Since the recorded data indicate that the longitudinal structure responses throughout the 3-span structure have a dominant response frequency at about 3.5 Hz and a minor response frequency at about 2 Hz, it is postulated that the frequency at 3.5 Hz is dominated by the stiffer Hayward BART Station structure. Thus the model properties of the stiffer model representing the Hayward BART Station were adjusted to reflect a fundamental frequency in the longitudinal direction of about 3.5 Hz.

CORRELATION OF ANALYTICAL AND MEASURED RESPONSES

Based on the longitudinal and transverse analytical models developed as described previously, dynamic responses of the models subjected to the inputs of the free-field acceleration time-histories in the NS and EW directions as recorded by Sensors 17 and 19, respectively, were computed. Since model parameters, such as soil and elastomeric material properties are uncertain and since the recorded data are not sufficient to deduce the needed information, numerous parametric variations were considered in the analysis. Included in these parameter variations were the stiffnesses of the elastomeric bearing pads, the foundation soil modulus and damping values, and the distance H used in characterizing the foundation embedment effect. The final values of these parameters were selected as those which resulted in the best correlations between the analytical predicted responses and the corresponding measured responses. The responses obtained from analyses using the best-estimate parameter values are compared with the corresponding measured responses in the form of 2%-damped acceleration response spectra calculated from the acceleration response time histories. These comparisons and discussions of the results are summarized below.

Longitudinal Responses - The 2%-damped acceleration response spectra for the analytically computed longitudinal response motions at sensor locations 6, (girder), 3 (pier-beam), and 2 (pier-base) are compared with the corresponding spectra for the measured response motions in Fig. 5. As shown by these comparisons, the analytical results capture the gross response behavior in the longitudinal direction reasonably well; however, as indicated from the spectra shown, the longitudinal response are dominated by the structural amplification peak at the frequency of 3.6 Hz which is attributable to the major structural system frequency of the stiffer Hayward BART Station structure. A future confirmation of this response characteristic is desirable.

Transverse Responses - The 2%-damped acceleration response spectra for the analytically predicted transverse response motions at sensor locations 11 (girder), 12 (pier-beam), and 13 (pier-base) are compared with the corresponding results obtained from the measured response motions also in Fig. 5. As indicated by these comparisons, the transverse analytical model captured the fundamental mode response at the frequency of 1.8 Hz very well; however, it is somewhat deficient in predicting the second mode response at the frequency of 3.6 Hz, which is basically due to the foundation rocking. Because of the lack of recorded data that could be used in separating the rocking component and translation component of the pier base motions, further refinements of the foundation model, which significantly controls the transverse structural response behavior, could not be achieved rationally.

ASSESSMENT OF STRUCTURAL PERFORMANCE AND DESIGN IMPLICATIONS

The earthquake response data recorded at the three-span section of the BART elevated structure offer a unique opportunity to assess the seismic response behavior of this structure during the Loma Prieta earthquake. From the results of analyses presented previously, valuable insights into the seismic performance of this section of the BART elevated structure have been obtained and their implications on design have been assessed as follows:

(1) The apparent structural damping value of the BART structure as indicated from the recorded data and as found to give reasonable correlations, is about 2.5% for the fixed-base structure and about 4% for the structure-foundation system, both of which are lower than the value of 5% normally used in design. This lower apparent damping value leads to a structural response amplification factor at the deck level of about 4 which is higher than peak elastic spectral amplification factor of 3 normally used for design. However, considering that the peak horizontal acceleration of the free-field motions during the earthquake was only 0.16g, the damping value of 5% and the peak elastic spectral amplification factor of 3 at the design level of 0.35g to 0.70g can be judged to be reasonable and conservative for design purposes.

(2) As indicated by the recorded data, as well as by the parametric correlation studies, the soil-structure interaction effect on seismic response of the structure is significant. This effect tends to lower the structure system frequencies appreciably. For example, the analytical model developed for transverse response prediction shows the fundamental fixed-based structure frequency to be 2.5 Hz which is considerably above the system frequency of 1.8 Hz obtained when soil-structure interaction is considered. In the design of the BART structure, a fixed-base structural model is normally used which tends to over-estimate the frequencies and under-estimate the response.

(3) The recorded data indicate that the BART elevated structures are highly coupled in the longitudinal direction due to the presence of the continuous rails which are rigidly fastened to the girders, even though the structure of each span is designed to be simply-supported and free to move at one end. This implies that the single-pier model used for design in this direction may not be appropriate, especially for those elevated sections which have large variations in the pier column heights. When the system is strongly coupled longitudinally the shorter columns tend to experience higher seismically induced internal forces; whereas, the single-pier model without this coupling may not predict such a result. Thus in such situations, a model consisting of structures of several spans and piers may be necessary. Furthermore, due to the apparent strong coupling of the rails, the axial forces induced in the rails across the girder joints should be assessed in such situations.

(4) As discussed previously, the apparent shear stiffnesses of the elastomeric bearing pads for the BART girders have been found to be higher than the code values, indicating potential degradation of the material due to aging or other environmental effects. It would be very useful, if and when these pads are replaced, to perform tests of the existing pads to determine their properties. Furthermore, since their properties in the current condition are uncertain, design or assessment of the structure should consider a wide variation of these properties.

(5) Since the soil-structure interaction effect is shown to be important, design procedures for estimating the pile foundation impedances and capacities such as those published in Ref. 4 should be evaluated using actual earthquake response data. However, to make this possible, more instruments should be placed on the foundation base such that they can produce sufficient data for evaluating separate modes of foundation response. The current CSMIP instrumentations are not sufficient for such an evaluation.

CONCLUSIONS AND RECOMMENDATIONS

Based on the analysis and structural performance assessment results obtained in this study, the following conclusions and recommendations can be made:

(1) The data recorded during the Loma Prieta earthquake by the CSMIP instruments on the Hayward-BART elevated structure provide valuable information for understanding the seismic response of this structure.

(2) Due to the high axial stiffness of the continuous rails, the seismic response behavior of this structure in the longitudinal direction was found to be quite different from that in the transverse direction. The former behavior is controlled by the response of the entire coupled system; whereas, the later is more or less controlled locally from span to span. The responses in both directions are significantly influenced by soil-structure interaction effects. In the more-critical transverse direction, these effects actually result in higher responses than those obtained using the fixed-base design analysis procedure by a factor of 1.3 to 1.5.

(3) During the Loma Prieta earthquake, the maximum seismically-induced column base moment was approximately 1/3 of the column's ultimate moment capacity. However, using response spectrum compatible accelerograms normalized to the Maximum Credible Earthquake PGA level of 0.7g, as currently specified in the BART Extension Program, the maximum induced seismic base moment predicted by the models calibrated in this study was found to exceed the design moment capacity by a factor of about 3.4.

(4) The studies conducted in this research program point out an urgent need of instrumentation that allows independent recordings of the rocking rotation responses at the bases of pier-columns. A need also exists to obtain longitudinal response data at locations closer to the Hayward BART Station. Thus, the current instrumentation layout on this section of structure can be improved by shifting some of the redundant sensors for recording the longitudinal motions of girders to pier bases for measuring base rocking motions and to locations closer to the BART Hayward Station for measuring the longitudinal motions.

(5) The findings of this study suggest the need for an assessment of current design procedures, including modelling for seismic response predictions and criteria for setting limits on ductility demands.

ACKNOWLEDGEMENT

The study as reported in this paper received principal funding from the California Strong Motion Instrumentation Program, California Department of Conservation, Division of Miens and Geology, Office of Strong Motion Studies and secondary funding from International Civil Engineering Consultants, Inc. Mr. Matt McDole and Mr. Mark Chu of Bay Area Rapid Transit (BART) District and Mr. Matt Hsiao of Bay Area Transit Consultants, Inc. provided much valuable information on the structure investigated. These funding and information sources are gratefully acknowledged.

REFERENCES

(1) Penzien, J. and Tseng, W. S., "Analytical Investigations of the Seismic Response of Tall Flexible Highway Bridges," Report No.UC-EERC 73-12, Earthquake Engineering Research Center, University of California, Berkeley, June 1973.

(2) Shakal, A., Huang, M. et al., "CSMIP Strong-Motion Records from the Santa Cruz Mountains (Loma Prieta), California Earthquake of 17 October 1989," Report No. OSMS 89-06, California Strong Motion Instrumentation Program, California Department of Conservation, Division of Mines and Geology, November 17, 1989.

(3) Abcarius, J. L., "Lateral Load Tests on Driven Pile Footings," Structure Notes, No. 22, California Department of Transportation (Caltrans), Division of Structures, March 1991.

(4) Lam, P. I. and Martin, G. R., "Seismic Design of Highway Bridge Foundations," Report No. FHWA/RD-86/101, Federal Highway Administration, Office of Engineering and Highway Operations, June 1986.

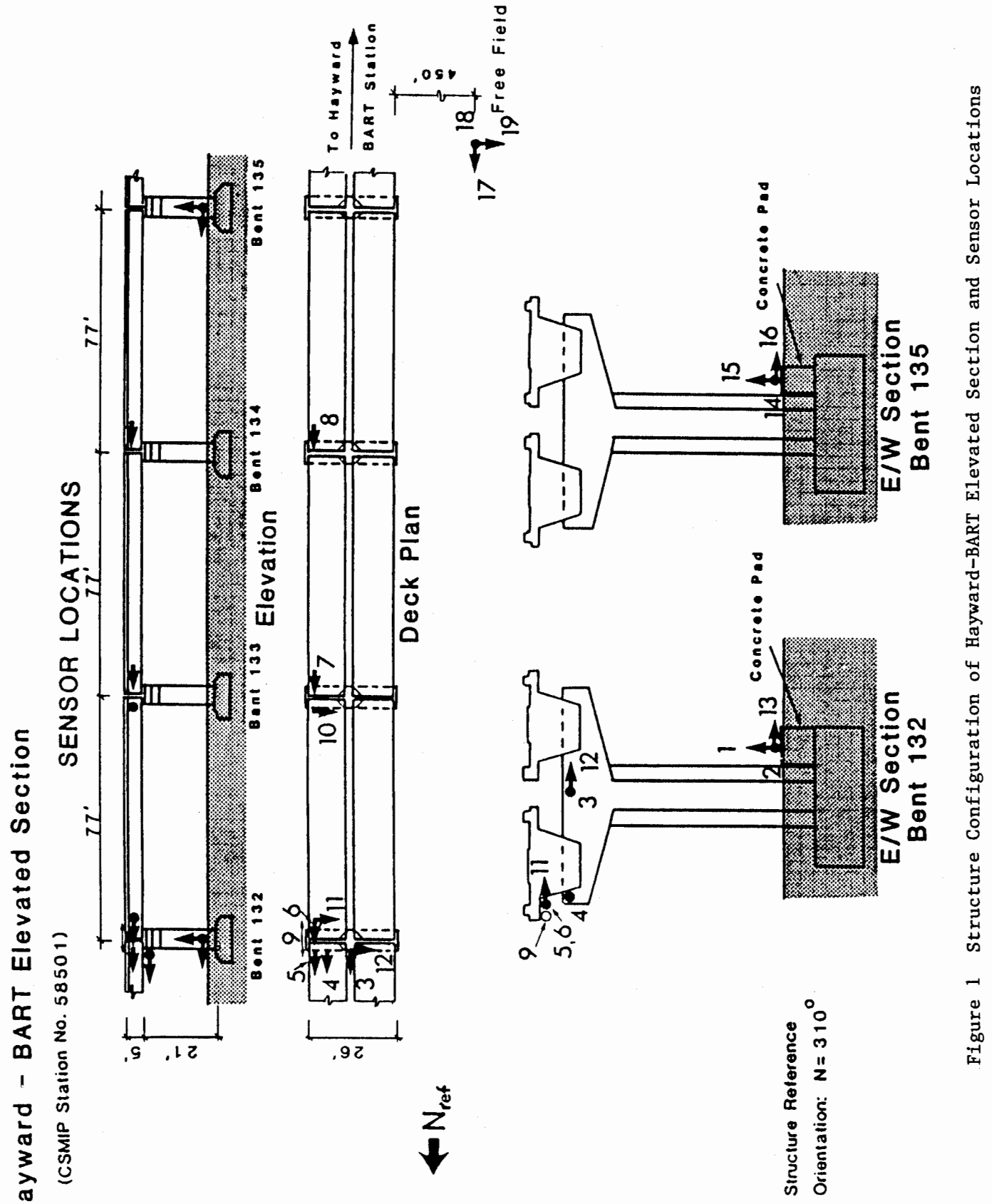

Figure 1 Structure Configuration of Hayward-BART Elevated Section and Sensor Locations

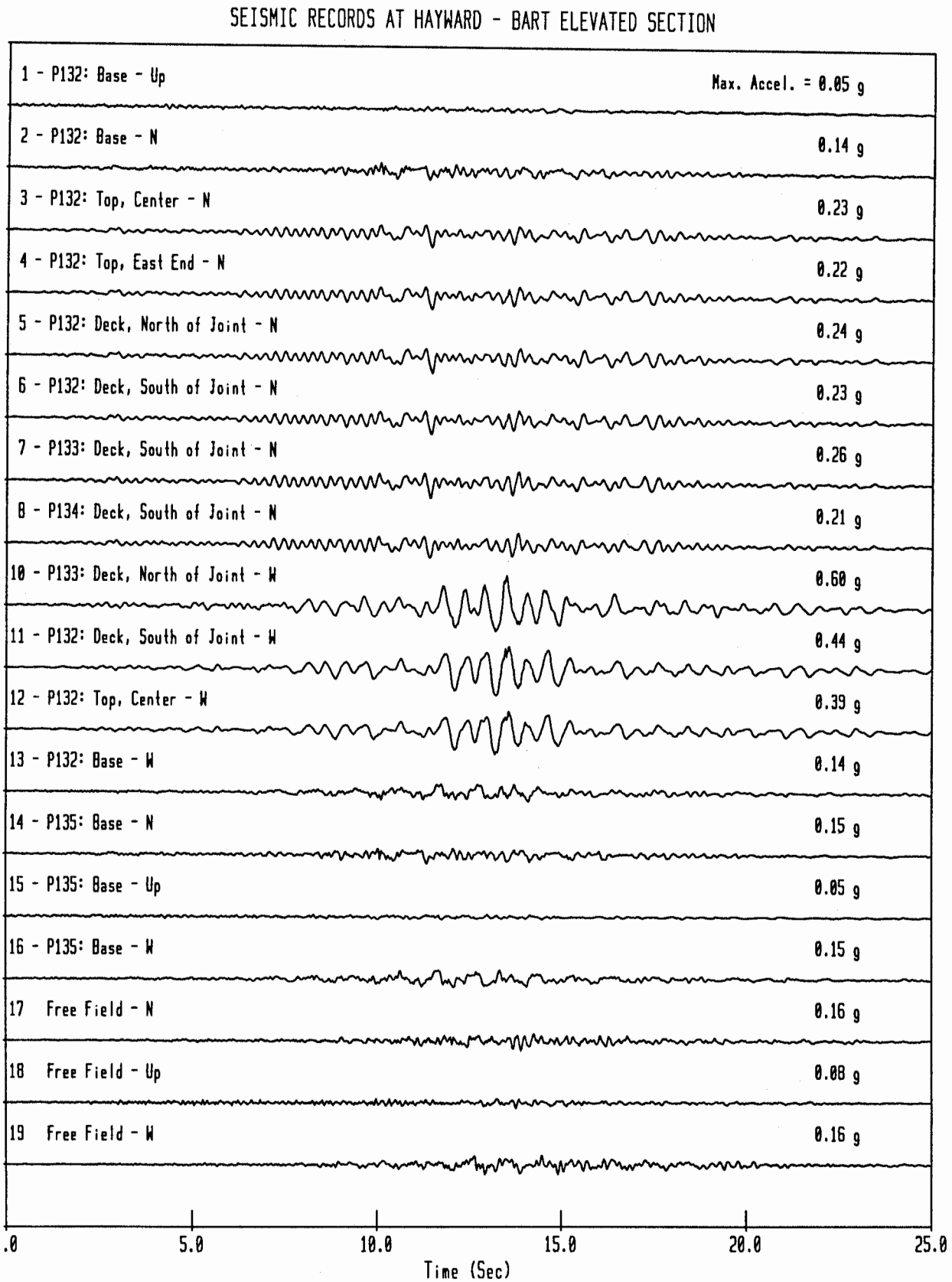

Figure 2 Accelerograms Recorded During the Loma Prieta Earthquake of 1989

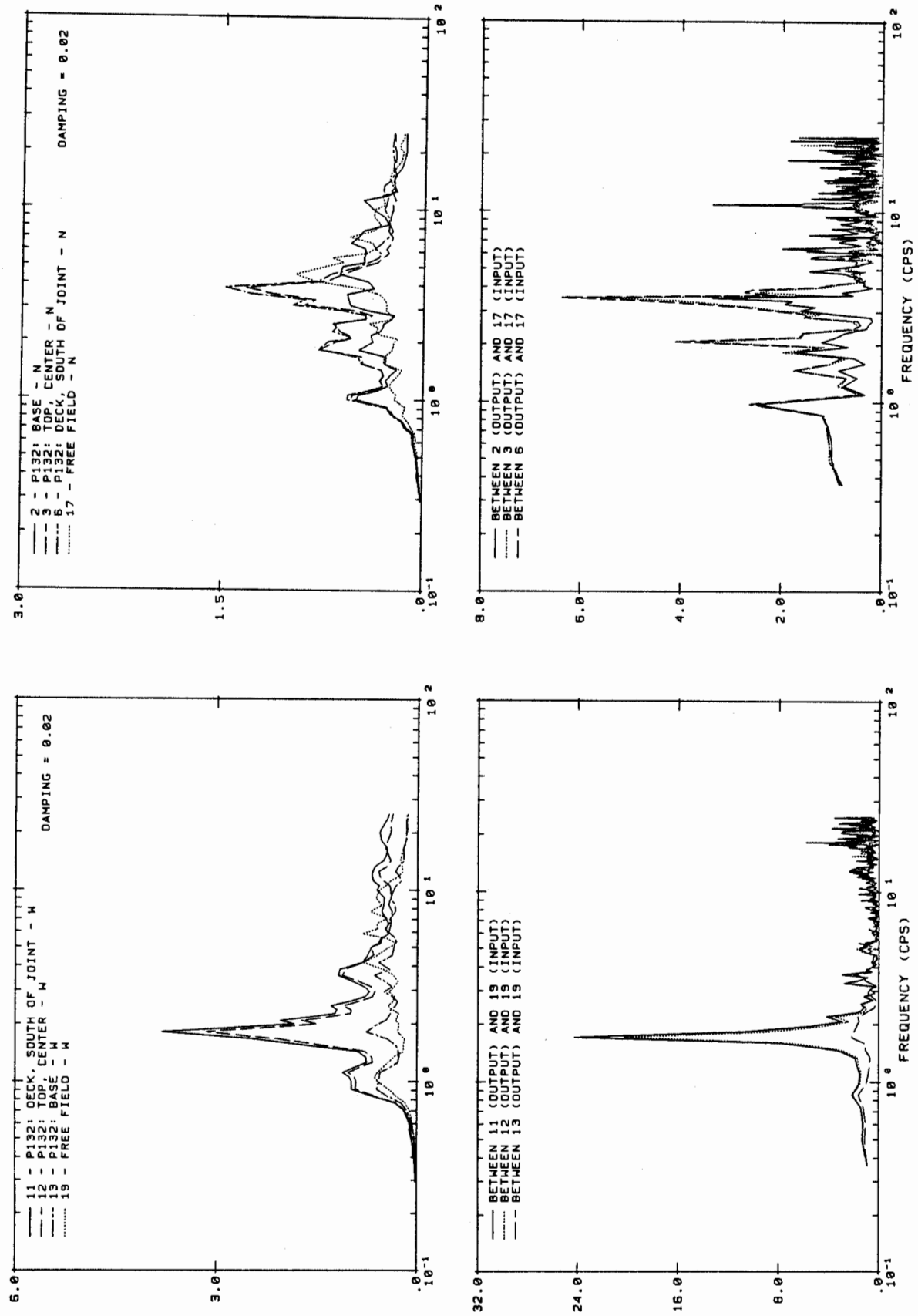

Figure 3 2%-Damped Acceleration Response Spectra and Transfer Function Amplitudes of Recorded Motions

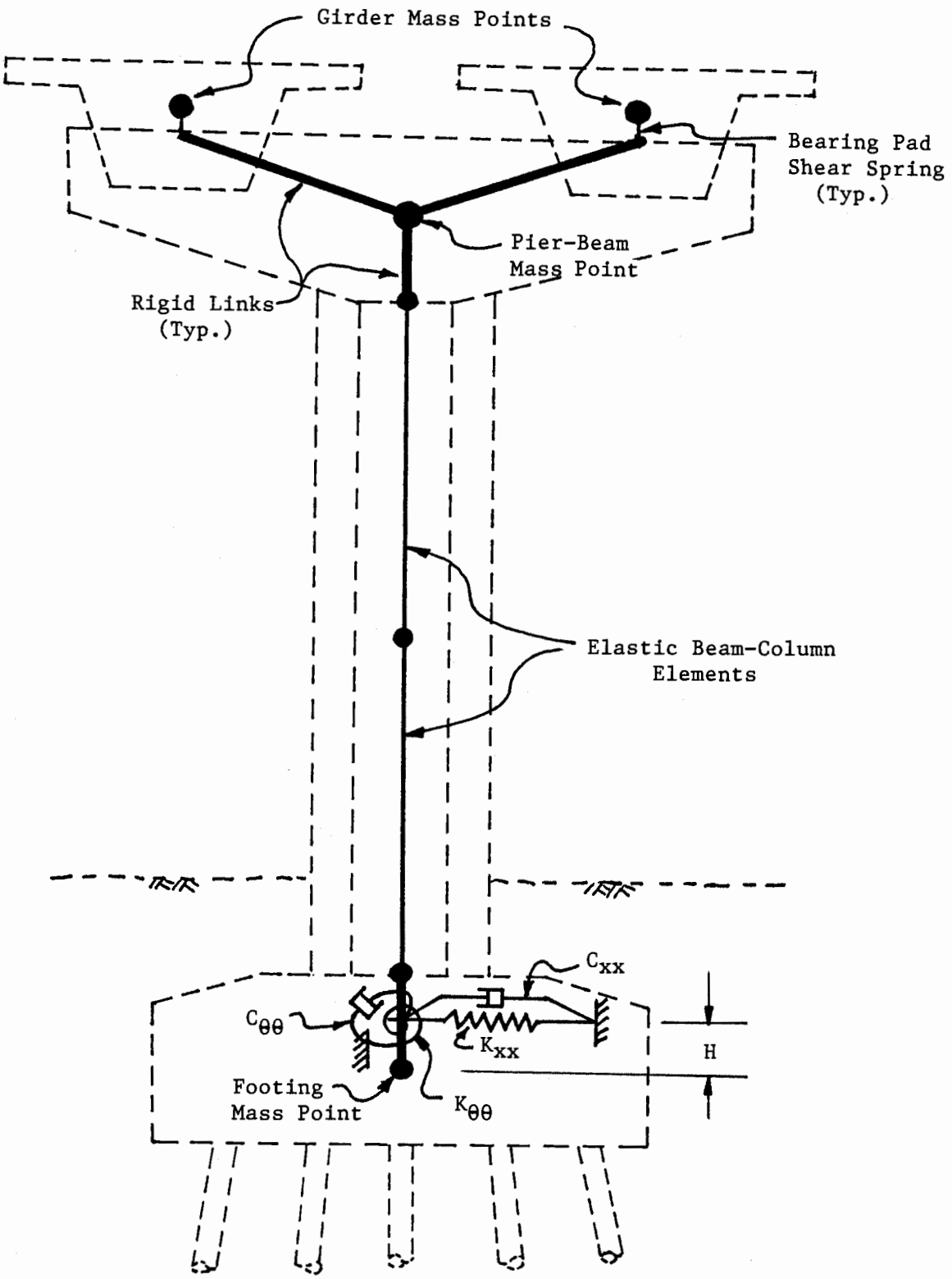

Figure 4 Analytical Model for the Transverse Response Analysis

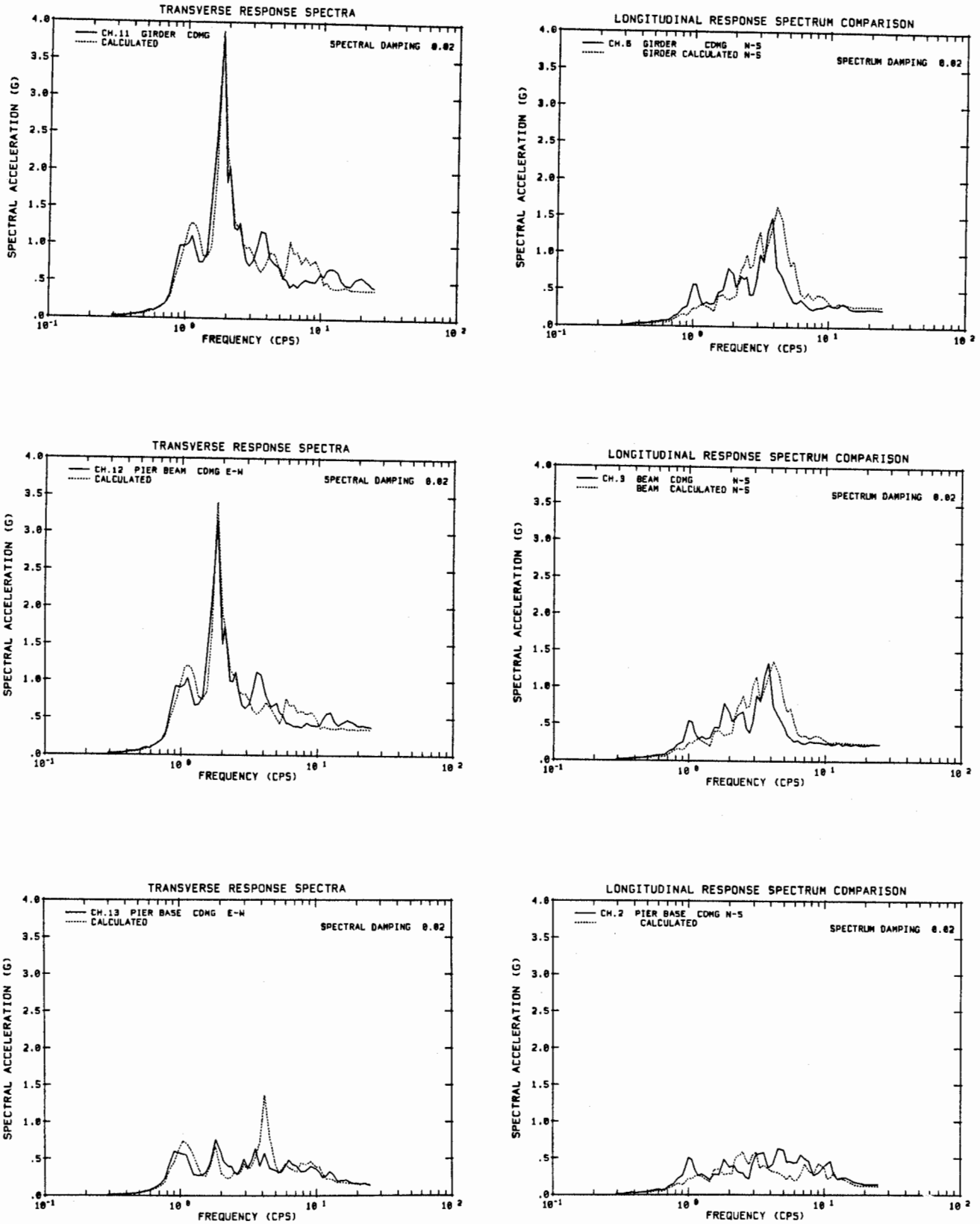

Figure 5 Comparisons of Analytically-Predicted and Measured Responses

ANALYSIS OF THE RECORDED RESPONSE OF LEXINGTON DAM DURING VARIOUS LEVELS OF GROUND SHAKING

F.I. Makdisi, C.Y. Chang, Z.L. Wang, and C.M. Mok
Geomatrix Consultants, Inc.
One Market Plaza, 717 Spear Street Tower
San Francisco, California 94105

ABSTRACT

Lexington Dam, a 200-foot-high compacted earthfill embankment, was strongly shaken by the Loma Prieta 1989 earthquake (M_W 7) as well as by two smaller events (M_L 5) in June 1988 and August 1989.

The dam was instrumented as part of the California Strong Motion Instrumentation Program. The recordings at Lexington Dam due to at least three different levels of ground shaking provided valuable data for examining the nonlinear strain-dependent behavior of the embankment materials due to earthquake shaking. This paper summarizes the results of analyses of the recordings at the dam crest and abutment for two of the three earthquakes described above. The analyses included Fourier spectral ratio computations (crest to abutment) to examine changes in the fundamental natural period of the dam due to different levels of shaking; and one- and two-dimensional dynamic response analyses to evaluate the nonlinear strain-dependent behavior of the embankment materials at two levels of earthquake shaking.

LEXINGTON DAM

Lexington Dam is located on the east flank of the Santa Cruz Mountains, off Highway 17 between San Jose and Santa Cruz, about 17 miles north of Santa Cruz. The dam is 205 ft high and has a crest length of 810 ft. It is a zoned earthfill embankment with a downstream slope of 3:1 (H:V) and an upstream slope of 5½:1. A cross section of the embankment through the maximum section is shown in Figure 1. The embankment consists of four zones, upstream and downstream shells of gravelly clayey sands, a thick core of sandy gravelly clay, and an internal drain zone between the core and downstream shell. The downstream shell contains about 15 to 35% fines and the upstream shell about 20 - 65%, in both cases the fines are medium plasticity clays with LL ≈ 33-39 and PI ≈ 14-24. The core, below a depth of 80 ft, is composed of 85% fines of medium to high plasticity (LL ≈ 61-67 and PI ≈ 38-44), between the crest and a depth of 80 ft, the core material resembles more the upstream shell material with about 30 to 50% fines of medium plasticity (LL ≈ 31-39 and PI ≈ 14-18).

The foundation and abutments consist of bedrock of the Franciscan formation, which is composed chiefly of interbedded sandstone and shale, greenstone, and minor amounts of chert and schist. The topsoil at the foundation area was stripped prior to dam construction.

Recorded Ground Motions

The dam is instrumented with 3 sets of strong motion accelerographs, one set is located at a rock outcrop at the left abutment (west of the concrete spillway), and two sets are located on the crest to measure the response of the embankment. The locations of these instruments are shown on a layout of the dam presented in Figure 1. At each of the three locations the accelerographs were oriented in three orthogonal directions: transverse (normal to the dam axis), longitudinal (along the dam axis), and vertical. During the Loma Prieta earthquake (M_W 7) of October 17, 1989, peak accelerations (in the transverse direction) of 0.39 and 0.45 g were recorded at the left and right crest of the dam, respectively, and 0.45 g at the rock formation of the left abutment. The dam response was also recorded during two smaller magnitude (M_L ~ 5) earthquakes around Lake Elseman, one event on June 27, 1988, and the other on August 8, 1989. Peak accelerations recorded in the transverse direction during these events were significantly smaller than those of the Loma Prieta earthquake: 0.11 to 0.16 g on the crest and 0.03 g at the left abutment, for the event of June 27, 1988; 0.16 to 0.18 g on the crest and 0.08 g at the left abutment, for the earthquake of August 8, 1989. These data and earthquake information are summarized in Table 1.

TABLE 1

RECORDED PEAK ACCELERATIONS AT LEXINGTON DAM
DURING VARIOUS EARTHQUAKES

Earthquake (Date)	Magnitude M_L	Approximate Distance to Rupture Zone (km)	Peak Acceleration Values (g)		
			Left Abutment	Left Crest	Right Crest
Loma Prieta (Oct. 17, 1989)	6.9	6	E-W: 0.41 Up: 0.15 N-S: 0.45	0.40 0.22 0.39	0.34 0.20 0.45
Lake Elseman (Aug. 8, 1989)	5.2	18	E-W: 0.11 Up: 0.03 N-S: 0.08	0.17 0.08 0.18	0.22 0.10 0.16
Lake Elseman (June 27, 1988)	5.0	19	E-W: 0.04 Up: 0.02 N-S: 0.03	0.11 0.07 0.11	0.12 0.07 0.16

The recordings from these three earthquakes were digitized by the staff of the Strong Motion Instrumentation Program (Shakal et al., 1989). Upon examination of the records from the June 27, 1988 event it was noticed that the records appeared to be missing the early portion of ground motions and that the instruments may have triggered late during this event. Accordingly, this set of records was not used in the analyses and dynamic response computations described in the subsequent sections of this paper. Plots of the 5% damped response spectra of recordings from the two larger events are presented in Figure 2.

Analysis of Recorded Motions

Fourier spectral ratios of the recorded motions at the crest and the abutment were computed to examine any changes in the fundamental natural period of the embankment due to different levels of ground shaking. An increase in period with an increase in level of shaking reflects a decrease in the shear modulus of the embankment material (Chang et al., 1989).

A plot of the Fourier spectral ratios (crest to abutment) for both the smaller (M_L 5) event and the Loma Prieta (M_W 7) earthquake are shown on Figure 3. An examination of Figure 3 shows a substantial increase in the fundamental natural period of the embankment from about 0.5 seconds for the M_L 5 earthquake to about 1.4 seconds for the Loma Prieta event. It should be noted that the level of shaking represented by the peak ground acceleration at the left abutment rock for the smaller event was about 0.16 g compared to a value of about 0.45 g for the Loma Prieta event. The increase in the fundamental period of the embankment suggests a significant reduction in shear modulus of the embankment material due to the Loma Prieta earthquake.

Analysis of Embankment Response

To analyze the embankment response to the two levels of recorded ground motions, one- and two-dimensional dynamic finite element analyses were performed. The analyses employed the method of complex response and an equivalent linear approximation of the strain dependent modulus and damping properties. The program SHAKE (Schnabel et al., 1972) was used for the one-dimensional analyses, and FLUSH (Lysmer et al., 1975), a plane strain finite element analysis program was used for the two-dimensional analyses. In all analyses described herein, the transverse component (component normal to the dam axis) of ground motion was used.

The values of shear modulus at low strain (G_{max}) for various zones of the embankment were estimated on the basis of field shear wave velocity measurements (Wahler Associates, 1982). These values are summarized in Table 2 below:

TABLE 2

Zone	Shear Wave Velocity (ft/sec)
All zones at shallow depth (0-20 ft)	1200
Lower core (below 80 ft depth)	1100 - 1500
Upper core and upstream shell	1400
Downstream shell (20-50 ft depth)	1700
Downstream shell (below 50 ft depth)	2200
Foundation rock	1800 - 3000

The results of the geophysical field survey revealed shear wave velocities in the foundation bedrock that varied between 1800 and 3000 ft/sec with average values in the shallow

foundation of about 2200 ft/sec. Theoretical studies of dams located in canyons with flexible rock foundations (Gazetas, 1991) showed that for cases where the ratio of canyon rock velocity to the dam velocity was less than 10, assuming a rigid rock foundation resulted in differences in the computed amplification function at the dam crest by more than 70%. Accordingly, it was considered more appropriate to model the upper 300 to 350 ft of rock foundation below the dam as a flexible rock foundation and include it in the finite element mesh. Figure 4 shows the two-dimensional finite element representation of Lexington Dam and its flexible rock foundation. Shear wave velocities in the rock foundation were specified as follows, 0 to 150 ft depth: v_s = 2500 ft/sec, 100 to 200 ft: v_s = 3000 ft/sec, and 200 to 350 ft depth: v_s = 4000 ft/sec. This distribution of rock shear wave velocities with depth was based on data from similar sites underlain by Franciscan rock formations where shear wave velocities have been measured with depth. The transverse component of the rock motion recorded at the left abutment outcrop was used as input to the finite element analysis and was specified as surface motion of a free field rock column. Horizontal transmitting boundaries were incorporated in the finite element idealization of the dam-foundation system. This assumption implies that rock motions at the abutment and at the valley floor are similar. One-dimensional wave propagation studies were made to verify this assumption as well as the use of results of two-dimensional finite element and finite difference studies of topographic effects on similar slopes at the Diablo Canyon site (Pacific Gas and Electric Co., 1988).

Relationships for variation of modulus and damping properties with strain were obtained from published literature on similar soils: Seed and Idriss (1970) and Seed et al. (1984) for cohesionless soils; and Sun et al. (1988) for cohesive soils. A number of parametric studies of the effects on the predicted response of using various modulus reduction and damping curves, different shear wave velocities, as well as the effects of assuming rigid rock foundation were made (Makdisi et al., 1991). For the results presented herein, the modulus reduction and damping curves used in the analyses are shown below in Table 3. These properties are based on the mid-range shear modulus reduction curve for Sands proposed by Seed and Idriss (1970) and the lower bound curve for damping proposed by the same authors.

TABLE 3.

Modulus Reduction and Damping Curves Used in Analyses

Shear Strain %	G/Gmax	Damping Ratio
10^{-4}	1.0	0.3
10^{-3}	0.97	0.8
10^{-2}	0.73	2.8
10^{-1}	0.30	10.0
1	0.05	21.0

The value of shear wave velocity for the lower core zone (Table 1) was specified at 1200 ft/sec.

Figure 5 shows the results of the two-dimensional finite element analyses for both events in terms of the computed and recorded 5% damped acceleration response spectra at the crest of the dam. There is reasonable agreement between the computed and recorded spectra for the Loma Prieta 1989 event at periods of 0.2 seconds and longer, although the peak acceleration is over-predicted by as much as 65%. For the smaller Lake Elseman event, although the analysis approximately predicts the first natural period of the embankment, the predicted spectral accelerations are about 60% of the recorded ones over the entire spectral range.

Figure 6 shows the computed Fourier amplitude transfer functions between the dam crest and left abutment recordings for both events analyzed. Again there is reasonable agreement between the computed transfer functions shown in Figure 6 and those obtained from the recorded motions shown in Figure 3. The computed first natural periods of the embankment using the finite element analysis are about 0.55 seconds for the smaller Lake Elseman event and about 1.3 seconds for the Loma Prieta event. The shift in the fundamental natural period of the embankment with the increase in level of ground shaking reflects the strain dependent nonlinear behavior of the embankment soils. This is shown in a plot of the G/Gmax and damping values vs. strain for the finite elements located at the centerline of the dam between the crest and the foundation and presented in Figure 7. This plot shows that for the Lake Elseman earthquake, the strain levels developed were in the range of about 0.004 - 0.03%, with corresponding reduction in Gmax of about 30% to 40%. In contrast with the Loma Prieta event, the developed strain level varied between about 0.1% and 1.0% with a corresponding reduction in shear modulus of about 60 to 95% of the initial low strain value.

SUMMARY AND CONCLUSIONS

The recorded response at Lexington during the Loma Prieta 1989 earthquake and two smaller events provided an opportunity to evaluate the nonlinear behavior of the embankment soils during various levels of ground shaking. Fourier spectral ratios of the recorded motions showed a definite shift in the fundamental natural period of the embankment with increased level of ground shaking. Two-dimensional finite element analyses of the embankment response using equivalent linear strain-dependent material properties provided predictions of embankment motions that are in reasonable agreement with the recorded motions.

ACKNOWLEDGEMENTS

The studies summarized in this paper were funded by the California Division of Mines and Geology, Office of Strong Motion Instrumentation Program. The authors wish to thank Bob Teppel of Santa Clara Valley Water District for providing valuable data on Lexington Dam, and the staff of the California Division of Safety of Dams (DSOD) for providing help during review of their files.

REFERENCES

Chang, C.-Y., Power, M.S., Tang, Y.K., and Mok, C.-M., 1989, Evidence of nonlinear soil response during a moderate earthquake: Proceedings of Twelfth International Conference on Soil Mechanics and Foundation Engineering, Rio de Janeiro, Brazil, August 13-18.

Gazetas, G., and Dakoulas, P., 1991, Aspects of seismic analysis and design of rockfill dams: State of the Art paper, Proceedings of the Second International conference on Recent Advances in Geotechnical and Earthquake Engineering and Soil Dynamics, Vol. II, March.

Lysmer, J., Udaka, T., Tsai, C.-F., and Seed, H.B., 1975, FLUSH - A computer program for approximate 3-D analysis of soil-structure interaction problems: Earthquake Engineering Research Center, Report No. EERC 75-30, University of California, Berkeley, November.

Makdisi, F.I., Chang, C.-Y., Wang, Z.-L., and Mok, C.-M., 1991, Analysis of the recorded responses of Lexington Dam during various levels of ground shaking: report in preparation for the California Division of Mines and Geology, Strong Motion Instrumentation Program, Geomatrix Consultants, Inc., San Francisco, California.

Schnabel, P.B., Lysmer, J., and Seed, H.B., 1972, SHAKE - A computer program for earthquake response analysis of horizontally layered sites: Earthquake Engineering Research Center, Report No. EERC 72-12, University of California, Berkeley, December.

Seed, H.B., Idriss, I.M., 1970, Soil moduli and damping factors for dynamic response analysis: Earthquake Engineering Research Center, Report No. EERC 70-10, University of California, Berkeley.

Seed, H.B., Wong, R.T., Idriss, I.M., and Tokimatsu, K., 1984, Moduli and damping factors for dynamic analyses of cohesionless soils: Earthquake Engineering Research Center, Report No. UCB/EERC 84/14, University of California, Berkeley, September.

Shakal, A., Huang, M., Reichle, M., Ventura, C., Cao, T., Sherburne, R., Savage, M., Darragh, R., and Peterson, C., 1989, CSMIP strong-motion records from the Santa Cruz Mountains (Loma Prieta), California earthquake of 17 October 1989: California Strong Motion Instrumentation Program Report No. OSMS 89-06, 195 p.

Sun, J.I., Golesorkhi, R., and Seed, H.B., 1988, Dynamic moduli and damping ratios for cohesive soils: Earthquake Engineering Research Center, Report No. UCB/EERC 88/15, University of California, Berkeley.

Wahler Associates, 1982, Seismic safety evaluation of Lexington Dam: Final report prepared submitted to Santa Clara Valley Water District, May.

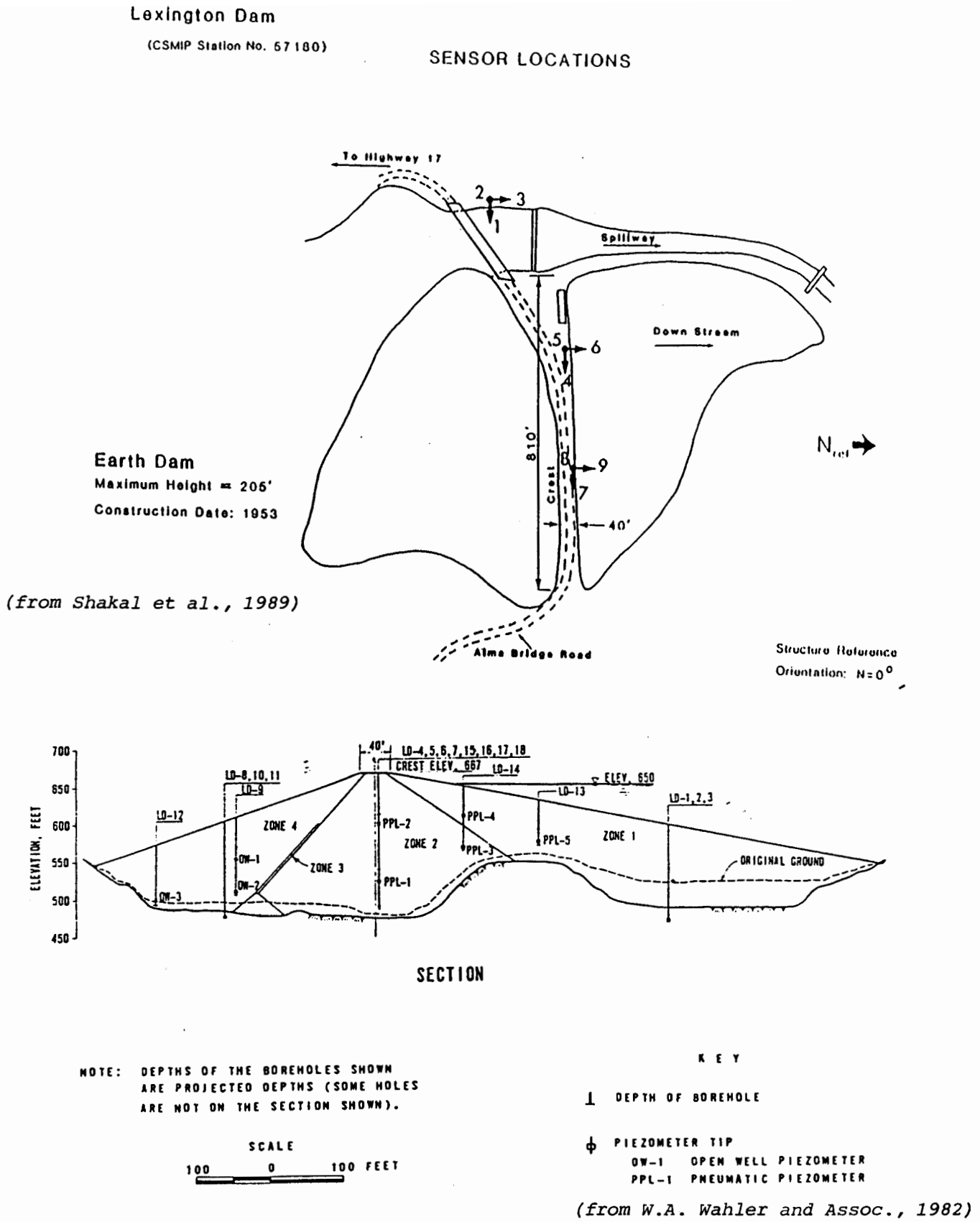

FIGURE 1. Plan of Lexington Dam showing locations of instruments and cross section showing various zones of embankment.

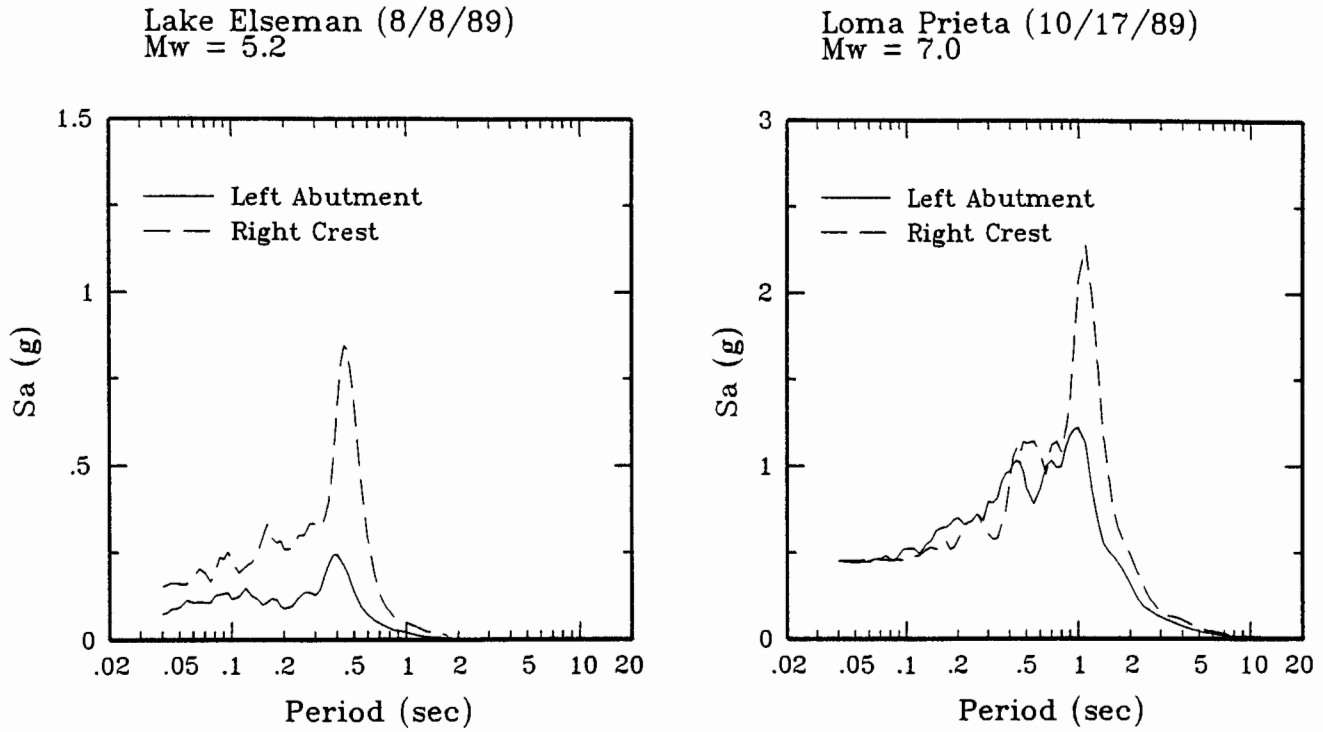

FIGURE 2. Response spectra of recorded motions at Lexington Dam for the transverse component (5% damping).

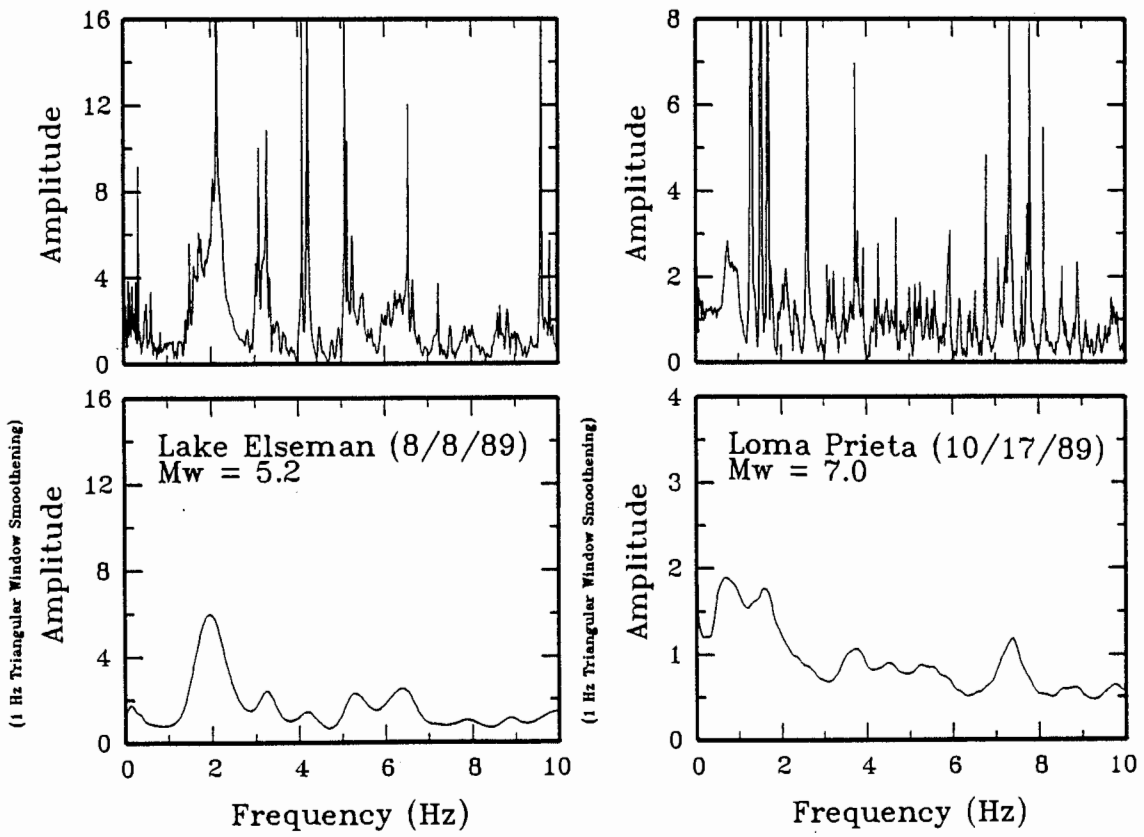

FIGURE 3. Fourier spectral ratios of crest to abutment recordings at Lexington Dam.

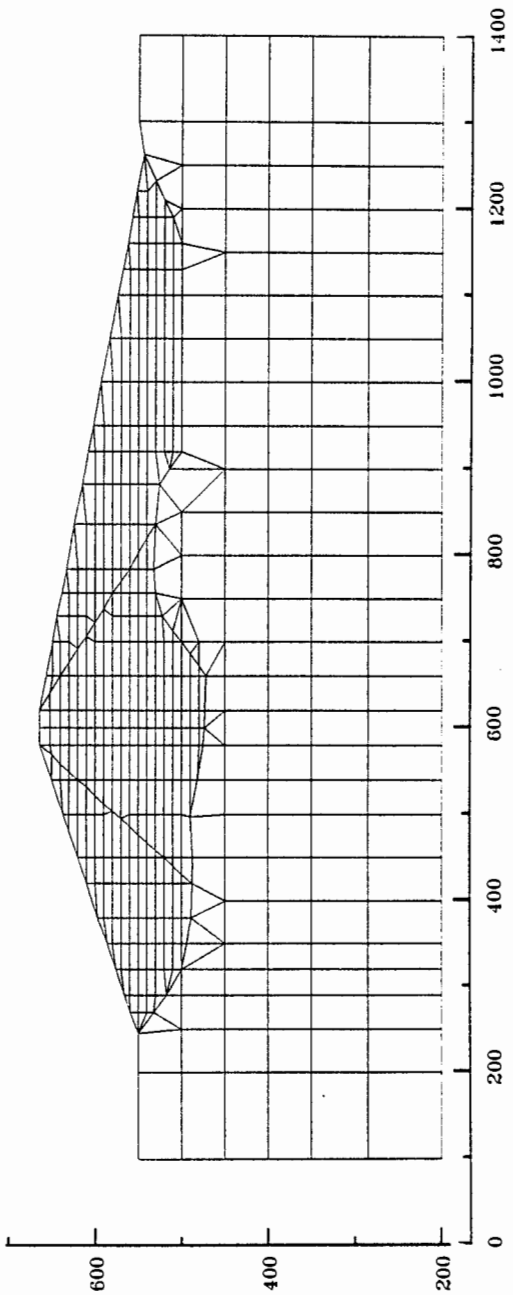

FIGURE 4. Finite element representation of Lexington Dam and its foundation.

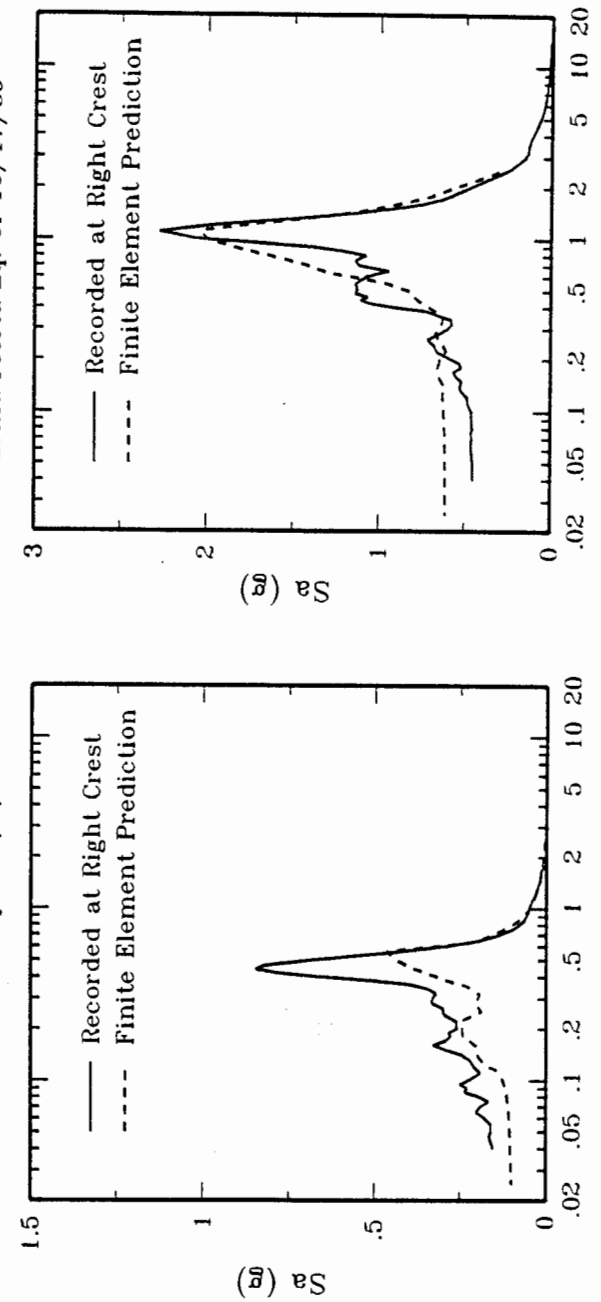

FIGURE 5. Comparison of computed and recorded response spectra at crest of Lexington Dam.

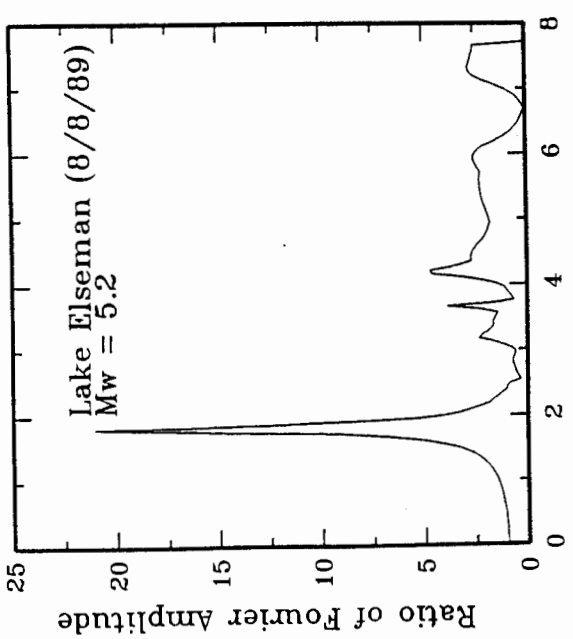

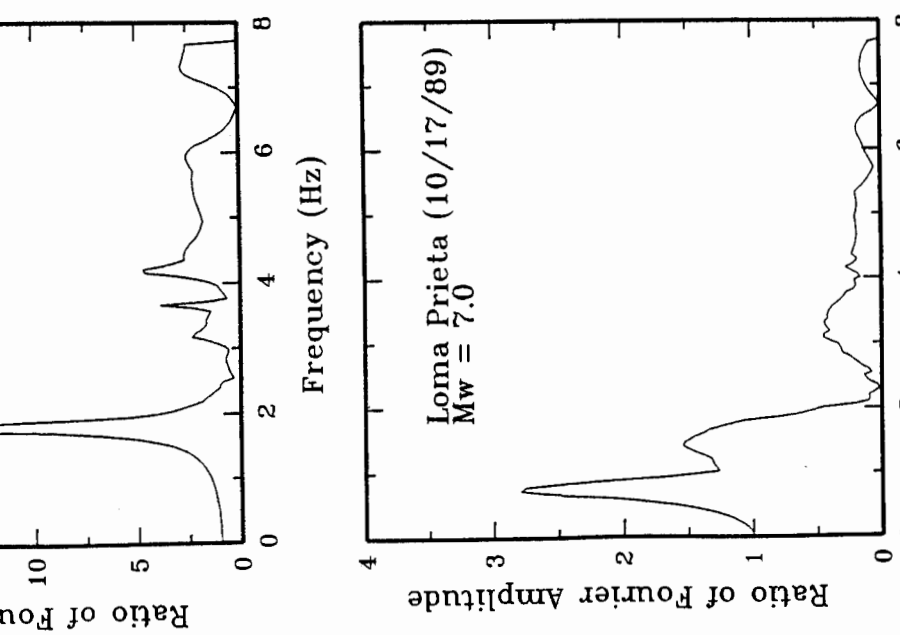

FIGURE 6. Computed Fourier amplitude transfer function (crest to abutment) at Lexington Dam.

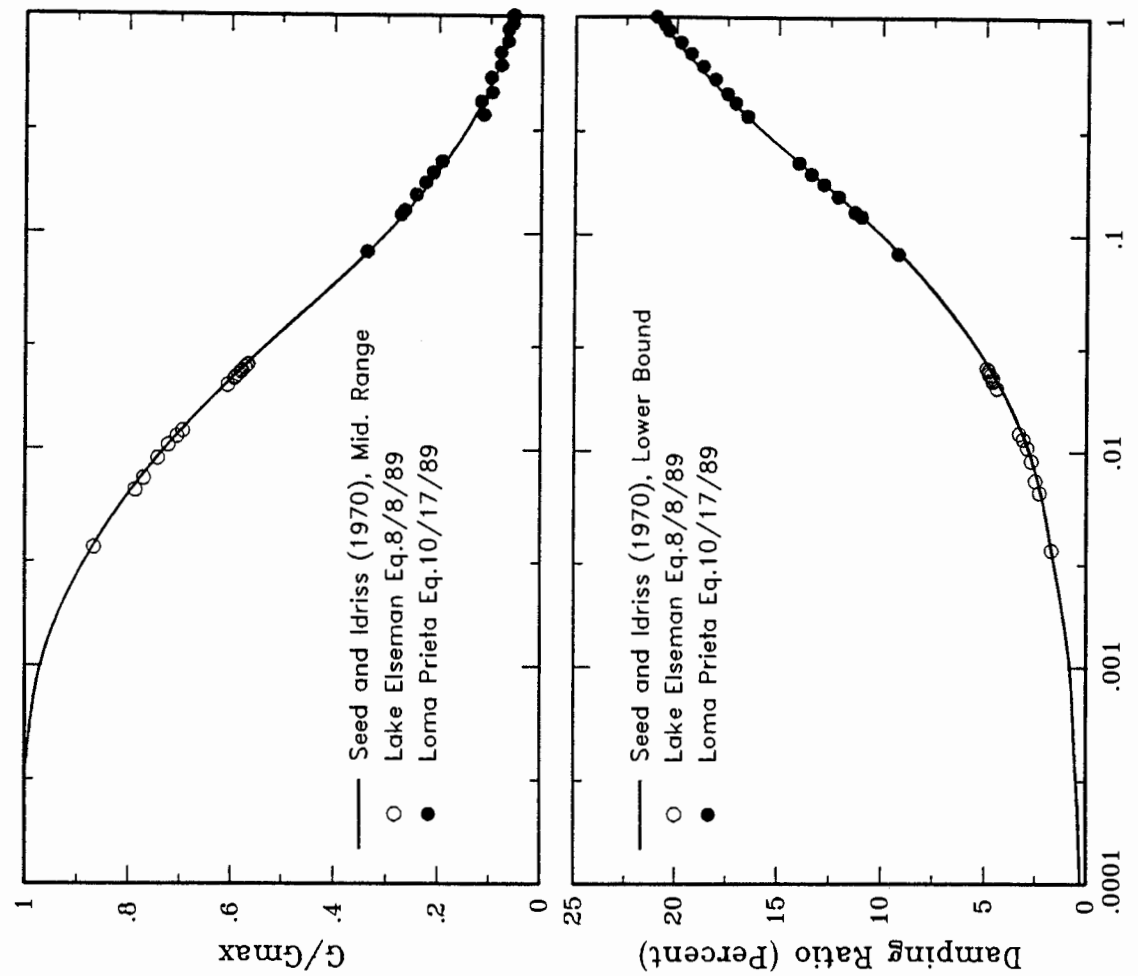

FIGURE 7. Variation of shear modulus and damping with strain for two events at Lexington Dam.

SOIL-FOUNDATION-STRUCTURE BEHAVIOR AT THE OAKLAND OUTER HARBOR WHARF

G. Norris and R. Siddharthan
Associate Professors, University of Nevada, Reno

Z. Zafir, S. Abdel-Ghaffar, and P. Gowda
Graduate Students, University of Nevada, Reno

ABSTRACT

This paper discusses the use of CSMIP records at Oakland Outer Harbor Wharf (along with that from Yerba Buena) to study the free-field motions at Oakland Outer Harbor, both at shallow depth and to bedrock, and the possible softening of soils surrounding the piles supporting the instrumented wharf. The paper also discusses the determination of the motion on the instrumented wharf using free-field motion input and deflection compatible lateral and vertical pile foundation stiffnesses. Such derived motion compares well with the recorded motions on the deck. While there was no reported liquefaction at the site, there was at nearby locations; and the consequence of an assumed lower relative density of the near-surface sand at Oakland Outer Harbor is discussed. Likewise, the consequence of a change in the orientation of the wharf or the incoming motions, assessed by interchanging the direction of the free-field motions, is presented. These latter changes reflect conditions under which a soil-foundation interaction failure or structural failure of the batter piles may have developed, failures that occurred at facilities nearby.

INTRODUCTION

During the Loma Prieta earthquake of October 17, 1989, there was considerable damage to facilities at Oakland harbor; however, there was no specific failure of the soil or damage to the structure of the CSMIP instrumented wharf (Berths 24,25,26) at Oakland Outer Harbor. This paper discusses the use of CSMIP records at the Oakland Outer Harbor Wharf to assess free-field motions in the soil supporting the piles of the wharf, the nonlinear variation in inertial interaction stiffnesses of the piles (with due consideration of free field strain and any softening due to developing pore pressures associated with unrealized liquefaction), and the assessed motion on the deck using free-field input through deflection compatible equivalent linear foundation springs. In addition, the paper discusses the consequence of a decrease in the relative density of the near-surface sand layer supporting the piles or the direction of incoming motions. Such changes reflect conditions under which there may have been liquefaction or a soil-foundation interaction failure or structural failure of the batter piles as observed at nearby facilities.

LAYOUT OF RECORDING INSTRUMENTS AND SOIL PROFILE

Figure 1 presents the layout of the instrumentation at Oakland Outer Harbor Wharf. Channels 1, 3, 10 and 12 are the horizontal free-field instruments located to the east of the wharf. They exhibited peak accelerations of 0.28g, 0.22g, 0.27g, and 0.29g, respectively, during the Loma Prieta earthquake.

Figure 2 represents the averaged soil profile used for the horizontal free-field response evaluation as constructed based on soil and geophysical data taken from a number of sources (see Acknowledgements).

SHEAR MODULUS AND DAMPING CURVES FOR THE SOIL LAYERS

In performing an equivalent linear one-dimensional ground response analysis using the commonly employed program, SHAKE (Schnabel et al., 1972), it is necessary to specify the soil type (SAND, CLAY or ROCK) and to supply the shear modulus reduction (G/G_{max}) and damping (β) curves for these materials. In the deep deposit considered here (approximately 495 ft. to Franciscan greywacke), the vertical effective stress σ'_{vo} increases to over 25000 lb/ft^2. There have been a number of laboratory studies, e.g., that by Hardin and Drnevich (1972), that have shown a dependency of G/G_{max} and β values on the level of σ'_{vo}. Therefore, a modified SHAKE analysis was used here in which such dependency was modeled.

Figure 3 shows curves for Bay Mud modified from the curves given by Seed and Sun (1989) using a relationship for overburden pressure established from the work of Hardin and Drnevich (1972). It should be noted that the Seed and Sun shear modulus curve for Bay Mud (σ'_{vo}=2000 lbs/ft^2) exhibits linearity (i.e., G/G_{max}=1) up to a greater strain ($1x10^{-2}$%) than that for other clays and a damping curve that falls near the lower range for the average of all clays (see Seed and Idriss, 1970). Similar stress-dependent modulus and damping curves were derived for sands as shown in Figure 4.

FREE FIELD RESPONSE

All free-field horizontal acceleration histories (Channels 1, 3, 10 and 12) were considered separately, and the motions at the top of the bedrock at a depth of 495 ft. were computed using deconvolution. Figure 5 shows the spectral acceleration curve for rock motion derived using the modified SHAKE program along with the spectral curve for the particular (ground surface) input motion for Channels 10 and 12. (The curves for Channel 1 are like those for Channel 10; and 3 like those 12.) One will note that the predominant period of base and surface motions is about 0.6 to 0.8 seconds and that the spectrum for motion in the long direction of the wharf (Channels 12 and 3) is wider indicating energy input over a wider range in frequency than that for motions transverse to the wharf (Channels 10 and 1). This raises the question of the possibility for damage to the wharf had the orientation of the wharf or the incoming motions been reversed.

The influence of the soil deposit can be judged from a consideration of the ratio of the spectral accelerations, surface to base, at different periods. From inspection of all sets of curves, it is clear that the maximum ratio occurs at about 1.3 to 1.4 seconds making this the effective period of the deposit.

Figure 6 provides a comparison of the spectral curves for derived motions with that for recorded motion on rock at Yerba Buena. For additional comparison, bedrock motion for Channel 12 was derived using the traditional SHAKE analysis (i.e., no modification for σ'_{vo}) and its spectral curve is compared with those

for Yerba Buena and the modified SHAKE analysis in Figure 7. It is seen that the already high peak at approximately 0.2 seconds in the modified SHAKE curve is unreasonably high for the traditional SHAKE analysis.

Given the agreement between the recorded rock motion and the deconvoluted spectra shown in Figure 6 and peak rock accelerations (0.12g deconvoluted versus 0.11g recorded maximum peak value on rock in the Bay area), it was decided that the modified SHAKE analysis gives sufficiently accurate free-field stresses and strains to proceed with both the liquefaction and pile stiffness evaluation studies as discussed subsequently.

Figure 8 shows the variation in equivalent shear strain with depth from deconvolution using the modified SHAKE program relative to all horizontal free field motion input. Figure 9, which is a plot of the effective modulus ratio with depth for Channel 3 and 12 input, is an indication of the nonlinearity of the responses induced in the different materials during the Loma Prieta earthquake. A shear modulus ratio of one signifies that the material is responding as an elastic material at its initial tangent shear modulus (G_{max}).

LIQUEFACTION ANALYSIS

Figure 10 indicates the soil layers representative of a longitudinal cross section taken midway across the slope of Figure 11. This is slightly different than the soil layering depicted in Figure 3 which represents conditions at the top of the slope where the free-field instruments are located. As indicated in Figure 11, the 37-ft. thick sand layer located near the top of the profile was allowed to take on different property values corresponding to the assumption of different relative densities (D_r) for the sand. Further, the modulus (G_{max}) and related shear wave velocity (V_s) values were allowed to vary with depth within the layer in relation to the change in the mean normal effective stress.

While the consulted soil reports and borings generally yield a corrected standard penetration test blow count (N_1) value of 70 or greater for this silty sand, an N_1 that corresponds to a Dr of 100%, it is known that both natural and hydraulic fill sand at other locations in the Oakland harbor (some of which liquefied during the earthquake) exhibit dramatically lower blow count values (down to 10 or less). Furthermore, it is this sand layer that provides the support for the wharf piles. Therefore, it was decided to evaluate the possibility of liquefaction at the site for other assumed combinations of D_r and N_1.

Rock motion for Channel 12 (i.e., the greater motion in the long direction of the wharf) was used to assess the equivalent shear stress (τ_{eq}) and, hence, the earthquake induced stress ratio ($R=\tau_{eq}/\sigma'_{vo}$) with depth through this layer for these different density states of the sand: D_r=100%, N_1=70; D_r=90%, N_1=44; D_r=58%, N_1=16; and D_r=40, N_1=6. Figure 12 shows the variation in stress ratio with depth through the sand as obtained from a modified SHAKE analysis. Realize, of course, that changes in the property values for the sand cause changes in the resulting near-surface response (i.e., strain, acceleration, etc.).

Superposed on the plot are vertical lines of the stress ratio necessary to cause liquefaction in four equivalent cycles of shaking for different N_1 and D_r values. While four equivalent cycles of excitation is a low value for the

typical magnitude 7 earthquake, this is the value assessed from the Channel 12 surface acceleration record using the weighting techniques after Seed et al. (1975).

The stress ratios to cause liquefaction were established from curves presented by Norris (1988) which are cross plotted from those given by Seed et al. (1983). Corrections relating to the percentage of fines derived from the relations presented by Seed et al. (1984), applied to the Norris (1988) curves, give the curves shown in Figure 13. Such treatment of fines is important in the present case because the near surface sand is silty. Table 1 presents the values to cause liquefaction in four cycles for various combinations of N_1 and percent fines. Only the values immediately bracketing the variation in induced stress ratio are shown in Figure 12.

It is clear from Figure 12 that, regardless of the difference in variation in induced stress ratio (i.e., for different N_1 and D_r combinations), clean sand with an N_1<25 to 30 blows (D_r<75 to 80%) or silty sand with an N_1<20 blows (D_r<70%) with between 15 and 35% fines would have liquefied had it been present in any form at this location (i.e., layer, seam or lens). This is undoubtedly what happened in areas immediately surrounding the instrumented wharf. On the other hand, at this level of density (70-85%) and above it is unlikely that there would have been any significant softening of the sand during the course of the Loma Prieta earthquake, i.e., any pore pressure buildup causing possibly greater slope or foundation movement would have been accompanied by a dilatant reaction that would have arrested any significant realization of such deformation. Therefore, either the sand was perfectly stable and not likely to soften or it would have liquefied.

PILE FOUNDATION STIFFNESSES

Figure 11 shows the vertical and batter piles used to support the wharf. These are driven 18-in. square prestressed concrete piles. There are approximately 1000 piles over the 1600 ft. length of the wharf. The spacing between the piles varies but it large enough that the piles can be considered as isolated (i.e., there is no group reduction factor to consider). Further, the piles have very little dead load to support and the tip load mobilized at the lower loads is so small that the piles can be considered symmetric as far as their axial response (tension versus compression) is concerned.

The nonlinear variation in vertical stiffness (at groundline) shown in Figure 14 was derived from similar shaped load-settlement curves from three pile load tests (two on piles from Row E and one on a pile from Row B) conducted at the time of construction. Superposed on this curve is a line of constant stiffness of 2000 kips/in which corresponds to the level of shear modulus and strain due to the free-field motions. In other words, due to the earthquake, the shear modulus in the supporting sand layer is already reduced to a certain level and the shear modulus of the soil would not be any higher than the (reduced) free-field value even if the vertical interaction displacements were less than the associated 0.03 in. value. Alternatively, when the interaction displacements and associated shear strains are higher, the soil shear modulus is lower and the vertical pile stiffness is governed by the inertial interaction response.

Using a laterally loaded pile analysis program by Gowda (1991), the lateral

stiffness of the piles was assessed over a wide range in deflection. The curves of Figure 15 are for groundline response for the moment condition of the lateral load applied at the deck times the unsupported length of the pile. One and one-half ft. of Bay Mud (undrained shear strength S_u=1440 lbs/ft^2) over dense sand (friction angle ϕ=39^o) was assumed for this analysis. The superposed cutoff for free-field conditions is not shown but would occur at a groundline inertial interaction or relative deflection of less than 0.02 in. This is smaller than the relative lateral deflections that derive from the dynamic analysis of the wharf described in the next section.

It should be noted that the batter piles were treated as if they have normal and axial stiffnesses equal to the lateral and axial stiffnesses of vertical piles of the same embedment and unsupported length.

Given the high relative density of the supporting sand layer, it was deemed that the above stiffnesses would apply during the earthquake, i.e., there would be no softening of the stiffness curves due to developing porewater pressures in the sand. This would not be the case if the blow count or relative density of the layer were lower than, say, N_1=20 or D_r=70%, but then as shown in the last section such sand would liquefy directly. Of course it may be that at other locations the sand is nonuniform and might liquefied locally without yielding a mechanism for slope failure. Therefore, there might be a momentary reduction in stiffnesses. More detrimental would be the loss of sand strength at shallow depth immediately below the thin cover of Bay Mud causing a significant reduction in lateral (as compared to vertical) stiffness and, hence, a greater transfer of lateral load to the batter piles.

DYNAMIC ANALYSIS OF THE WHARF

The program IMAGES-3D (Leung, 1988) was used for the dynamic analysis of the wharf. A repeatable 48-ft. long by 62-ft. wide section of the deck and supporting piles was modeled with brick elements (for the deck) and three-dimensional beam elements (for the pile). Lateral (two directions) and axial spring stiffnesses were assigned at groundline corresponding to the level of assumed (maximum) relative displacements. The stiffnesses were then changed in successive runs until displacement compatible values from the curves of Figures 14 and 15 were obtained. This takes a couple of iterations; but, unless it is done, it cannot be said that the proper distribution of the loads to the structure has been achieved. It should be noted that the pile connection at the deck was handled by embedding a beam element in the brick (deck) element.

A modal analysis was performed to establish the frequencies, mode shapes, modal weights and participation factors of the modeled wharf. Only the first three modes were considered in the dynamic analysis. Damping was taken constant in all modes at a value of 5%, a reasonable value for elastic analysis of reinforced concrete structures. The transverse response of the structure was evaluated based on Channel 1 free-field motion input. Figure 16 is a comparison of computed (Node 18) and recorded (Channel 4) accelerations. Similar good comparison was achieved between Node 34 and Channel 5.

The peak relative displacements at groundline for piles of the different rows varied as follows: 4.16 in. lateral maximum for piles of Row A to a minimum peak value of 0.02 of piles of Row C (outboard); and 0.022 in. axial displacement

for piles of Row D to).0006 in. displacement for piles of Row A.

Channel 12 motion was input to the model to ascertain the response had the incoming motions or the orientation of the wharf been reversed. The computed response at Node 18 for the reversed motion is about the same as that for the actual input.

Based on the above analysis the peak shear forces at the pile head of the batter piles varied from 23.7 to 15.3 kips for the true input (Channel 1) and from 15.4 to 9.2 kips for the reversed input (Channel 12). These shear loads are well within that allowed and would not cause damage to the piles. Therefore, the piles damaged at other locations were likely embedded in a nonuniform sand deposit where liquefaction occurred locally below the thin cover of Bay Mud thus causing reduced lateral stiffness and, hence, even greater transfer of lateral force to the batter piles. This hypothesis is still to be tested but it can be accomplished in a straightforward manner by simply reducing the lateral/normal stiffness of all piles to a very low value (say, 0.5 kip/in) while maintaining compatible vertical stiffnesses. The resulting shear loads at the heads of the batter piles will indicate whether this was a likely mechanism for damage.

CONCLUSIONS

The current study has been useful in looking at free-field motion, soil-foundation interaction response and foundation-structure behavior. However, the dramatic response that occurred at nearby facilities seemed far from developing at the instrumented Oakland Outer Harbor Wharf due largely to the high relative density of the near-surface sand in which the piles supporting the wharf are founded. Simply assuming a lower density of the whole layer will not explain the likelihood for pile damage because the induced stress ratio in the layer is so large that the sand would need to be of such high density (D_r>70%) to survive liquefaction that it would not be subject to softening due to developing porewater pressures. Alternatively, a mechanism of damage arising from a loss in lateral stiffness due to local near-surface liquefaction is still being investigated. There was no particular effect due to a change in the orientation of the incoming motions. In total, the present study has shown the usefulness of the CSMIP records in the attempted verification of methodologies for soil-foundation-structure interaction analysis; though, at the instrumented Oakland Outer Harbor Wharf, there was nothing of dire consequence to report. Basically, the structure was of such small mass that, in such competent soil, there was no significant interaction response, i.e., the structure was forced to follow free-field soil motion.

ACKNOWLEDGEMENTS

This study was supported by a grant from the Office of Strong Motion Studies of the Division of Mines and Geology of the California Department of Conservation. The authors would also like to thank Jerry Serventi of the Port of Oakland, Dave Rogers of Rogers Pacific, Dick Short of Kaldveer, Bob Darrah of Dames and Moore, Mark Best of Pioneer Drilling, and Ad Goldschmidt of CALTRANS for providing a variety of information (soil reports, boring logs, pile load test results, driving records, etc.) relative to the Oakland harbor and Cypress area.

REFERENCES

1. Gowda, P. (1991), "Laterally Loaded Pile Analysis for Layered Soil Based on the Strain Wedge Model," M.S. Thesis, University of Nevada, Reno, in preparation.

2. Hardin, B.O., and Drnevich, V.P. (1972), "Shear Modulus and Damping in Soils: Design Equations and Curves," Journal of Soil Mechanics and Foundations Division, ASCE, Vol. 98, No. SM7, pp. 667-692.

3. Leung, W.H. (1988), "IMAGES-3D: Interactive Microcomputer and Graphics of Engineering Systems-3 Dimensional," Celestial Software, Inc., Berkeley, California.

4. Norris, G.M. (1988), "Liquefaction of the Meloland Overcrossing During the Imperial Valley Earthquake of 1979," Bulletin of the Association of Engineering Geologists, AEG, Vol. XXV, No. 2, pp. 235-247.

5. Seed, H.B. and Idriss, I.M. (1970), "Soil Moduli and Damping Factors for Dynamic Response Analyses," Report No. EERC 70-10, Earthquake Engineering Research Center, University of California, Berkeley.

6. Seed, H.B., Idriss, I.M., and Arango, I. (1983), "Evaluation of Liquefaction Potential Using Field Performance Data," Journal of the Geotechnical Division, ASCE, Vol. 109, No. 3, March, pp. 458-482.

7. Seed, H.B., Idriss, I.M., Makdisi, F., and Banerjee, N. (1975), "Representation of Irregular Stress Time Histories by Equivalent Uniform Stress Series in Liquefaction Analyses," Report No. EERC 75-29, Earthquake Engineering Research Center, University of California, Berkeley.

8. Seed, H.B. and Sun, J.I. (1989), "Implications of Site Effects in the Mexico Earthquake of Sept. 19, 1985 for Earthquake-Resistant Design Criteria in the San Francisco Bay Area of California," Report No. UCB/EERC-89/03, Earthquake Engineering Research Center, University of California, Berkeley.

9. Seed, H.B., Tokimatsu, K., Harder, L.F.,and Chung, R.M. (1984), "The Influence of SPT Procedures in Soil Liquefaction Resistance Evaluations," Report No. UCB/EERC-84/15, Earthquake Engineering Research Center, University of California, Berkeley.

10. Schnabel, P.B., Lysmer, J., and Seed, H.B. (1972), "SHAKE: A Computer Program for Earthquake Response Analysis of Horizontally Layered Sites," Report No. EERC 72-12, Earthquake Engineering Research Center, University of California, Berkeley.

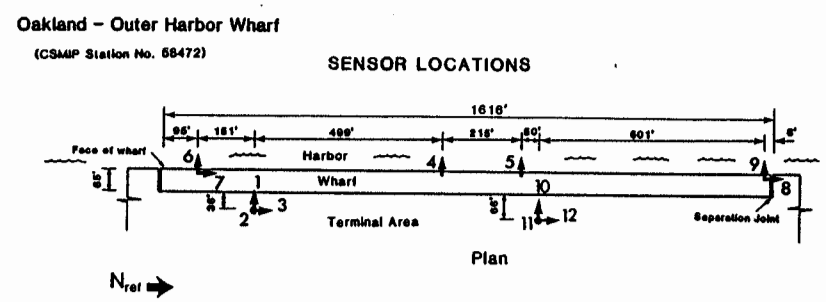

Fig. 1 Sensor location at Oakland Outer Harbor Wharf

▽			
18'	Sand	σ'_{vo} = 563 psf	V_s = 500 ft/sec
4'	Clay	1226	350
43'	Sand	2671	1100
80'	Clay	6035	1000
20'	Clay	8560	1200
65'	Clay	10706	1200
25'	Clay	12978	1200
45'	Clay	14746	1400
85'	Sand	18538	1750
15'	Clay	21573	1250
95'	Sand	24921	1750
Half Space (Franciscan Greywacke)			V_s = 2000 ft/sec

Fig. 2 Soil profile used for one-dimensional deconvolution studies

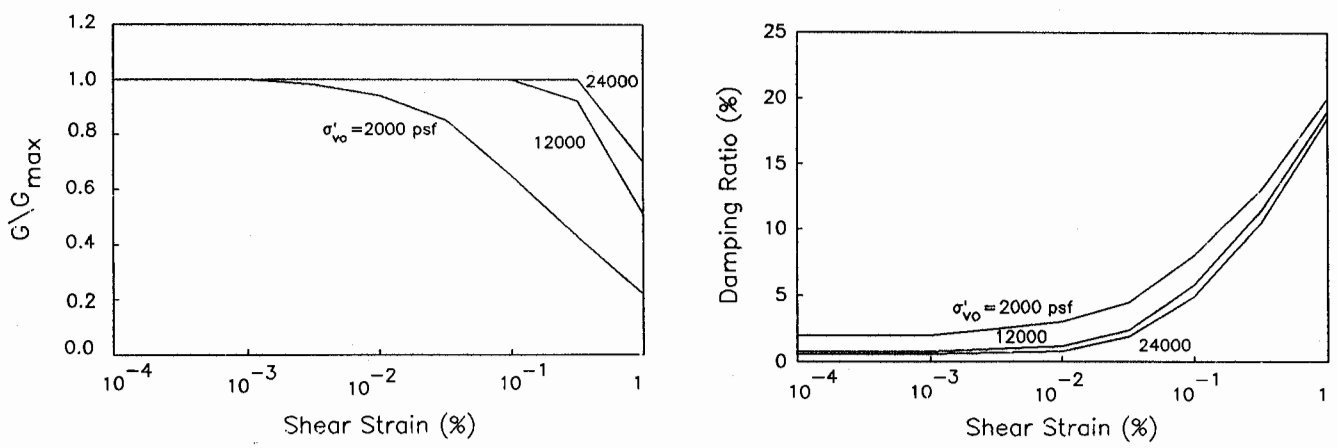

Fig. 3 Shear modulus reduction and Damping curves for Bay Mud for different σ'_{vo}

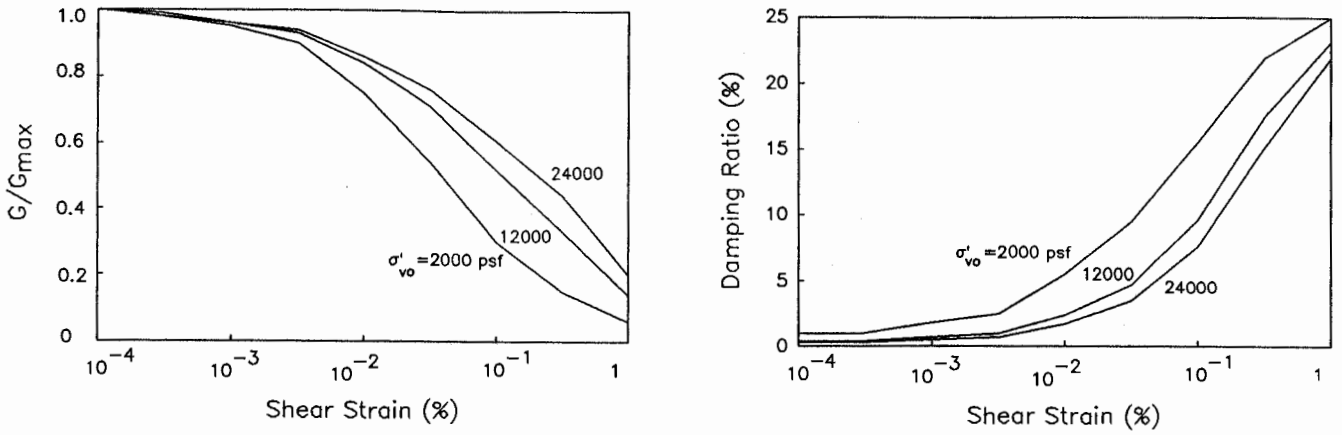

Fig. 4 Shear modulus reduction and Damping curves for sand for different σ'_{vo}

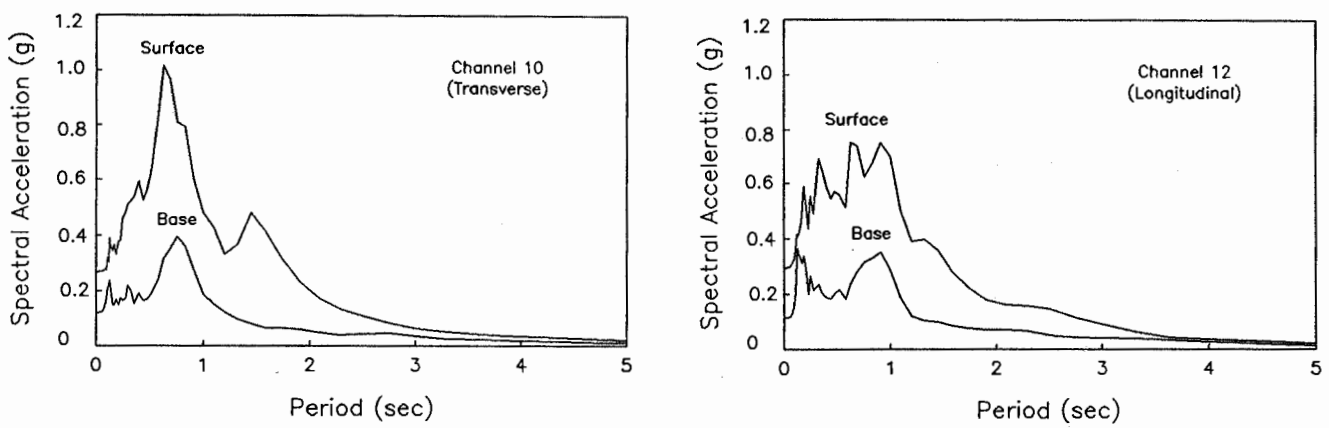

Fig. 5 Surface and (deconvoluted) rock spectral acceleration curves, Channel 10 & 12

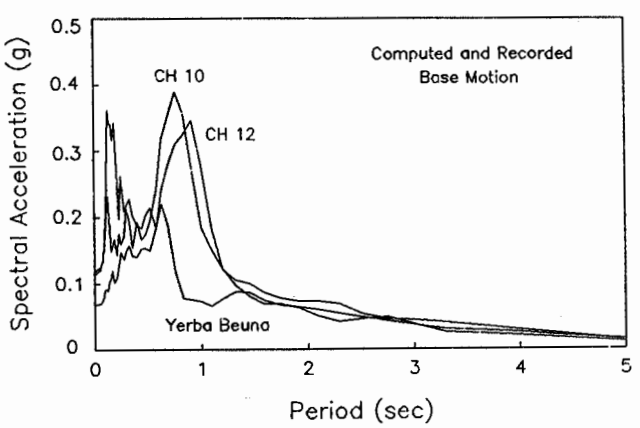

Fig. 6 Spectral acceleration curve for rock motions, Channels 10 & 12 and Yerba Buena

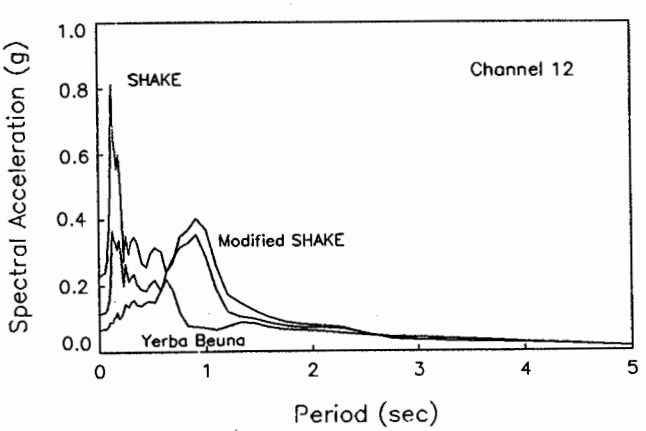

Fig. 7 Spectral acceleration curves for rock, Channel 12 modified SHAKE vs. traditional SHAKE analysis and Yerba Buena

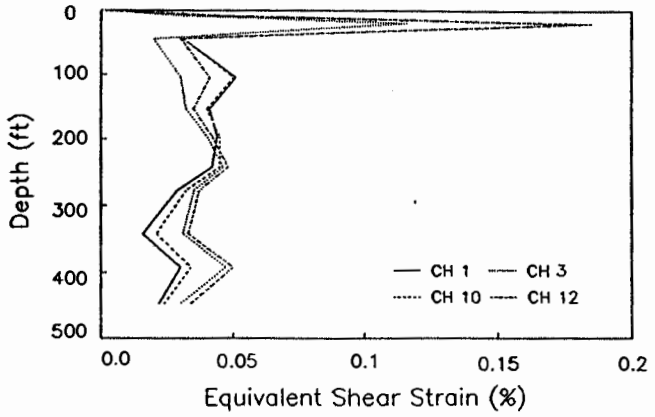

Fig. 8 Variation in equivalent shear strain

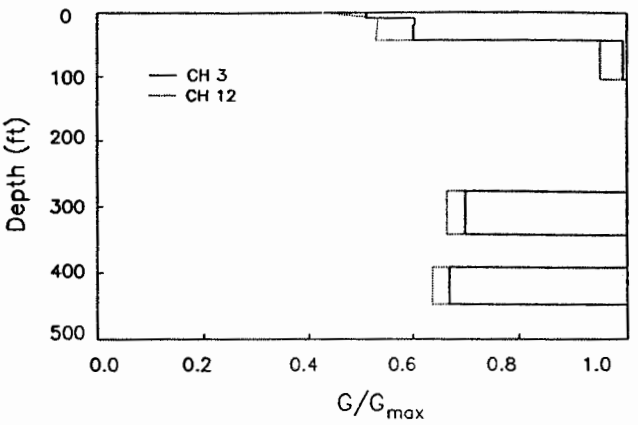

Fig. 9 Variation in modulus reduction

15'	Clay	σ'_{vo} = 1226 psf	V_s = 500 ft/sec
37'	Sand	2671	Variable
80'	Clay	6035	1000
20'	Clay	8560	1200
65'	Clay	10706	1200
25'	Clay	12978	1200
45'	Clay	14746	1400
85'	Sand	18538	1750
15'	Clay	21573	1250
95'	Sand	24921	1750
Half Space (Franciscan Greywacke)			V_s = 2000 ft/sec

Fig. 10 Soil profile taken and slope for liquefaction studies

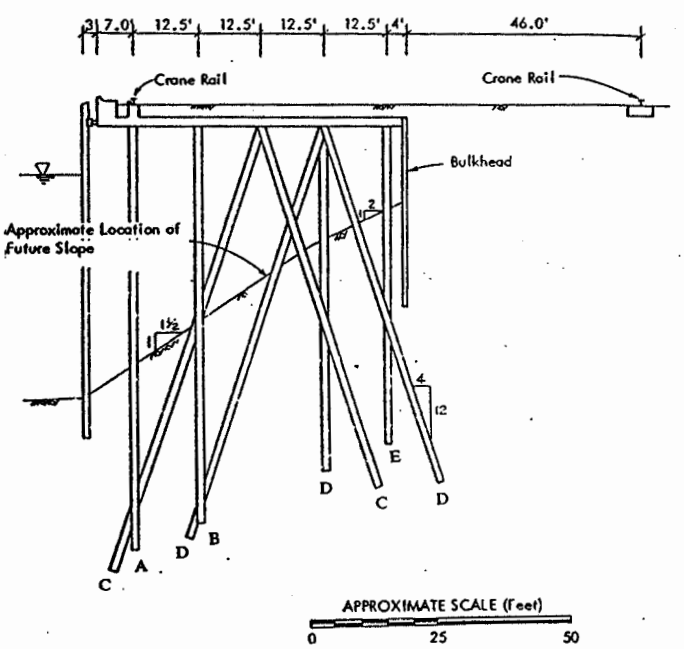

Fig. 11 Pile arrangement

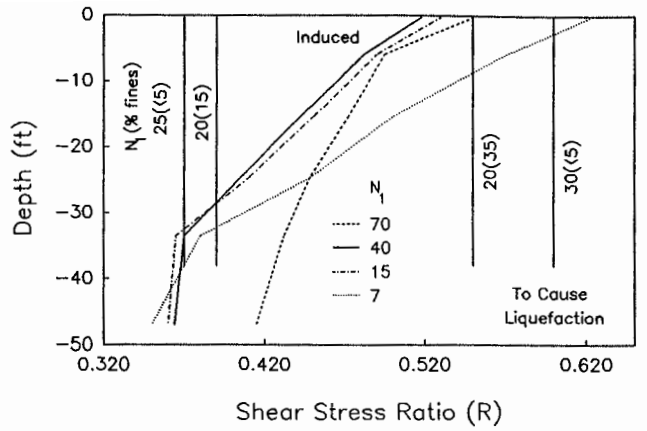

Fig. 12 Variation in stress ratio R for Channel 12 motion

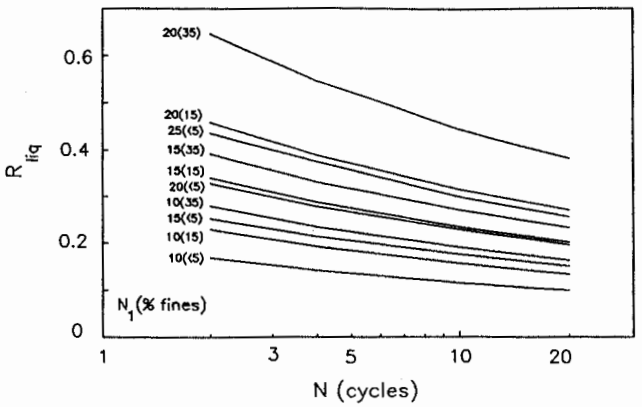

Fig. 13 Liquefaction Curves

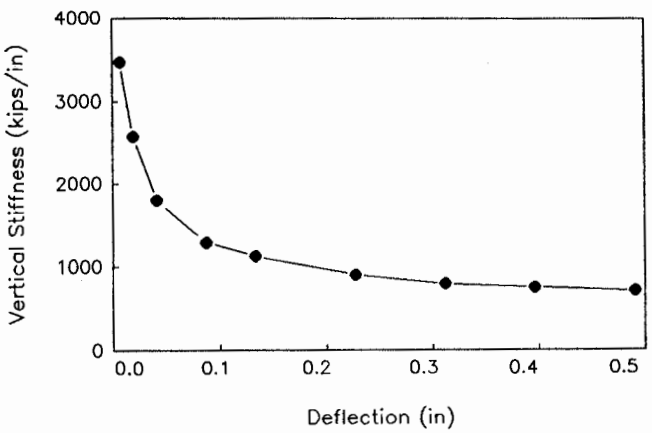

Fig. 14 Axial stiffness variation, all piles

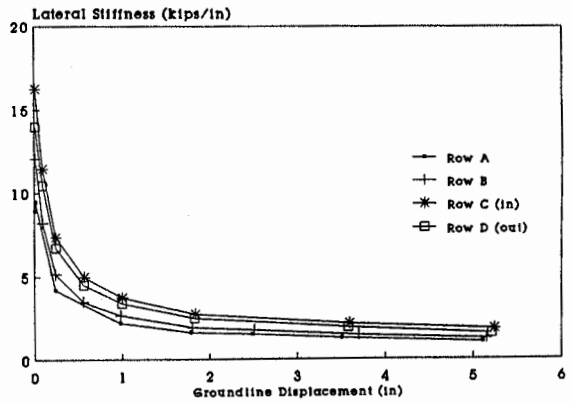

Fig. 15 Lateral stiffness variation, piles of Row A, B, C, D (Others not shown)

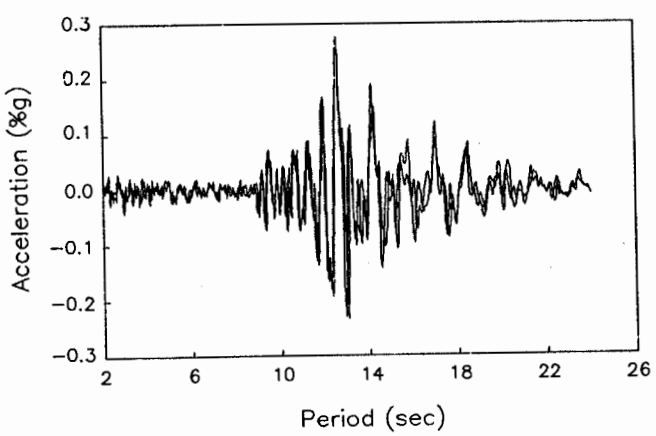

Fig. 16 Computed (Node 34) using Channel 1 input versus recorded (Channel 5) accelerations on the wharf

Table 1. Stress Rate to Cause Liquefaction in Four Cycles for Different Blow Counts and Percent Fines

N_1 blows (% fines)	R_{liq}
25(≥15)	∞
30(≤5)	≈0.6
20(35)	.55
20(15)	.39
25(≤5)	.37
15(35)	.33
20(≤5)	.29
15(15)	.28
10(35)	.23
15(≤5)	.21
10(15)	.19
10(≤5)	.14

RESPONSE OF BASE-ISOLATED STRUCTURES IN RECENT CALIFORNIAN EARTHQUAKES

James M. Kelly, Ian D. Aiken, and Peter W. Clark

ABSTRACT

The October 1989 Loma Prieta and February 1990 Upland earthquakes both affected base-isolated structures and provided the first significant earthquake response data from base-isolated structures in the U.S. In the Loma Prieta earthquake, California Strong Motion Instrumentation Program (CSMIP) sensors on the Sierra Point Overhead were triggered, and in the Upland earthquake, the Foothill Communities Law and Justice Center (FCLJC) in Rancho Cucamonga experienced significant ground accelerations, CSMIP instruments again recording the motions.

The responses of the two structures are investigated in a study of the strong-motion data. Isolation system characteristics are determined from the data and these are used in analytical studies of the structure responses. Implications of the results on current design approaches and code requirements for base-isolated structures are addressed.

1. INTRODUCTION

1.1 Description of Structures

FCLJC - The FCLJC is a four story plus basement braced steel frame. The building was designed in 1983 and construction was completed in 1985. The building is 414 ft by 110 ft in plan, and the height of the main roof above the isolation bearings is 76.5 ft (Fig. 1). At the basement level, 14-inch thick concrete shear walls extend the full height of the basement. These walls serve to spread overturning actions in the braced frames onto the bearings. The foundation system consists of individual spread footings for each isolation bearing. The site is underlain by sand, silty sands, gravel, and a coarse-to-fine alluvial sequence, with basement rock at a depth of about 800 ft.

The FCLJC was the first base-isolated structure in the United States, and as such, a number of conservative assumptions were made in the design of the building. The County of San Bernardino requested that the building would experience only minor structural damage in the Maximum Probable Earthquake — the maximum event that could be expected during a period of 100 years — and would not suffer permanent damage to the basic structure in a Maximum Credible Earthquake — the worst seismic event that is postulated within the geotechnical framework of the site [1]. The Maximum Credible Earthquake was defined as a Richter magnitude 8.3 event on the San Andreas Fault, 13.5 miles from the site. This event corresponds to a motion with PGA = 0.6 g, a spectrum with constant velocity of 50 in/s in the period range beyond 0.8 second, and a duration longer than 35—40 seconds. The extremely long (414 ft) plan dimension of the building resulted in very large torsional effects when the 5% eccentricity code requirement was included in the analyses. The FCLJC isolation system is discussed in detail in section 2.

Sierra Point Overhead - The Sierra Point Overhead is an 8-lane, 616 ft long bridge on U.S. Route 101 north of San Francisco International Airport. The 117 ft wide, 10-span bridge is

skew in plan, with the north and south abutments skewed 59° and 72°, respectively, to the radial line.

The bridge was designed in 1955, constructed in 1957, widened in 1969, and base-isolated as part of a seismic upgrade project in 1984-85 [2]. Plan and typical section views of the structure are shown in Fig. 2. The superstructure consists of a concrete deck slab on steel girders supported on lead-rubber isolation bearings. The bent columns are cantilevered from individual spread footings on hard sandstone. There are a total of 27 concrete columns, 36 inches in diameter, and they are generally arranged in 4-column bents. The bents at the ends of the bridge have only one, two, or three columns because of the skew alignment. The columns vary in length from 11 ft, 19 ft, and 27-30 ft, with the shorter columns being nearer the abutments. The bridge carries traffic over two railroad tracks. Three pre-cast, reinforced-concrete collision walls, 13.75 ft high and 3 ft thick extend between bent columns parallel to the railroad alignment as shown in Fig. 3.

The bridge was originally designed under 1953 AASHO specifications and in a 1982 structural review was found to be deficient in column strength. Base isolation was chosen as an alternate solution to reconstruction, and was able to reduce the horizontal earthquake loads subjected to the vulnerable columns. The structure was isolated by replacing the spherical steel pin-type bearings with lead-rubber isolation bearings. The design earthquake was a Richter magnitude 8.3 occurring on the San Andreas fault 4½ miles west of the site. The isolation system is discussed in detail in section 2.

1.2 Earthquake Motions

The epicenter of the M_L = 5.5 February 28, 1990 Upland earthquake was located about 8 miles east of the FCLJC building. The maximum free-field acceleration recorded at the site was 236 gals, and 40 seconds of data were acquired. The free-field accelerations were significantly larger than those experienced by the building. Instrumentation on the FCLJC consists of 16 accelerometers on the structure itself, and an additional 3 free-field accelerometers located approximately 350 ft SE of the building. The instrumentation locations are shown in Fig. 1.

The M_L = 7.1, October 17, 1989 Loma Prieta earthquake was centered about 50 miles south of the Sierra Point Overhead bridge. The maximum site free-field acceleration was 104 gals, and 38 seconds of data were acquired. Instrumentation on the bridge consists of 13 accelerometers located on two adjacent columns (Fig. 2). Accelerations are measured above and below two isolators and at the base of one of the columns. Three additional sensors are located in the free-field, on a sidehill bench on sandstone bedrock 200 ft NW of the bridge, at approximately the same elevation as the bridge deck.

No damage occurred in either of the structures as a result of the earthquakes.

2. DESCRIPTION OF ISOLATION SYSTEMS

FCLJC - The building is supported on 98 high-damping natural rubber bearings and has a design period of approximately 2.0 seconds under the Maximum Credible Earthquake. There are eight different bearing types incorporated in the design. All of the bearings are 20 inches in diameter and the total height of rubber in each case is 11.97 inches. A view of one of the bearings during construction is shown in Fig. 4. Four different rubber compounds were used in the manufacture of the isolators, aspects of which are discussed in more detail in section 3. The maximum displacement in the isolators under the Maximum Credible Earthquake was calculated to be 15 inches. To accommodate this displacement, a seismic gap of 16 inches is

provided on all sides of the building. Ball joints were added to piping and utility connections across the isolation interface to allow the large horizontal displacements. The isolation bearings possess substantial inherent damping, which varies from about 9 to 12% depending on the level of deformation in the isolators. The first two fixed-base translational periods were calculated to be 0.62 second and 0.72 second in the N/S and E/W directions, respectively. Connection of the bearings to the foundation and superstructure is by steel pin shear dowels into the bearing end plates.

Each isolator used was tested at the time of manufacture at shear strain levels of 2%, 10%, 25%, and 50% [1]. First cycle (unscragged) and tenth cycle (fully scragged) stiffnesses were obtained. The composite stiffnesses of the entire isolation system (unscragged and scragged) are given in Table 2. In addition to these tests, four bearings were tested to the full design displacement of 15 inches [3].

Sierra Point Overhead - The Sierra Point Overhead isolation system consists of 33 lead-rubber and natural rubber bearings. There are a total of six different bearing designs in the system. There are two bearings sizes: 18 inches square or 22 inches in diameter; the square bearings have either no lead plug or a lead plug of 3 inches or 6 inches in diameter. The circular bearings have 4 inch diameter lead plugs. The total height of rubber in the bearings is either 5.625 inches or 6.375 inches. The natural rubber used in the bearings is an unfilled compound with a relatively low inherent damping and a moderately nonlinear low-strain stiffness behavior. The abutment details were not changed in the isolation retrofit, and remain the same as in the original 1957 construction, being 1 inch gaps filled with expansion joint material. The maximum displacement of the deck with respect to the footings in the design earthquake was calculated to be 7-9 inches, involving about 1½ inches in the columns and the remaining displacement in the isolators themselves. The maximum isolator displacement was calculated to be 7½ inches.

Clearly, the required seismic gap has not been provided. The reason for not doing so at the time of the upgrade was given as economic. In the event of a major earthquake and consequent damage to the haunch at the top of the abutment backwalls, the required seismic gap would be provided at the time of repair.

The overall design of the bearings was influenced by several dimensional constraints. The removal of the spherical steel pin type bearings provided a clear gap of only 9 or 10 inches between the top of the columns and the underside of the bent cap girders. The plan size of the bearings was limited by the overall size (36 inches diameter) of the columns. Because of the height restrictions, steel dowels were not used for the connection between the upper and lower bearing plates and the isolators themselves. The bearings are kept in place by keeper plates welded to the sole plates.

3. RUBBER COMPOUNDS

FCLJC - Four distinct compounds were used in the FCLJC isolators, all identified as high-damping natural rubber. The compounds are designated by the supplier, LTV Energy Products, Arlington, Texas (in order of decreasing shear modulus), as 246-70, 243-65, 2x-69, 2x-71.

All of these high-damping compounds have a highly non-linear stress-strain behavior that is particularly advantageous for base-isolated systems. The materials are very stiff for cycles of shear at small strain levels. The effective modulus decreases as the strain level increases up to about 100% and for cycles of shear strain beyond this level it stiffens up again. Thus, the system is stiff for wind loads, environmental disturbance, and small earthquake input. It

softens for large earthquake input providing a long period isolation effect and if the motion is much greater than that assumed in the design, the stiffness increases and the displacements are controlled.

Another aspect of the mechanical behavior of these compounds that is important in interpreting isolation system performance is the fact that the material undergoes a reversible process known as scragging. When tested to a specific level of cyclic shear strain, the stiffness in the first cycle is higher than the subsequent cycles. The material rapidly reaches a steady-state and all cycles after about the third are identical. When the compounds are tested under standard test conditions, the accepted procedure is to quote only the fully-scragged properties. The properties associated with the first few cycles are generally ignored. After testing the material will revert to its unscragged state in a matter of hours or sometimes days. Thus, an isolation system that has been unshaken for several years will respond with higher initial stiffness than would be anticipated for fully-scragged properties.

The combined effects of non-linearity due to low strain level and of scragging will mean that the period of the building is much less than the period specified in the design.

The shear moduli of the various compounds were evaluated at the time of manufacture of the isolators and the values obtained are listed in Table 1. The average ratio of the unscragged 2% modulus to the scragged 50% modulus (the design level) is 6.24, and this would predict that the 1.50 second period (if the superstructure were taken to be rigid) would be reduced to a period of 0.8 second. This result agrees with the period identified from the earthquake response data.

Sierra Point Overhead - The elastomer used in the bearings is a lightly-filled rubber designated by the manufacturer, LTV Energy Products, as 247-55. It is a high-strength, low-damping natural rubber compound which is less nonlinear than the high-damping compounds. The scragged 2% shear modulus is about 250 psi compared to the scragged 50% modulus of about 100 psi. No information is available on the unscragged moduli for this compound.

4. EARTHQUAKE RESPONSE OF THE STRUCTURES

CSMIP processed data was used in the response studies of both structures. Typical CSMIP accelerogram processing involves instrument correction, baseline correction, high and lowpass (bandpass) filtering, and then numerical integration to obtain velocity and displacement. The FCLJC accelerograms were bandpass filtered with ramps at 0.3—0.6 Hz and 23—25 Hz, while the Sierra Point Overhead filter ramps were 0.15—0.30 Hz and 23—25 Hz. This means that all long-period content greater than 1.67 seconds and 3.33 seconds was removed from the FCLJC and Sierra Point Overhead records, respectively.

FCLJC - The peak building response and free-field accelerations are given in Table 3. Plots of the N/S foundation, basement, 2nd floor, and roof accelerations are shown in Fig. 5. Linear-elastic 5%-damped response spectra for these responses are shown in Fig. 6. The two figures indicate that the isolation system reduced the high-frequency content of the input ground motion to the superstructure. The structure response period in the N/S direction is 0.7 second from the response spectra (Fig. 6). The maximum displacements of the isolation system were 0.25 inch (2% shear strain) and 0.10 inch (0.8% shear strain) in the N/S and E/W directions, respectively. Frequency-domain analyses of the data indicate that the structure responded with a period of approximately 0.7 second in both the N/S and E/W directions. A single-degree-of-freedom analysis of the isolation system using 2% unscragged properties for the bearings gives a period of approximately 0.7 second. Information from the original design calculations and computer analyses of the structure indicate that the first translational periods of

the superstructure are approximately 0.7 second in both the N/S and E/W directions. These results suggest that the FCLJC response in the Upland earthquake involved coupled response of the closely-spaced first isolated and superstructure modes. Time-history analyses of the FCLJC subjected to the foundation motions recorded in the Upland earthquake have been performed with good agreement between analytical and measured responses.

The torsional response was investigated by evaluation of the torsional displacements of the isolation system and of the superstructure above the isolators. While found not to be significant, about one-half of the total torsional displacement occurring at the roof level was due to the isolation system. Vertical deformations in the isolators on the north and south sides of the building were calculated. The deformations were found to be extremely small (0.02 inch) and did not cause any appreciable rocking motion in the superstructure.

Sierra Point Overhead - The peak structural response and free-field accelerations are given in Table 4. Plots of the longitudinal (N/S) west column above-isolator, below-isolator (top of column), base of column, and free-field accelerations are shown in Fig. 7. The above-isolator peak acceleration (264.5 gals) is slightly less than that below the isolator (304.5 gals) and some reduction of high-frequency content is evident. Linear-elastic 5%-damped acceleration response spectra for these responses (excluding the free-field) are shown in Fig. 8. For the high-frequency peak at about 0.1 second there is some reduction in the spectral ordinate from below the isolator to above the isolator, but for periods greater than about 0.2 second the accelerations above the isolator are equal to or greater than those below it.

The maximum displacements in the isolation system were 0.20 inch (3.6% shear strain) and 0.12 inch (2% shear strain) in the longitudinal (N/S) and transverse (E/W) directions, respectively. These maxima both occurred in the west column isolator. Calculation of the force-deformation relationship for the west column isolator indicates that this level of deformation corresponds approximately to the point of first yield of the lead plug. The force-deformation relationships for all of the six different types of bearings were calculated and the composite system stiffness at pre-yield deformation levels determined. The isolated period was calculated to be approximately 0.75 second. It was not possible to identify a structural period from frequency-domain analyses or response spectra, and thus this calculated period could not be confirmed. However, because of the lack of clearance at the abutments (a nominal 1-inch gap filled with expansion joint material) the deck is not free to move as if it were properly isolated.

As put forward in [4] the 3 to 4-fold increase in superstructure accelerations over those in the footing indicates that either

(a) the composite backfill-abutment-superstructure system is almost rigid and responded to a spike in the site response spectrum (which is not evident in the spectra), or

(b) the conglomeration of loosely-connected superstructure members (the longitudinal stringers that span between the bent caps are fixed at one end and sit on a rocker bearing with additional restrainer-bar seismic restraint at the other) responded dynamically by moving with respect to each other and transmitted frequencies throughout the steel superstructure which were recorded by the instruments. If this were the case, then the accelerations recorded would not be representative of the inertial forces subjected to the columns.

Because of the restricted clearance and restraint existing at the abutments and the segmental nature of the bridge superstructure, it is not possible to make a more detailed interpretation of the records.

5. CONCLUSIONS

It is clear that both of these base-isolated structures did not act under recent earthquake loading in the manner intended for a base-isolated structure. In the case of the FCLJC the response is satisfactorily explained by the fact that the effective isolation period at the level of deformation induced in the elastomer is about the same as that of the fixed-base superstructure. Isolation as a concept is based on there being a large separation between the isolation period and the fixed-base structure period. The advantages of isolation derive from the low participation factors of the higher modes. The small amplification in accelerations seen in the FCLJC is a consequence of the fact that the building did not fulfill this requirement at that level of input. The degree of attenuation of the free-field motion under the building was also surprising but due to the proximity of the epicenter and the depth of the earthquake the motion was most probably generated by vertically-propagating shear waves. The waves striking the free surface reflect in a different way than waves impacting the covered surface under the foundation and this rather than the degree of embedment could explain the attenuation. Although the isolators were about 8 times stiffer than assumed in design, the damping was very high assuring a substantial degree of energy absorption. The structure did perform with smaller drifts and smaller forces than would the fixed-base structure subjected to the same input motion.

In the case of the Sierra Point Overhead the fact that the abutments prevented movement explains the unusual response. This, combined with the high stiffness of the bearings at low levels of strain combine to prevent isolation action.

The conclusion to be drawn from this study is that over-conservatism in the design of base isolation systems is not necessarily a correct approach. Since the FCLJC building was the first base-isolated building in the United States, a great deal of conservatism was incorporated into the design. In recent years extensive tests to failure of isolators for nuclear power plant applications have shown that properly designed and manufactured isolators are capable of very large strains under load and have remarkable margins of safety beyond the design level. This implies that designers should be careful with their conservatism in designing base isolation systems. The structure should be designed on the same basis as a conventional structure with the confidence that if the design-level earthquake is exceeded, the isolators will not fail but the failure will be in the superstructure with exactly the same mechanisms as in a conventional structure. In this way, when the structure is struck by the type of moderate earthquake which is highly likely during the lifetime of the structure, its performance will include those aspects for which isolation is used, namely, reduction of acceleration in the superstructure, no participation of the higher modes and reduced input to building contents.

Analysis of the Sierra Point Overhead Loma Prieta data revealed that the bridge instrumentation layout involves unnecessary redundancy in some channels. It is recommended that the layout be evaluated and redesigned to provide a more informative response data-set for future earthquakes.

REFERENCES

[1] Tarics, A.G., Way, D., and Kelly, J.M., "The Implementation of Base Isolation for the Foothill Communities Law and Justice Center," A Report to the National Science Foundation and the County of San Bernardino, Reid and Tarics Associates, San Francisco (November 1984).

[2] Pomeroy, E.G., "Sierra Point Overhead Seismic Isolation Retrofit," *ATC-17*, Applied Technology Council, pp. 123-132 (March 1986).

[3] Kelly, J.M. and Celebi, M., "Verification Testing of Prototype Bearings for a Base-Isolated Building," *Report No. UCB/SESM-84-01*, University of California, Berkeley (March 1984).

[4] Buckle, I.G., "Recent Progress in Base Isolation for Bridges in the United States," *Proceedings*, 6th U.S.-Japan Bridge Engineering Workshop, Lake Tahoe, Nevada (May 1990).

Table 1 Shear Moduli for FCLJC Rubber Compounds

Compound	Shear Modulus (psi)					
	2%		50%		100%	
	unsc.	scr.	unsc.	scr.	unscr.	scr.
246-70	1083	500	240	163	176	156
243-65	1083	417	205	143	146	130
2x-69	617	402	150	114	111	100
2x-71	542	259	125	100	96	89

Table 2 Isolation System Stiffnesses

	Shear Stiffness (kips/in)			
	2%	10%	25%	50%
unscragged	4949	2288	1412	955
scragged	1700	1000	800	640

Table 3 Summary of Peak Accelerations, FCLJC

Component	Accelerations (gals)	
	N/S	E/W
roof	152.8	85.7
2nd floor	69.4	-
basement[1]	52.6	37.8
foundation[2]	138.9	106.2
free-field	235.6	228.5

Superstructure N/S channels are at center of building
1 - above isolators
2 - below isolators

Table 4 Summary of Peak Accelerations, Sierra Pt. Overhead

Component	Accelerations (gals)		
	N/S	E/W	Vertical
above W. col isolator	264.5	190.3	85.2
below W col. isolator	305.4	204.2	-
above E col. isolator	283.3	179.7	-
below E col. isolator	307.5	188.3	-
base of W column	88.0	44.4	28.9
free-field	103.6	56.6	31.2

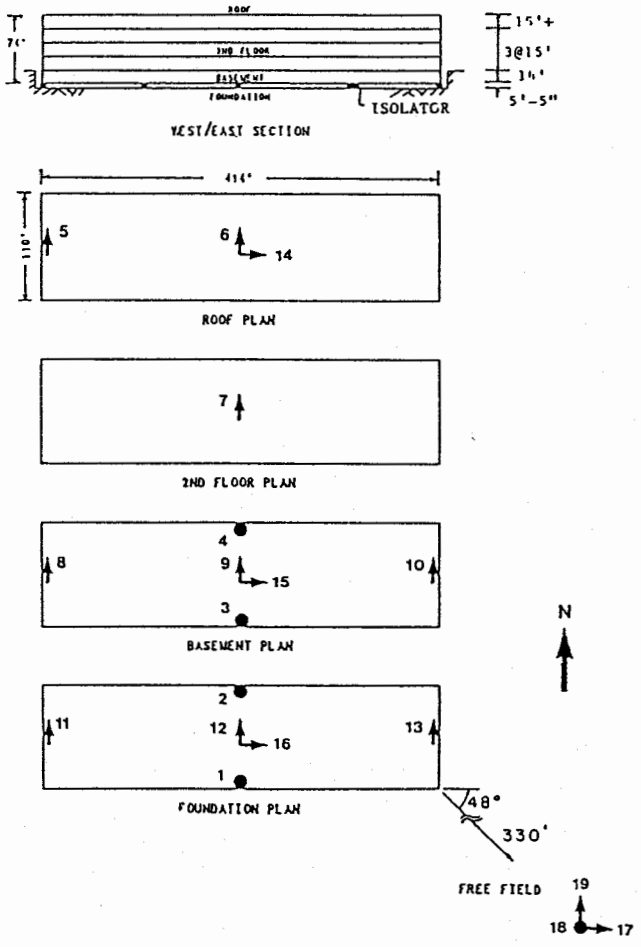

Fig. 1 FCLJC Plan and Elevation with Instrumentation Layout

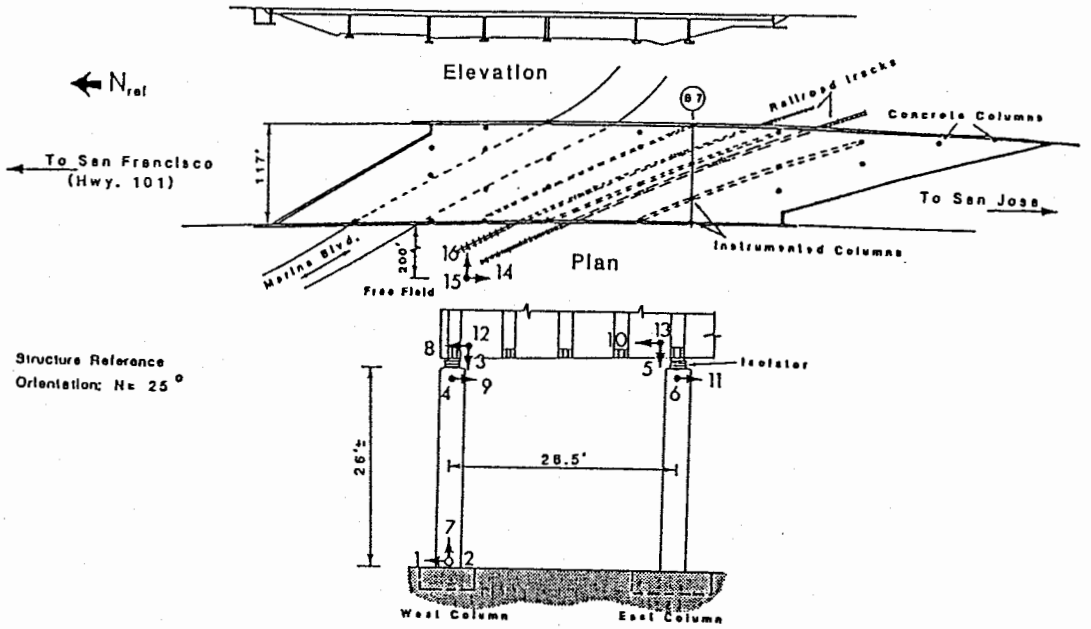

Fig. 2 Sierra Pt Overhead Plan and Elevation with Instrumentation Layout

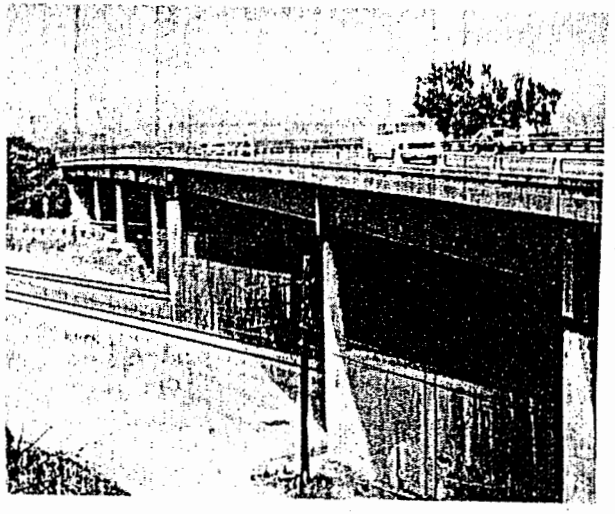

Fig. 3 General View of West Side of Sierra Pt Overhead

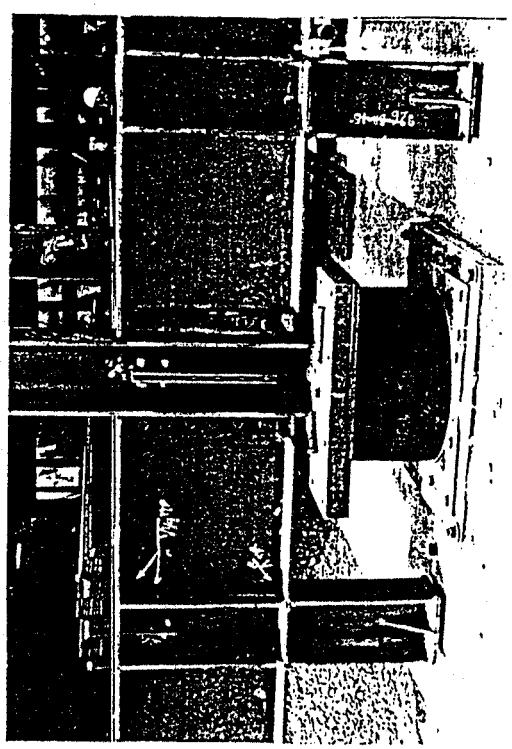

Fig. 4 FCLJC Bearing Installed During Construction

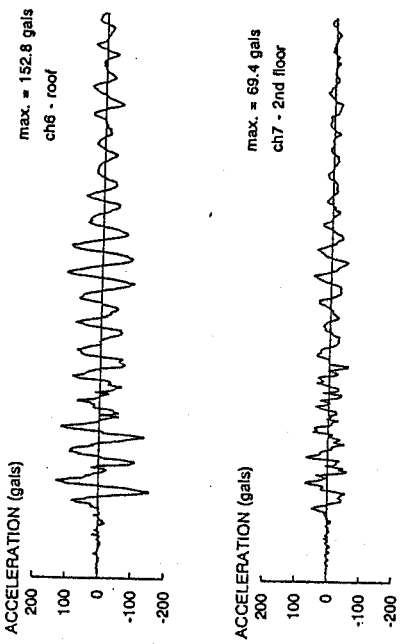

Fig. 5 FCLJC Transverse (N/S) Response Accelerations

Fig. 6 FCLJC 5%-Damped Response Spectra, Transverse (N/S) Accelerations

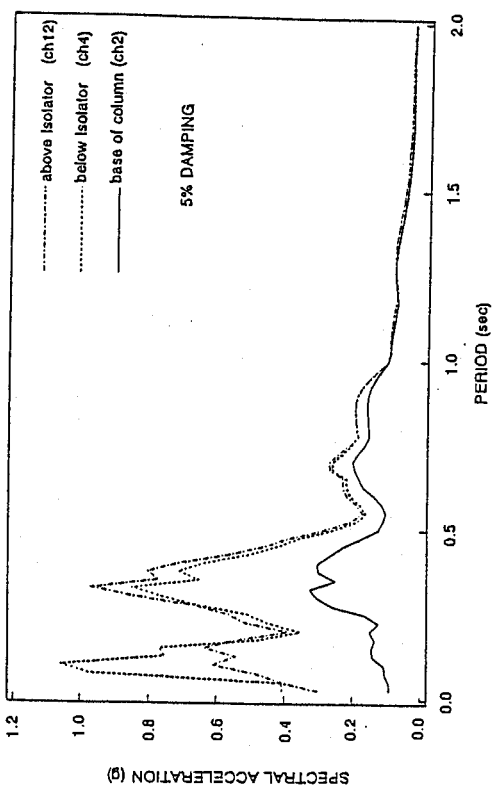

(a) West Column Longitudinal (N/S)

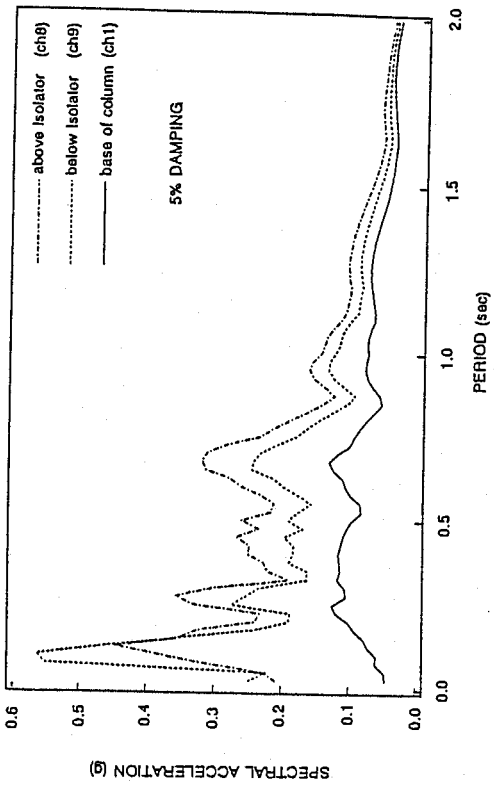

(b) West Column Transverse (E/W)

Fig. 8 Sierra Pt Overhead 5%-Damped Response Spectra

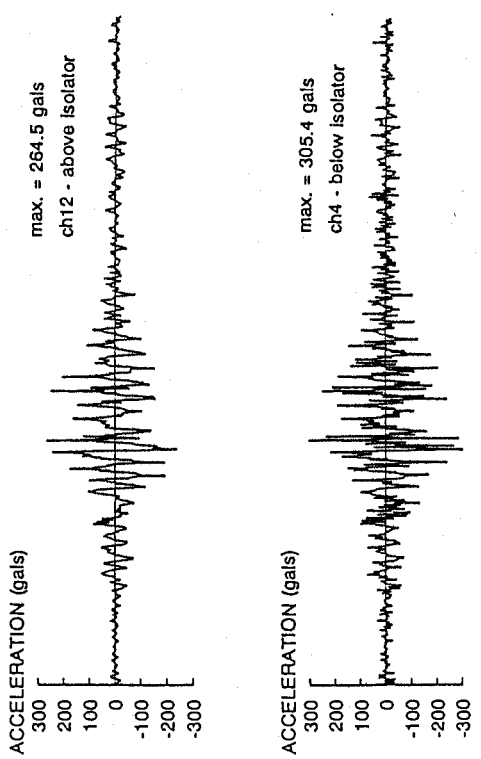

Fig. 7 Sierra Pt Overhead Longitudinal (N/S) Response Accelerations

ANALYSIS OF A TWO STORY OAKLAND OFFICE BUILDING DURING THE LOMA PRIETA EARTHQUAKE

Frank E. McClure
Consulting Structural Engineer

ABSTRACT

A three-dimensional model of a two story Oakland office building was subjected to response spectra and time history analyses developed from the California Division of Mines and Geology Strong Motion Instrumentation Program (SMIP) Loma Prieta earthquake records. Although the building had a severe plan torsional irregularity, and was subjected to large peak ground, second floor and roof accelerations, the building suffered no damage. These dynamic analyses showed that the building was twice as stiff and strong as required by current 1988 Uniform Building Code provisions.

INTRODUCTION

The purpose of this study is to obtain a better understanding of the excellent performance of a two story building in Oakland which was subjected to large peak ground and spectral accelerations during the Loma Prieta earthquake. The building was instrumented by the State of California, Department of Conservation, Division of Mines and Geology Strong Motion Instrumentation Program in 1974. The building is designated as an Oakland two story office building, CSMIP Station No. 58224. The location of the ten sensors is shown in Figure 1. The acceleration records for these sensors are shown in Figure 2.

This report is written from the viewpoint of structural engineers who design new buildings and evaluate the performance of existing buildings. They are concerned with the maximum response of any particular element of the building, the duration of strong ground and building shaking, the periods of the significant modes of vibrations, and the maximum displacements. Strong motion records provide the data to be used with computer analyses to obtain the above information.

From the maximum response of an element, the structural engineer can design the member to resist the forces on the member. Duration and magnitude of shaking gives an indication of the number of cycles of large member forces and displacements. These data are important for the design and evaluation of ductile, semi-ductile and brittle members. The maximum displacement and inter-story drift give clues to possible damage to non-structural elements of a building. Designing a building with low inter-story drift criteria reduces the displacements of and damage to the non-structural elements.

BUILDING DESCRIPTION

The building is a two story office building located in Oakland, California, designed in 1964, and built in 1965. The plan dimensions are 150 ft. in the east-west direction and 163 ft. in the north-south direction with 14 ft. 6 in. story heights. See Fig. 3. The building was designed to have a future third story which was never built. It is located on the north-east corner of the street intersection with a three story building to the north and a one story building to the east.

The building is a structural steel moment frame structure with reinforced concrete fill over roof and second floor metal decking welded to the steel frame. The first floor is a reinforced concrete slab on grade. The foundations are reinforced concrete spread footings for the interior columns and continuous deep footings for the exterior walls and columns.

The building structure has a two story complete welded structural steel frame. All beam and girder to column connections are moment connections. The top and bottom flanges of each beam and girder to column connections are full penetration butt welded to stiffener and continuity plates which were full penetration butt welded to column flanges and webs. The beam and girder web connections consist of single web plates that are butt welded to the column web and flanges, and fillet welded to the beam and girder webs the full height of the web plates with return fillet welds top and bottom. There are no web doubler plates. These beam and girder to column welded connections are similar to "Special" steel moment-resisting space frame connections used in current construction, even though they were constructed over twenty-five years ago.

The north and east walls are on the property lines and are non-bearing four hour fire walls. They are constructed of 8" stack bond solid grouted reinforced concrete block. These concrete block walls are well anchored to the structural steel columns and beams, and the roof and second floor reinforced concrete fill. The exterior south and west walls are non-structural walls constructed of 6" nailable steel studs @ 16" o.c.

The north and east continuous 8" concrete block walls with the structural steel moment frames throughout the building produce a building with a severe torsional plan irregularity. The center of rigidity of the lateral force resisting system is located close to the intersection of the north and east continuous block walls. This torsional plan irregularity was recognized early in the architectural and structural design of the building. The architectural design was modified to allow closer column spacing in the west and south street window walls which increased the in-plane lateral force stiffness of these walls.

There are fifteen columns in the south wall frame as compared to six in the other east-west frames. Fourteen columns are located in the west wall frame as compared to seven columns in the other north-south frames. See Fig. 3.

The exterior west and south window walls are finished with interior plaster and exterior stucco. These walls are non-bearing walls and have

almost continuous narrow height strip windows in the second story and large window openings in the first story. After the Loma Prieta earthquake, the interior plaster and exterior stucco south and west walls showed only minor cracks which could have been shrinkage cracks there before the earthquake.

The 1961 soils investigation report shows three soil borings to forty-two feet. The typical soil profile is firm silty sand to sand of the Merritt Formation underlie the site to depths of 30 to 40 feet. Below the Merritt Formation is sandy and clayey silt of the Alameda Formation extending to the depths explored. The static ground water, in 1961, was at 24 foot depth. According to the 1988 Uniform Building Code, Table 23-J, an S-2 soil with an S factor = 1.2 is appropriate for the site with a soil profile of dense or stiff soil conditions, where the soil depth exceeds 200 feet.

1964 BUILDING DESIGN

Frank E. McClure of Frank E. McClure and David L. Messinger, Consulting Structural Engineers, was the partner in charge, designer and engineer of record.

The building was designed to conform to the 1961 Oakland Building Code which followed the 1961 Uniform Building Code (UBC) lateral force provisions. It was designed as a three story office building with a mechanical space within the future third story. The design lateral base shear was calculated using the following formula: V = ZKCW, where Z = 1.0, K = 0.67, C = 0.05/ T**1/3 exp. power, T = 0.10 N = .30 sec., producing C = 0.075. V = 1.0 x .67 x .075 W = .05 W. The tributary weights of the future roof, future third, and second floor were 1,150 k, 2,840 k, and 2050 k, respectively, or a total weight of 6,040 k. Base shear V = .05 W = .05 x 6,040 = 302 k.

It is important to note that in the 1961 UBC, K = 0.67 could be used for buildings with a moment resisting space frame which, when assumed to act independently of any other more rigid elements, is capable of resisting 100 per cent of the total required lateral forces in the frame alone. There were no "Ordinary" and "Special" steel moment frame provisions.

The 1961 UBC drift requirements consisted of the following statement: "Lateral deflections or drift of a story relative to its adjacent stories shall be considered in accordance with accepted engineering practice." It was required to increase horizontal torsional moments resulting from an eccentricity between the center of mass and center of rigidity of not less than five per cent of the maximum building dimension.

With the plan torsional irregularity in the lateral force resisting system resulting from the stiff 8" concrete block walls on the east and north property lines, it was necessary to provide a stiff framing system in the south and west walls. A stiff structural steel moment frame was designed for these walls recognizing that it would be almost impossible for these frames to be as stiff as the concrete block property line walls.

The building was designed with 100% of the design lateral forces being resisted by the 8" reinforced concrete block wall parallel to the lateral

forces. A separate design was prepared, wherein the 8" block walls were neglected, and 100% of the design lateral forces were resisted by the complete structural steel moment frames parallel to the lateral forces. All beam and girder to column connections were welded moment connections, not just in the south and west wall perimeter frames.

Based on very rough approximations of relative rigidities of the structural steel frames and engineering judgment, the south and west frames were designed for V = 116 k or about 40% of the total building lateral force parallel to each of these frames. This design base shear was much larger than would have been obtained by rigorous seismic analysis taking into consideration the relative rigidities of the concrete block walls and the steel moment frames, including the increase in the torsional moments due to a 5% additional accidental torsional eccentricity.

The 1961 UBC design requirements for structural steel frames were simpler than those in the 1988 UBC. Panel zone shear and drift calculations were not required. No column web doubler plates were provided. The steel frames as built do not conform with the panel zone shear requirements of the 1988 UBC. However, the beam and girder to column connections develop the flexural capacity of the beams and girders. Continuity and stiffener plates were provided which would conform to the 1988 UBC provisions for "Special" steel moment-resisting space frames. The structural steel frames in the south and west walls more than meet the drift and AISC unity check requirements of the 1988 UBC.

AMBIENT WIND AND FORCED VIBRATION MEASUREMENTS

In April 1965, the United States Coast and Geodetic Surveys measured the first mode period of the building using a Sprengnether Portable Seismograph and a Ranger Lunar seismometer. The wind excited period of the building in the north-south direction was 0.47 sec. and 0.48 sec. in the east-west direction. At the time of these measurements, the concrete block walls and the complete structure were in place. The south and west street exterior metal stud walls were in place but had not been plastered.

Later in 1965, forced vibration tests were performed on the building when the construction was almost complete. Only minor plastering of the mechanical penthouse walls and completion of the painting of the building remained to be completed. A complete description of these vibration tests and the results can be found in a paper, "Dynamic Response of a Two Story Steel Frame Structure," J. G. Bouwkamp and J. K. Blohm, Vol. 56, No. 6, Bulletin of the Seismological Society of America, December 1966.

Based on the forced vibration measurements, the first mode period was 0.426 sec. and the second mode period was 0.130 sec. The decrease in these periods, as compared with the ambient wind periods, can be attributed to the increase in the stiffness of the building due to the added stiffness of the exterior plastered south and west walls.

Having the first and second modes of vibration from the forced vibration measurements provided a unique opportunity to validate the computer modeling

assumptions, if the computer model first and second modes of vibration were close to the forced vibration values.

COMPUTER MATHEMATICAL MODEL

A rigorous three-dimensional mathematical model of the building was prepared with 196 nodes, 321 beam-column elements and 88 membrane elements. This model included consideration of the flexibility of the roof and second floor diaphragms and the stiffness of the non-structural elements. The IMAGES-3D Finite Element Analysis Program developed by Celestial Software, Inc. was used.

In the development of a computer mathematical model to simulate the building's dynamic characteristics, the modeling of the non-structural elements can have an influence on the periods of the modes of vibrations for low levels of building excitation. Under the current study, computer analyses of the building without plastered exterior walls produced a first mode period = 0.63 sec. and a second mode period = 0.20 sec. as compared to a first mode period = 0.463 sec. and a second mode period = 0.172 sec. for the building with plastered exterior walls.

The model with the plastered exterior walls was considered a viable model when it produced a first mode period = 0.463 sec. and second mode period = 0.172 sec. as compared with the forced vibration first mode period = 0.426 sec. and second mode period = 0.130 sec.

Referring to Fig. 2. structural response record for south-east roof corner Sensor 3, the peak roof acceleration of 0.65 g occurred at about 14 seconds into the record. Prior to this peak acceleration, the period of the roof response was about 0.50 sec. and about 0.60 sec. after the peak acceleration. This period lengthening can be explained since after the peak response, the non-structural elements were not as well-connected to the structure and their lateral stiffness was diminished.

1988 UNIFORM BUILDING CODE SEISMIC ANALYSIS

Using the above computer model, a conventional 1988 UBC lateral force analysis was performed that took into account the flexibility of the roof and second floor diaphragms. The roof and second floor horizontal seismic forces were distributed throughout the building to the appropriate nodes based on their tributary nodal masses.

Based on the as-built two story building with a mechanical penthouse, the 1988 UBC lateral force base shear, V = ZICW/Rw, where Z = 0.40, I = 1.0, C = 1.25 S/T**2/3 exp. power, S for S2 soil = 1.2, T = Ct x (hn)**3/4 exp. power = 0.035 x (29)**3/4 exp. power = 0.437 sec. Therefore, C = 1.25 x 1.2/ 0.437**2/3 exp. power = 2.59, and V = .40 x 1.0 x 2.59 W/Rw. It was assumed that the structural steel frame met the requirements of a "Special" steel moment frame because of the detailing of the beam and girder to column connection with stiffener and continuity plates butt welded to the column web and flanges. Therefore, Rw = 12 was used. V = .40 x 1.0 x 2.59 W/12 = 0.086 W for Rw = 12.

The tributary weights of the roof and second floor were 2,200 k and 2,050 k, or a total weight of 4,250 k. Base shear V = 0.086 x 4,250 k = 366 k. This base shear of 366 k is about 20% greater than the 1961 UBC base shear = 302 k.

In order to compare the results of the 1988 UBC equivalent static lateral force analysis with the response spectra and time history analyses, it was decided to focus on the response of the south wall structural steel frame, designated as "Frame 7." Frame 7 is parallel to the orientation of Roof Sensor 3, Second Floor Sensor 5, and Ground Floor Sensor 7. The base shear forces on Frame 7 and its roof computed response were used to compare the results of the 1988 UBC equivalent static force analyses, the response spectra and time history analyses. These base shear forces, roof displacements and columns bending stresses are shown in Table 1.

The total 1988 UBC east west base shear = 366 k. The total base shear without accidental torsion for Frame 7 = 110 k or about 30% of the total building east west base shear. Accidental torsion added 9.8 k additional base shear to Frame 7, and amplified torsion required by Section 2312 e (6), 1988 UBC, added 2.78 times the accidental torsion of 9.8 k or 27 k base shear. The total Frame 7 base shear = 137 k which represents 37% of the total building base shear. It is interesting to note that the 1961 UBC Frame 7 base shear was about 40% of the total building base shear or 116 k without the use of computer analysis.

TABLE 1.

MAXIMUM RESPONSE OF SOUTH WALL STRUCTURAL STEEL FRAME

	INPUT	BASE SHEAR	ROOF DISPLACEMENT	COLUMN BENDING STRESS
1.	1961 UBC	116 k	0.40 in.	7,900 psi
2.	1988 UBC	137 k	0.47 in.	9,300 psi
3.	Response Spectra 5% Damping	203 k	1.19 in.	14,500 psi
4.	Time History 2% Damping	160 k	0.89 in.	12,200 psi
5.	Time History 5% Damping	133 k	0.80 in.	9,900 psi
6.	SMIP Sensor 7		0.80 in.	

LOMA PRIETA RESPONSE SPECTRA ANALYSES

Three-dimensional 5% damped response spectra analyses were performed, using Complete Quadratic Combination (CQC) combined 9 modes of vibration, which included 96 per cent of the participating mass of the structure. The requirements that orthogonal effects be considered was satisfied by using 100% of the east-west plus 30% of the north-south response spectra.

The total building base shear, V = 921 k or 22% of the total weight of the building. This building base shear resulting from the response spectra analysis is 921 k / 366 k = 2.5 times greater than the 1988 UBC base shear.

The base shear, V, for Frame 7 = 203 k. The Frame 7 columns members had bending stresses = 14,500 psi, or about one-half the 1988 UBC allowable bending stresses. The roof displacement = 1.19 in. or an inter-story drift of (.0036) or 70% of the 1988 UBC allowable inter-story drift of (.0050). See Table 1.

LOMA PRIETA TIME HISTORY ANALYSES

Three-dimensional time history analyses, using 2% and 5% damping, were performed, which included the time histories of the east-west, north-south, and vertical ground motions run concurrently. The largest total building shear, V = 608 k or 14% of the total weight of the building. This building base shear is 608 k / 366 k = 1.66 times greater than the 1988 Uniform Building Code base shear.

The 5% damped time history, maximum base shear, V, for Frame 7 = 133 k, and its roof displacement = 0.80 in. which corresponds to the Sensor 7 displacement of 0.80 in. This displacement represents an inter-story drift of (.0024) or one-half the 1988 UBC allowable inter-story drift of (.0050). The 2% damped time history responses were slightly greater and the column member bending stresses = 12,200 psi or 40% of the 1988 UBC allowable bending stresses. See Table 1.

FINDINGS AND CONCLUSIONS

1. A three-dimensional computer model was validated based on its first and second modes of vibrations which matched the forced vibration first and second modes. Using this model and the SMIP strong motion ground motion records, the time history analyses produced the displacements of the roof and second floor which were very close to the displacements shown in the strong motion records.

2. During the Loma Prieta earthquake, the roof, second floor, and ground were subjected to peak accelerations of 0.65 g, 0.39 g, and 0.26 g, respectively. However, according to the time history analyses, the total maximum base shear force on the building at any one time was 14% of the weight of the building.

3. Without performing response spectra and time history analyses, it is difficult to explain the excellent performance of the building when just comparing the design base shear, V equals 5.0% x the weight of the building with the maximum recorded peak ground acceleration equal to 26% g. Depending on the type of structural system and its configuration, buildings can resist peak ground accelerations many times greater than their design base shears, expressed as a percentage of gravity.

4. According to the time history analyses, the south wall structural steel frame was subjected to a lateral force about equal to the 1988 UBC lateral forces including the provisions for amplified torsion. The steel frame members were subjected to 34% of their maximum UBC allowable bending stresses. The frame deflected 50% of the 1988 UBC allowable drifts. In other words, the structural steel frame was designed to be more than twice as strong and twice as stiff as required by the 1988 UBC provisions.

5. This inter-story drift stiffness helps explain the lack of any damage in the building despite its severe plan torsional irregularity. Minimizing the inter-story drifts by designing a stiff structural steel frame along the two street window walls helped mitigate the stiffness of the opposite property line masonry walls. The use of over-strength and stiffness can mitigate severe plan torsional irregularities.

6. Time history analyses provide better information concerning the performance of an existing building than response spectra analyses. A better understanding of the variation with time of the displacements and stresses in the members is possible by "stepping" through the response of a building in 0.02 sec. time history intervals. Response spectra analyses, particularly using smoothed design response spectra, are more appropriate for the design ofnew buildings. Use of response spectra analyses, developed from on-site ground strong motion records, tend to overstate the response as compared to time history analyses, using the same ground strong motion records.

7. Multi-channel strong motion instrumentation records provide important data to validate the performance of a building during an earthquake. The records provide data concerning the acceleration, velocity and displacements at various locations of the building, which aids in the validation of the computer models used to evaluate the building. Computer analyses which can reproduce the measured responses in the building are more credible than computer analyses without such validation.

8. For buildings with plan torsional irregularities, the 1988 UBC provisions require inclusion of amplified torsion up to 3.0 times the accidental torsion. This amplified torsion provision requires increasing the design forces in the perimeter structural elements in the building. If damage control is a design goal, then reduction of the allowable inter-story drifts for these elements also should be considered. The excellent performance of the subject building can be attributed mainly to the stiffness in the street window wall structural steel frames.

ACKNOWLEDGEMENT

The contents of this report were developed under Contract No. 1089-509 from the California Department of Conservation, Division of Mines and Geology, Strong Motion Instrumentation Program. However, those contents do not necessarily represent the policy of that agency nor endorsement by the State Government.

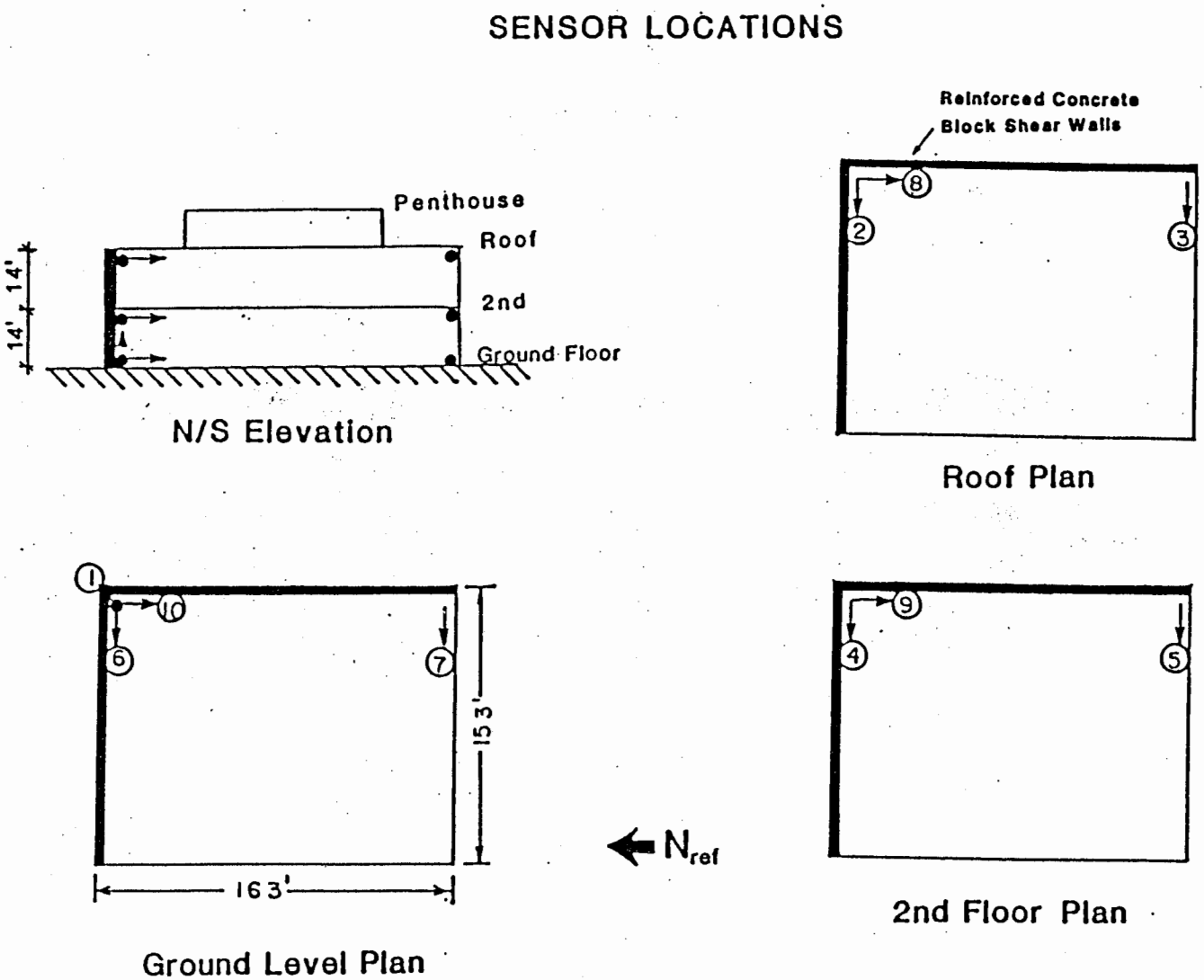

Figure 1

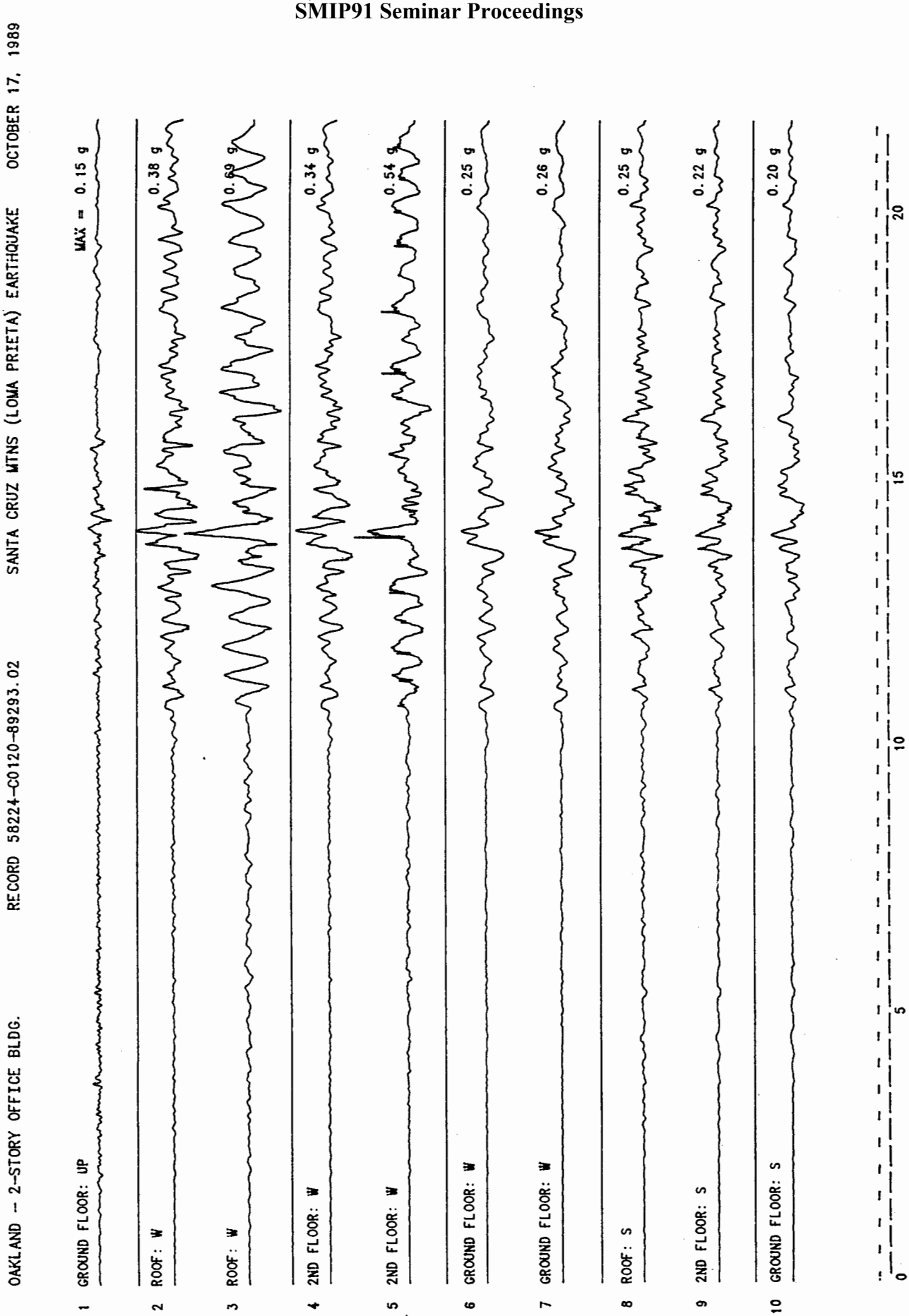
OAKLAND -- 2-STORY OFFICE BLDG.
RECORD 58224-C0120-89293.02
SANTA CRUZ MTNS (LOMA PRIETA) EARTHQUAKE
OCTOBER 17, 1989
1 GROUND FLOOR: UP
MAX = 0.15 g
2 ROOF: W
0.38 g
3 ROOF: W
0.69 g
4 2ND FLOOR: W
0.34 g
5 2ND FLOOR: W
0.54 g
6 GROUND FLOOR: W
0.25 g
7 GROUND FLOOR: W
0.26 g
8 ROOF: S
0.25 g
9 2ND FLOOR: S
0.22 g
10 GROUND FLOOR: S
0.20 g
0
5
10
15
20
TIME - SECONDS

Figure 2

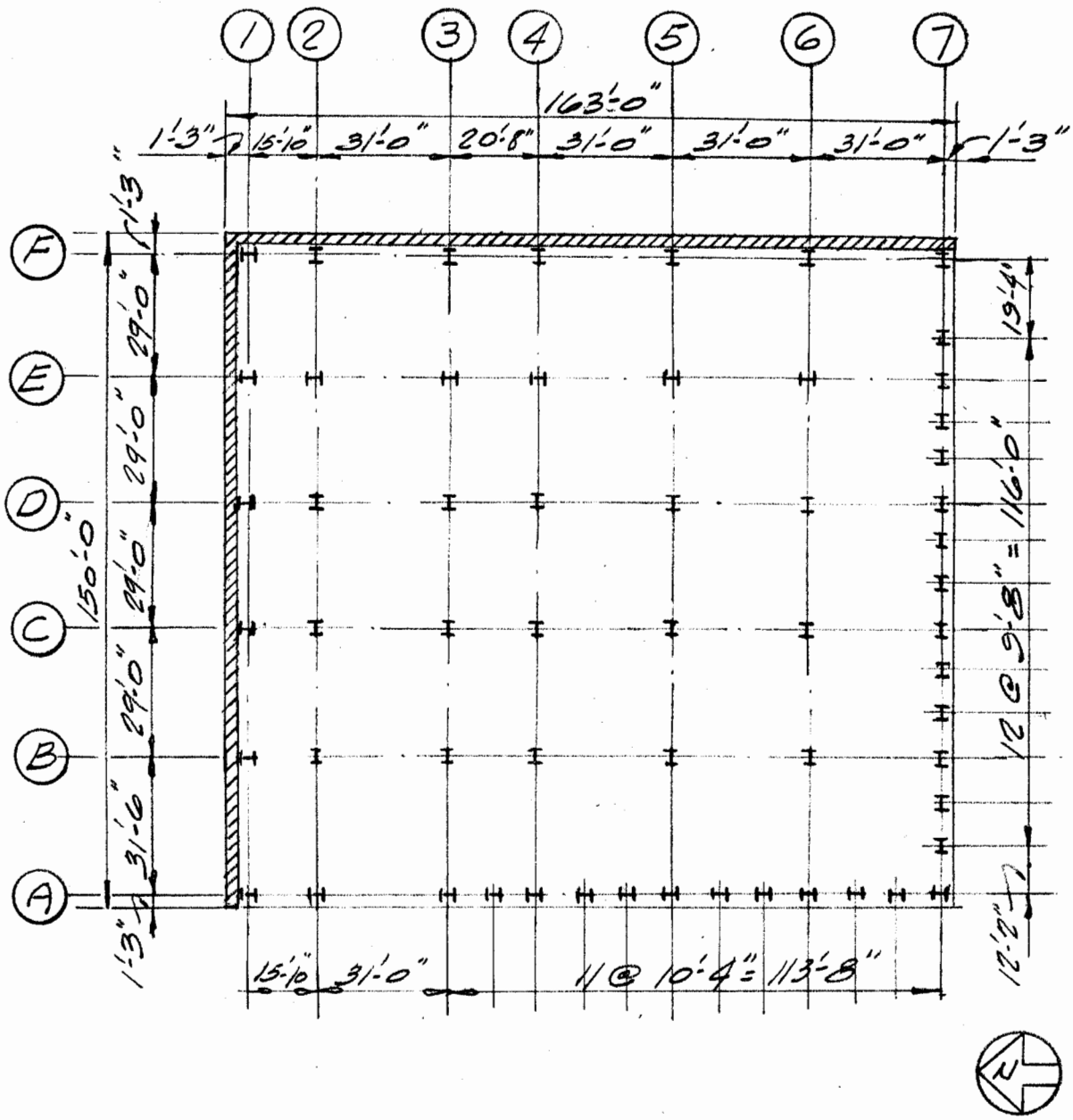

PLAN

Figure 3

CORRELATION BETWEEN RECORDED BUILDING DATA AND NON-STRUCTURAL DAMAGE DURING THE LOMA PRIETA EARTHQUAKE

Dr. Satwant S. Rihal
Professor, Architectural Engineering Department
Cal Poly State University, San Luis Obispo, CA 93407

ABSTRACT

A study of non-structural damage observed in the instrumented Santa Clara County Government Center building, during the Loma Prieta, California, earthquake of October 17, 1989, has been carried out, to correlate the recorded CSMIP response data with observed non-structural component damage. A methodology is presented to assess the performance and behavior of non-structural building components during earthquakes.

INTRODUCTION

Widespread non-structural component damage was observed and reported in a broad class of buildings during the Loma Prieta, California earthquake of October 17, 1989. Such damage was distributed over the San Francisco Bay Area, including the cities of Oakland and San Francisco as well as San Jose. The major consequences of the non-structural component damage are the severe economic impact posed by such damage as well as possible life-hazard in some cases. It is worth noting that as expected non-structural damage was observed mainly in modern multi-story buildings which otherwise behaved satisfactorily during the Loma Prieta, California Earthquake. The objective of the project is to analyze recorded SMIP data and study the correlation between available recorded data and non-structural component damage in instrumented buildings during the Loma Prieta earthquake of October 17, 1989.

INSTRUMENTED BUILDING CASE-STUDY SANTA CLARA COUNTY SERVICES BUILDING - SAN JOSE

After initial study it was decided to lead this research project with a case-study of the Santa Clara County Government Center Building located in downtown San Jose. This building has been the source of recorded data from two previous earthquakes in 1984 and 1986, and has been the subject of studies during these previous earthquakes. The overall view of this case-study building is presented in Figures 1 and 2.

DESCRIPTION OF BUILDING STRUCTURAL SYSTEM

This thirteen story building is essentially square in plan configuration. The structural system consists of moment-resisting frames at 26 ft. o.c. in both directions. Wings along the west and south sides of the building are used primarily for circulation, e.g., elevators and stairs as well as for mechanical systems. These wings are offset in plan and that is

the only plan irregularity in the layout of the primary structural system. Furthermore, these wings extend one floor above the roof which is the main vertical irregularity in the building structural system. There is a non-structural irregularity on the southwest corner between the two wings discussed above. From the ground floor to the fifth floor there is a glass enclosed architectural space. The main foundation system consists of a solid mat foundation. The typical floor framing plan is presented in Figure 3. Typical moment-resistng-frame elevations are shown in Figures 4 and 5.

OBSERVED NON-STRUCTURAL DAMAGE

Non-structural building components are classified to include partitions, suspended ceilings, curtain walls, facades and cladding, and contents, e.g., filing cabinets, book shelves, computer equipment, office furniture, etc.

The non-structural damage observed in the Santa Clara County Government Center Building falls mainly in the category of contents damage including damage to interior space-enclosure partial-height partitions.

In general, valuable non-structural damage data gets lost soon after an earthquake due to the need and necessity to quickly repair such damage to bring building facilities back into operation. For this case-study, the Santa Clara County Government Center Building, a video tape documenting non-structural damage observed soon after the Loma Prieta earthquake, was obtained [5] for study and analysis.

A review of the video tape [5] of observed non-structural damage shows that there was substantial damage to contents in this building facility, mainly at the 7th, 9th, 10th and 11th floor levels.

A classification of non-structural components (contents) and corresponding observed damage and location is presented in Table 1.

RECORDED MOTIONS

The typical recorded and processed data obtained from the strong motion instruments in the Santa Clara County Services Building, as provided by the CSMIP program [4] is shown in Figure 6.

A typical floor acceleration response spectrum for the 7th floor (NW corner) based on CSMIP vol. 3 [4] data for this building is presented in Figure 7.

CORRELATION BETWEEN RECORDED DATA AND OBSERVED NON-STRUCTURAL DAMAGE

Non-structural component damage in buildings is characterized by both acceleration as well as inter-story drift effects. A study of the observed non-structural damage data recorded on video tape showed that in general, there was no damage observed below the fifth floor level. The majority of the non-structural component damage is concentrated at the 7th and 11th floor

levels, with lesser damage observed at the 8th, 9th and 10th floor levels. Efforts are now under way to complete the correlation between floor responses (accelerations and displacements) and corresponding observed non-structural component damage. It is planned to develop a non-structural damage index as one means of quantifying the observed non-structural damage in relation to corresponding recorded response data (accelerations, displacements, etc.).

Summaries of the peak responses recorded at different levels in the Santa Clara County Government Center Building, during the 1989 Loma Prieta, California, earthquake as well as the 1984 Morgan Hill, California, earthquake are presented in Tables 2 and 3.

OBSERVATIONS/PRELIMINARY RESULTS/CONCLUSIONS

A comparison of peak recorded motions at different levels in the Santa Clara County Government Center Building during the 1989 Loma Prieta earthquake and the 1984 Morgan Hill earthquake shows that the peak recorded response floor accelerations and displacements during the 1989 Loma Prieta earthquake were almost twice those recorded during the 1984 Morgan Hill earthquake @ the 12th floor and roof levels and approximately 2.5 times @ the 7th floor level. According to damage data provided by Van Osdol [5], this building suffered non-structural component damage during the 1984 Morgan Hill earthquake and the 1986 Mt. Lewis earthquake also. Since that time certain levels of upgrading and retrofit of non-structural building components has been carried out, which helped reduce level of non-structural damage during the 1989 Loma Prieta earthquake. Work is now underway to carry out a seismic analysis of the building system using the computer program ETABS [1] to develop a better correlation between results of analysis, recorded data and observed non-structural component damage in the Santa Clara County Government Center Building.

ACKNOWLEDGEMENTS

This study is supported by a research grant from the Strong Motion Instrumentation Program of the California Department of Conservation. This support is gratefully acknowledged. The author would like to thank Dr. Moh Huang and Dr. Tony Shakal of the CSMIP for their encouragement, help and support. The valuable assistance of Mr. Wes Van Osdol of the County of Santa Clara, General Services Agency during this study is gratefully acknowledged. The author acknowledges the contribution of Robert Reitherman during the course of this investigation. The author acknowledges the valuable assistance of project research assistants Evelyn Pratt, John Laporta and Paul Philbaum during the course of this research study.

REFERENCES

1. ETABS, Computers and Structures, Inc., Berkeley, California.

2. Reitherman, Robert, Personal Communication, 1991.

3. Shakal, A., Huang, M., et al., "CSMIP Strong-Motion Records and Processed Data from the 1984 Morgan Hill Earthquake," California Department of Conservation, Division of Mines and Geology, Office of Strong Motion Studies, OSMS 85-05.

4. Shakal, A., Huang, M., et al., "CSMIP Strong-Motion Records and Processed Data from the 1989 Loma Prieta Earthquake," California Department of Conservation, Division of Mines and Geology, Office of Strong Motion Studies, 1991.

5. Van Osdol, Wes., Personal Communication, 1991.

TABLE 1
CLASSIFICATION OF OBSERVED NON-STRUCTURAL DAMAGE

LEVEL	NON-STRUCTURAL COMPONENT	DESCRIPTION OF NON-STRUCTURAL DAMAGE										
		Toppled Foreward	Toppled Backward	Opened	Moved Rel. to Original Position	Fell Down	Jumped Up	Torsion on Component	Chip-ped	Scat-tered	Warped	In Plane Buck-ling
7	File Cabinets	x	x	x	x			x				
7,11	Drawers in Desks			x	x	x		x				
7	Phone				x							
7,11	5+' Partitions	x	x		x	x						
7,11	6'Book-shelves	x	x		x	x						
7	Ceiling Plaster								x			
7	HP Computer	x			x			x				
7	Ceiling Molding				x	x						
7	Microfiche Files				x					x		
7	Desks				x							
7,11	Computer Screen		x		x			x				
7,11	Book-shelves				x							
7,11	General Supplies				x	x				x		
11	Laser Printer				x							

TABLE 1
CLASSIFICATION OF OBSERVED NON-STRUCTURAL DAMAGE
(Continued)

LEVEL	NON-STRUCTURAL COMPONENT	DESCRIPTION OF NON-STRUCTURAL DAMAGE										
		Toppled Foreward	Toppled Backward	Opened	Moved Rel. to Original Position	Fell Down	Jumped Up	Torsion on Component	Chip-ped	Scat-tered	Warped	In Plane Buck-ling
11	Laser Ptr. Cart				x							
8,10, 11	Plant Pots Broken				x	x			x	x		
11	Bookshelves on wall				x							
9	Microwave		x		x	x						
9	Bookshelves Standing									x		
10	ComputerSys. on wheels				x							
5,7	Ceiling Moulding					x						
4	Ceiling Tile/Pipes					x						
4	Concrete Column							x	x	x		
4	Supporting Staircase											
4	Baseboard Molding				x						x	
7	Xerox Machine				x							
7	Air Condi-tion vents				x	x						
7	Bookshelves Library	x			x	x				x		x

TABLE 2
Summary of Peak Recorded Motions/Damage Data by Levels
1989 Loma Prieta Earthquake

Level (1)	East-West Component				North-South Component				Non-Structural Damage Index*
	Peak acc. g.	Peak displ. in.	Peak spectral response @ T. sec.	Duration, sec., ≥ 0.10 g *	Peak acc., g.	Peak displ. in.	Peak spectral response @ T. sec.	Duration sec., ≥ 0.10 g *	
Lower	-0.091	-3.75			-0.106	-2.79			
2	-0.152	-6.1			-0.108	-4.53			
7	0.257	11.18	2.4		0.223	-10.91	2.4		
12	0.271	15.24	2.2		-0.261	-13.94			
Roof	0.334	14.53	2.2		-0.343	-14.57	2.4		

* under preparation

TABLE 3
Summary of Peak Recorded Motions/Damage Data by Levels
1984 Morgan Hill Earthquake

Level (1)	East-West Component				North-South Component				Non-Structural Damage Index*
	Peak acc. g.	Peak displ. in.	Peak spectral response @ T. sec.	Duration, sec., ≥ 0.10 g *	Peak acc., g.	Peak displ. in.	Peak spectral response @ T. sec.	Duration sec., ≥ 0.10 g *	
Lower	0.041	-1.04	2.2		-0.035	-1.26	3		
2	-0.057	1.53	2.2		0.049	-1.60	3		
7	-0.117	4.57	2.2		0.104	4.25	2.2		
12	0.160	6.97	2.2		0.168	-7.17	2.3		
Roof	0.174	7.56	2.2		0.169	-7.28	2.2		

* under preparation

Figure 1. Santa Clara County Government Center - San Jose
Overall View from South-West

Figure 2. Santa Clara County Government Center - San Jose
Overall View from the North-West

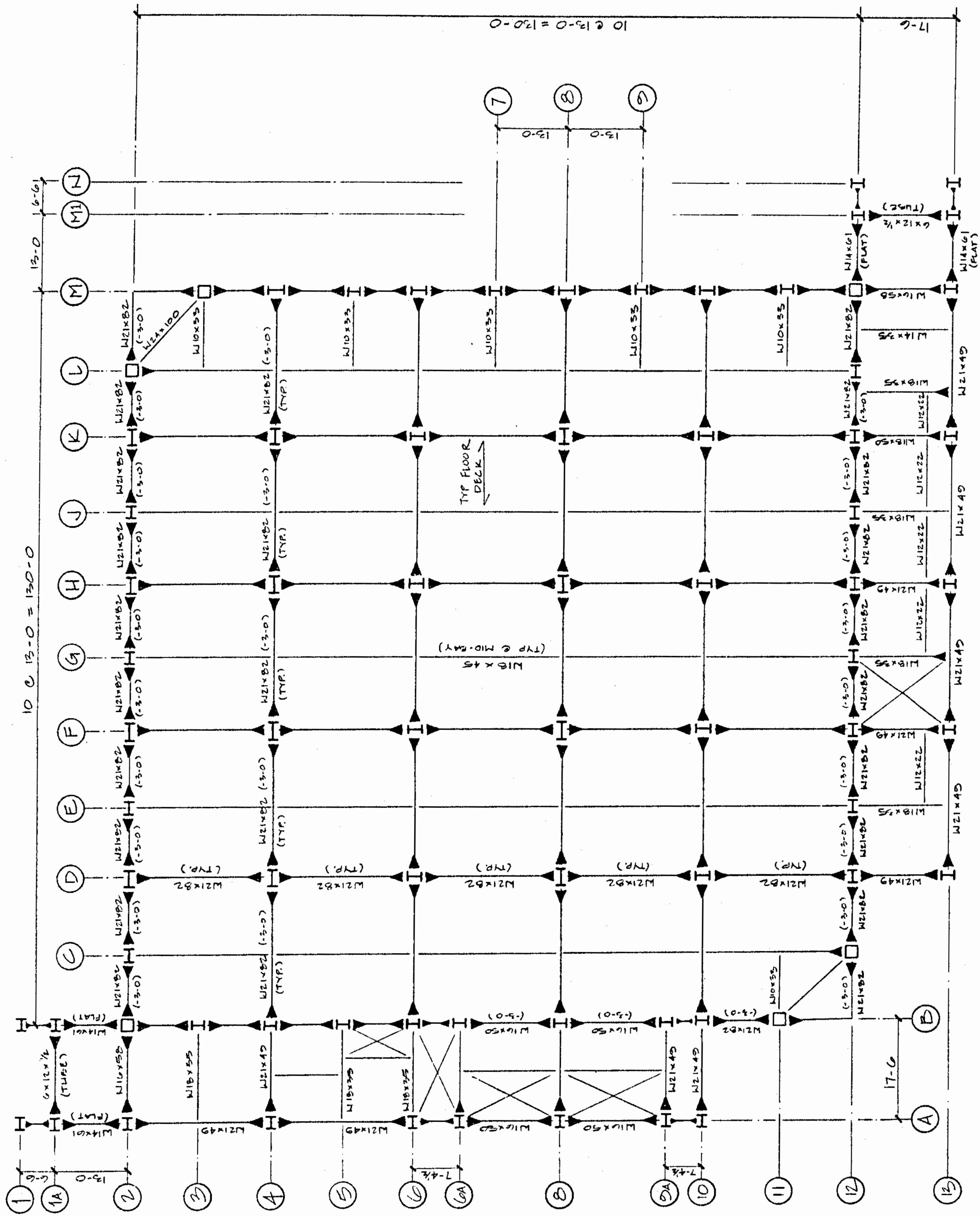

Figure 3. Santa Clara County Government Center - San Jose
Typical Structural Floor Framing Plan

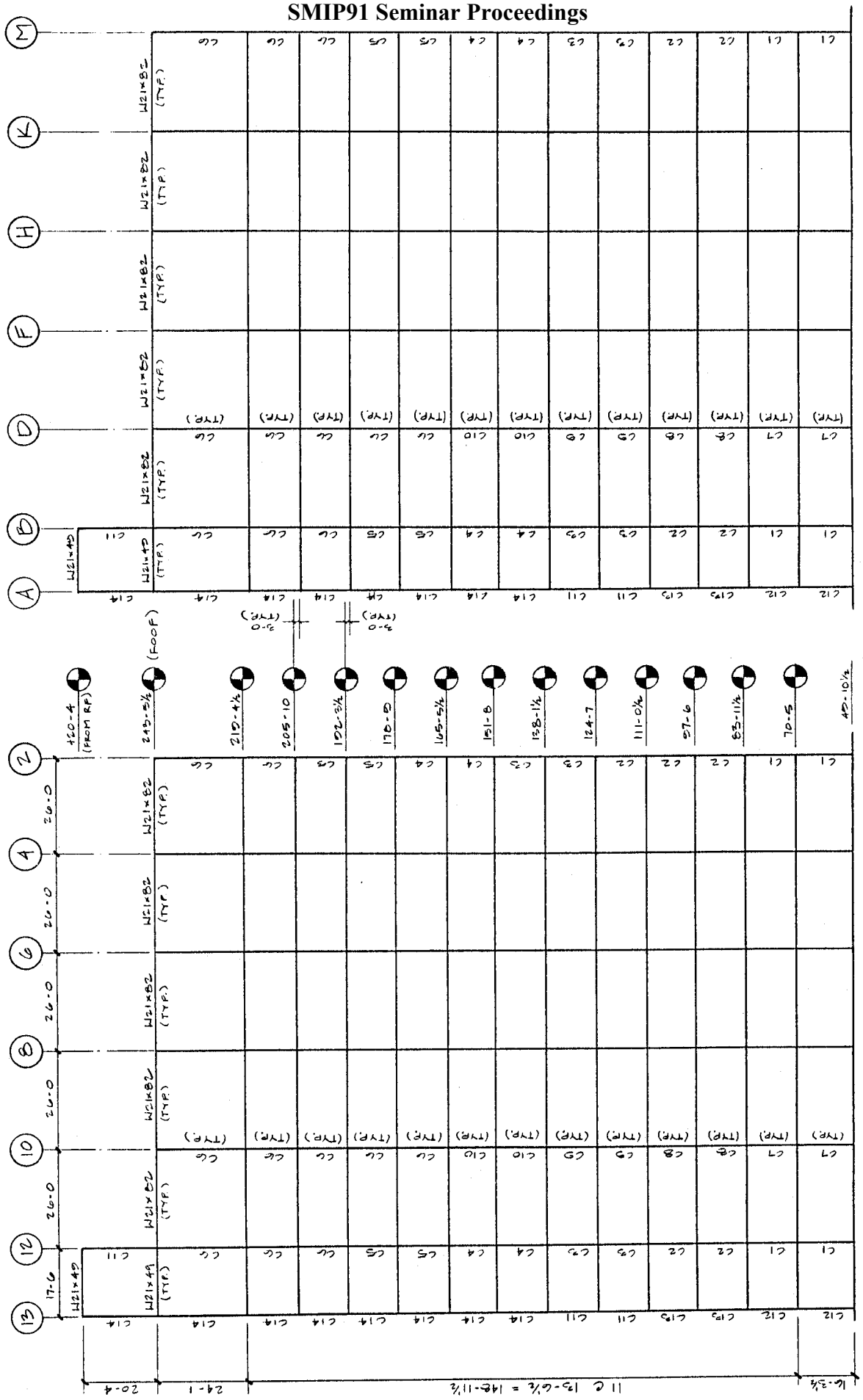

Figure 4. Santa Clara County Government Center - San Jose
Typical North-South Moment-Resisting-Frame Elevations

Figure 5. Santa Clara County Government Center - San Jose
Typical East-West Moment-Resisting-Frame Elevation

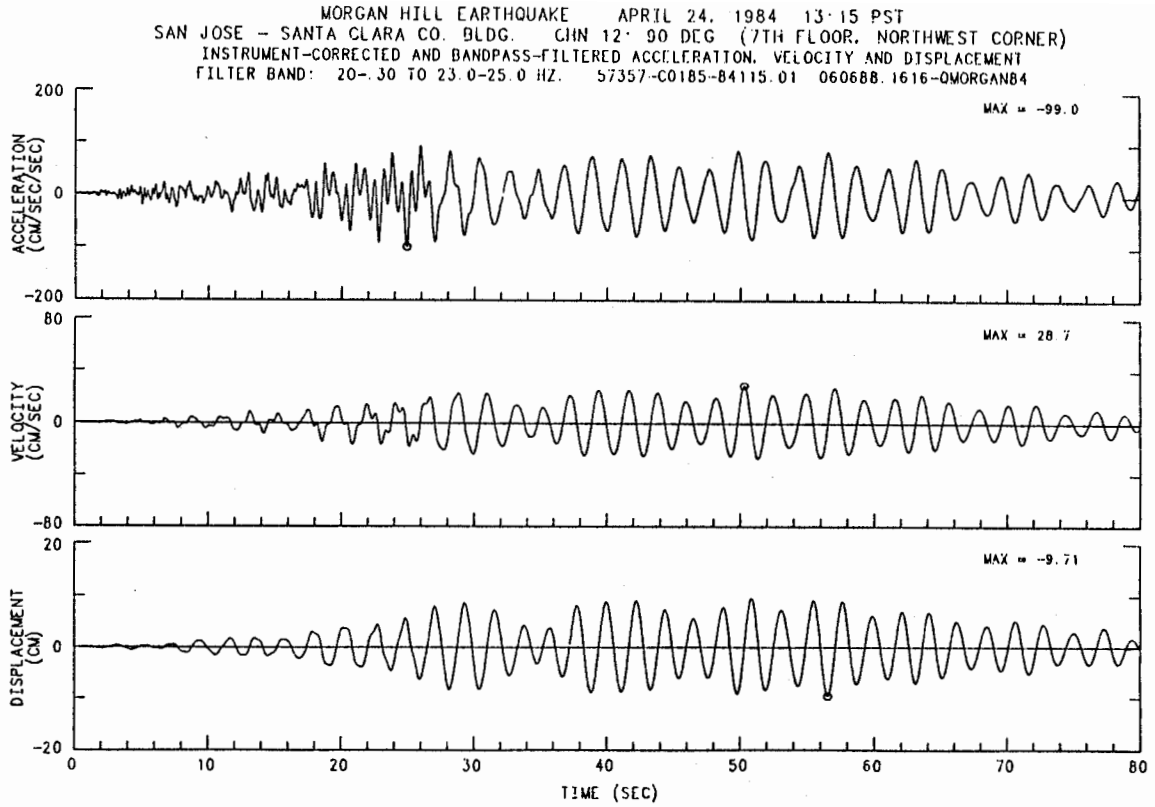

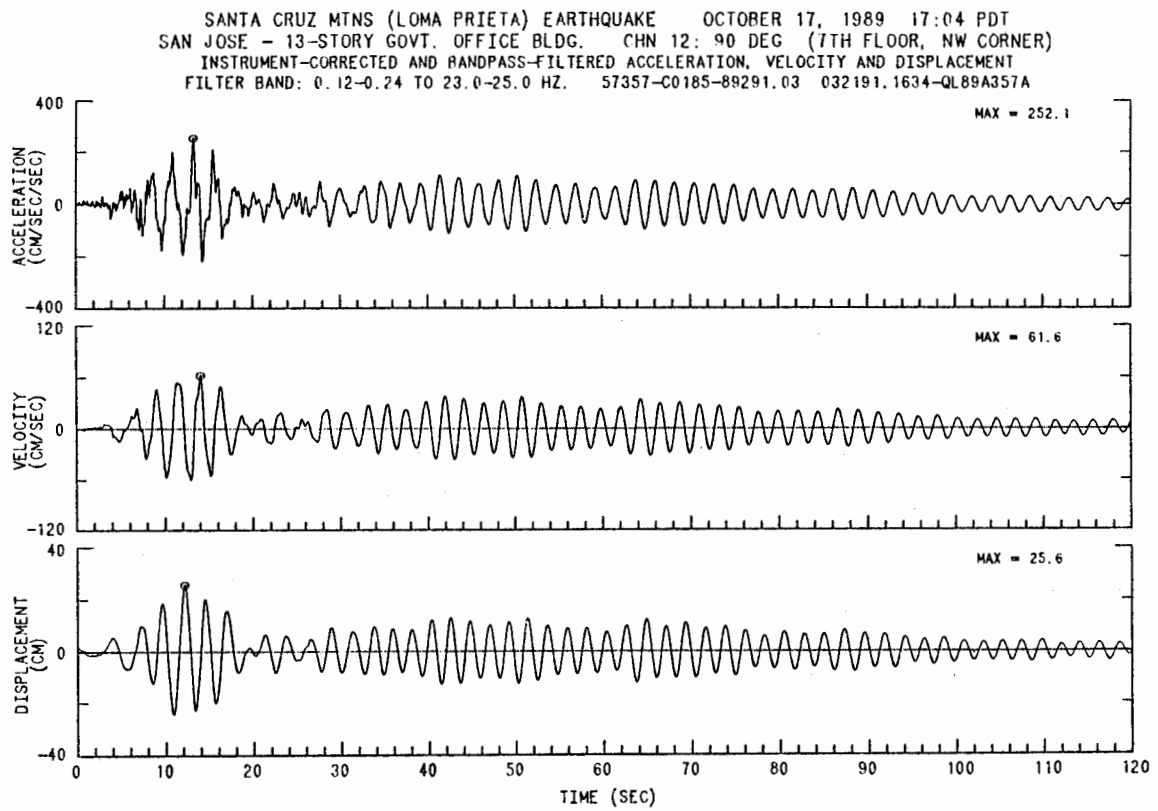

Figure 6
Source: Ref. [3], [4]

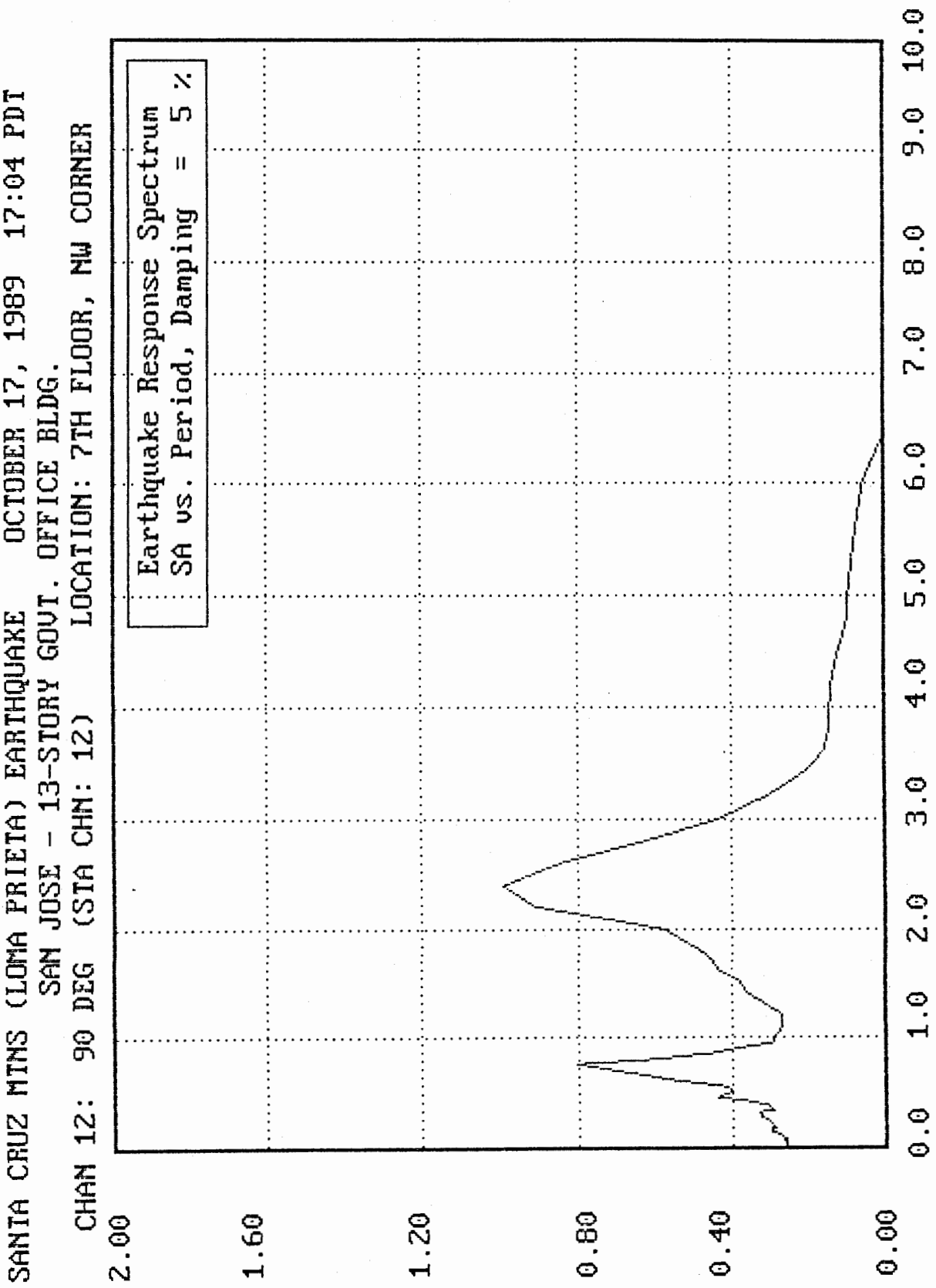
SANTA CRUZ MTNS (LOMA PRIETA) EARTHQUAKE OCTOBER 17, 1989 17:04 PDT
SAN JOSE - 13-STORY GOVT. OFFICE BLDG.
CHAN 12: 90 DEG (STA CHN: 12) LOCATION: 7TH FLOOR, NW CORNER
Earthquake Response Spectrum
SA vs. Period, Damping = 5 %
S A
2.00
1.60
1.20
0.80
0.40
0.00
0.0
1.0
2.0
3.0
4.0
5.0
6.0
7.0
8.0
9.0
10.0
Period

Figure 7

An Investigation of Serviceability Requirements of the 1988 UBC Seismic Provisions

Chia-Ming Uang
Assistant Professor, Northeastern University
Ahmed Maarouf
Graduate student, Northeastern University

ABSTRACT

The Uniform Building Code (UBC) serviceability requirements to control story drift and member forces for the ''moderate'' design earthquake are examined. It is shown from the UBC drift limits that the intensity of the UBC-implied moderate design earthquake for buildings taller than 65 ft. is only one-sixth that of the severe design earthquake. Recorded responses of one steel and one reinforced concrete building frames which were subjected to ground excitations with an intensity similar to the UBC moderate design earthquakes are studied. The results show that, for certain ductile building systems, the UBC one-phase design procedure cannot avoid excessive story drifts and structural yielding.

INTRODUCTION

Modern building seismic design provisions generally require that a well designed building should be able to (i) resist minor earthquakes without damage, (ii) resist moderate earthquakes without structural damage, but probably experience some nonstructural damage, and (iii) resist major earthquakes without collapse (6). The 1988 UBC (9) seismic design provisions focus mainly on the third criterion, which is commonly referred to as the ultimate limit state. The first two criteria can be referred to as the serviceability limit state — a limit state which is overlooked in the UBC. While the ultimate limit state deals with the life-safety considerations for severe earthquakes, the serviceability limit state attempts to reduce economic losses by minimizing nonstructural damage and by avoiding structural yielding in moderate earthquakes.

For design purposes UBC specifies an elastic design spectrum (C_{eu}) for the severe design earthquake. The design base shear ratio (C_w) for working stress design is computed as follows (see Fig. 1):

$$C_w = \frac{C_{eu}}{R_w} \tag{1}$$

where R_w = system performance factor. Since the R_w factor is a force reduction factor to account for structural ductility, structural overstrength, and the difference between the working stress and strength design formats (7), the C_w spectrum in Fig. 1 represents the *inelastic* design spectrum for the severe design earthquake. Note that the level of the C_w spectrum varies with the R_w factor. To consider the serviceability limit state, it is necessary to know the elastic design spectrum (C_{es}) for the moderate design earthquake. In this study it is assumed that the levels between the severe and moderate design

earthquakes differ by a factor R_{ser}

$$C_{es} = \frac{C_{eu}}{R_{ser}} \tag{2}$$

Fig. 1 shows the C_{eu}, C_{es}, and C_w spectra. Note that the C_w spectrum is the inelastic design spectrum for the severe design earthquake, while the C_{es} spectrum is the *elastic* design spectrum for the moderate design earthquake.

To determine the R_{ser} value implied by UBC, it is necessary to consider the UBC drift limits. For buildings with an R_w value greater than 7.5 and a height taller than 65 ft., UBC requires that the design story drifts ratio not exceed $0.03/R_w$ (see point A in Fig. 2). Accepting a limit of story drift ratio equal to 0.005 in order to control nonstructural damage, the ordinate of point B in Fig. 2 can be determined by proportions

$$R_{ser} = \frac{0.03/R_w}{0.005} R_w = 6 \tag{3}$$

Since UBC uses an effective peak acceleration (EPA) equal to 0.4 g in high seismic regions, Eq. 3 implies that the EPA for the UBC moderate design earthquake is about 0.07 g — a level of excitations which has been experienced by many buildings in the Bay Area during the Loma Prieta earthquake.

For steel design the allowable stress for seismic load combinations is equal to $0.88F_y$ (= 0.66 $F_y\times$ 4/3). The UBC-implied allowable stress, $F_a^{(es)}$, for the moderate design earthquake can be computed by proportions (see Fig. 2)

$$\frac{F_a^{(es)}}{0.88F_y} = \frac{C_{es}}{C_w} = \frac{C_{eu}/R_{ser}}{C_{eu}/R_w} = \frac{R_w}{R_{ser}} \tag{4}$$

that is,

$$F_a^{(es)} = \frac{R_w}{R_{ser}} \times 0.88F_y = \frac{R_w}{6} \times 0.88F_y \tag{5}$$

The above equation shows that the UBC-implied allowable stress at the moderate design earthquake level is excessive for ductile frame systems. For example, $F_a^{(es)}$ is equal to $1.76F_y$ for R_w = 12. When the gravity load effects are considered, a general expression for $F_a^{(es)}$ can be derived (8). Gravity load effects can reduce but cannot eliminate member overstress in moderate earthquakes.

OBJECTIVE AND SCOPE

The main objective of this research is to study the serviceability performance (i.e., control of story drift and member forces) of multistory buildings. Two buildings (CSMIP Station Nos. 57355 and 57357) have been selected for this study because the recorded base motions of these buildings have an intensity similar to that of the UBC-implied moderate design earthquake.

METHOD OF ANALYSIS

For each building it is necessary to compute member forces and story drift ratios. Since only a limited number of floors were instrumented to measure the lateral motions, and no member force measurements were made by CDMG (2), a static analysis procedure using the computer program ETABS (4) has been developed. For each building the analysis procedure involves the following steps.

1. Establish a 3-dimensional finite element model based on the design drawings.
2. Estimate dead loads and realistic live loads.
3. Based on the analytical mode shapes and the relative displacements of the instrumented floors, compute the relative displacements of the other uninstrumented floors. Fig. 3 shows schematically the procedure for a 10-story building which is instrumented at the fifth floor and roof.
4. Perform structural analyses at peak responses by applying the gravity loads and by imposing the relative displacements obtained from step 3 to the model. Detailed structural responses are thus obtained.

SUMMARY OF RESULTS

CSMIP Station No. 57357 — This is a 13-story office building located in San Jose (see Fig. 4b). It was designed in 1972. The lateral force resisting system is a steel moment-resisting space frame. The fundamental periods predicted by the 1988 UBC empirical formula is 1.77 sec. The reactive weight of the building is estimated to be 25,200 kips. The building is founded on alluvial soil with a mat foundation. The 1988 UBC design base shear ratio is 0.043 for R_w = 12. A review of the design based on the 1988 UBC (see Fig. 5a) indicates that the maximum story drift ratio is 90% of the UBC limit (= $0.03/R_w$ = 0.025), and the member stress ratios are low ($\approx$ 0.4).

Table 1 shows the natural periods computed from the responses recorded during the 1984 Morgan Hill earthquake (3) and the 1989 Loma Prieta earthquake. The elongation of the natural period is insignificant (less than 10%), which is typical for steel structures.

The EPA of the base horizontal motion is 0.08 g. The ETABS analysis shows that the maximum story drift ratio is 1.28% (see Fig. 5b). Fig. 5b shows that the stress ratio produced by the Loma Prieta earthquake can be as high as 2.1 if the structure were to respond elastically. Apparently this type of building does not satisfy the serviceability requirements to minimize nonstructural component damage and to avoid significant member yielding even under minor to moderate earthquake excitations.

CSMIP Station No. 57355 — The building was designed in 1964 and constructed in 1967 (Fig. 4a). This reinforced concrete office building consists of 10 stories above grade and one story below the ground level. The lateral force resisting system consists of two end reinforced concrete shear walls and six interior frames in the E-W direction, and four frames in the N-S direction. The building is founded on alluvial soil with a mat foundation. The reactive weight of the building is estimated to be 24,500 kips. The R_w value in the N-S (moment frame) direction could be taken as either 12, 7, or 5, depending on the

ductility (or detailing) provided. Except for the UBC detailing requirements, this building satisfy the UBC strength and stiffness requirements for an R_w value equal to 12.

The stress ratios of the structural elements (see Fig. 6) show that the beams control the design and the columns are under-stressed. The gravity load effect is significant on these beams. The design story drift ratios produced by the 1988 UBC design seismic forces are much smaller than the UBC limits.

A comparison of the measured periods (see Table 1) during the 1984 Morgan Hill earthquake (5), and the 1989 Loma Prieta earthquake shows some elongation of fundamental periods in the longitudinal and transverse directions. The elongation of the periods suggests a loss of stiffness of about 23% in the E-W direction and 40% in the N-S direction. Considering that the rocking motion is significant in the E-W direction during the Morgan Hill earthquake (1), the N-S direction was judged to be critical in resisting ground excitations.

Because of the large lateral stiffness, which is a characteristic of reinforced concrete buildings in general, the maximum story drift ratio (= 0.17%) during the Loma Prieta earthquake did not exceed the serviceability limit of 0.5%.

The member forces obtained at the peak responses of the building show that a number of beams have exceeded the yield moment, which is defined by the initial yielding of the longitudinal reinforcements. The ratios between the actual member forces produced by the earthquake and the UBC required strength have reached 1.05 in the beams and 1.7 in the columns (Fig. 6). Significant structural yielding might have occurred had these members been proportioned to just satisfy the UBC strength requirement.

CONCLUSIONS

The Uniform Building Code seismic design procedure does not address the serviceability limit state explicitly. Therefore a building structure which satisfy the UBC might experience significant nonstructural and structural damages. The serviceability problem is more pronounced for ductile frames with less gravity loads. A simple analytical study shows that the intensity of the UBC-implied moderate design earthquake for buildings taller than 65 ft. is only one-sixth that of the severe design earthquake. For ductile frame systems the member forces may exceed member capacity significantly if the structure were to respond elastically. This is confirmed by the study of a 13-story steel frame; the actual stress ratio may be as high as 2.1, and the maximum story drift ratio is 1.28%. Because of the large lateral stiffness, the serviceability performance tends to be satisfactory for the type of reinforced concrete structures studied.

ACKNOWLEDGMENTS

This research is supported by a grant from the Strong Motion Instrumentation Program of the California Department of Conservation. Much appreciation is given to the staff of the SMIP, especially Drs. A. F. Shakal and M. J. Huang, for providing processed data and design drawings.

REFERENCES

1. Bard, P., "The Importance of Rocking in Building Motion: An Experimental Evidence," *Proc. 9th World Conf. Earthquake Engrg.*, vol. VIII, pp. 333-338, Int. Assoc. for Earthquake Engrg., Tokyo, Japan, 1988.
2. "CSMIP Strong-Motion Records of the Santa Cruz (Loma Prieta) California Earthquake of 17 October, 1989," *Reprt OSMS 89-06*, Calif. Strong Motion Instrumentation Program, Calif. Div. Mines Geology, Sacramento, Calif., 1989.
3. Mahin, S. A., Boroschek, R., and Zeris, C., "Engineering Interpretation of the Responses of Three Instrumented Buildings in San Jose," *Preprints*, SMIP89 Seminar, CDMG, Sacramento, Calif., 1989.
4. Maison, B. F. and Neuss, C. F., "SUPER-ETABS: An Enhanced Version of the ETABS Program," Technical Report to the National Science Foundation, J. G. Bouwkamp, Inc., Berkeley, Calif., 1983.
5. Papageorgiou, A. S. and Lin, B. C., "Influence of Lateral Load Resisting System on the Earthquake Response of Structures - A System Identification Study," *Earthquake Engrg. Struct. Dyn.*, vol. 18, pp. 799-814, 1989.
6. *Recommended Lateral Force Requirements and Commentary*, Struct. Engrs. Assoc. of Calif., San Francisco, Calif., 1990.
7. Uang, C.-M., "Establishing R (or R_w) and C_d Factors for Building Seismic Provisions," *J. Struct. Engrg.*, vol. 117, no. 1, pp. 19-28, ASCE, 1991.
8. Uang, C.-M. and Bertero, V. V., "UBC Seismic Serviceability Regulations: Critical Review," *J. Struct. Engrg.*, vol. 117, no. 7, pp. 2055-2068, ASCE, 1991.
9. *Uniform Building Code (UBC)*, Int. Conf. of Bldg. Officials, Whittier, Calif., 1988.

Building	Direction	Morgan Hill	Loma Prieta	Model
CSMIP-57355	N-S	0.91 (5)	1.08	1.08
	E-W	0.64	0.71	0.70
	torsion	0.39	0.47	0.37
CSMIP-57357	N-S	2.1 (3)	2.28	2.01
	E-W	2.2	2.24	2.17
	torsion	1.7	1.75	1.62

Table 1 Comparison of Natural Periods

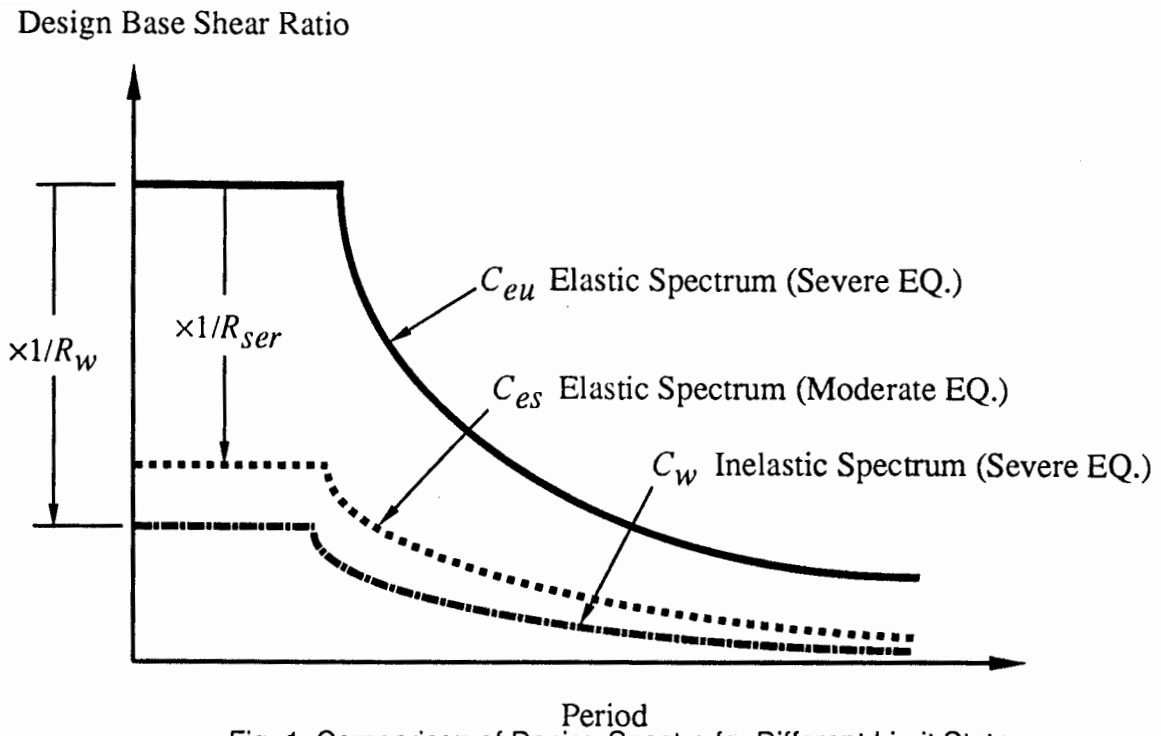

Fig. 1 Comparison of Design Spectra for Different Limit States

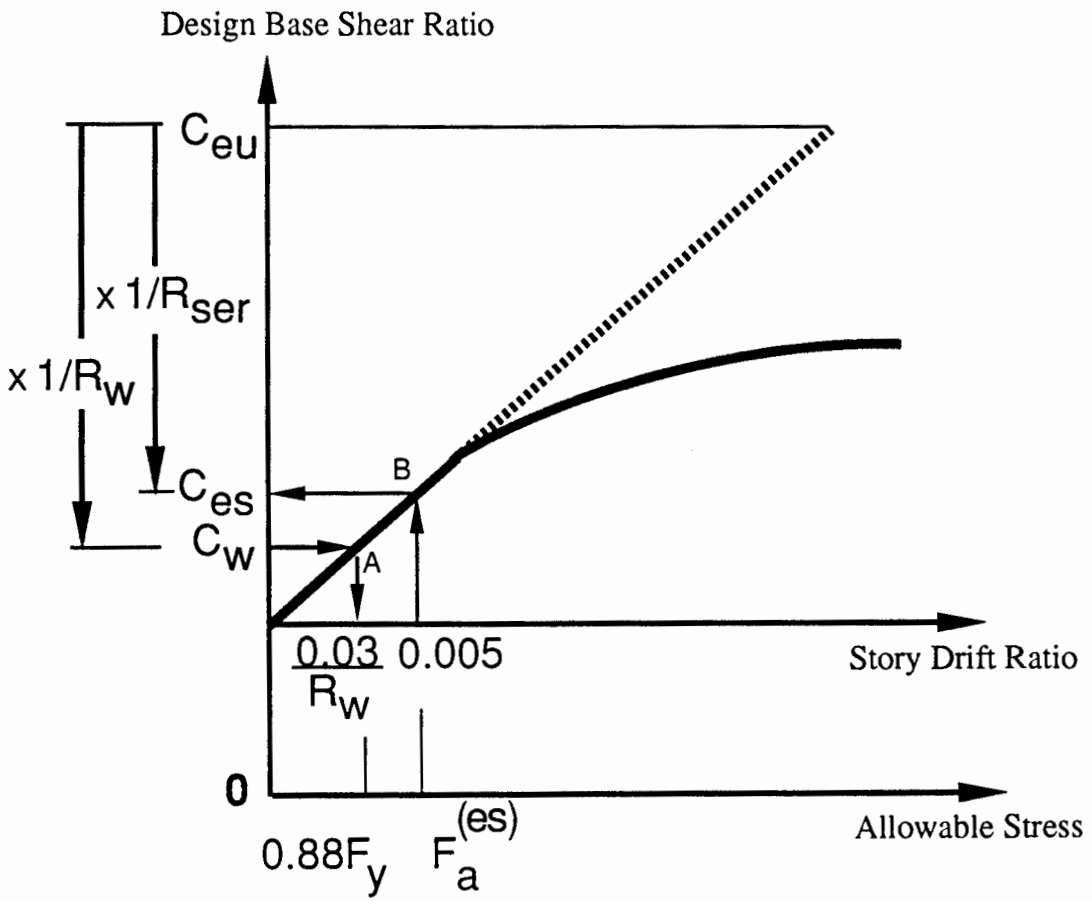

Fig. 2 Relationship between UBC Inelastic Design Force Level and Moderate Earthquake Design Force Level

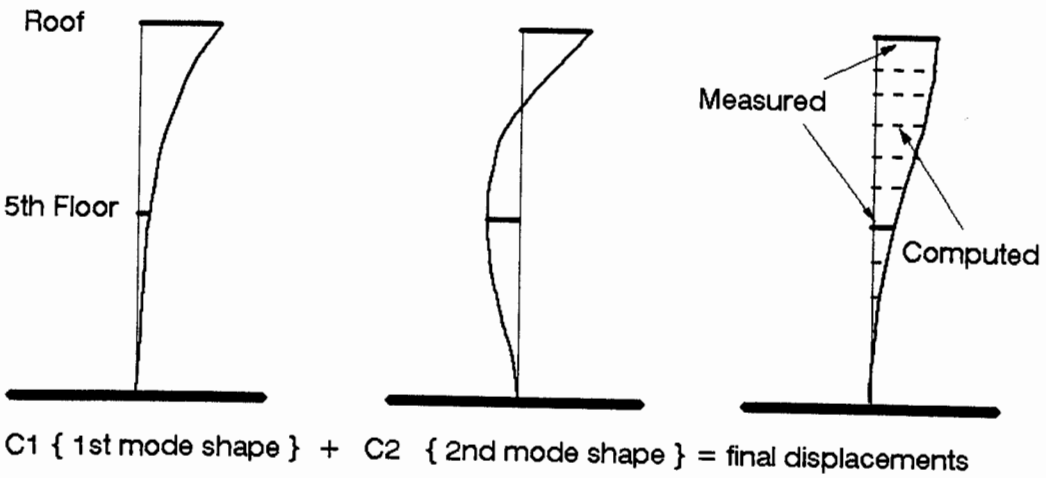

Fig. 3 Procedure to Compute Relative Displacements

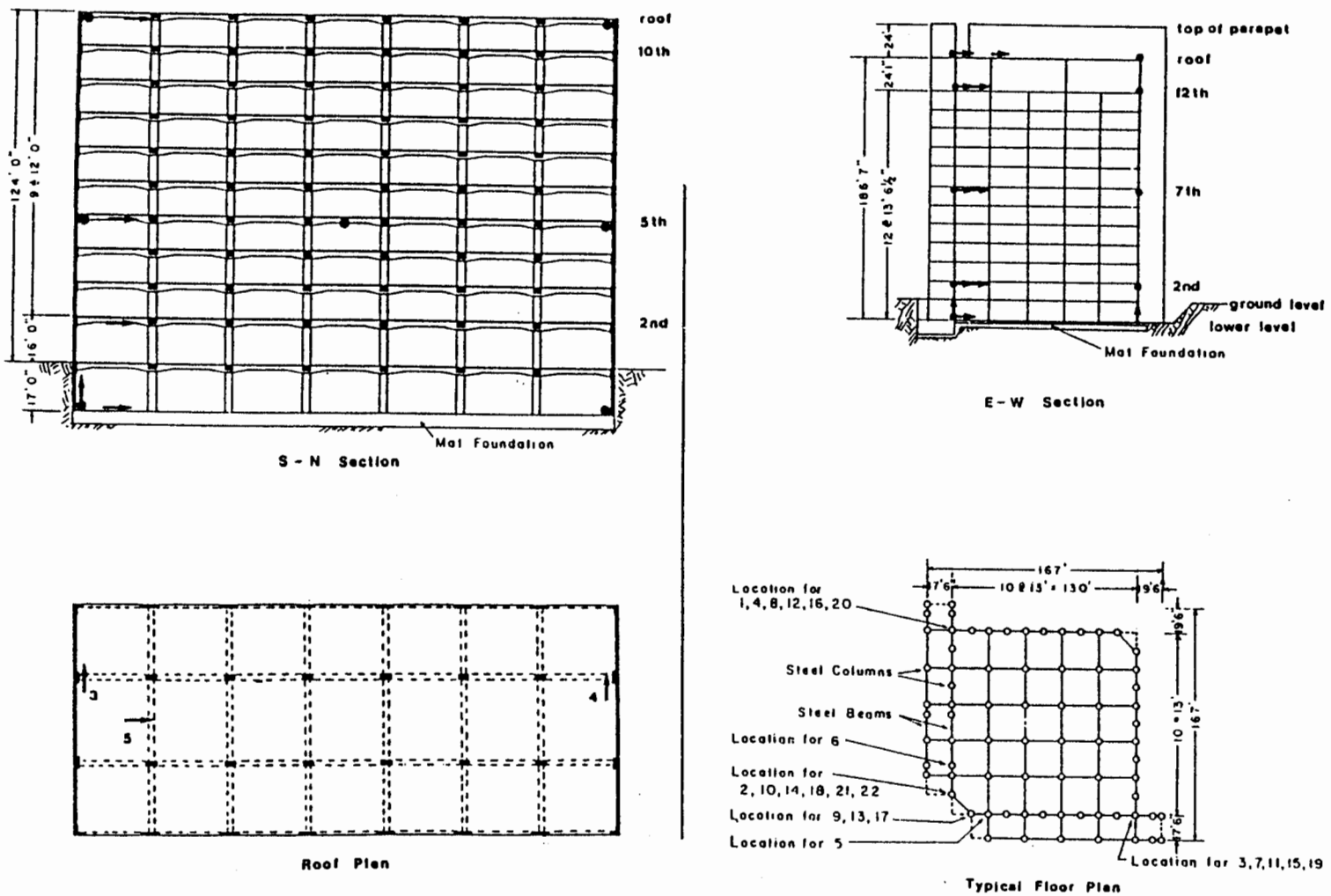

Fig. 4 Plan and Elevations of Buildings

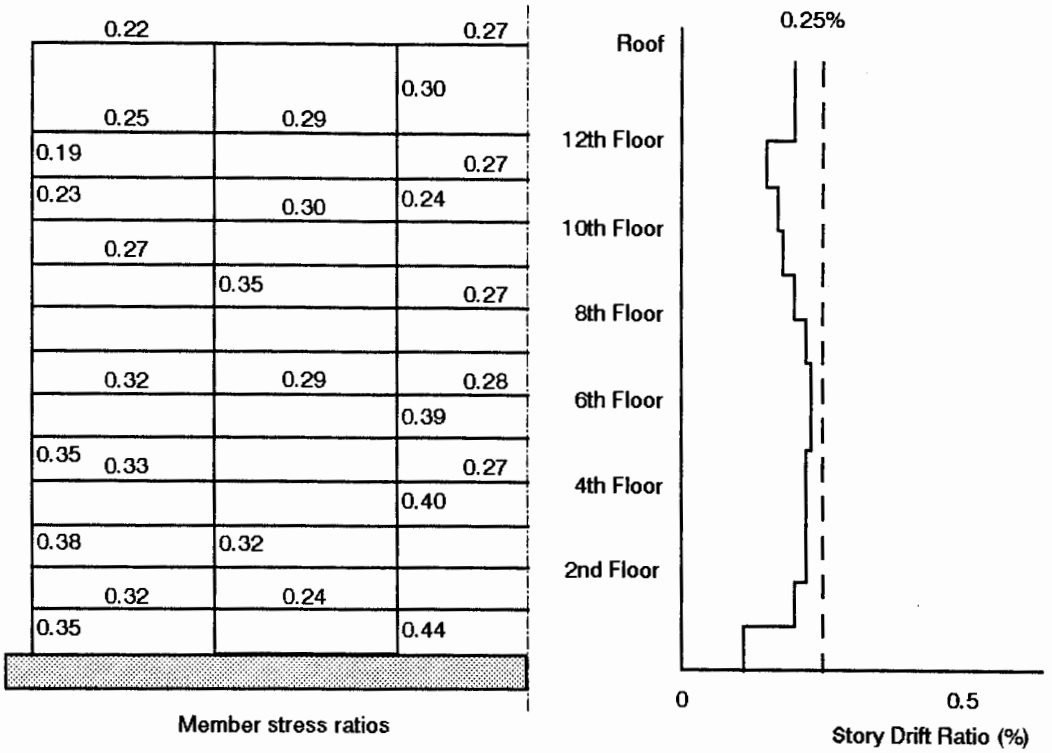

(a) 1988 UBC Design

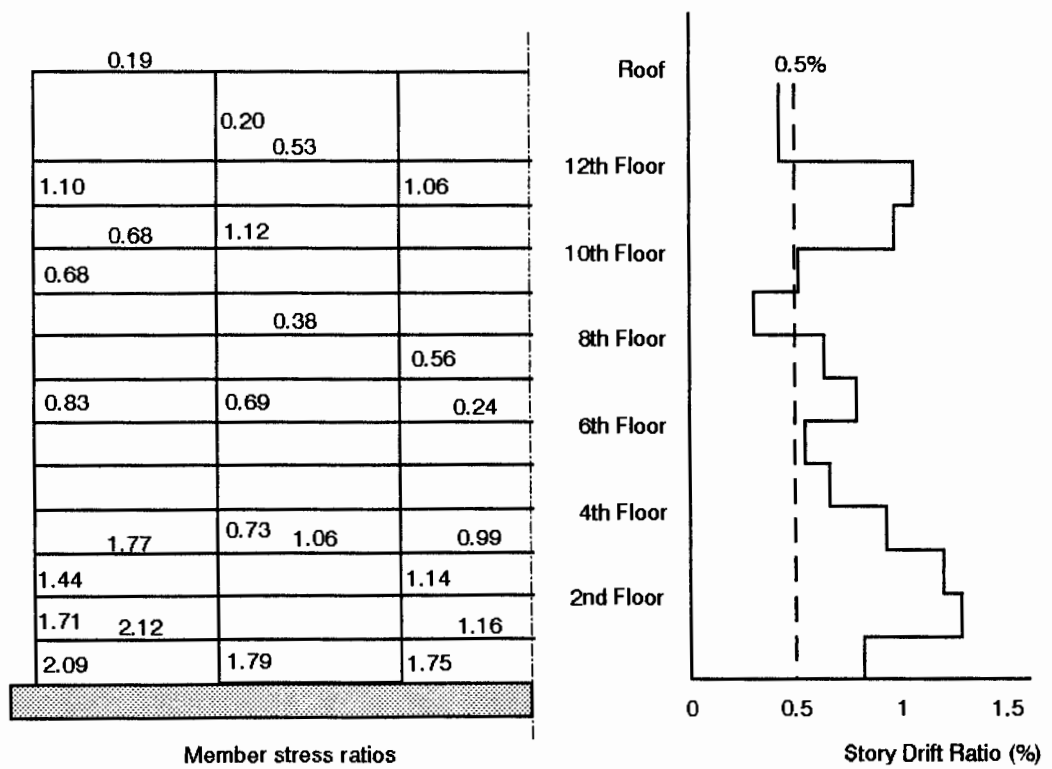

(b) 1989 Loma Prieta Earthquake

Fig. 5 Member Stress Ratios and Story Drift Ratios (CSMIP No. 57357)

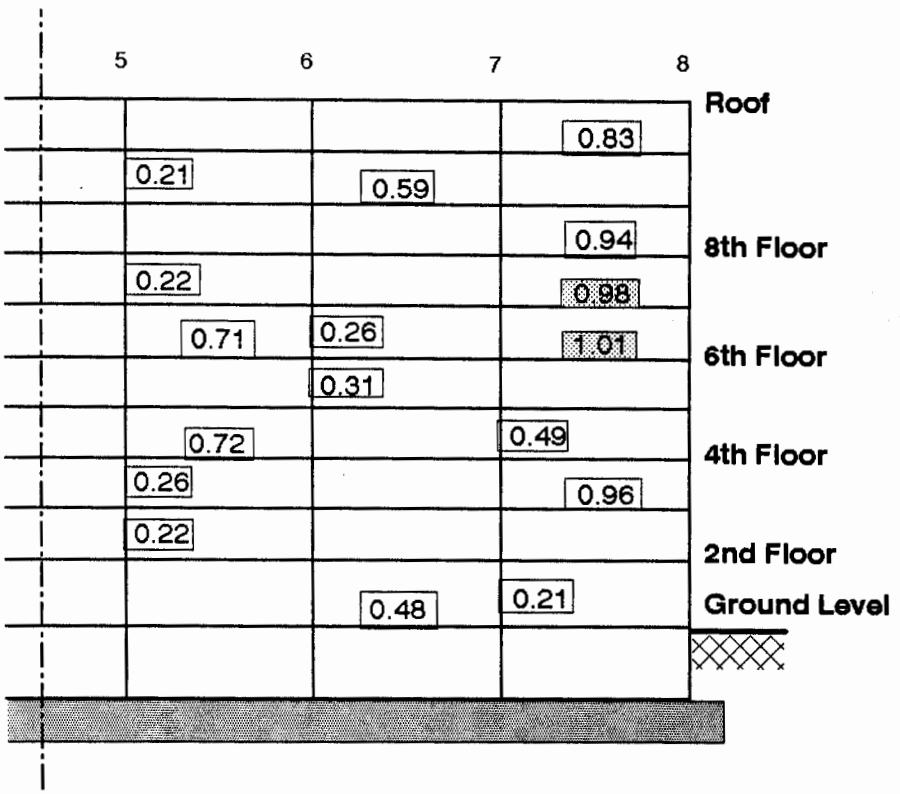

Fig. 6 Member Stress Ratios for 1988 UBC Design (CSMIP No. 57355)

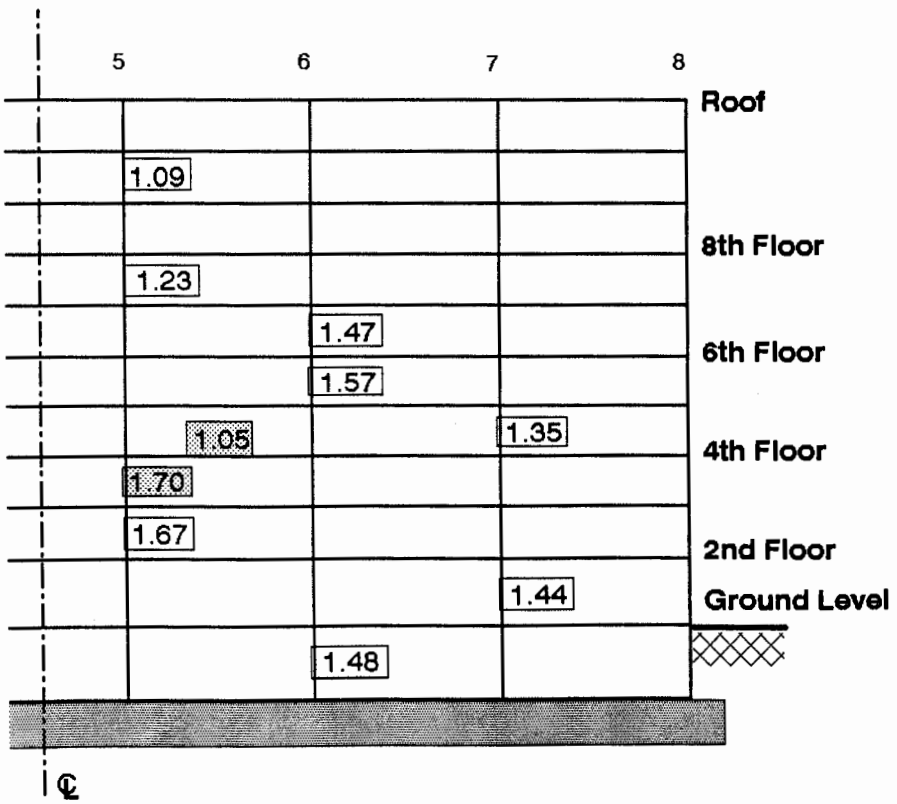

Fig. 7 Ratios between Member Forces Produced by Loma Prieta Earthquake and UBC Design Seismic Forces (CSMIP No. 57355)

DYNAMIC AMPLIFICATION OF GROUND MOTIONS BY LOW-RISE, STIFF SHEAR WALL BUILDINGS

Jon D. Raggett
J. D. Raggett & Associates, Inc.

Christopher Rojahn
Executive Director
Applied Technology Council

ABSTRACT

Dynamic amplification was defined as the ratio of actual peak base shear to an equivalent rigid-body base shear. Peak base shear was determined by summing the product of mass-times-acceleration for every element of mass in the building. An acceleration distribution over the entire building was assumed in terms of recorded acceleration time histories at several locations. Time histories from four buildings were studied. Due to diaphragm flexibility primarily, the dynamic response of these buildings did not differ significantly from that which would have occurred from a five-to seven-story steel frame. Actual peak base shears for this class of buildings was as high as 1.76 times equivalent rigid body base shears.

OBJECTIVES OF STUDY

The original objective of this study was to analyze existing strong motion data of low-rise, unreinforced masonry shear wall buildings with flexible diaphragms, to determine the extent to which ground motions are amplified by wall. Since there is only one unreinforced masonry building heavily instrumented, and since that instrumentation is not as complete as desired, the principal objective was expanded to include all low-rise buildings with stiff (masonry or concrete) shear walls and to include the affects of wall and diaphragm flexibility. A secondary objective of this study was to determine if any improvements to exiting strong motion instrumentation plans were warranted.

DESCRIPTION OF THE EVALUATION PROCEDURE

The principal objective of this study requires that amplification of ground motion be defined. Amplification of ground motion can be defined in a number of ways. It can be an instantaneous ratio of building motion to corresponding ground motion, it can be some averaged ratio, it can be a distortion reference to a corresponding absolute motion, and so forth. The best measure of amplification of ground motion should relate to the quantities used to design this class of buildings.

Typically, low-rise, masonry and concrete shear wall buildings with flexible diaphragms are designed using a distribution of static-equivalent forces. The most commonly referenced single measure of this set of static-equivalent forces is the design base shear, V. Amplification of ground motion will therefore be defined as the ratio of peak base shear allowing wall and diaphragm flexibility to that which would occur if the building were a rigid body.

Specifically for this study, peak base shear is defined as the maximum, total, seismically induced force transmitted to the foundation by all shear walls and frames parallel to the motion being considered. Out-of-plane wall forces at the ground level are not included. Three peak base shears are defined (one real and two hypothetical). The first is the actual, measured, peak base shear (V3) including all of the contributions due to actual wall and diaphragm flexibilities. The second is a hypothetical, "what if", peak base shear (V2) that would have occurred if diaphragms were infinitely rigid. In this analysis, diaphragm motions are assumed to equal the average of the motions of the walls to which they are attached. The third is another hypothetical, "what if", peak base shear (V1) that would have occurred if all diaphragms and walls were infinitely rigid.

Peak base shears (for each building, for each earthquake, for each principal direction) were computed by numerically summing the product of each element of mass and its corresponding acceleration, over the entire building, for each increment of time, for the actual and the two hypothetical cases. It is relatively easy to determine the mass of every element. If the building has been instrumented well, it is also reasonably easy to approximate the acceleration of every element in terms of the measured accelerations. A building (whether high-rise or low-rise) is instrumented well if all significant motions excited by an earthquake, for all parts of the building, can be approximated with accuracy from the recorded motions. For the class of structures considered in this study, the building is instrumented very well if, for each principal direction (typically transverse and longitudinal) the horizontal motions at a) the mid-points of every diaphragm are recorded, b) the intersections of every shear wall line and every diaphragm are recorded, and c) the bases of shear walls are recorded. If base rocking motion is expected to be significant, then at least a pair of vertical motions must be recorded for each shear wall, as well. Certainly, some approximations can be made with fewer instruments (such as approximating the base motions of several parallel shear walls with the base motion of a single shear wall).

For example, consider the assumed acceleration distribution for a simple, one-story, rectangular warehouse building. It is instrumented well if, for each direction, the base motion of each end wall is recorded, the in-plane motion at the top of each end wall is recorded, and the mid-span horizontal diaphragm motion is recorded. End wall accelerations are assumed to vary linearly

between the base and top motions. The horizontal motion of the roof diaphragm (and tributary mass of the out-of-plane walls) is assumed to vary as a half-sine-wave between end wall top motions. Acceleration distributions are constructed similarly for multi-bay and multistory buildings.

For each building, for each principal direction, for each earthquake, the three base shears defined previously were computed from the building properties and the recorded accelerations. For each time history, extreme values of V1, V2, V3 were identified (from the time histories V1(t), V2(t), V3(t) respectively).

DESCRIPTION OF BUILDINGS STUDIED

The basic criteria used to select buildings for this study were a) that the building have masonry or concrete shear walls and flexible diaphragms, b) that the building was sufficiently well instrumented so the acceleration distribution over the entire building could be determined with accuracy, and c) that strong-motion records for the building exist. Few buildings, other than those instrumented under the California Strong-Motion Instrumentation Program (CSMIP) are instrumented well enough to meet the above criteria. Therefore, those buildings in the CSMIP constitute the primary data base.

Only one unreinforced masonry building (for which strong-motion earthquake records exist) is instrumented in CSMIP. It is a 2-story rectangular building located in Gilroy, California. The strong-motion instrumentation, in both principal directions, does not meet the minimum requirements for this analysis. This building was included in this study, however, because it is the only building of its type, and some upper/lower bound analyses of its motions can be made that will yield at least some information regarding unreinforced masonry building behavior.

The second building is a rectangular reinforced concrete tilt-up warehouse building in Hollister, California with plan dimensions of 100 feet by 300 feet. The building has a wood, penalized roof system. The building is instrumented well. See Figure 7 for its elevations and Figure 8 for its instrumentation plan.

The third building is also a rectangular reinforced concrete tilt-up warehouse building in Redlands, California with plan dimensions of 90 feet by 235 feet. The building has a wood, penalized roof system. The building is instrumented well.

The fourth building is a 2-story rectangular office building in Milpitas, California with plan dimensions of 125 feet by 168 feet. It has precast, reinforced concrete tilt-up walls with large and uniformly spaced openings on all elevations. The second floor diaphragm has metal decking over open-web joists

with a concrete topping. The roof diaphragm is plywood over wood framing. The building is instrumented well.

EARTHQUAKE STRONG MOTION RECORDS ANALYZED

The earthquake motions analyzed for this study are summarized in the following table:

BUILDING	EARTHQUAKE	PEAK GROUND ACCELERATION LONG	PEAK GROUND ACCELERATION TRANS	PEAK ROOF ACCELERATION LONG	PEAK ROOF ACCELERATION TRANS	EQ MAG
Gilroy URM	Loma Prieta (10/17/89)	.24	.28	.55	.98	7.1
Hollister Warehouse	Loma Prieta (10/17/89)	.36	.25	.45	.82	7.1
	Hollister (1/26/86)	.14	.12	.25	.30	5.5
	Morgan Hill (4/24/84)	.07	.08	.12	.25	6.2
Redlands Warehouse	Palm Springs (7/8/86)	.04	.05	.11	.13	5.9
Milpitas Building	Loma Prieta (10/17/89)	.14	.10	.59	.33	7.1

DISCUSSION OF RESULTS

For this paper the motions of only one building, the Hollister Warehouse, will be discussed. The complete results of this study will be presented by the Applied Technology Council in ATC-27.

Shown in Figure 1 are schematic elevations of the Hollister Warehouse. Shown in Figure 2 are the strong-motion instrument numbers and locations.

Results are presented in two ways. Shown on Figure 3 is a sample of the three inertial force time histories (V1(t), V2(t), and V3(t)) defined previously that were obtained, for each building, for each earthquake studied, and for each direction of motion considered (transverse or longitudinal). The inertial

total force time histories do not equal precisely base shear time histories. The base shear time history equals the inertial time history plus a velocity dependent (damping force) time history. However, at the peaks of a total inertial force time history, the velocity is zero. Therefore, the PEAK inertial forces do equal the PEAK base shears. On the figure, the peak values of V1, V2, and V3 are identified. Shown on Figure 4 are the peak base shears (equal to the peak inertial forces) for the Hollister Warehouse normalized with respect to the peak rigid body base shear, V1 (the measure of amplification in this study due to wall, or wall-plus-diaphragm, flexibility).

Amplification due to wall flexibility only is evaluated with peak base shear, V2. For both directions of motion, for all earthquakes, V2 maximum observed was 1.14. Generally, for this class of buildings, there is insignificant amplification due to wall amplification alone. The 14% amplification observed for transverse motions of the Hollister warehouse for the Morgan Hill earthquake may be due to base rocking more than due to wall flexibility, but it was not observed in the other two earthquakes studied for this warehouse. It comes as no surprise that amplification due to wall flexibility alone for this class of buildings, is insignificant.

Amplification due to wall and diaphragm flexibility (the actual behavior) for warehouse structures can be very significant, depending upon the aspect ratio of the diaphragm. For longitudinal motions (a width to depth aspect ratio of 0.33) actual peak base shears are only marginally greater than the equivalent rigid body base shear (the maximum amplification is 7%). This again is to be expected; it is intuitively obvious. For transverse motions (aspect ratio of 3.00) actual peak base shears were found to be 76%, 55%, and 15% greater than their rigid body equivalents. These amplifications can be very significant, but obviously are not uniformly large for all earthquakes. This behavior is expected if a long, narrow warehouse is modeled as an equivalent 2-story shear wall building. The "first story" shear walls are the actual, very stiff concrete, end shear walls of the warehouse. The "second story" shear walls are the relatively flexible, plywood, horizontal half-diaphragms to mid-span. The "second story" lumped mass consists of approximately two-thirds of the entire roof and out-of-plane wall mass. This "second story" lumped mass can be very large, particularly when the out-of-plane walls are concrete, are 300 feet long, and are 31 feet high (as they are for the Hollister warehouse). This two-mass system with large masses and one soft spring (the plywood roof diaphragm) can have a fairly long fundamental period: approximately 0.65 seconds for the Hollister warehouse. This period is apparent from the V3(t) time history (shown in Figure 3 for the Hollister Warehouse). This fundamental period is typical for a five- to seven-story steel frame building, and is not generally associated with a one-story building having solid concrete shear walls. Once it is understood that a long, narrow warehouse is dynamically similar

to a five- to seven-story steel frame building, then the observed amplification of motion is not at all surprising. The behavior of the other three buildings studied was similar.

Thus far, effects of wall and diaphragm flexibility on overall building base shear have been studied . The effects of diaphragm flexibility on the diaphragm itself is even more dramatic.

Three plywood shear time histories were computed for transverse motions of the Hollister warehouse for the Loma Prieta earthquake. The first was the actual plywood time history observed. The actual peak plywood shear observed was 3103 plf. The plywood is 3/4 inch CDX with 10d nailing at 1-3/4" on centers. Allowable shear is approximately 930 plf. The peak value was 3.34 times the design value, with apparently no damage. If the roof diaphragm motions were assumed to equal the wall-top motions, the peak plywood shear would have been 1510 plf; and, if the roof diaphragm motions were assumed to equal the ground motion (assuming the building responded rigidly to the earthquake), the peak plywood shear would have been 1430 plf. Amplification of plywood shear due to wall and diaphragm flexibility (over rigid body behavior) was 117%.

Amplification of wall anchorage due to wall and diaphragm flexibility was even greater. Out-of-plane wall anchorage time histories for transverse motions of the Hollister warehouse to the Loma Prieta earthquake were also computed. The plywood diaphragm is nailed directly to a 4x plate, which is bolted directly to the top of the wall; there are no joist or purlin anchors. Actual peak roof-to-wall anchorage load at diaphragm mid-span was 1081 plf. The actual peak roof-to-wall anchorage load adjacent to an end wall was 345 plf. The peak roof-to-wall anchorage assuming rigid body behavior would have been 327 plf. The amplification of wall-to-roof anchorage due to wall flexibility was 221%. The allowable load on the anchor bolt-to-wood nailer is equivalent to 306 plf. The peak value measured was 3.53 times this allowable value, with apparently no damage.

CONCLUSIONS

Low-rise, shear wall buildings are generally expected to be stiff, and are not expected to have dynamic amplification factors much greater than one. If the low-rise buildings have heavy, stiff walls and flexible horizontal diaphragms their behavior in earthquakes can be quite different.

The strong-motion records from four low-rise buildings (with stiff shear walls and flexible diaphragms) were analyzed. Peak base shears were amplified as much as 82% over what the peak base shear would have been if the building was assumed to behave as a rigid body.

The amplification of elements of such buildings obviously was greater than the amplification of the peak base shear for the entire building. For one building, the Hollister warehouse, the actual roof plywood shear was found to be (for transverse motions) 117% greater than what it would have been had the building behaved as a rigid body; and wall-to-roof anchorage, 221% greater.

Transverse motions of buildings of this class will behave very similarly to five- to seven-story steel frame buildings. Similar amplifications of motion can be expected. The longitudinal motions of such buildings show little amplification of motion because the primary contributor to that amplification, diaphragm flexibility, is expected to be small.

Although no complete set of strong-motion records were available for a unreinforced building, because their floor diaphragms typically are very flexible, it can be expected that their peak base shears can be greatly amplified. The upper and lower bound analyses made in this study for one unreinforced masonry building, with a diaphragm aspect ratio of only 1.06, showed this to be the case.

For this class of buildings, deformations that vary horizontally are just as important as deformations that vary with height. Consequently, the number of strong motion-instruments required to describe the complete acceleration distribution with accuracy can be large. In general, in order that building motions be described unambiguously, the motion of every horizontal diaphragm, the motion of every wall-to-diaphragm connection, and the motion of each shear-wall-to-ground connection should be recorded.

ACKNOWLEDGEMENTS

The authors gratefully acknowledge the guidance and insight provided by the advisory Project Engineering Panel: Karl Deppe, M. J. Huang, Donald Kay (ATC Board Representative), Fred Willsea and Theodore Zsutty. The funding provided by the Division of Mines and Geology is also gratefully acknowledged.

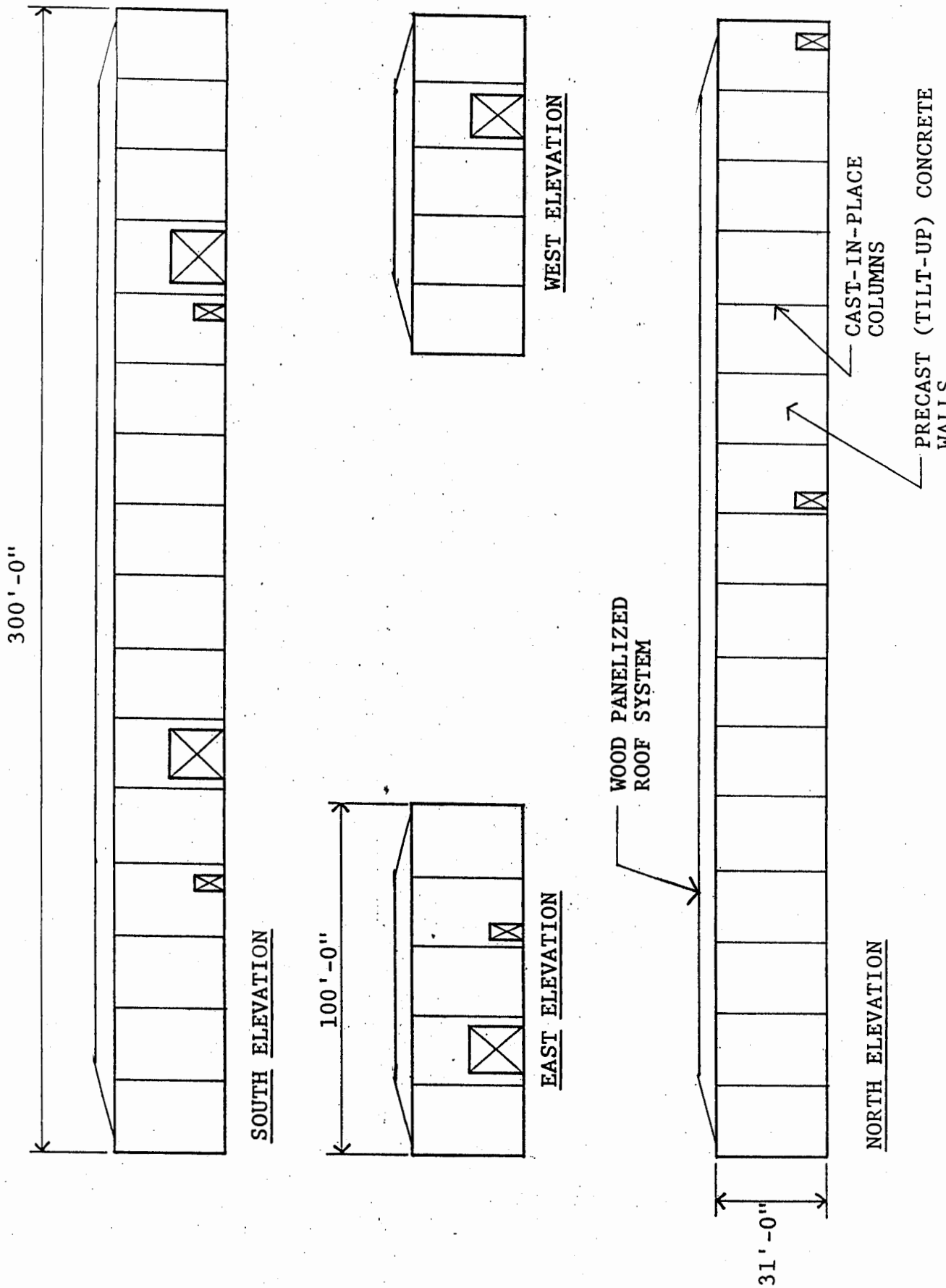

FIGURE 1 - 1-STORY WAREHOUSE BUILDING
HOLLISTER, CALIFORNIA

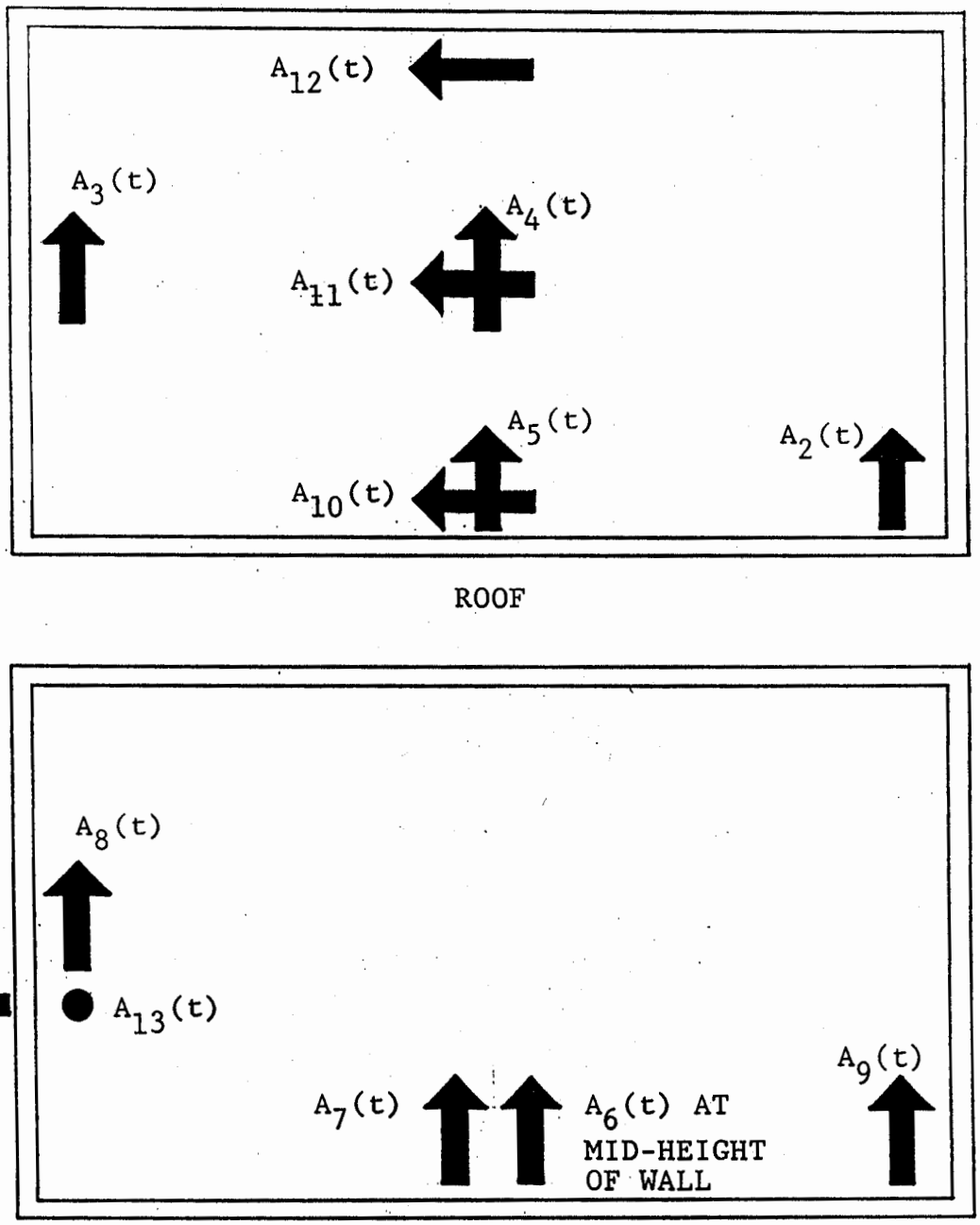

FIGURE 2 - INSTRUMENTATION PLAN
1-STORY WAREHOUSE BUILDING
HOLLISTER, CALIFORNIA

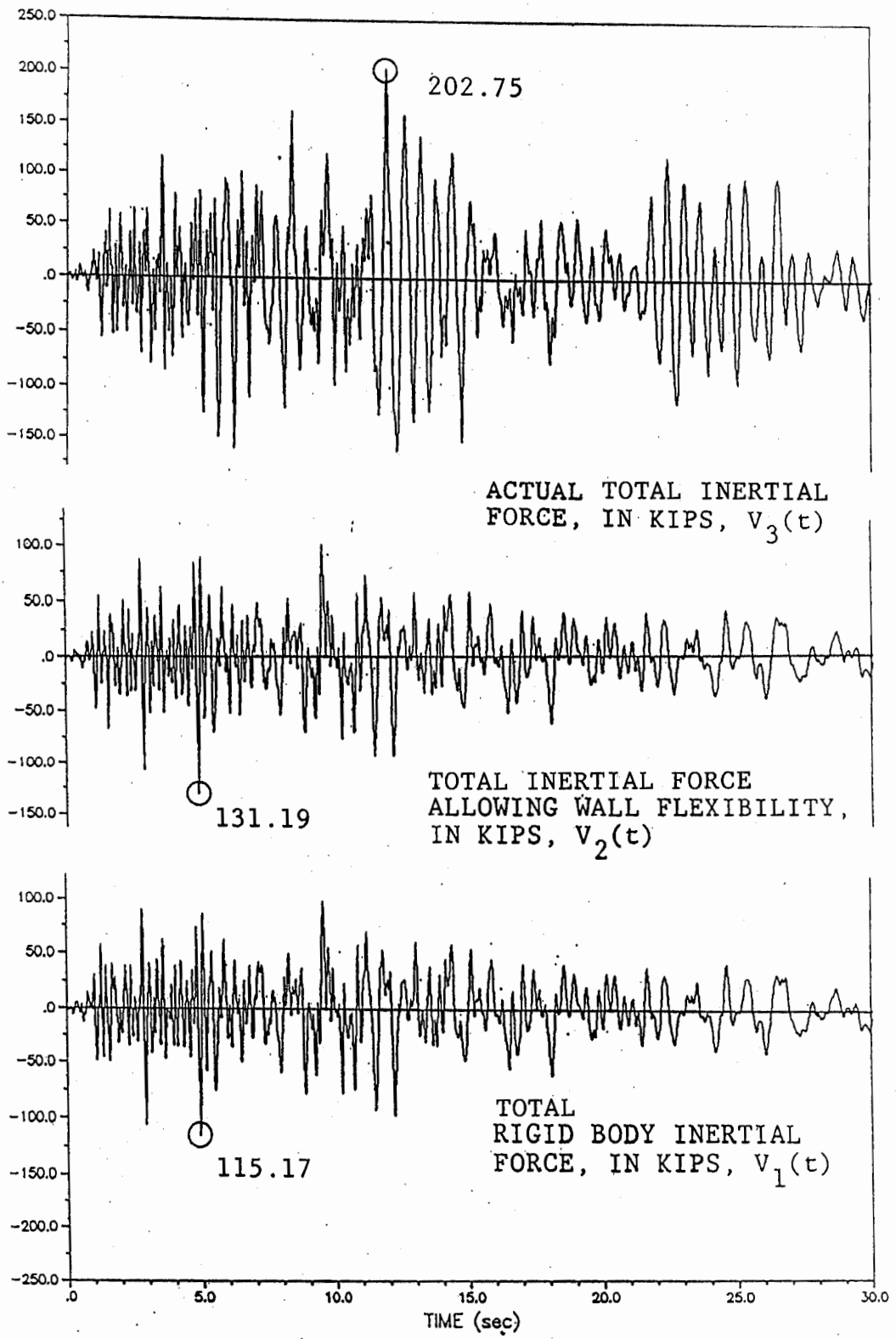

TRANSVERSE MOTION

FIGURE 3 1-STORY HOLLISTER WAREHOUSE
MORGAN HILL EARTHQUAKE (4/24/84)

V_1 - PEAK RIGID BODY BASE SHEAR

V_2 - PEAK BASE SHEAR ALLOWING WALL FLEXIBILITY

V_3 - PEAK BASE SHEAR ALLOWING WALL AND DIAPHRAGM FLEXIBILTY (ACTUAL CASE)

FIGURE 4
PEAK BASE SHEARS
1-STORY HOLLISTER WAREHOUSE